Static Resistance Functions for Unbonded Retrofit Unreinforced Concrete Masonry Walls with Plate Connection for Blast Design Applications

by

Eric Gagnet

A thesis submitted to the Graduate Faculty of
Auburn University
in partial fulfillment of the
requirements for the Degree of
Master of Science

Auburn, Alabama
August 3, 2013

Approved by

James S. Davidson, Chair, Professor
Robert W. Barnes, James J. Mallett Associate Professor
Justin D. Marshall, Assistant Professor

Abstract

Over the past two decades the use of explosives to attack both commercial and government buildings has increased. A substantial amount of research has been conducted to be able to protect not only the occupants but the structure also. New construction practices have been developed to mitigate the damages, but retrofit of existing buildings does not have a single answer. The resistance functions of all the components of the wall including a retrofit system are needed to be able to model an accurate simulation to ensure safe design of the retrofit.

For design purposes the amount of energy dissipation is important; however, the design codes, such as UFC 3-340-02, do not use energy dissipation as a criterion for safe design. Rather deflection and rotation limits are set for different levels of protection. In order to determine if a wall meets these limits, a dynamic analysis is performed to determine the maximum deflection a wall will exhibit during a loading. Typically a single-degree-of-freedom (SDOF) model is used to solve for the midspan deflection. This simplified method requires a definition of the relationship between resistance and deflection.

Unreinforced, ungrouted masonry (URM) walls are commonly found throughout the world. Masonry buildings have been around for thousands of years and comprise over 70% of buildings worldwide. Because of their popularity and susceptibility to fragmentation, it is imperative to ensure masonry walls are capable of withstanding a

blast load. The two main categories of URM walls examined are non-arching walls and arching walls. Several methods have been developed to simulate how these walls will resist a lateral load and an in depth comparison is presented.

Many methods have also been developed for the resistance definition of an unbonded retrofit system. These methods have also been heavily examined. An analytical method was developed to incorporate the effects of the retrofit connection on the resistance function. This method was validated using finite element modeling. Many different geometric models were used to assess the validity of the algorithm.

Lastly, all of the components of the walls resistance definitions were combined to form the total resistance of the wall. This resistance was used in a single-degree-of-freedom model to generate a retrofit system for a specific design example.

Table of Contents

List of Figures

List of Tables

Notation

a	=	length over which arching force acts
A	=	Cross sectional area
b	=	Unsupported length of membrane
B	=	distance from support to yield location divided by span length = 0.5
c	=	Distance from centroid to most extreme fiber
C_1	=	Compression force per unit width in shell
C_2	=	Compression force per unit width in web
CMU	=	Concrete masonry unit
E	=	Modulus of elasticity of retrofit
E_c	=	Concrete masonry modulus of elasticity
FBD	=	Free body diagram
f_{cr}	=	Cracking stress of masonry
f'_m	=	Crushing stress of masonry
f_r	=	Modulus of rupture
g_{max}	=	Maximum allowable gap between wall and support
H	=	Height of wall
H	=	Horizontal reaction
h'	=	Distance between supports
H_{bottom}	=	Horizontal reaction at the bottom of the wall
H_T	=	Horizontal reaction at the top of the wall
I	=	Moment of inertia for membrane
I_g	=	Gross (uncracked) moment of inertia
j	=	Constant
k	=	Solid ratio of masonry through webs (k = 0 assumed for horizontal span arching if not fully grouted)
K_e	=	Elastic Stiffness
L	=	Length of membrane
L'	=	Arch length of membrane
L_d	=	Original length of diagonal for half wall
L_p	=	Length of plate from hinge to edge
M	=	Moment caused by lateral pressure
P	=	Lateral pressure

P	=	Axial Load
Q_1	=	Maximum allowable flexural resistance
Q_2	=	Pressure of decaying wall
Q_y	=	Yield load
R	=	Vertical reaction
r_1	=	Resistance due to flexure
r_2	=	Decaying resistance
R_m	=	Moment arm of arching masonry wall
SBEDS	=	Single-degree-of-freedom Blast Effects Design Spreadsheet
SFR	=	Solid fraction ratio
T	=	Thickness of wall
T	=	Tension force at ends of retrofit
t_p	=	Thickness of plate
T_s	=	Thickness of membrane
t_{ms}	=	Masonry shell thickness
T_v	=	Vertical component of membrane axial force
UFC	=	Unified facilities criteria
URM	=	Unreinforced masonry
V_{top}	=	Arching force at top of the wall
W_i	=	Self-weight of wall
α	=	Support fixity
β	=	Curvature ratio
γ	=	Incremental displacement for retrofit
δ	=	Shortening of wall
Δ	=	Lateral deflection at mid-span
Δ_1	=	Deflection at Q_1
Δ_2	=	Deflection at Q_2
Δ_c	=	Distance midspan moves while closing gap
Δ_{cr}	=	Deflection at mid-span at cracking of CMU wall
Δ_{crG}	=	Deflection at mid-span at crack growth
δ_g	=	Gap distance between wall and support
$\Delta_{max\ elastic}$	=	Maximum elastic mid-span deflection of CMU wall
Δ_{st}	=	Deflection at the point of snap though
E	=	Strain
ε'	=	Compression strain due to arching forces and support movement strains
ε_d	=	Strain of diagonal in CMU at failure
θ	=	Angle of membrane at ends
λ	=	Angle of masonry wall
λ	=	Change in rotation of plate

ν = Poisson's ratio
σ = Stress in extreme fiber
σ_t = Ultimate dynamic tensile stress of masonry
σ_y = Stress in extreme fiber at yielding
φ = Angle of rotation of plate
ψ = Additional displacement added by rotation of plate

Chapter 1: Introduction

1.1 Background

Terrorist attacks have increased in frequency over the years. In a study conducted by the National Research Council (NRC), explosions account for 46 percent of all terrorist attacks worldwide. This number is substantially higher within the United States, 77 percent (NRC 1995). Explosives are cheap and easy to make but can cause significant damage to both the structure and the occupants.

In 1993, the New York World Trade Center was one of the first major U.S. buildings to come under attack. A Terrorist drove a 1500 lb explosive into the basement (Terrorism 2004). When detonated, a 100-ft crater was created killing six people and injuring over a 1000 (FBI 2008). The explosive was constructed using readily available materials at a cost of less than $400 (NRC 1995). At that time, this attack was the largest terrorist attack using explosives on American soil.

On April 19th 1995, the Alfred P. Murrah Federal Building came under attack from a homegrown terrorist. A rented trunk placed next to the building contained the explosive. Upon detonation, 168 people were killed and over five hundred were wounded (Terrorism 2004). Damage from the attack is shown in Figure 1.1.

Figure 1.1 Structural Damage of the 1995 Oklahoma Building Bombing (AP Photo, Newman 2013)

In 1998, two US embassies were attacked simultaneously; one in Kenya, the other in Tanzania. Again the explosives were thought to be stored inside of a truck parked near the buildings. The explosion in Kenya killed 11 while injuring 86. The Tanzania explosion killed 213 people, 12 of which were Americans, and injured over 5000 (Terrorism 2004).

The use of explosives can be attributed to several factors: to obtain publicity, political or symbolic statements, destroy assets, religious imperative, injure and kill occupants, and lastly for revenge. For these reasons, commercial and military structures are the two main targets (NRC 1995). Due to these attacks the military has implemented strict security measures in attempts to prevent explosives from entering the building. As a result, exterior elements are more prone to attacks and increase the need to be able to resist blast loads. Government facilities may require blast loading as a part of design

loads whereas most of the commercial market does not require a building be designed to resist an explosion.

Blast loading is dynamic in nature. It is commonly compared to earthquake loading, which is incorrect (NRC 1995). An earthquake has a low intensity and a long duration, whereas a blast typically has a high intensity over a very short duration (NRC 1995). For this reason new techniques need to be developed to mitigate damage.

Unreinforced, ungrouted masonry (URM) walls are commonly found throughout the world. Masonry buildings have been around for thousands of years and comprise over 70% of the buildings worldwide (The Mason Contractors Association of America, n.d.). Today buildings with a high risk of being subjected to a blast loading have been designed to withstand external detonation. However, many existing buildings were not designed to resist blast loading. Davidson et al. (2005) state that most injuries sustained during a blast are not directly caused by the detonation: pressure, heat or container fragmentation. Rather most injuries result from secondary fragmentation resulting in blunt trauma or penetration resulting from the disintegration of the CMU and the windows being propelled at high velocity. Because of secondary fragmentation it is important to ensure that these elements are able to resist the loading without producing hazardous debris.

Since Wiehle and co-researchers at The Stanford Research Institute started researching how to develop a static resistance function for URM walls subjected to a lateral load in 1969, many different theories and methodologies have been developed. Due to the brittle nature of URM walls, laboratory testing is very difficult and unreliable, especially during the decay phase of the resistance function. For these reasons, many

have developed their own resistance functions based on differing assumptions. These assumptions can change the resistance curve significantly.

The three types of systems to be considered in this report are: 1) non-arching walls 2) arching walls 3) unbonded retrofit. The first two systems involve URM walls while the third system describes how an unbonded membrane will resist an out-of-plane load. The first URM wall system will describe how a simply supported wall, where the supports do not resist rotation, will respond to the lateral load, while the second details how a wall with an arching force will react to the lateral load.

Since 1995, a great deal of research and testing has been conducted by the Air Force Research Laboratory (AFRL) at Tyndall Air Force Base, Florida to develop inexpensive and practical methods to strengthen URM walls against blast (Davidson et al. 2004). An important factor that is considered is the ability for the retrofit system to be implemented worldwide where limited equipment is available during the installation. For this reason AFRL, along with other agencies, have explored the use of fiber reinforced composites, aramid composite fabrics, etc.

For unbonded membrane many different methods have been developed to generate a resistance definition. These methods are examined in the same manner as the masonry methods. Several laboratory tests have been conducted to examine how the retrofit connections will affect the resistance curve, but no analytical method has been developed to describe this effect.

1.2 Objective

The overall objective of the research represented by this report was to develop a resistance function to be used in SDOF-based blast analyses of membrane retrofitted unreinforced masonry walls.

1.3 Methodology and Scope

The following tasks were required to achieve that broader goal stated above: 1) assess resistance definitions that are currently used for blast analyses of non-arching and arching unreinforced masonry walls, compare them to experimental data, and determine which is the most accurate; 2) evaluate the different membrane resistance definitions and validate them using finite element software; and 3) develop a method to incorporate the connection flexibility into the membrane resistance function used for the analyses of unbonded retrofit masonry walls subjected to blast loading and validate the method using full-scale explosion test results.

Over the years several different methods have been developed to form a resistance curve for both the wall and retrofit system. It is important to know how each of these methods was developed and what assumptions were used to develop these methods. Finally with each of these components, which method should be used for design purposes?

Research was conducted to find valid resistance functions for various types of URM walls. For each method the original source was reviewed to validate the reasoning and ensure it should be used. This process was also used for the membrane resistance methods.

The connection algorithm was developed to mimic the response of the retrofit against previous lab tests and finite element models. The algorithms were developed using equilibrium, compatibility, and the stress-strain curve. The assumptions made to generate this algorithm produce a slightly conservative resistance curve by generating a slightly lower resistance. For design purposes this is acceptable.

The resistance of the wall system is a critical input component of single-degree-of-freedom models used for blast design. For design of retrofit systems, it is important to determine the peak deflection of the system. This deflection corresponds to a wall rotation that is compared to response limits. These response limits determine the level of protection that is provided.

Chapter 2: Literature Review

2.1 Overview

Over the past several years much research has been done in order to evaluate methods of retrofitting unreinforced concrete masonry (URM) walls. Many older buildings are not reinforced against lateral loads. Due to the brittle nature of concrete masonry there is little resistance when an out-of-plane load is applied. Buildings being constructed for a high blast resistance typically use grouted CMU with steel reinforcement. It is both expensive and impractical to demolish and rebuild the wall. A practical solution is to retrofit the existing wall with a membrane. Many different materials can be applied as a backing to the CMU wall to add resistance to a blast load. As a blast wave propagates through a wall it encounters several forms of resistance that will help provide strength, ductility and dissipate the energy to reduce the lethality of a blast. Every part of the wall and retrofit system should be considered to ensure an accurate and proper design.

According to Knox et al. (2000) the overall objective of a blast analysis is to determine the maximum deflection that would be acceptable to ensure minimal injury or death to the occupants. The use of a single-degree-of-freedom system simplifies the analysis as a mass on a spring with a defined resistance. Analytical formulas have been developed to formulate the resistance of the concrete masonry unit (CMU) wall and the unbonded retrofit. With some assumptions, Knox et al. (2000) stated that the overall

resistance of the wall is the sum of the resistance of the individual components at the corresponding displacement.

Many analytical models have been developed to describe the resistance of the CMU and the unbonded retrofit. The way the retrofit is installed has been studied extensively and determined that the connection can increase the ductility of the system (Hoemann et al. 2010; Johnson et al. 2009).

2.2 Masonry Wall

CMU walls can resist lateral loading in one of two ways. If the wall supports cannot resist rotations, the only way the wall will resist the load is through flexural resistance (Drysdale et al. 1994). If the supports are rigid the wall will have a compressive force to resist rotation of the wall. When the wall is bent due to the lateral loads the tension face will elongate. If the supports are rigid this elongation is met with a compression force at the supports. This type of interaction is referred to as an arching boundary condition. The two types of walls are separated based on the support conditions and will be classified as either arching walls or non-arching walls.

Buchan and Chen (2007) looked at 40 CMU walls subjected to explosions reported in 6 different papers. The tests included both URM walls and partially grouted, lightly reinforced walls. Of those categories some were retrofit and others were not. The retrofit under consideration was a fiber reinforced polymer membrane. It was concluded that the retrofitted walls resisted a peak pressure 50% greater than the non-retrofit walls. Along with an increase in peak pressure, the retrofit walls had a reduction in debris scatter compared to the non-retrofit walls.

For all masonry walls, ACI 530-08 outlines the design criteria that must be satisfied for strength design of ungrouted unreinforced masonry walls subjected to both moments and an axial load. The four design assumptions used in ACI 530-08 are:

a) Strength design of masonry members shall be in accordance with principles of engineering mechanics

b) Strain in masonry shall be directly proportional to the distance from the neutral axis

c) Flexural tension in masonry shall be assumed to be directly proportional to the strain

d) Flexural compressive stress in combination with compressive stress shall be assumed to be directly proportional to strain

Using these assumptions the strength of the masonry can be determined so that the compressive stress in the masonry does not exceed $0.80 f'_m$ and the tensile stress in the masonry does not exceed the modulus of rupture for masonry. Design values for the modulus of rupture for masonry is given in Table 2.1.

Table 2.1 Modulus of Rupture for Masonry, psi (kPa) (ACI 530-08)

Direction of flexural tensile stress and masonry type	Mortar types			
	Portland cement/lime or mortar cement		Masonry cement or air entrained portland cement/lime	
	M or S	N	M or S	N
Normal to bed joints in running or stack bond				
Solid units	100 (689)	75 (517)	60 (413)	38 (262)
Hollow units[1]				
Ungrouted	63 (431)	48 (331)	38 (262)	23 (158)
Fully grouted	163 (1124)	158 (1089)	153 (1055)	145 (1000)
Parallel to bed joints in running bond				
Solid units	200 (1379)	150 (1033)	120 (827)	75 (517)
Hollow units				
Ungrouted and partially grouted	125 (862)	95 (655)	75 (517)	48 (331)
Fully grouted	200 (1379)	150 (1033)	120 (827)	75 (517)
Parallel to bed joints in stack bond				
Continuous grout section parallel to bed joints	250 (1734)	250 (1734)	250 (1734)	250 (1734)
Other	0 (0)	0 (0)	0 (0)	0 (0)

[1] For partially grouted masonry, modulus of rupture values shall be determined on the basis of linear interpolation between fully grouted hollow units and ungrouted hollow units based on amount (percentage) of grouting.

2.2.1 Non-Arching walls

Wiehle et al. (1969) was one of the first to outline the process of developing a static resistance function for masonry walls. Wiehle et al (1969) assumed the resistance can be idealized in five regions: elastic, elastic-plastic, strain hardening, plastic, and decaying. An idealized representation of the resistance functions is shown in Figure 2.1.

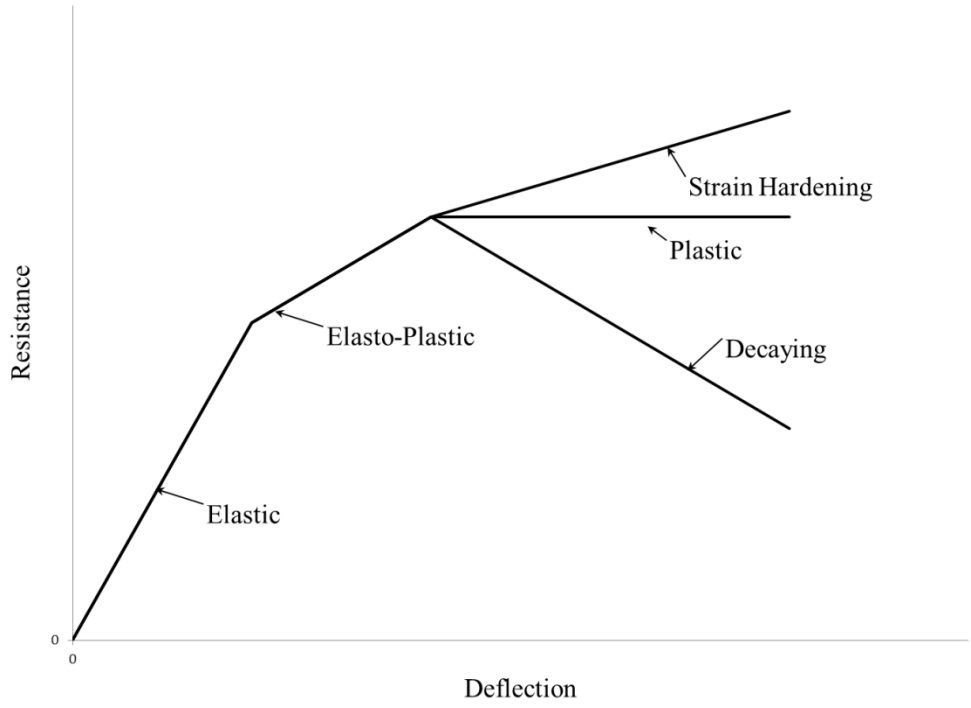

Figure 2.1 Idealized Resistance Curves

The resistance definition used by Wiehle et al. (1969) considered the wall as only having two phases: an elastic and decaying phase. During the elastic phase the wall behaves in the same way as an elastic beam. Wiehle et al. (1969) does consider the tensile bond of the mortar. Once cracked, the wall is idealized as two rigid beams connected at the crack. After cracking, the wall will have a discontinuity due to the sudden loss of the flexural strength if no axial load is applied. The geometry of the wall along with the weight and axial load are the only forces considered resisting the lateral load. A preexisting axial load increases the resistance by keeping the crack closed. Wiehle et al. (1969) place the axial load at the wall centerline and assumes the eccentricity negligible.

Slawson (1995), Johnson et al. (2008), and Jones (1989) use this resistance function as the analytical method for URM walls.

Paulay and Priestley (1992) describe the mechanics of masonry walls under lateral loads and what determines failure of a CMU wall. “The formation of cracks does not constitute wall failure” (Paulay and Priestley 1992). The failure of the wall is dependent on the resultant of the compressive force moving past the line of action for the axial load and self-weight of the wall.

Paulay and Priestley (1992) make the assumption that there will be no tensile resistance of the masonry wall. Figure 2.2 illustrates how the resultant force moves as the crack propagates.

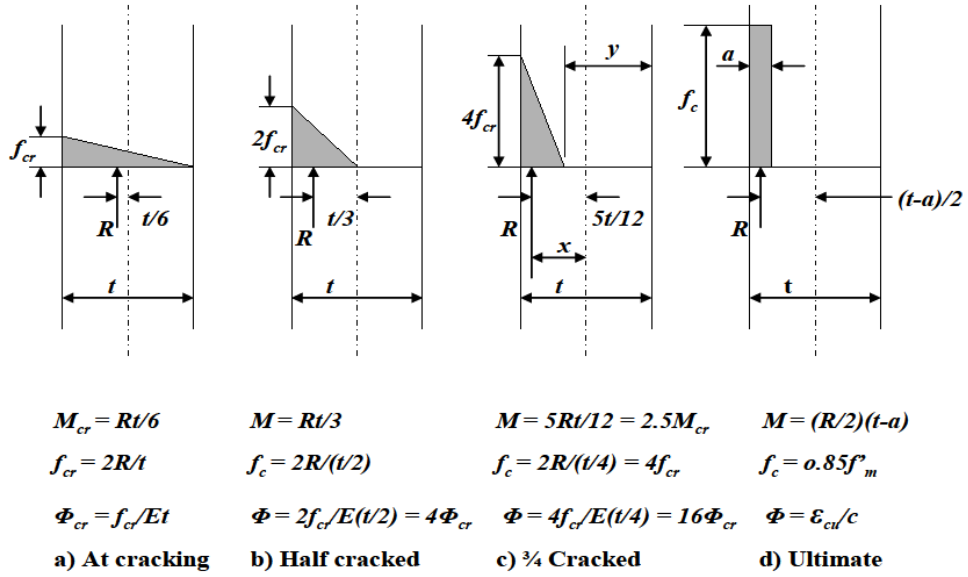

Figure 2.2 Compressive Resultant Force (Paulay and Priestley 1992)

It is noted that the intensity of the compressive stress increases; however, the area decreases as the crack spreads. Because of this, the resultant force, *R*, remains the same throughout if there is no arching force. Paulay and Priestley (1992) state that as a

conservative estimate, the deflection of the wall increases proportionally with the curvature of the centerline.

The bond of the mortar and CMU can define the maximum tensile stress and therefore the ultimate strength of the wall (Drysdale et al. 1994). However, the strength of the bond can vary by as much as 20% in the laboratory testing. With a highly variable mortar tensile bond the crack can easily be initiated before the ultimate strength is reached. It only takes a small portion of the mortar in a bed to have lower strength to compromise the entire wall. "The crack initiates along two or three units […] and then immediately propagates for the full length of the wall" (Drysdale et al. 1994). The mortar tensile bond itself is very low and reduced because of its variability making it appear negligible. However, the addition of tensile stresses to the walls resistance can more than double the strength of the wall (Drysdale et al 1994).

Based on the ideas from Drysdale et al. (1994) and Paulay and Priestley (1992), Moradi and Davidson (2008) developed a resistance definition for non-arching URM walls. However, one major difference is that the Moradi resistance definition assumes that tensile stresses are negligible. The ACI 530-08 code indicates that some tensile stress can be used; however Moradi and Davidson use a value of zero mortar tensile bond. One major advantage of Moradi and Davidson's method is that it considers partial fixity at the supports. If the fixity is below 75% the wall will fail at the mid-span. The conservative assumption is to assume no fixity at the top and bottom; however, if some restraint is known it will help increase the resistance of the wall. The axial load applied will remain along the centerline of the wall all the way through failure. With this resistance function, tensile stresses cannot be resisted and result in cracking of the wall. The wall will fail

when the resultant of the compressive stresses moves outside the line of action of the gravity loads. The compressive stresses developed in the wall cross-section can reach the linear elastic ultimate compressive stress without constituting failure of the wall.

Moradi and Davidson's (2008) general resistance definition is not a closed form solution; it must be solved by incrementally changing the displacement in order to achieve the full resistance function. The overall process involves solving for the pressure and deflection just before cracking. After cracking, the crack length is increased incrementally allowing for the deflection and pressure to then be calculated. Since Moradi and Davidson's resistance function does not consider tensile stresses it will fail well below the Wiehle et al. (1969) curve.

Single-Degree-of-Freedom Blast Effects Design Spreadsheet (SBEDS) Methodology Manual (PDC 2008) does not recommend using non-arching since static test shows little resistance of the masonry past the yield point. It is stated that the moment capacity of the wall is controlled primarily by the tensile bond strength between units. SBEDS Methodology Manual (PDC 2008) recommends using a dynamic mortar tensile bond of 200 psi if no test data is available; however for static resistance this should be reduced.

Because there is no restoring force the resistance of a simply supported CMU wall will rely solely on flexural resistance. After the onset of the crack the masonry resistance drops to an almost negligible value (Johnson 2008). It is noted that without arching supports, there is little resistance to blast loading (Johnson 2008).

2.2.2 Arching Wall Resistance Functions

Arching walls provide a significant increase in resistance due to the addition of compressive force acting on the wall after cracking. If masonry walls are placed inside a rigid frame substantial resistance can be developed. McDowell et al. (1956) states that the resistance of an arching wall can be up to six times the resistance of a plain CMU wall. Again it is assumed that the wall can be represented as two rigid beams rotating about the supports and hinged at the center. Once the wall cracks, coupled forces develop at the supports and the center crack. Theses coupled forces are what psrovides the additional resistance (McDowell 1956), the coupled forces are shown in Figure 2.3.

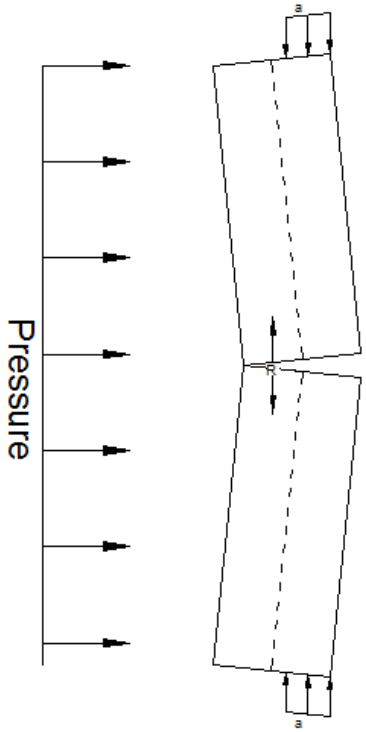

Figure 2.3 Idealized Arching Wall Forces

Where *a* represents the arching force applied by the supports and *R* is the restoring force at the midspan. The forces are developed from the crushing of the masonry wall. Once the coupled forces vanish the wall is destroyed (McDowell 1956).

Several assumptions about the geometry and the material properties are needed. The material properties of the masonry wall play a significant role. The first major assumption is the inability of the masonry to withstand any tensile forces. It is assumed that the wall behaves as a classic elastic-plastic material. The plastic phase represents the crushing of the masonry. Once the masonry is crushed the masonry will not be able to develop any additional stress. Therefore, the masonry does not have any strength recovery (McDowell 1956).

The first development of the resistance function for arching wall is presented in Wiehle et al. (1969). All the previous assumptions made by Wiehle et al. (1969) about non-arching walls are still viable. One major distinction between arching and non-arching walls is that the maximum elastic resistance does not occur at cracking as it does for non-arching walls. For arching walls, the maximum elastic resistance is developed when the supports reach their maximum moment. The decay phase of the arching wall is assumed to behave in the same manner as the non-arching wall. This method was implemented by Jones (1989), Slawson (1995) and Johnson (2008).

As the axial forces and moments at the supports increase, the wall will crush at the wall ends first followed by the crushing at the midspan (Drysdale et al. 1994). A three hinged arch will be formed by crushing at these three locations. The arching force is dictated by the mortar joint not the masonry properties (Drysdale 1994).

Drysdale et al. (1994) address the issue of gap arching. The presence of a gap will reduce the resistance of the wall compared to fully fixed supports and will have larger resistance than a simply supported wall. Gaps between the wall and support are common and have several causes, including poor construction, shrinkage and creep, or intentional. Even though a gap is present, arching forces can still develop. When a lateral load is applied, the wall must rotate about the base until the gap is closed. Once the gap has been closed the wall will begin to resist the load. Figure 2.4 illustrates how a gapped wall moves under lateral loading.

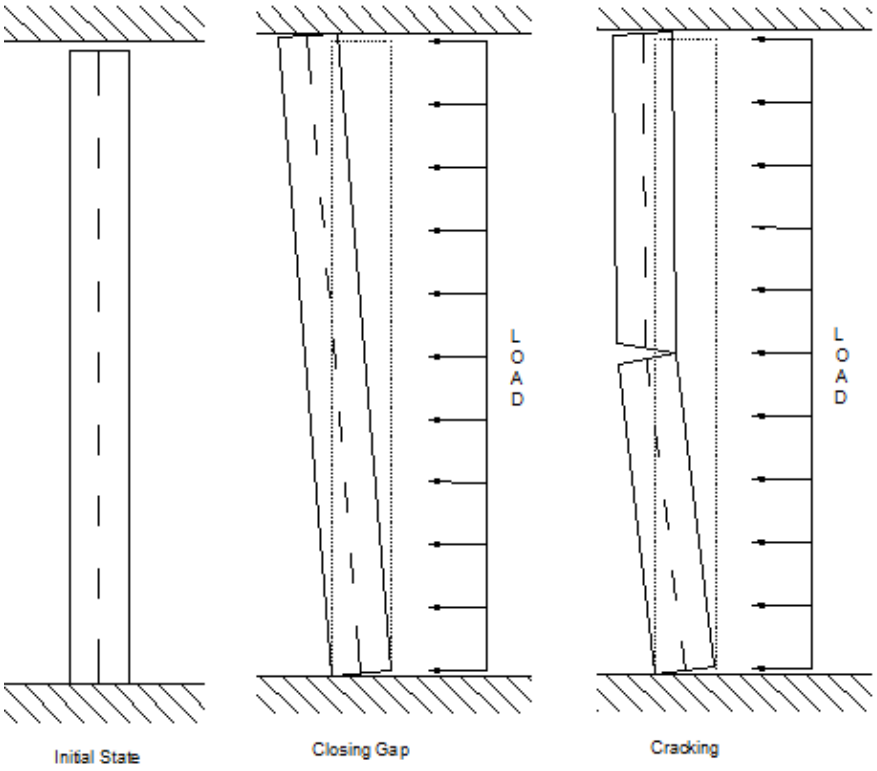

Figure 2.4 Arching Mechanism for Gapped Wall

The gap increases the deflection at cracking since the wall must rotate before cracking can happen. There is a maximum amount of gap allowed to ensure the wall will touch the

support and develop the compressive reaction. The maximum allowable gap is given by Drysdale et al. (1994) and presented in Equation 2.1.

$$g_{max} = \sqrt{h^2 + t^2} - h \tag{2.1}$$

Where g_{max} is the maximum allowable gap, h is the height of the wall and t is the thickness of the wall.

Hoemann et al. (2010) looked at the connection's ability to increase the arching resistance of a gapped wall. If an angle is placed at the top of a wall it will eliminate the need for the wall to rotate about the base before arching resistance can be exerted. The angle will allow the wall to form the hinged condition needed to exert the downward thrust if the roof support can be considered rigid.

Moradi and Davidson (2008) examined the use of mechanical properties of the masonry and the geometric properties to develop a resistance function for arching walls. Using the ideas developed by Paulay and Priestly (1992) and Drysdale et al. (1994), Moradi and Davidson developed a resistance function for non-gapped CMU walls. Assuming the arching force is developed as the wall deflects and increases in intensity as the deflection grows until failure. The arching force is assumed to act only on the face shell thickness or if the face thickness is unknown using the simplified formula below (Drysdale et al. 1994).

$$a = 0.1t \tag{2.2}$$

Where a is the length over which the arching force acts and t is the thickness of the masonry block. The axial load applied to the wall is assumed to act at the top center of

the wall for the duration of the loading. This assumption is for simplicity since the axial load moving to the point of contact once arching exists will complicate the calculations.

SBEDS Methodology Manual (2008) developed the resistance functions based on Park and Gamble (2000). Park and Gamble (2000) developed resistance functions for reinforced concrete slabs based on mechanical and geometric properties as well as experimental data. The formulas developed by SBEDS neglect reinforcement and incorporate voids to simulate ungrouted CMU. SBEDS incorporates not only tensile strength of the mortar but the dynamic mortar tensile bond which should be reduced for use in static resistance curves. Most masonry walls will have a gap of 0.25 in. to 0.5 in. to allow for thermal expansion. This gap is often filled with a flexible material and needs to be examined when developing a resistance function for existing walls (SBEDS Methodology 2008).

2.3 Unbonded Retrofit System

Since URM is very brittle and lacks ductility there is a need to retrofit walls to provide ductility. The retrofit may also catch the fragmented parts of the wall which could be deadly if unrestrained. There are two methods of retrofitting a pre-existing CMU walls: bonded and unbonded. The unbonded method is commonly referred to as a catcher system since it will catch the wall debris. An unbonded retrofit system drawing and installation are shown in Figures 2.5 and 2.6 respectively. The installation picture comes from testing done at the Air Force Research Laboratory (AFRL).

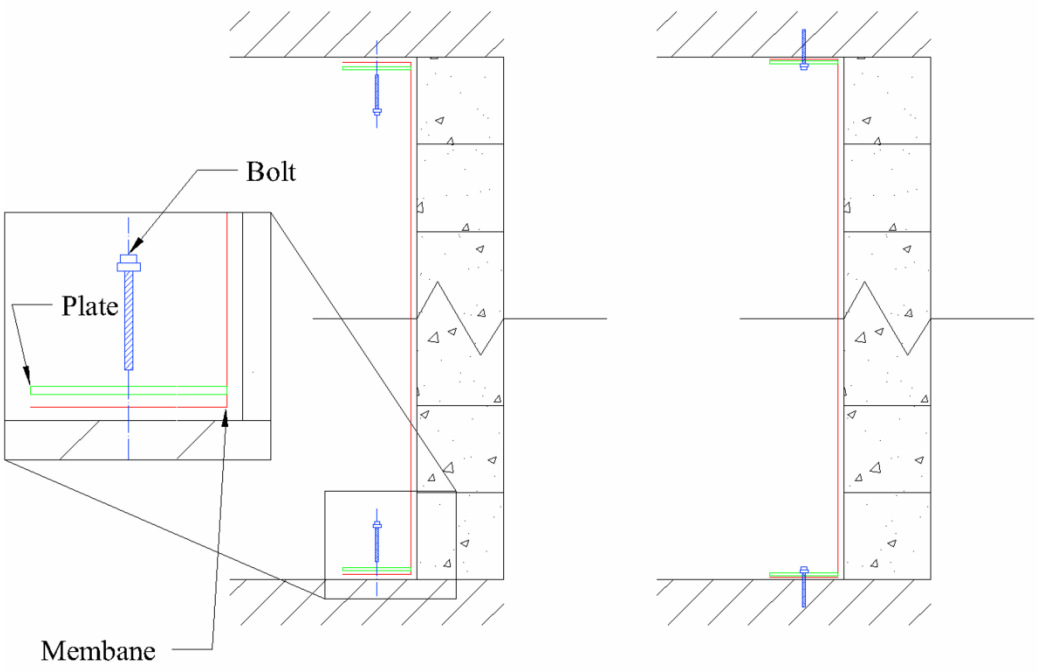

Figure 2.5 Membrane Retrofit System Drawing

Figure 2.6 Installation of Membrane Retrofit System

An unbonded system is commonly attached to the floor and ceiling behind the wall. Many different materials can be used for the retrofit. The materials range from stiff steel to a plastic membrane commonly found at hardware stores.

Three methods for determining the resistance of the membrane have been developed. Young et. al (2012) presents a formula for the resistance of thin elastic flexible membranes. The deflection at mid-span corresponds to a cubic root relationship. The formula was developed assuming the membrane acts as a slender perfectly flexible cable that is loaded transversely and in tension. Figure 2.7 is the free body diagram of the cable (Young et a. 2012).

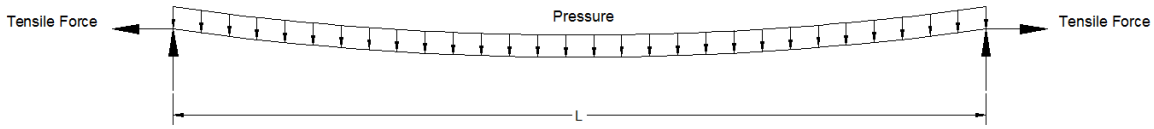

Figure 2.7 Free Body Diagram of Cable Analogy

The use of Young's formula was proposed by Salim et al. (2006). After yielding the use of a formula for plastic deformation proposed by Lane (2003) could be used. This set of equations will provide an approximate elastic-plastic resistance function for the retrofit (Salim 2006). The formula presented by Young (2012) can be used after yielding if the modulus of elasticity is updated at each step.

The second method was developed by Seide (1977). This formula was developed assuming all edges are straight with negligible in-plane shear stress and do not translate once the load is applied. The width to height ratio is assumed to be large, greater than 5. The formula proposed by Seide (1977) was considered for use by Sudame (2004).

One of the more widely used methods for developing the resistance function of the membrane starts with theory developed by Lane (2003). Lane determined that steel studs subjected to lateral pressures deflect in a parabolic shape. Lane (2003) developed a method to solve for the arc length of the stud assuming a parabolic shape. This method was used and re-derived by Fitzmaurice et al. (2006), Salim et al. (2007), Johnson (2008 and 2009) and referenced by Hoemann et al. (2010). This method involves incrementing the deflection and calculating the new arc length of the retrofit. The development and process will be detailed in Chapter 4.

Two Engineering Technical Letters (ETL) provide guidelines for use of geotextile fabrics for use in an unbonded system. ETL 00-09 defines geotextile as "a planer, permeable, polymeric textile material, which may be nonwoven, knitted, or woven" (Department of the Air Force 2000). Both ETL 110-3-494 and ETL 00-09 developed guidance based on a 8-in thick masonry and a 12-ft wall. The selection of these parameters will allow for a design for shorter and thicker walls that will have lower deflections (Protective Design Center 1999). It should be noted that this method only works for walls without windows (Department of the Air Force 2000). Figure 2.8 is a schematic illustrating the suggested design.

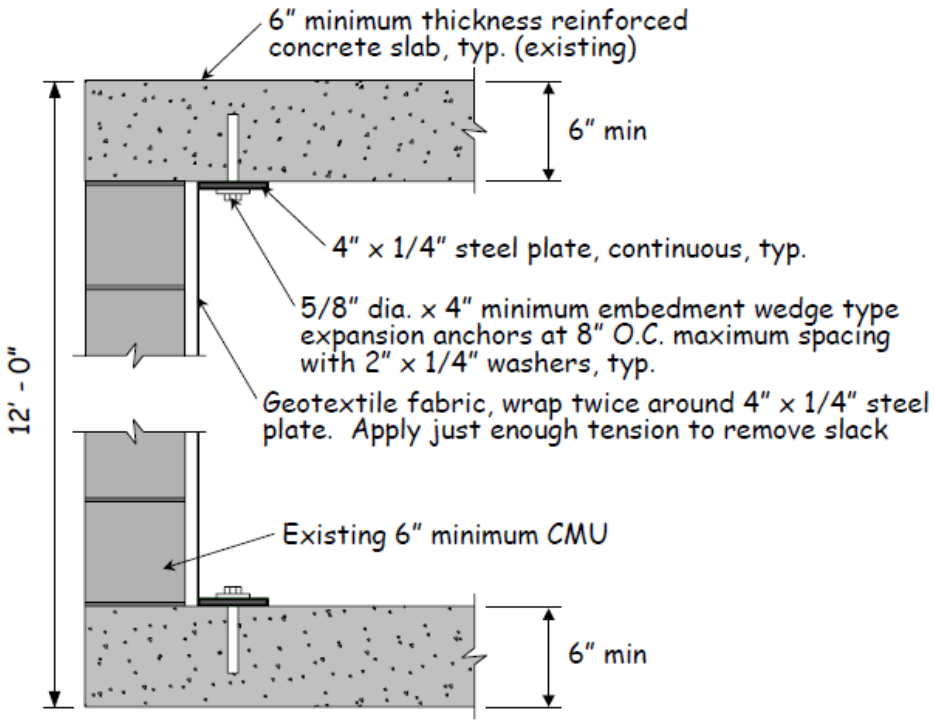

Figure 2.8 Suggested Catcher System Design (Department of the Air Force 2000)

A 4-in anchor is suggested as a minimum for 4000 psi concrete restraints. Longer anchorage will allow for more ductile failure of the connection (Department of the Air Force 2000). The average cost of a geotextile with installation is approximately $80 per linear foot along the width of the wall with labor and material consuming most of the expense (Department of the Air Force 2000).

2.4 Unbonded Retrofit System Connection

Several tests have been performed to demonstrate the importance and need for an analytical expression for the connections role in the overall resistance and ductility of the system. The first of these laboratory tests were performed by Salim et al. (2006). Two different setups were used to determine both the ductility and strength of the connection and how it will react with the membrane's lateral loading. To determine the ductility of

the connections, an axial tensile test was performed on three different thickness membranes bent at 90° at the top and bottom. Two different thickness plates were used to connect the sheets to the loading frame with a 12 and 16 inch bolt spacing. Ten tensile tests were reported. The second setup was a 16 point loading tree that would simulate a lateral load applied to the retrofit system. Only one test was performed to assess the viability of the resistance definition developed.

More in-depth tensile testing was performed by Fitzmaurice et al. (2006). Using the same setup as Salim et al. (2006); however, Fitzmaurice et al. used polymers instead of steel sheeting. Sixteen different tests were conducted to determine which connection scheme would allow for adequate strength without cumbersome construction. Three bolt spacing's were used: 8, 12, and 16 inches. Two different thicknesses of plate were used to clamp the membrane to the loading frame: 0.125 in and 0.25 in. The goal of the plate is to allow the membrane to develop significant stresses without contributing to premature failure. It was noted that most of the test conducted with the 0.125 in. plate, the plate was bent significantly, which allowed for the membrane to tear out at the bolts. For this reason, Fitzmaurice et al. (2006) recommend using a 0.25 in. plate. The polymer allows for significant ductility of the system (Fitzmaurice et al. 2006).

Using energy dissipation as the criteria to determine which bolt spacing would be adequate, it was determined that the 5/8-in bolts spaced at 16 in. allowed for sufficient energy dissipation (Fitzmaurice et al. 2006). 12 in. spacing was considered adequate as well. The plate's preparation before attaching the retrofit can decrease the strength of the membrane significantly. If the edges are allowed to remain square at the surface in contact with the membrane, the edge might cut the membrane preventing it from

achieving its full strength before failure. These sharp edges may reduce the capacity of the retrofit by as much as 50% (Fitzmaurice et al 2005).

Salim et al. (2007) performed a 16 point loading tree test on several different materials with plate configurations in order to determine if the plate edge affects the ultimate strength of the system. Three tests were conducted, two of the tests used toed plates. The toed plates were bent to eliminate a sharp edge from the system. The toed edges allowed for more ductility of the system. However, the toed plate bent more than a flat plate, allowing a bearing failure of the membrane at the bolts and decreasing the ultimate pressure (Salim et al. 2007).

Johnson et al. (2009) conducted two series of test on retrofit systems to determine which connection configuration would allow the membrane to achieve its ultimate strength. Series A used an axial tension approach to determine if sandwiching the membrane between an angle and a plate would eliminate the problem of a sharp edge. Figure 2.9 details the tensile set up used by Johnson et al. (2009).

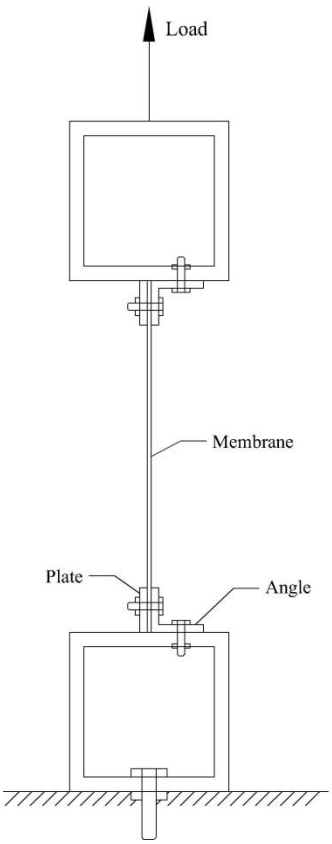

Figure 2.9: Tensile Test using Angles for Connection

This test revealed that the angles and plates did not bend, however they still allowed for bearing stresses around the bolts to form. These bearing stresses resulted in a 59% reduction in theoretical strength predicted by the analytical model. The bolt spacing used by Johnson et al. (2009) were 2 in., 4 in., and 8 in. The bolt spacing that produced the largest resistance reduced of strength by 60% used a 2 in bolt spacing. This configuration is very labor intensive, cumbersome, and ineffective.

Johnson et al. (2009) performed a second series of test using the same 16 point loading tree as Salim et al. (2006). This test was conducted with four different configurations to determine adequate bolt spacing and plate thickness. Using a bolt spacing of 8 in. and 12 in., the test again only achieved 41% of the optimum strength

before the test was terminated. However, instead of the test being truncated because of failure, the loading frame ran out of travel room making additional loading impossible. The average deflection of the four tests was a little over 20 in. All of the tests produced data lower than the analytical model because the ductility of the wall is heavily affected by the connections. With a thick membrane, two forms of failure were exhibited by the system. The first was a bearing failure of the bolts on the plate. The bolts were ripped out of the 0.125 in. thickness plate. The second failure was a bearing failure of the membrane on the bolts experienced by previous research. The membrane was allowed to bear on the bolts after the plate was bent approximately 45° (Johnson et al. 2009).

In an attempt to simplify the design and detailing of anchorage, Hoemann et al. (2010) simplified the anchorage into three cases. Case 1 involves the tension of the membrane being transferred directly into the plate with no moment arm. Without a moment arm the anchorage needed to resist the tension is simply the tensile force. In Case 2, the anchorage is placed in the center of the plate creating a pivot at the end opposite the applied load. The pivot point will amplify the tensile force causing the anchorage to be double the tension force. Case 3 is a transition case that accounts for the plate yielding and a plastic hinge forming in the plate. The force applied will bend the plate decreasing the moment arm until it is negligible. In Case 3 the anchorage force transitions from twice the applied load to the applied load. Figure 2.10 is an illustration of the three cases.

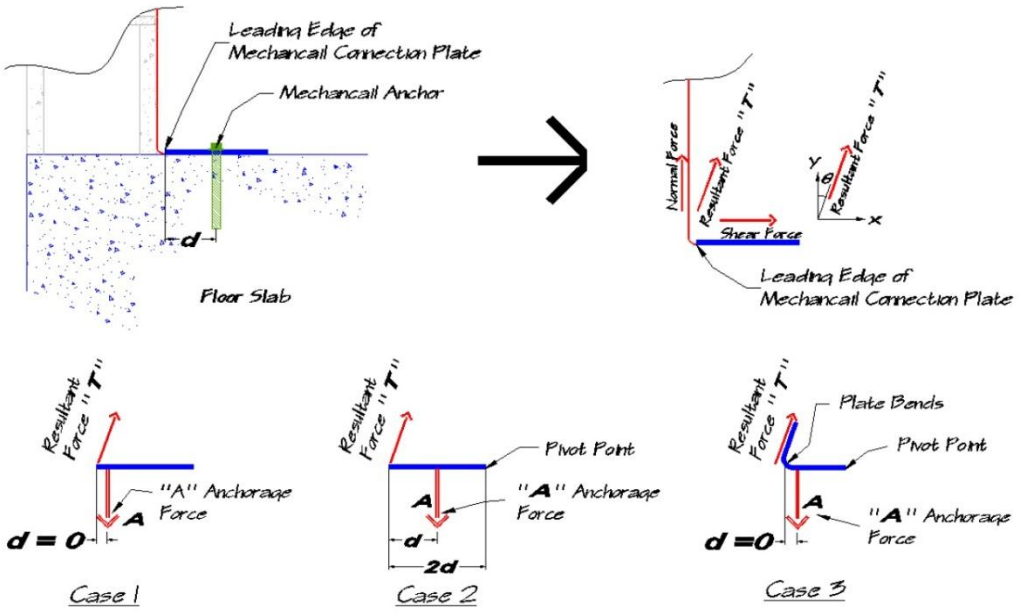

Figure 2.10: Idealized FBD of Mechanical Connections (Hoemann et al. 2010)

Case 2 is ideal for very soft low moduli membrane materials such as PVC membranes due to the inability to significantly bend or yield the connection (Hoemann et al. 2010). For stiffer materials that can bend the plate Case 3 should be considered. The capabilities of most drills will create a moment arm since the bolt will be a distance from the wall. Most drills will not be able to tighten the bolt if it is less than 3 in. from the wall (Hoemann et al. 2010).

2.5 Combination of Systems

A composite resistance curve, including both the wall and retrofit resistance, is needed in order to implement a SDOF model for blast analyses. In order to create a complete model, two methods may be used to determine the total resistance function. The first is a laboratory test of the entire wall system. This method is both expensive and cumbersome to do for every wall. The second is to determine a way of taking individual resistance functions and combining them into one system.

Knox et al. (2000) proposed a theory to combine different components of the wall system. In order to develop this model, Knox et al. (2000) made several assumptions about the system. The first assumption is that all the components will have the same deflection at midspan at every interval. The second is that no shear stresses will be transmitted between components. This assumption implies that all surfaces are frictionless and therefore unbonded. And lastly all static pressures will be applied normal to the surface of the wall. If all assumptions are satisfied the individual resistances can be added to determine the total resistance of the wall. Figure 2.11 is an idealized resistance curve combination if only the URM wall and retrofit are considered.

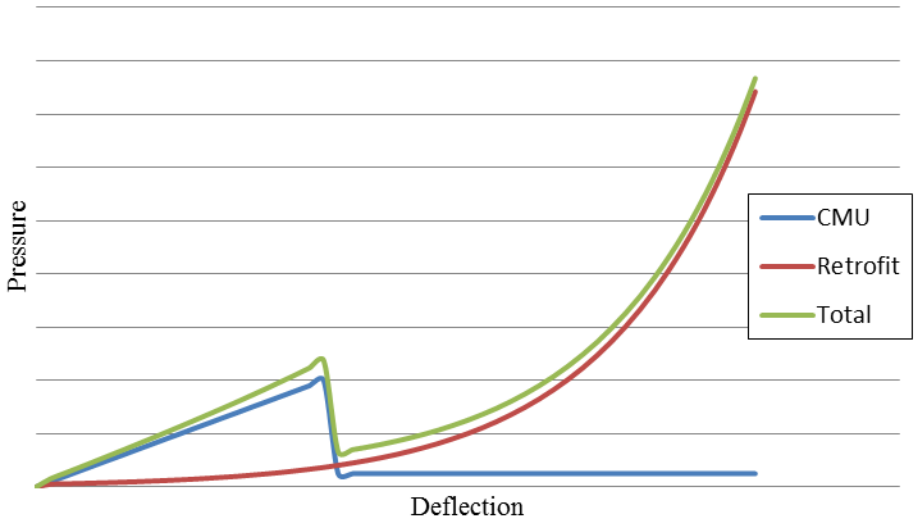

Figure 2.11: Idealized Resistance Curve Combination

The URM wall will have significant resistance at the onset of the load application and then dissipate once the wall has failed. The retrofit requires tension to develop before significant resistance can be observed. Individually these two components may not have adequate resistance to a blast loading whereas their combination may provide the needed resistance.

2.6 Material Selection

The effectiveness of the retrofit is primarily based in the selection of the material used. Many different materials have been tested for use in blast retrofitting. No one material will be ideal for every situation therefore it is necessary to explore different materials. Some materials have been designed for use as blast retrofits and provide adequate resistance. However, many materials used in other industries can be used for retrofitting URM walls. Examples of these materials are PVC membrane liners (Hoemann 2010), geotextiles (ETL 2000), steel membranes (Salim 2006), and polypropylene (Johnson 2009).

The selection of a material is heavily dependent on the material properties, such as modulus of toughness and percent elongation at failure, but construction may also contribute to the selection process. Stiff materials, like steel and chain link fence, will have low deflections with very large ultimate pressures; however they come with large construction cost (Hoemann 2010). The thickness of the material may also play a contributing role in selection. Thicker materials have shown to resist larger pressures however bending a 3-mm membrane of polypropylene requires significantly more effort and time, up to 12 hours more than a thinner membrane (Johnson 2009).

Thornburg (2004) reported ASTM standard uniaxial tension tests on 3 samples of 53 different materials. The three main characteristics observed were: ultimate stress, percent elongation at failure, and modulus of toughness. The ultimate stress is used to determine the ultimate load a membrane can withstand. The percent elongation correlates to the amount of deflection that might be exhibited during loading. Lastly, the modulus of toughness is a representation of the amount of energy that will be absorbed by the system

before failure (Thornburg 2004). The three categories are what designers should consider when selecting a material but materials tend to perform well in two categories and poorly in a third (Thornburg 2004). Materials ranged from stiff to very soft. Stiff materials tend to have low elongations with large ultimate pressures but low modulus of toughness, whereas soft materials have large modulus of toughness and adequate pressures but very large deflections.

The material properties needed for analysis depend significantly on the method used to perform the analysis. SBEDS Methodology (PDC 2008) requires a lot of material data about masonry including the dynamic properties, where Wiehle et al. (1969) requires only basic properties about the masonry. The same is true about the membrane material. The method proposed by Lane (2003) requires a true-stress true-strain curve and the method used by Young et al. (2012) only use area and Young's modulus of elasticity.

2.7 Response Limits

New building design has the ability to estimate what the threat level might be and design the structure to resist the loads to a certain level of protection (LOP). Retrofit systems do not have the ability to always bring a building within a high level of protection if the threat is high. The idea of the retrofit is to bring the structure within an acceptable and feasible LOP. For retrofitting a building the process goes as follows:

1) Define loading
2) Analyze the masonry without retrofit
3) Determine what the provided LOP is
4) Analyze the structure with the retrofit system
5) Determine the change in the LOP

6) Iterate if the LOP with the retrofit is not adequate

The LOP of a building is directly related to the expected damage to the system. The LOPs of building structures from PDC-TR 06-06 "Single-Degree-of-Freedom Structural Response Limits for Antiterrorism Design" are outlined in Table 2.2.

Table 2.2: Structural Damage Associated with Building Levels of Protection (U.S Army Corps of Engineers 2008)

Building Level of Protection	Descriptions of Potential Overall Structural Damage
Below AT standards[1]	Severe Damage - Progressive collapse likely. Space in and around damaged area is unusable.
Very Low	Heavy Damage - Onset of structural collapse. Progressive collapse is unlikely. Space in and around damaged area is unusable.
Low	Unrepairable Damage - Progressive collapse will not occur. Space in and around damaged area is unusable.
Medium	Repairable Damage - Space in and around damaged area can be used and is fully functional after cleanup and repairs.
High	Superficial Damage - No permanent deformations. The facility is immediately operable.

1 - This is not a level of protection, and should never be a design goal. It only defines a realm of more severe structural response, and may provide useful information in some cases.

For masonry structures, the masonry is commonly cracked and failed as a result of loading. Different structural elements are allowed to have different response levels depending on the type of element. This means that for a given building not all the elements must conform to the same criteria. The types of elements are outlined in Table 2.3.

Table 2.3: Component Descriptions (U.S. Army Corps of Engineers 2008)

Component	Description
Primary Structural	Members whose loss would affect a number of other components supported by that member and whose loss could potentially affect the overall structural stability of the building in the area of loss. Examples of primary structural components include: columns, girders, and other primary framing components directly or in-directly supporting other structural or non-structural members, and any load-bearing structural components such as walls.
Secondary Structural	Structural component supported by a primary framing component. Examples of secondary structural components include non-load bearing infill masonry walls, metal panels, and standing seam roofs.
Non-Structural	Components whose loss would have little effect on the overall structural stability of the building in the area of loss. Examples of non-structural components include interior non-load bearing walls, and architectural items attached to building structural components.

For masonry walls, depending on whether or not they are load bearing will fall into either the primary structural or secondary structural category. The damage associated with a structural component is related to the weight and standoff of the explosive and shown in Figure 2.12.

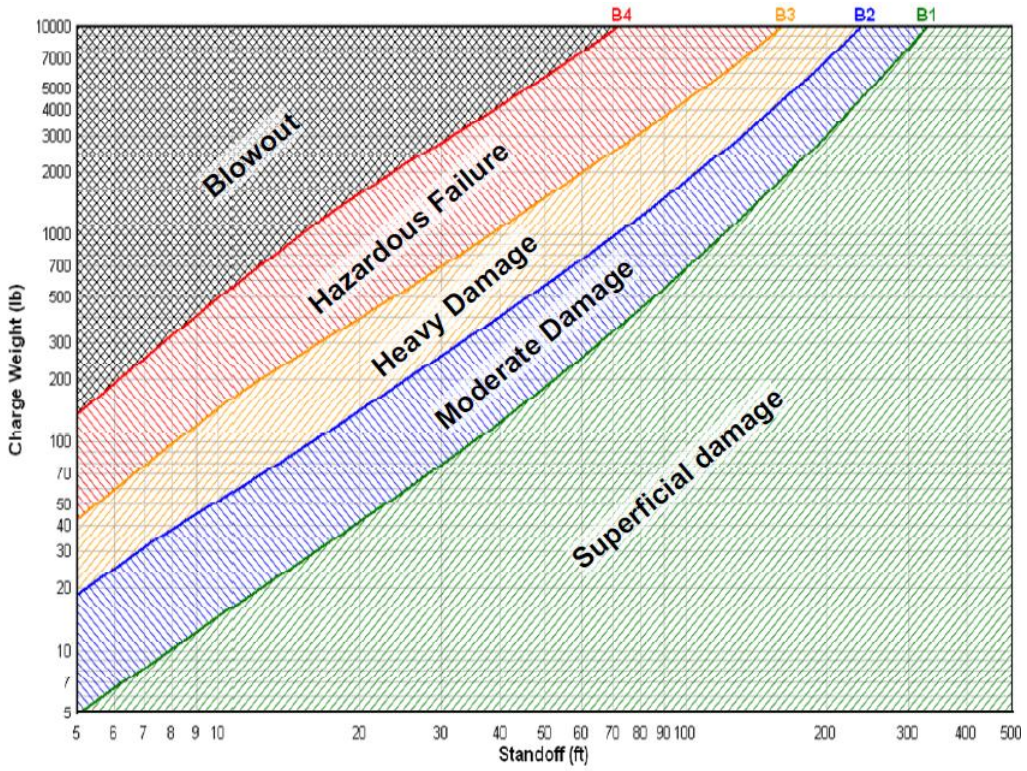

Figure 2.12: Component Damage Levels (PDC-TR 06-08 2008)

The damage to a component is specified as visible effects after loading happens. However, for design purposes response limits were developed to determine if damage would be declared superficial or hazardous. These response limits are described using two criteria. The first is a ductility ratio, μ, which is the ratio between the maximum deflection and the deflection at first yield. The second is the rotation of the wall at the support. Table 2.4 are the response limits for masonry walls from PDC-TR 06-08 modified to only show unreinforced masonry.

Table 2.4: Response Limits for Unreinforced Masonry

Member	B1		B2		B3		B4	
	μ	θ	μ	θ	μ	θ	μ	θ
Flexure	1	-	-	1.5°	-	4.0°	-	8°
Combined Flexure & Compression	1	-	-	1.5°	-	1.5°	-	1.5°

The design of a retrofit should bring the masonry wall within acceptable standards for a specific level of protection. As stated previously, due to the flexural response of unreinforced masonry superficial damage may not be applicable regardless of the amount of retrofit applied. Chapter 8 presents a design example that illustrates how the entire system masonry wall, membrane and membrane connection will work and how design of a retrofit could be done.

Chapter 3: Review of Design Resistance Functions for Unreinforced Masonry

3.1 Overview

The brittle nature of unreinforced non-grouted masonry walls makes a resistance definition difficult to derive and test. The resistance of a masonry wall depends heavily on the support conditions. Two support conditions have been considered. The first is when the supports provide no rotational resistance, which is represented as a simple support. With simple supports the wall resist lateral loads using only its flexural strength and any axial loads such as self-weight. Since unreinforced masonry does not have a large flexural resistance, it is generally considered negligible (PDC 2008).

The second support condition is a fully rigid support. If the wall supports are rigid, the support will resist rotation as the wall attempts to rotate. As the wall attempts to rotate into the support, the support reacts and pushes back at the corner of the wall. Since the support is assumed to be at the longitudinal edge of the wall, it will create a moment arm. The moment arm and force create a restoring moment. This restoring moment increases the resistance of the wall significantly (Drysdale et al. 1994).

3.2 Non-Arching Masonry Resistance Functions

If the wall supports cannot resist the rotation of the wall then the wall is assumed to be simple supported. The wall must be attached to the supports in such a way that no translation is permitted at the supports. If the wall is simply supported it is considered to be a beam with some flexural resistance up to cracking. After the wall cracks at midspan,

the resistance of the wall decreases significantly with very little additional displacement if no axial load is applied.

3.2.1 Wiehle Resistance Function

One of the first methods derived for the development of resistance functions for simply supported masonry walls against lateral loads was presented by Wiehle et al (1969). Wiehle et al. describe the resistance function in two phases. First is an elastic phase where the masonry wall is uncracked and resists the load through its flexural strength. The second phase is a decaying phase. The decaying phase depends heavily on the axial loads applied to the wall as the source of resistance.

To develop a resistance curve, the elastic peak pressure, p_1, and deflection at the maximum elastic pressure, Δ_1, is the first point calculated

$$p_1 = \frac{4t}{3h^2}\left(f_r t + P\right) \tag{3.1}$$

$$\Delta_1 = \frac{5\, p_1 h^4}{384\, E\, I_g} \tag{3.2}$$

Where t is the thickness of the wall, h the height of the wall, and P is the axial load applied through the center of the wall. f_r corresponds to either the modulus of rupture or the tensile bond strength depending on the design assumptions. Johnson (2009) used bond strength of 65 psi. This value is widely variable: 30 psi to 250 psi (Drysdale et al. 1994). The elastic resistance of the wall in Equation 3.1 uses a moment of inertia for a solid rectangular block, which does not incorporate the hollow sections of the CMU.

Once the elastic portion of the curve is known, the decay portion is determined using the formula for p_2 and incrementing the deflection.

$$p_2 = \frac{4}{h^2}(t - \Delta_2)(2P + W_i) \qquad 3.3$$

Depending on the axial load applied to the wall, three different decay phases are possible, Figure 3.1. The axial load can increase the resistance above the elastic phase. The axial load may allow the decay phase to start where the elastic portion ends or if the load is low enough the decay phase will start below the elastic portion.

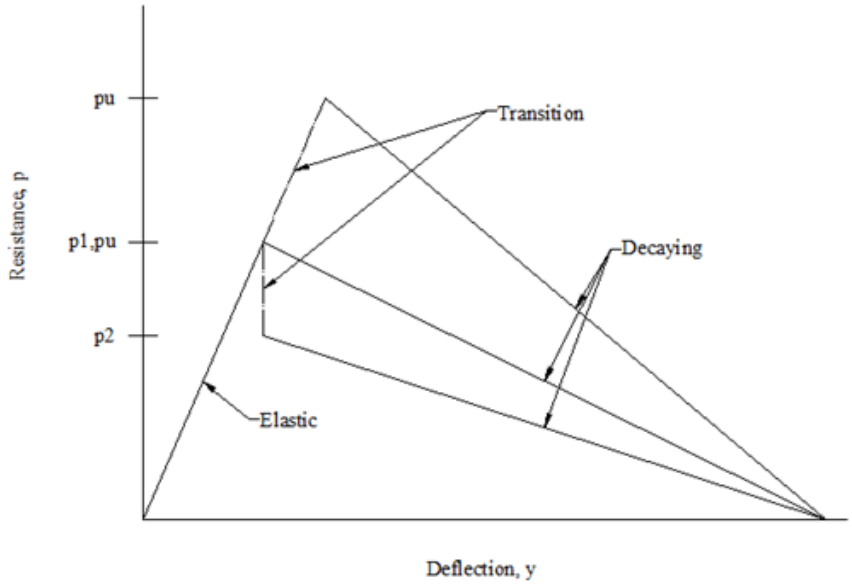

Figure 3.1: Decaying Phases Assumed by Wiehle et al. (1969)

There is an assumed linear relationship from the origin to the elastic limit. If the decay phase is below the elastic limit a vertical drop is assumed. When the ultimate pressure is above the elastic limit the transition has the same slope as the elastic portion until it reaches the decay phase.

3.2.2 Moradi Method

Moradi and Davidson (2008) developed a resistance function that would allow for different degrees of fixity of the supports. Using theories developed by Paulay and Priestly (1992) and those presented in Drysdale et al. (1994), Moradi and Davidson (2008) developed a resistance function. The major distinction of the Moradi method is that the tensile strength of the mortar is neglected, which reduces the resistance of the URM wall and allows for a very conservative design. Figure 3.2 is a free body diagram of the wall used by Moradi (2008).

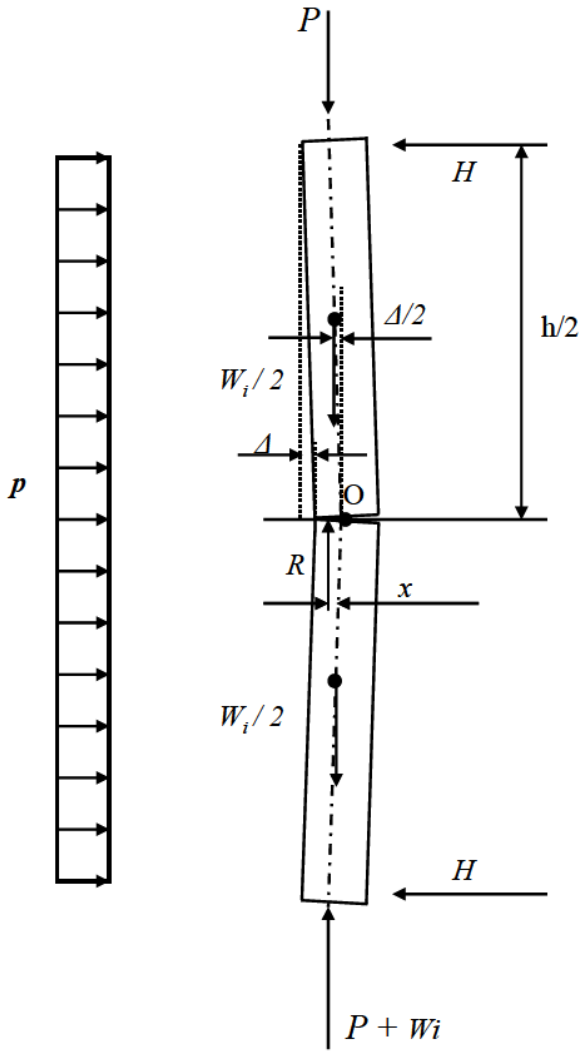

Figure 3.2: Free Body Diagram of Non-Arching Wall (Moradi et al. 2010)

To start, the pressure at the elastic limit is determined. The elastic pressure is calculated by setting Equations 3.4 and 3.5 equal to one another.

$$\Delta = \frac{t}{6} + \frac{y}{3} - \frac{(3-2\alpha)\,ph^2}{12W_i + 24P} \qquad 3.4$$

$$\Delta_{\max elastic} = \frac{(5-4\alpha)\,ph^4}{384E_c I_g} \qquad 3.5$$

Where E_c is the concrete masonry modulus of elasticity and I_g is the gross (uncracked) moment of inertia, α is the support fixity, with 0 being a pinned condition and 1 being a fully fixed condition, and y is the crack length of the URM wall. For the elastic phase there is no crack in the wall, therefore y=0. Once the pressure at cracking is known, the maximum elastic deflection can be calculated using Equation 3.5.

For the decay phase of the resistance function, the crack length is increased incrementally. Moradi and Davidson (2008) assumed that the displacement at midspan is proportional to the curvature of the wall. The deflection after cracking is calculated as follows:

$$\Delta_{crG} = \beta \Delta_{cr} \tag{3.6}$$

$$\text{Where: } \beta = \frac{R_{crG} t^2}{R_{cr}(t-y)^2} \tag{3.7}$$

Where *cr* denotes cracking and *crG* denotes crack growth. Since R does not change as the crack grows, R_{cr} and R_{crG} cancel each other out leaving:

$$\beta = \frac{t^2}{(t-y)^2} \tag{3.8}$$

Using the deflection after cracking and plugging it into Equation 3.4, the pressure can be determined. This process is continued until failure. The process for developing the resistance function is outlined in Figure 3.3.

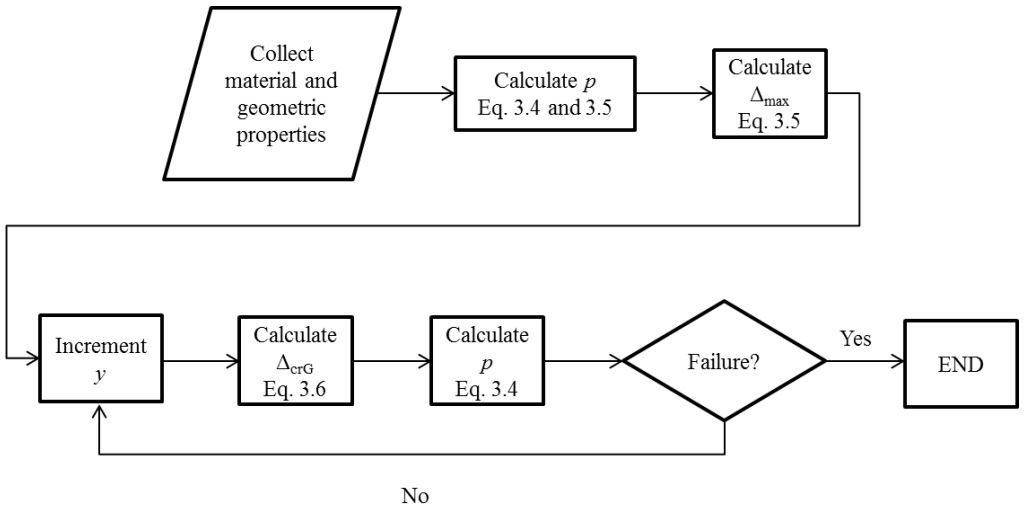

Figure 3.3: Moradi Method for a Non-Arching Resistance Curve Flow Chart

3.2.3 SBEDS Methodology

SBEDS User Manual (PDC 2008) considers two forms of URM wall response. The first is an elastic-plastic flexural response. This response is not recommended since static testing shows that masonry walls do not exhibit a plastic response (PDC 2008). SBEDS User Manual (PDC 2008) explains that the only reason it is included is due to the limited plastic response that has been used in the past. The second response type considered and is recommended is brittle flexural response with axial load.

From the bending stress formula the maximum moment capacity can be calculated.

$$\sigma_t + \frac{P}{A} = \frac{Mc}{I} \tag{3.9}$$

$$\text{Where } A = t \times SFR \tag{3.10}$$

Where σ_t is the ultimate tensile stress of the masonry and *SFR* is the solid fractional ratio of the masonry. If the exact cross sectional area is known, that should be used. Once the

maximum moment is known, beam mechanics are used to determine the lateral load that causes that moment as well as the deflection due to elastic bending.

$$r_1 = \frac{8M}{h^2} \text{ where: } M = S\left(f_t + \frac{P}{t} \right) \tag{3.11}$$

$$\Delta_{\text{max elastic}} = \frac{5 r_1 h^4}{384 E_c I_g} \tag{3.12}$$

Where r_1 is the resistance due to flexure and S is the elastic section modulus. A second point is calculated to determine if the axial load will increase or decrease the resistance of the wall and to what extent. The SBEDS User Manual (PDC 2008) suggests using 10% of the compressive strength or 200 psi, whichever is greater. First the resistance after cracking is calculated.

$$r_2 = \frac{8}{h^2}(t - \Delta_{max})\left(P + \frac{W_i h}{2} \right) \tag{3.13}$$

Where Δ_{max} refers to the maximum elastic deflection found in Equation 3.12. The deflection corresponding to r_2, Δ_2, is then calculated assuming a linear relationship. If the resistance after the elastic region is greater than the elastic resistance then the sign of the elastic stiffness, K_e, is positive; otherwise the sign is negative, Figure 3.4.

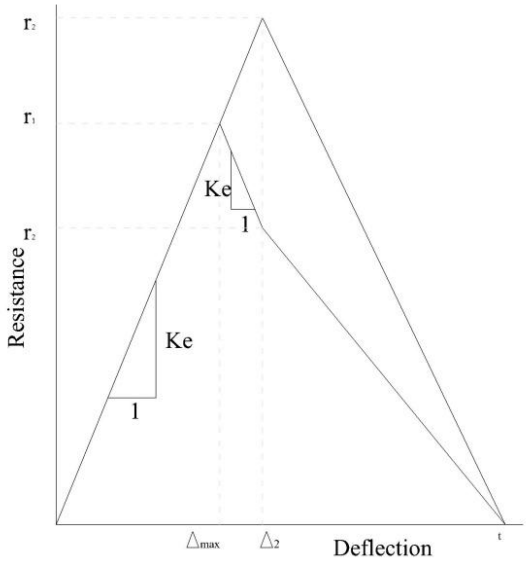

Figure 3.4: Idealized Resistance-Deflection Curve for SBEDS

$$\Delta_2 = \Delta_{max} + \frac{r_2 - r_1}{K_e} \tag{3.14}$$

$$K_e = \frac{r_1}{\Delta_{max}} \tag{3.15}$$

From this point the resistance curve is assumed linear until the wall has no resistance. The deflection corresponding to failure is assumed to be the thickness of the wall (PDC 2008). This method was presented by Oswald and Zehrt (2010) for the update to UFC 3-340-02.

3.2.4 Unified Facilities Criteria (UFC) 3-340-02 Methodology

TM 5-1300 is superseded by UFC 3-340-02 so it was not considered. UFC (2008) does not derive or present any formulas for a resistance curve for a simply supported wall. If a wall is simply supported the modulus of rupture will determine the maximum resistance of the wall (UFC 2008). Additional axial loads may be considered if they exist. An example presented by UFC (2008) for a simply supported wall is shown in Figure 3.5.

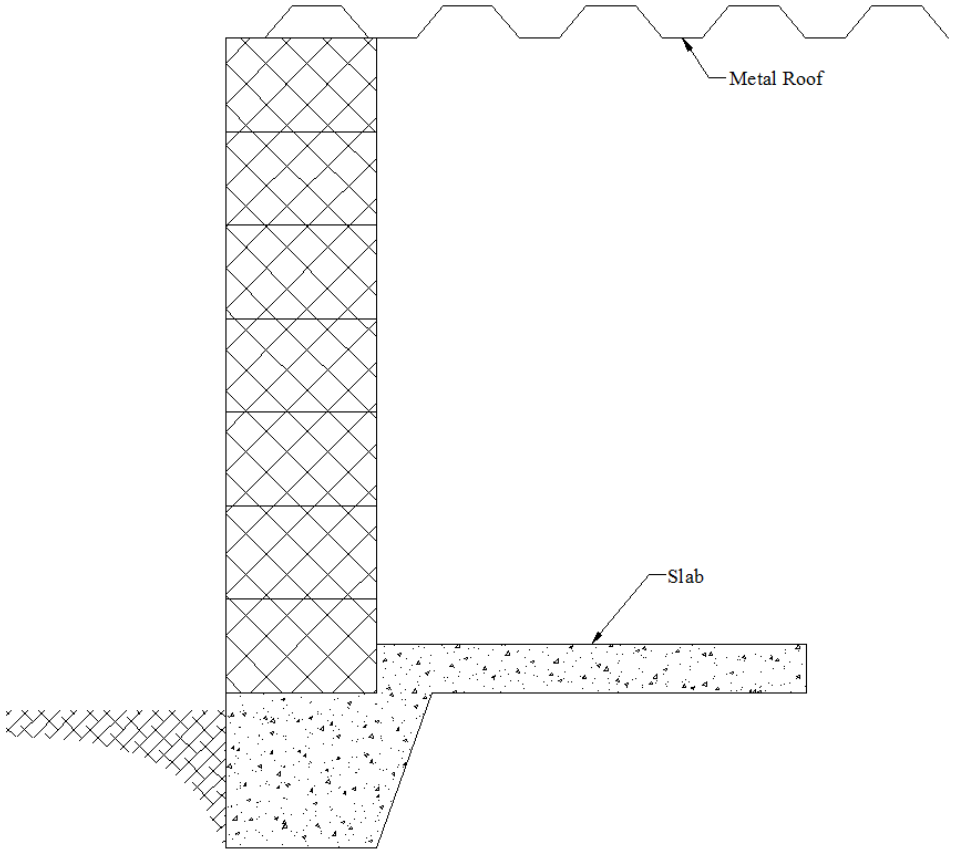

Figure 3.5: UFC Simply Supported Wall

The wall will have supports that resist lateral movements but cannot resist rotation. An update to the masonry chapter of UFC 3-340-02 was released by Oswald and Zerht (2010) and for non-arching walls the method presented is the same as the SBEDS method.

3.2.5 Comparison of Non-Arching Resistance Functions

A resistance function should be able to accurately predict the pressures required to deflect any size wall. Three different criteria are compared using each of the three methods. The three criteria examined are the wall thickness, brick type, and axial load. The baseline case will be an 8-in CMU brick wall with a height of 12 ft with no axial load. When exploring how these models change with varying wall properties, only one of the properties of the baseline case will be changed.

First how the models compare to one another is important to understand. Figure 3.6 shows how the models compare to one another. All the models have similar shape and all follow the same linear elastic path. The main differences are the peak pressure and how much the wall decays after cracking. The modulus of rupture proposed by Johnson (2008) was used for the Wiehle Method. SBEDS has a minimum of 200 psi for mortar tensile bond and this number was used for the SBEDS method.

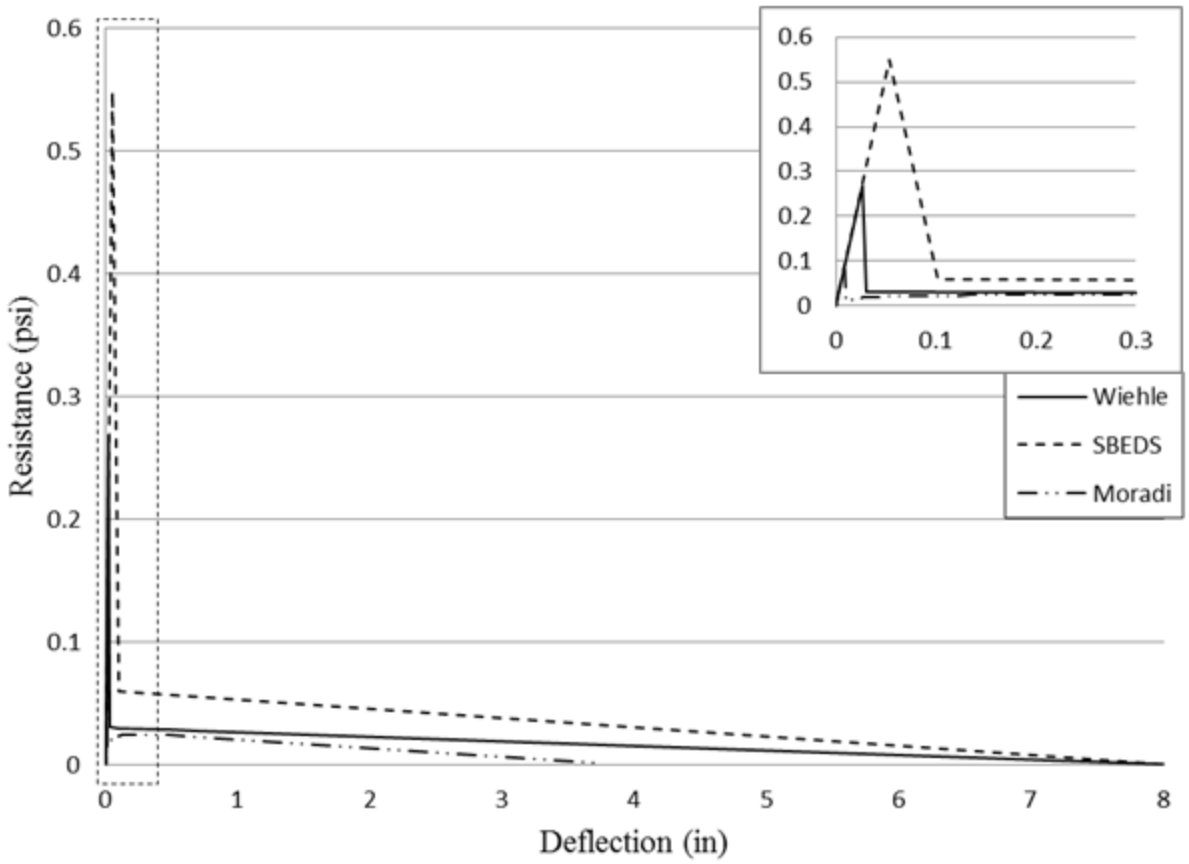

Figure 3.6: Comparison of Non-Arching Methods

SBEDS gives the largest prediction for the peak pressure followed by the Wiehle method. The Moradi method produces a resistance curve much lower than the other two. This is due to the assumption that the wall cannot resist any tensile stresses. This assumption allows for the lowest peak resistance. The Moradi method determines a peak pressure of 0.095 psi while the SBEDS and Wiehle methods predict 0.55 psi and 0.27 psi, respectively. The second important consideration is that for the Moradi method the wall deflection is less than half that of the other two models at failure.

To investigate how the thickness of the block changes the resistance function, three CMU block sizes were used, 6-in, 8-in, and 12-in. All of the properties were taken from SBEDS methodology (PDC 2008) and shown in Table 3.1.

Table 3.1: Masonry Properties of Three CMU Blocks

Brick	Density (pcf)	Weight (psf)	Face Shell Thickness (in)	Solid Thickness (%)	Moment of inertia (in^4/in)	Section Modulus (in^3/in)
6-in	120	33.0	1.25	55	12.8	4.5
8-in		39.2	1.25	49	28.4	7.4
12-in		48.0	1.25	40	82.4	14.2

The other properties such as modulus of rupture was taken from Johnson (2009) (65 psi), mortar tensile bond from SBEDS (PDC 2008) (200 psi), and support fixity from Moradi (2007) (0%) all remain the same.

How the thickness of the wall affects the models is examined by looking at how each model changes with respect to varying thicknesses rather than comparing every curve. The first method examined is the Wiehle method presented in Figure 3.7.

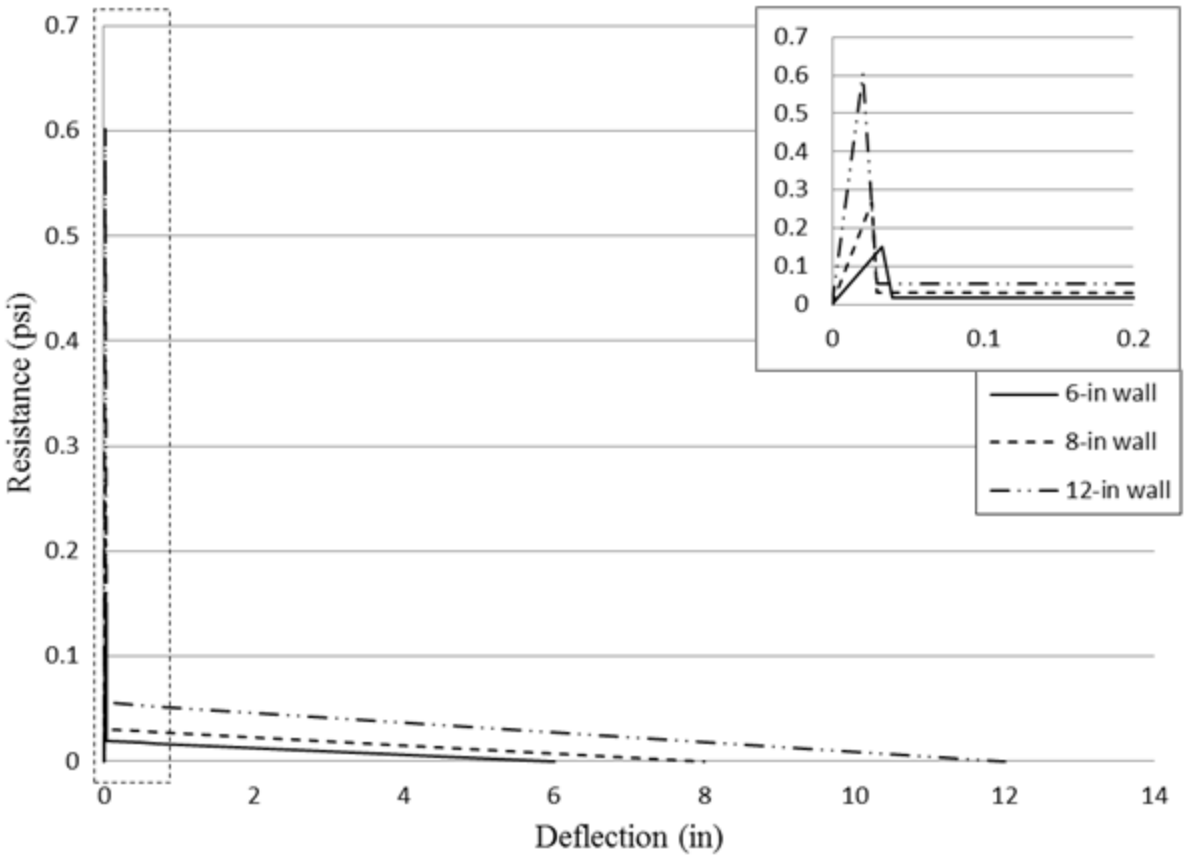

Figure 3.7: Wiehle Non-Arching Variable Wall Thickness

When the thickness of the wall is increased by 30% the resistance for the wall increases by a factor of approximately 1.75 and when the wall thickness is doubled the resistance is increased by a factor of four. Because of the way the formula is set up the thickness of the wall has a squared effect on the resistance of the wall. The deflection of the wall at the maximum pressure does not change significantly; however, it is important to note that the thinner walls have a larger midspan deflection at the ultimate pressure.

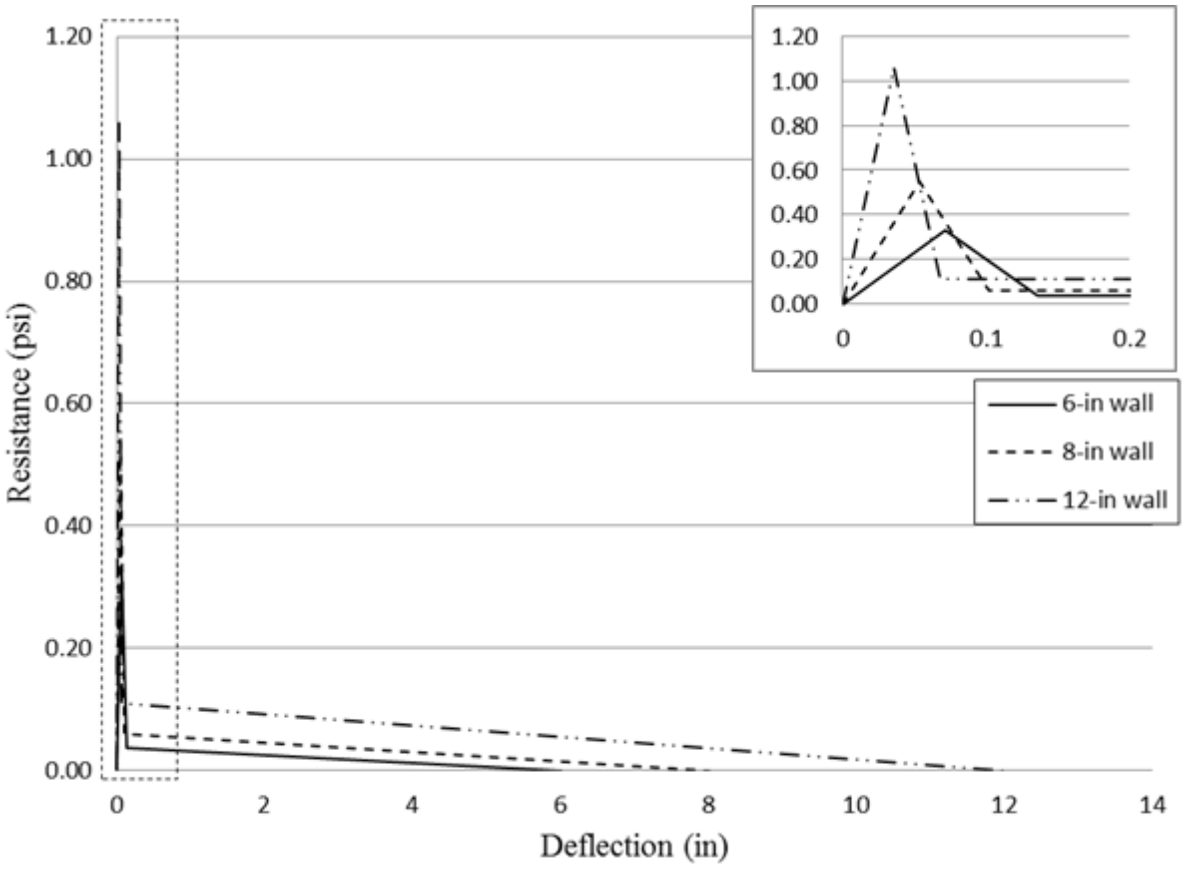

Figure 3.8: SBEDS Non-Arching Variable Wall Thickness

Figure 3.8 shows how the SBEDS method varies with block thickness. Once again the larger bricks produce a larger resistance. This method produces much larger deflection compared to the Wiehle method. The 6-in wall produced a pressure of 0.33 psi, the 8-in wall produced a pressure of 0.55 psi, and the 12-in wall generated a pressure of 1.1 psi at the peak pressure.

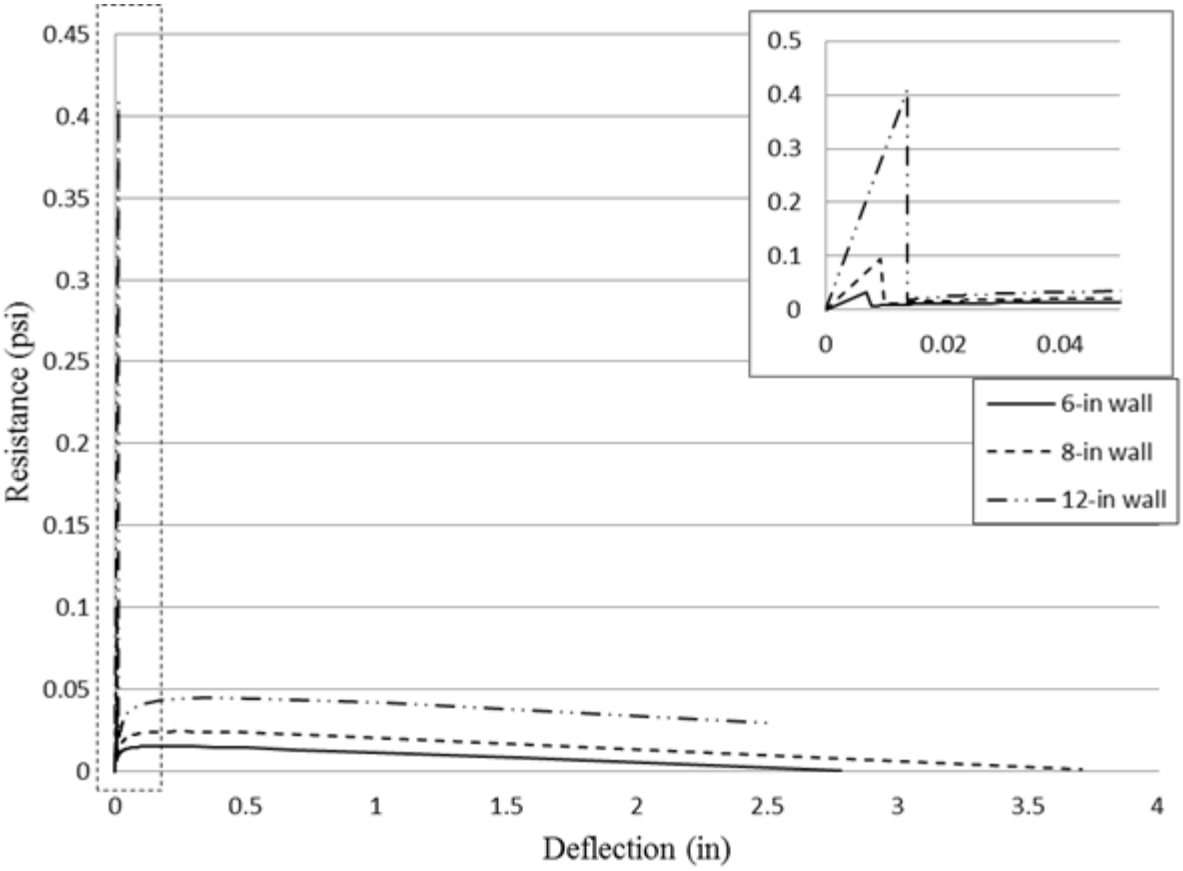

Figure 3.9: Moradi Non-Arching Variable Wall Thickness

The effect of block thickness on the Moradi method is shown in Figure 3.9. The Moradi method again produces larger pressures for thicker walls. For the 6-in wall, the peak pressure is 0.032 psi, the 8-in wall pressure is 0.094 psi, and the 12-in wall peak pressure is 0.41 psi. As the thickness of the wall increases the deflection at the peak pressure also increases, which is contrary to the other two methods.

The second characteristic to examine is the type of brick used. Three styles of bricks are used to examine how the models react to varying brick materials. The three type of bricks selected are: an adobe brick, CMU, and an European block. All bricks will have a thickness of 8 inches the other parameters are shown in Table 3.2.

Table 3.2: Material Properties of Varying Blocks

Brick	Density (pcf)	Weight (psf)	Compresive strength (psi)	Tensile Strength (psi)	Solid Thickness (%)	Moment of inertia (in^4/in)	Section Modulus (in^3/in)	Young's Modulus (psi)
Adobe	115	76.7	435.1	156	100	42.7	10.7	435100
CMU	120	39.2	1350	200	49	28.4	7.4	2000000
European	90	30.0	1350	200	50	12.8	3.2	2000000

The tensile strength of the adobe is calculated using the equation presented by ACI 318.

$$f_t = 7.5\sqrt{f_c'} \tag{3.16}$$

The modulus of rupture for adobe is 50 psi (IBC 2006). Since the Wiehle method use the modulus of rupture as the primary means to determine the peak pressure, the resistance can change significantly depending on the testing of the adobe. The effect that block type has on the Wiehle method is shown in Figure 3.10.

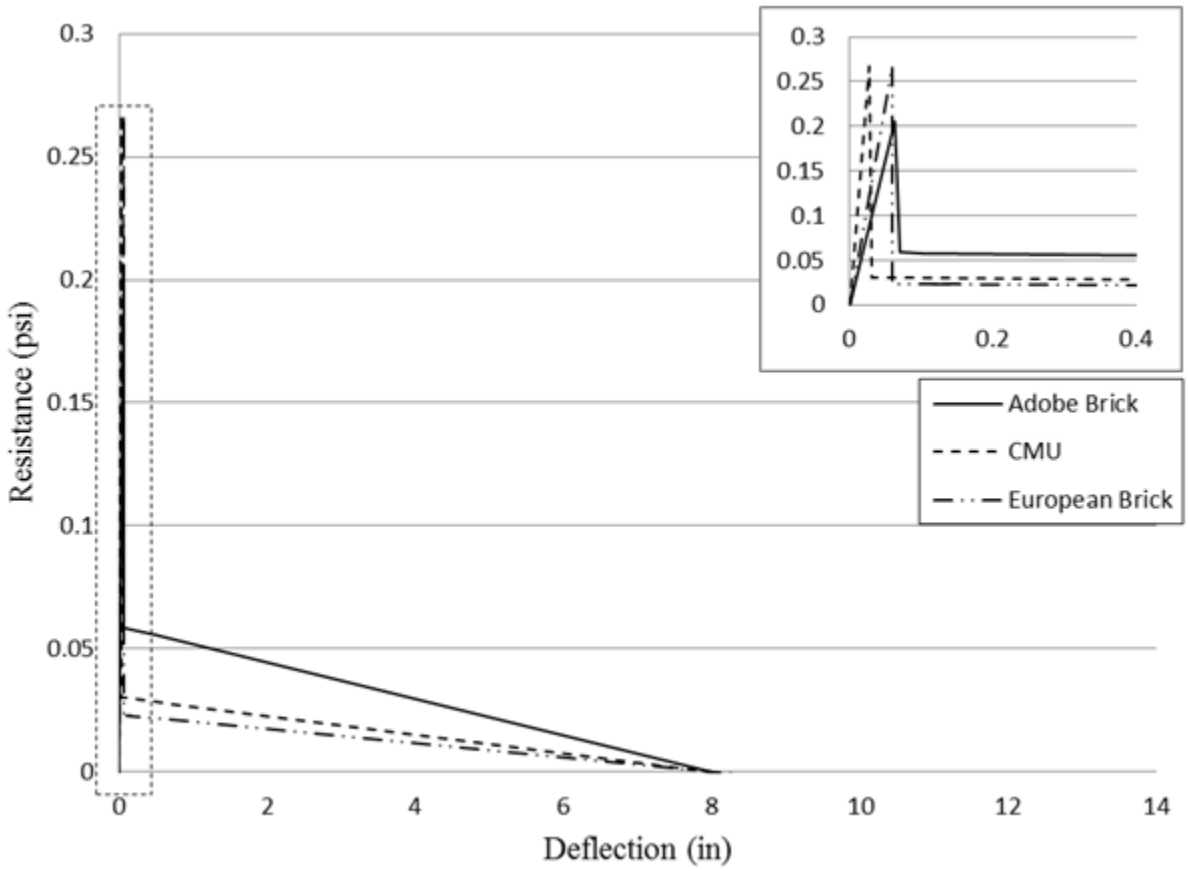

Figure 3.10: Wiehle Non-Arching Variable Brick Type

The Wiehle method uses the modulus of rupture as the main criteria to determine when the wall cracks and loses its flexural rigidity. Since the modulus of rupture for concrete is the same for the CMU blocks and the European blocks the peak pressures are the same. Table 3.3 summarizes the resistance and deflections at the peak resistance.

Table 3.3: Wiehle Method Summary of Deflections at Peak Resitance for Non-Arching Masonry with Varying Brick Types

	Deflection (in)	Pressure (psi)
CMU	0.026	0.267
Adobe Brick	0.062	0.206
European Brick	0.059	0.267

Since the moment of inertia is lower for the European brick the deflection at the peak resistance is greater. The difference between modulus of rupture of concrete and adobe is only 10 psi. This causes the peak resistance to be very close. The effect of brick type on the SBEDS method is shown in Figure 3.11.

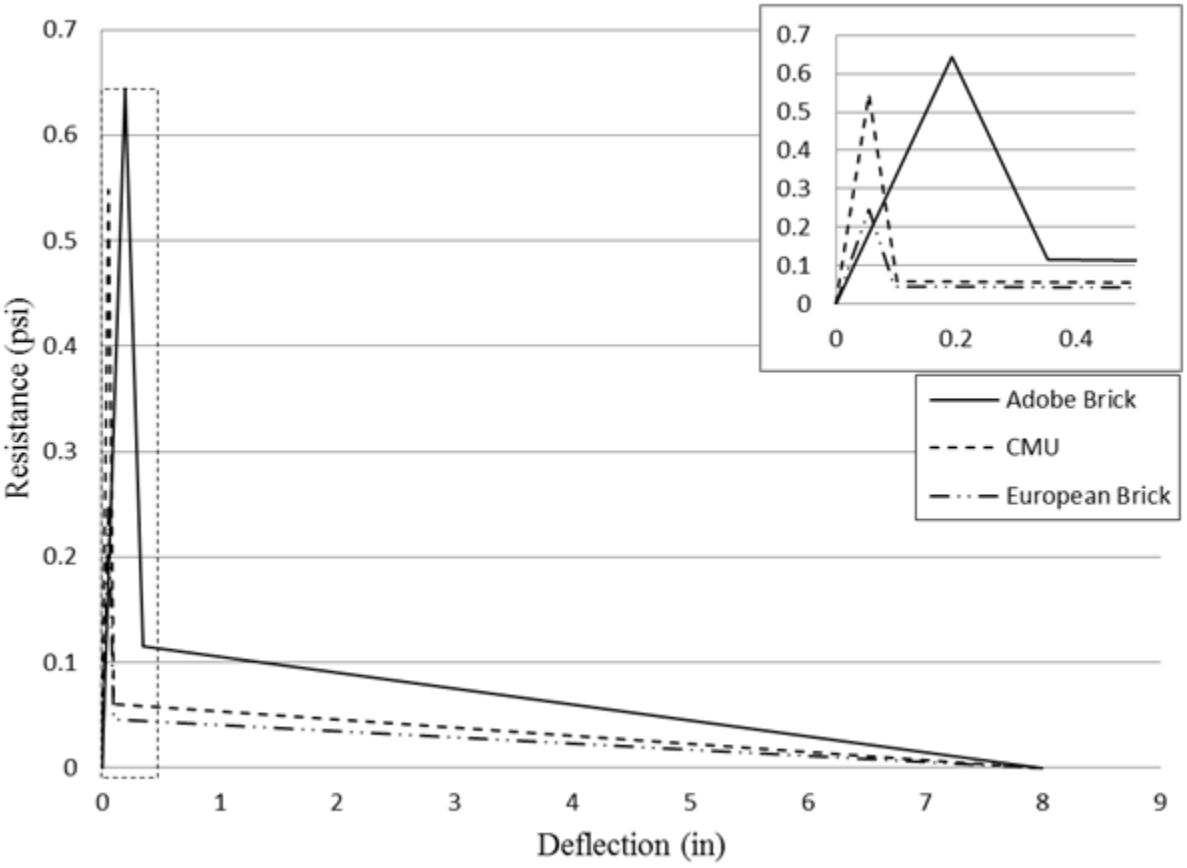

Figure 3.11: SBEDS Non-Arching Variable Brick Type

The SBEDS method does not follow the same pattern as the Wiehle method. The adobe again produces a large deflection at peak resistance while the European brick has the lowest resistance at the same deflection as the CMU brick. Table 3.4 summarizes the deflections at the peak resistance.

Table 3.4: SBEDS Method Summary of Deflections at Peak Resistance for Non-Arching Masonry with Varying Brick Types

	Deflection (in)	Pressure (psi)
CMU	0.054	0.548
Adobe Brick	0.194	0.644
European Brick	0.054	0.247

The moment of inertia of the bricks is important in determining the maximum pressure; however, it appears that the moment of inertia does not have a significant effect on deflection. The moment of inertia of the CMU block is twice that of the European block yet they have the same deflection at peak resistance. For this reason, the deflection of the European block and the CMU are the same. The effect of brick type on the Moradi method is shown in Figure 3.12.

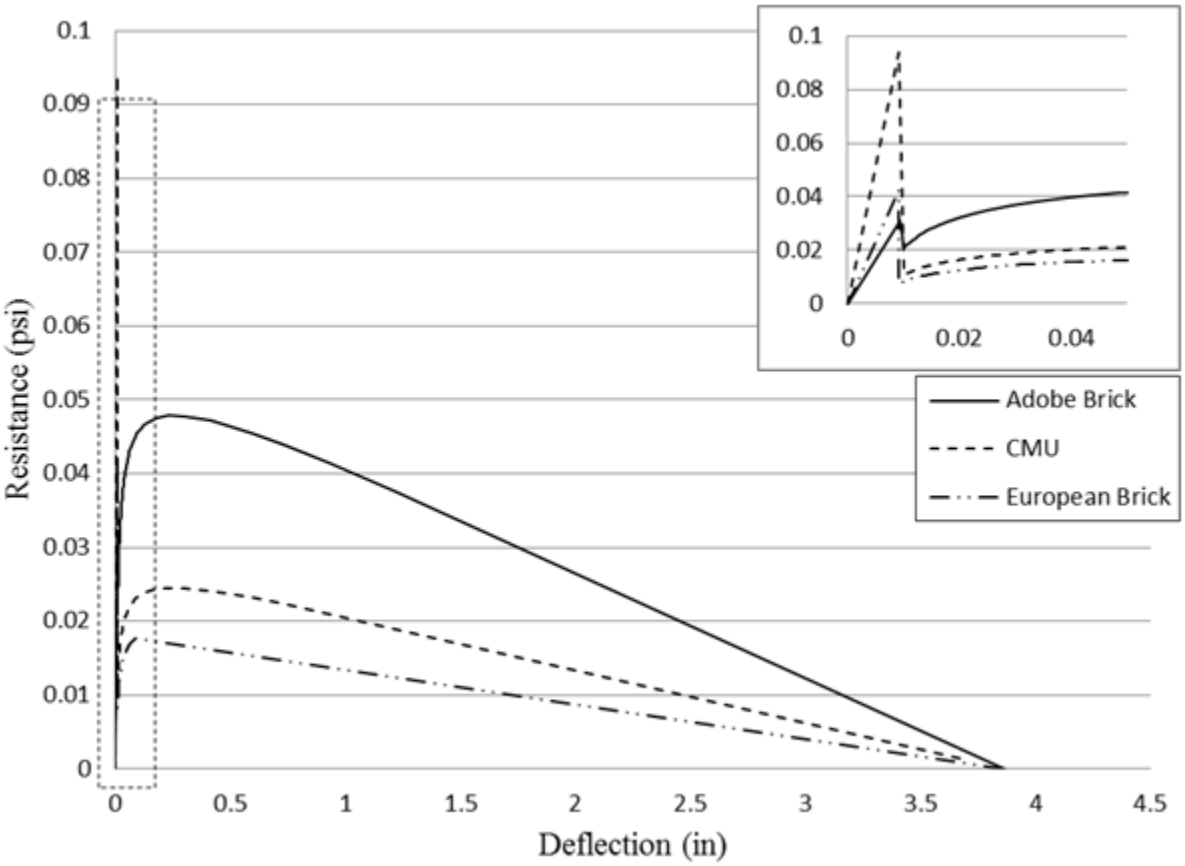

Figure 3.12: Moradi Non-Arching Variable Brick Type

The modulus of elasticity of the adobe is much less than that of the concrete blocks and the Moradi method uses this characteristic to determine the peak resistance. For this reason the peak resistance of the adobe is less than that of the other two blocks. In this graph it is easy to see how the cracking of the masonry affects the Moradi method. At the onset of the crack, there is not a significant amount of stresses developed to resist the lateral pressures. The crack must propagate to approximately 83% of the thickness until the second peak resistance is observed. The second peak is caused by the self-weight of the wall moving and helping to restore the system.

The last important factor that defines the shape of the resistance curve for non-arching masonry walls is the axial load. An axial load may be present if the roof or upper floor is supported by the wall. If the presence of an axial load is unknown or the designer is unsure as to what amount should be assumed, then the axial load is taken as zero when determining the resistance curve. The axial load acts as a restoring force and increases the lateral load resistance. Three axial loads will be examined to determine how they affect the resistance curves: 0 lb/in, 220 lb/in, and 500 lb/in. How axial load effects the Wiehle method is shown in Figure 3.13.

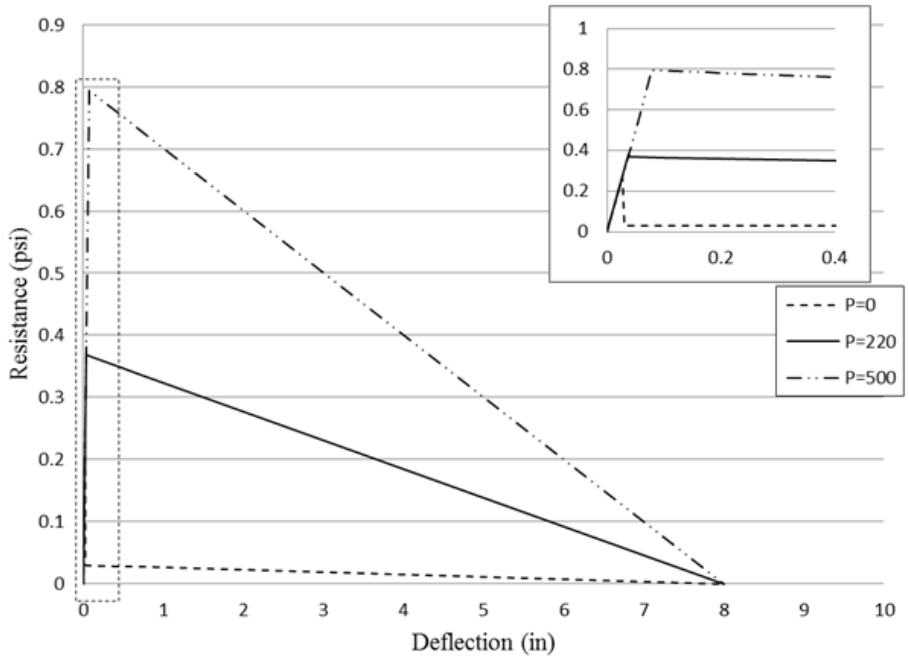

Figure 3.13: Wiehle Non-Arching Variable Axial Loads

The large axial load generates the largest resistance after the flexural resistance of the wall vanishes allowing the larger axial load to produce a larger peak resistance and deflection. The two walls with axial loads do not have a drop in resistance after the flexural resistance is gone. This is because the middle axial load was selected specifically

so the decay function would start approximately at the same point where the elastic function ended. How axial load effects the SBEDS method is shown in Figure 3.14.

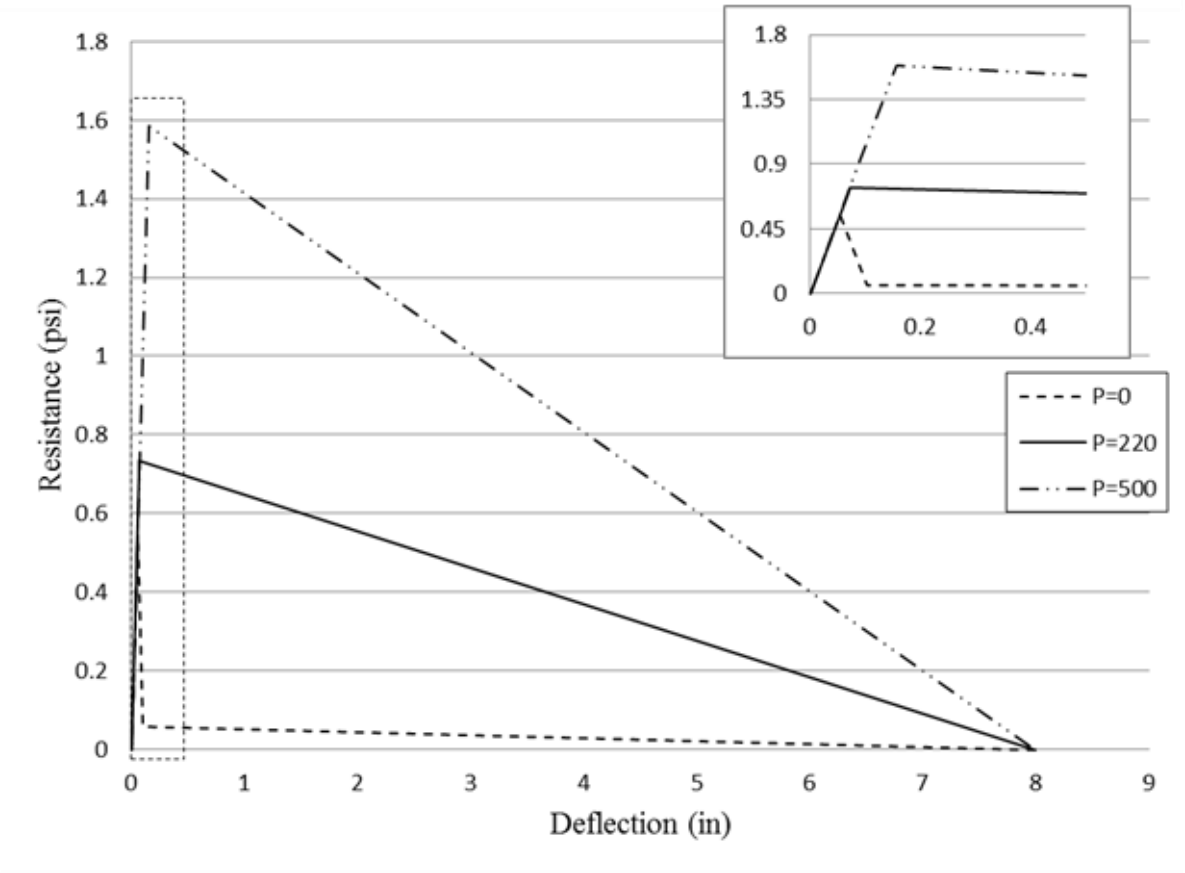

Figure 3.14: SBEDS Non-Arching Variable Axial Loads

The SBEDS method produces resistance curves that are similar to the Wiehle method. There is a similar pattern where the larger axial load generates the largest peak pressure followed by the middle axial load. One notable distinction between SBEDS and the Wiehle method is that the SBEDS pressures and deflection are about double that of the Wiehle method. Axial load effects on the Moradi method are shown in Figure 3.15.

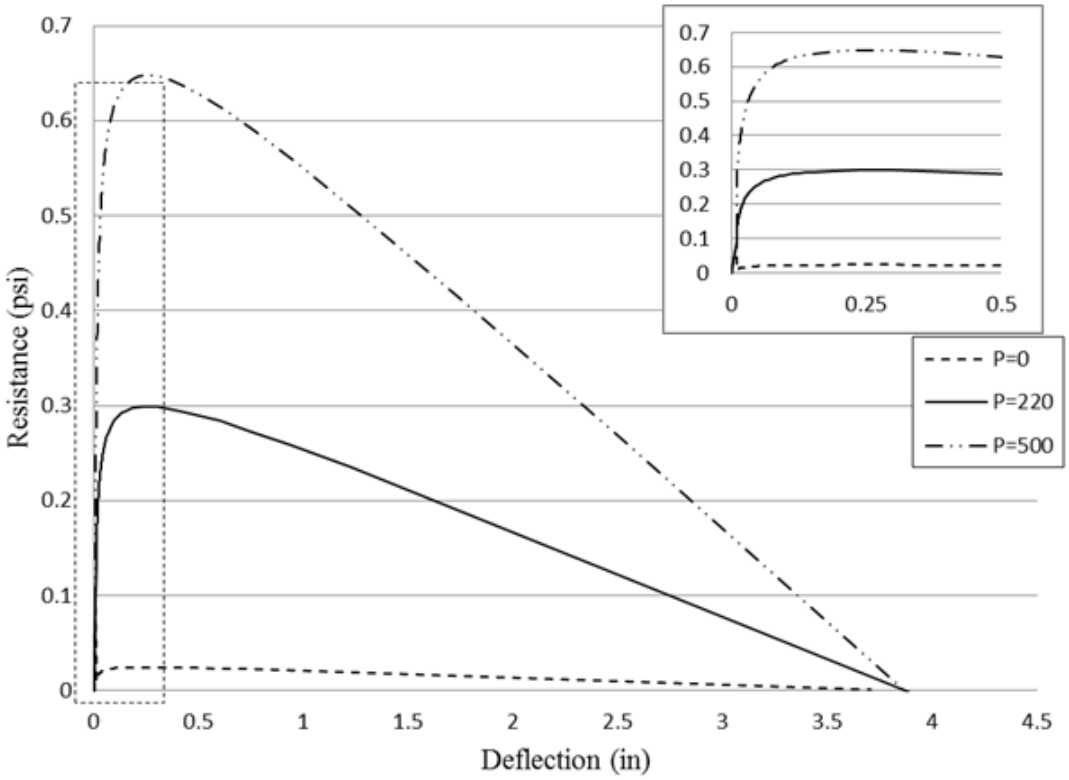

Figure 3.15: Moradi Non-Arching Variable Axial Loads

The Moradi method produces smoother curves due to the incremental changes made at every step. The resistances generated for the walls with an axial load are comparable to those generated by the Wiehle method. These pressures are still the lowest of the three methods but still follow the general order of which wall produces the largest pressures.

A comparison of the peak pressures for each variable and method is depicted in Figure 3.16. Three of the variables shown come from the same wall. One standard example was chosen to compare how changing variables affects the resistance curves. This is why the 8-in, CMU and P=0 bars all have the same pressure for a specific method.

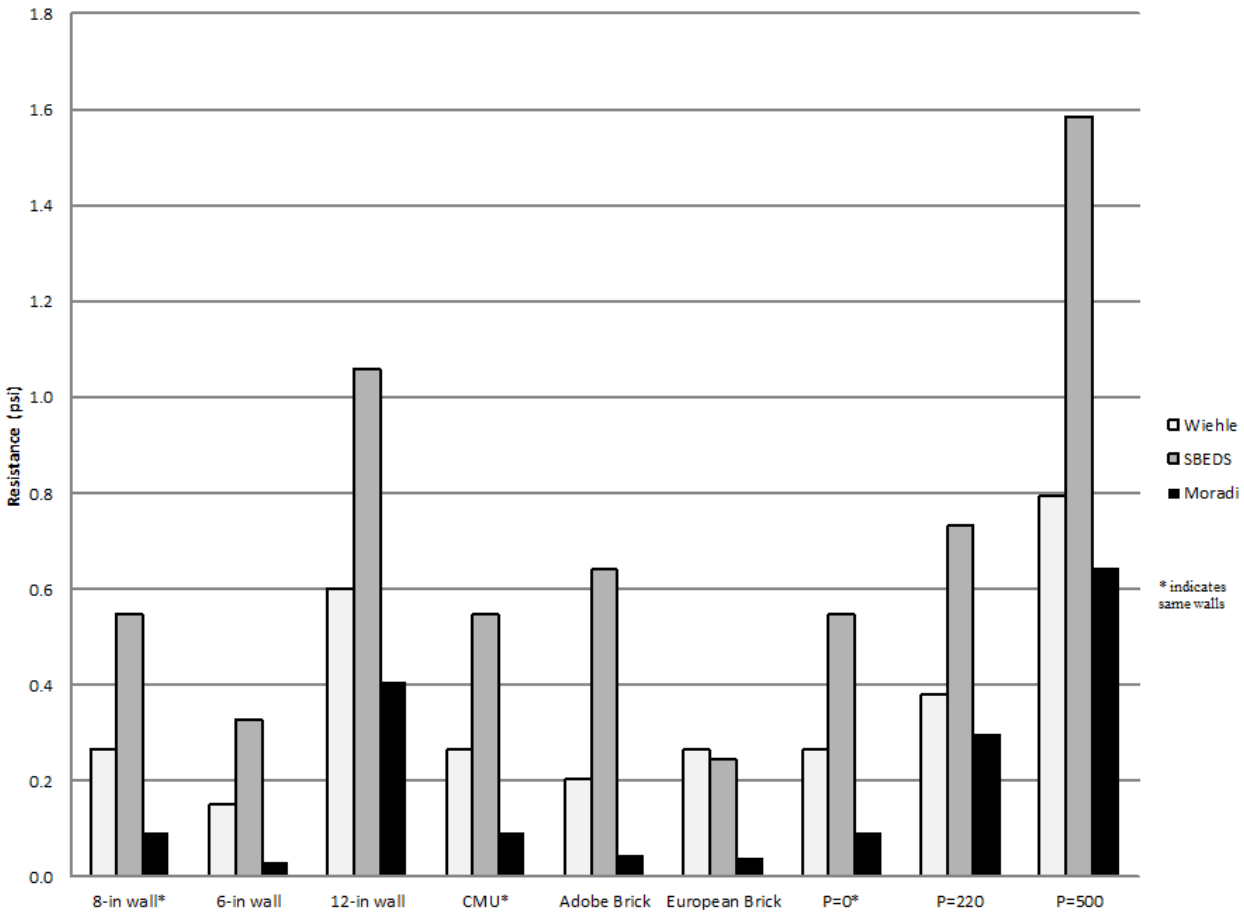

Figure 3.16: Comparison of All Non-Arching Walls

For all three characteristics, the Moradi method produces the lowest pressures. For most of the cases the differences between the Moradi method and the other two are significant. However, when an axial load is applied to the wall there is a substantial decrease in the difference between the methods. The SBEDS method produced the largest pressures for all but the European brick.

The deflections at the peak pressure do not follow a unique trend. For most of the cases the SBEDS method tends to generate the largest deflections. However, the Moradi and Wiehle methods both generate large deflections for different characteristics. Most of the deflections are approximately 0.05 in. with the maximum being approximately 0.25 in. for walls with large axial loads applied. Figure 3.17 compares the deflections at midspan.

The amount of energy dissipation, proportional to the area under the curve, a wall will absorb before failure is a key characteristic for comparison. The comparison of how each wall did in terms of energy dissipation is shown in Figure 3.18. The ideal wall can dissipate more energy than the load can impart. When an axial load is applied to the wall the amount of energy dissipated before failure is drastically increased. The SBEDS method produces a larger energy dissipation for every case. The Wiehle method used a moment of inertia for a solid rectangle. This assumption is inaccurate for ungrouted CMU. Due to the wide range of bond strengths of mortar to masonry, the Moradi method does not consider tensile stress.

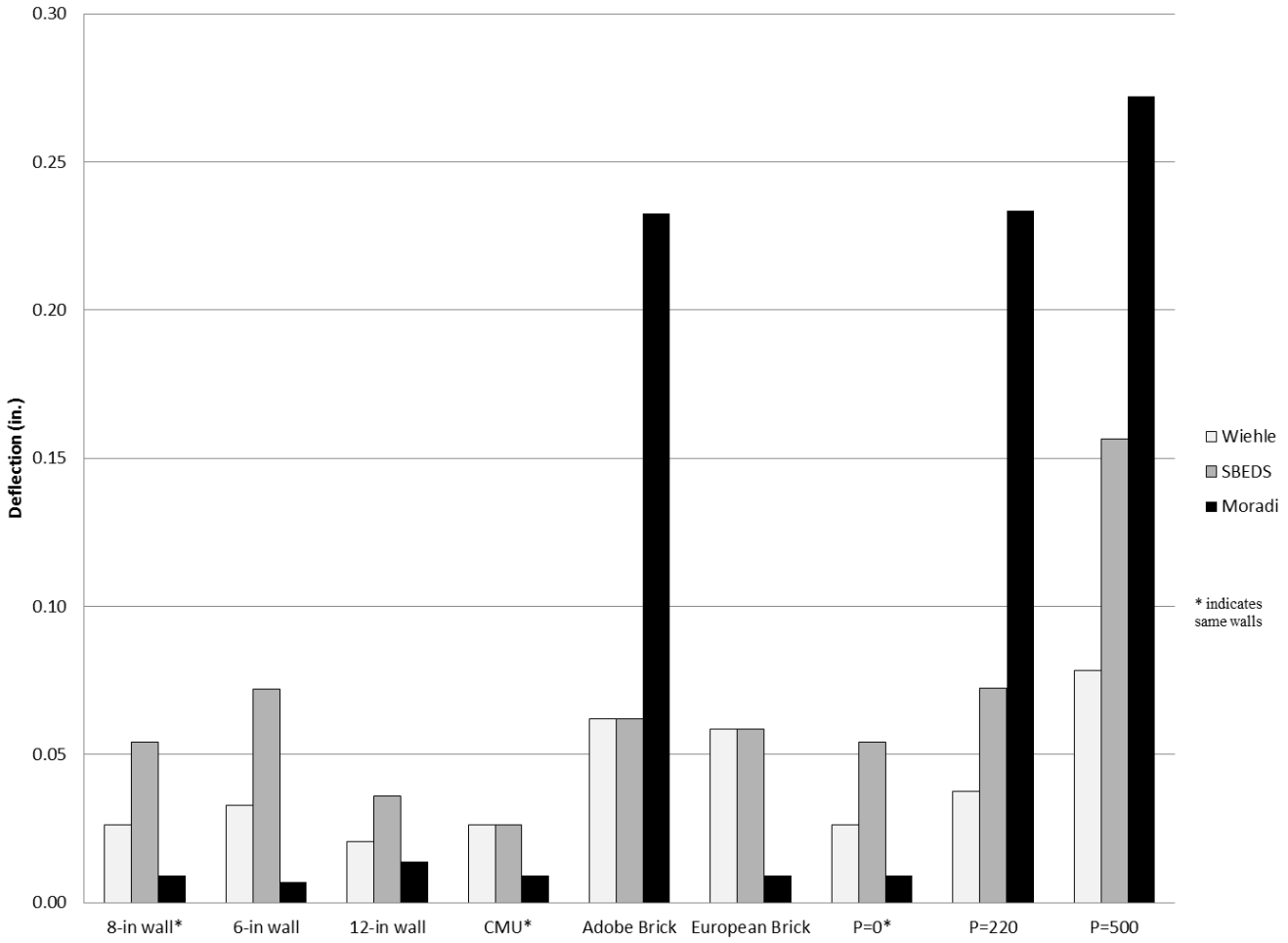

Figure 3.17: Deflection at Peak Pressure for Non-Arching Walls

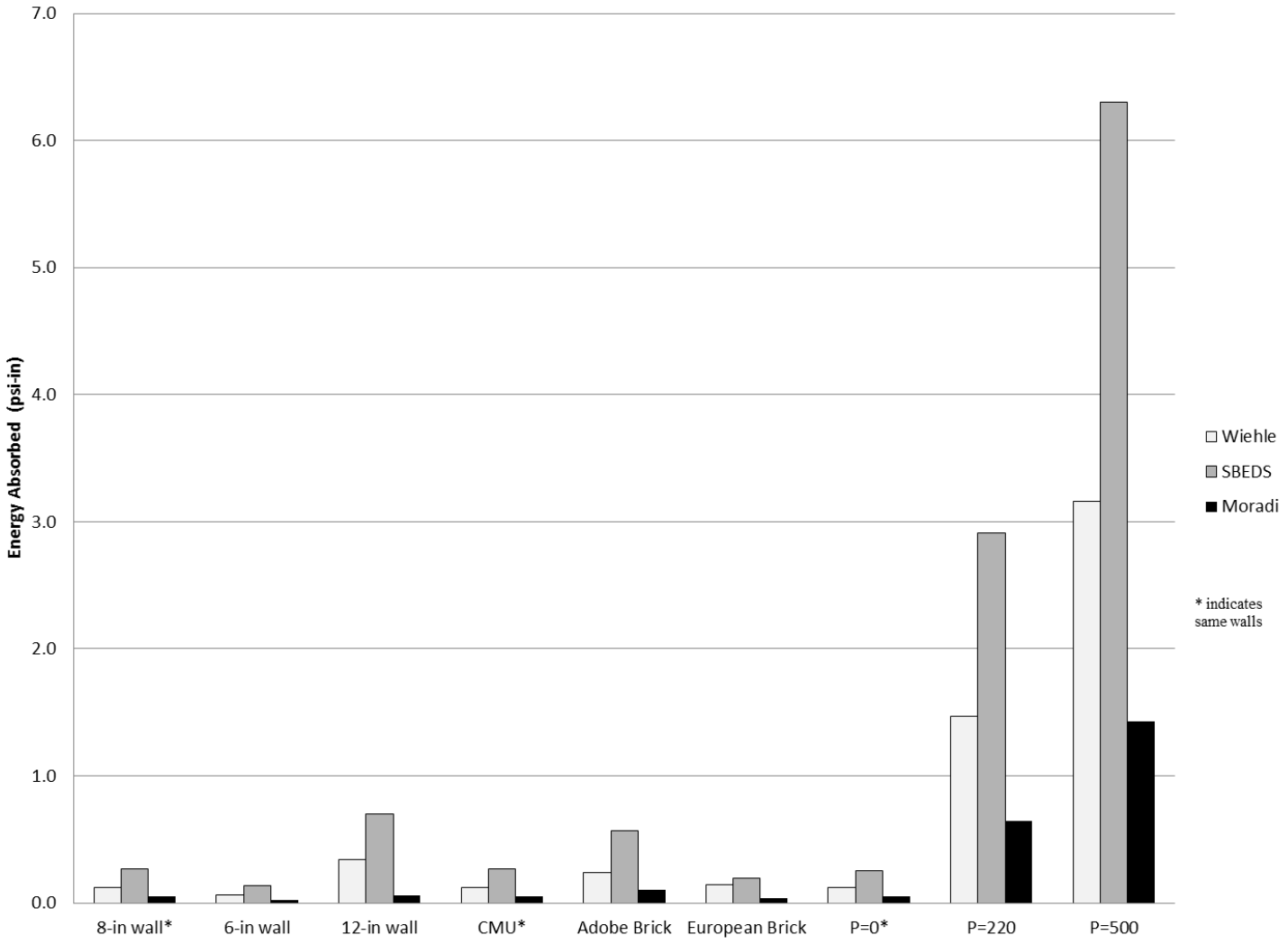

Figure 3.18: Energy Dissipation for Non-Arching Walls

3.3 Arching Masonry Resistance Functions

Depending on the support conditions, the wall may be modeled as a beam between two fixed supports. These supports must be able to resist the rotation of the wall. If the supports are stiff enough the wall can be modeled as an arching wall, which will give significant resistance to lateral loads (Pauley and Priestley 1992). When the wall is bent due to the lateral loads the tension face will elongate. If the supports are rigid this elongation is met with a compression force at the supports. This compressive force will act as a restoring force and help increase the resistance of the wall by almost 2.5 times (Drysdale et al. 1994).

There are four methods considered when developing the arching resistance function. The first one developed was by Wiehle et al. (1968) followed by Moradi and Davidson (2008), SBEDS Methodology (PDC 2008), and lastly UFC (DOD 2008).

3.3.1 Wiehle Arching Resistance Curve

The Wiehle method is used by Johnson (2008), Slawson (1995), and Jones (1989). Several assumptions were needed to generate the resistance curve. The first is that the lateral loads are registered entirely by the compressive forces generated and any flexural strength from tension is neglected. The second is that the wall acts as two rigid halves rotating about the supports. Any additional axial load applied is neglected.

The resistance function starts by calculating the deflection at the point when the wall starts to crack. Once the deflection is known the pressure at yielding can be calculated.

$$\Delta_1 = \frac{t\, f_m^{'}}{E_c} \frac{L_d}{L_d - \frac{h}{2}} \tag{3.17}$$

$$\text{Where: } L_d = \sqrt{\left(\frac{h}{2}\right)^2 + t^2} \tag{3.18}$$

$$p_y = \frac{2\, f_m^{'}}{h^2}\left(t - \Delta_1\right)^2 \tag{3.19}$$

These values identify the yield load for the masonry wall. This is the only point that will describe the elastic region of the wall. When the wall deflection is greater than the yield deflection, the midspan deflection is incremented and the resulting load is calculated.

$$p_2 = \frac{2\, f_m^{'}}{h^2}\left(t - \Delta\right)^2 \qquad \Delta > \Delta_1 \tag{3.20}$$

Once the deflection at midspan is the same as the thickness of the wall, the resistance is assumed to go to zero.

The UFC presents a set of equations for arching walls with a gap. This method works if the wall is braced at the top to resist translation but allows rotation of the wall until the wall is in contact with the rigid support. Figure 3.19 describes how the wall deflects during the loading.

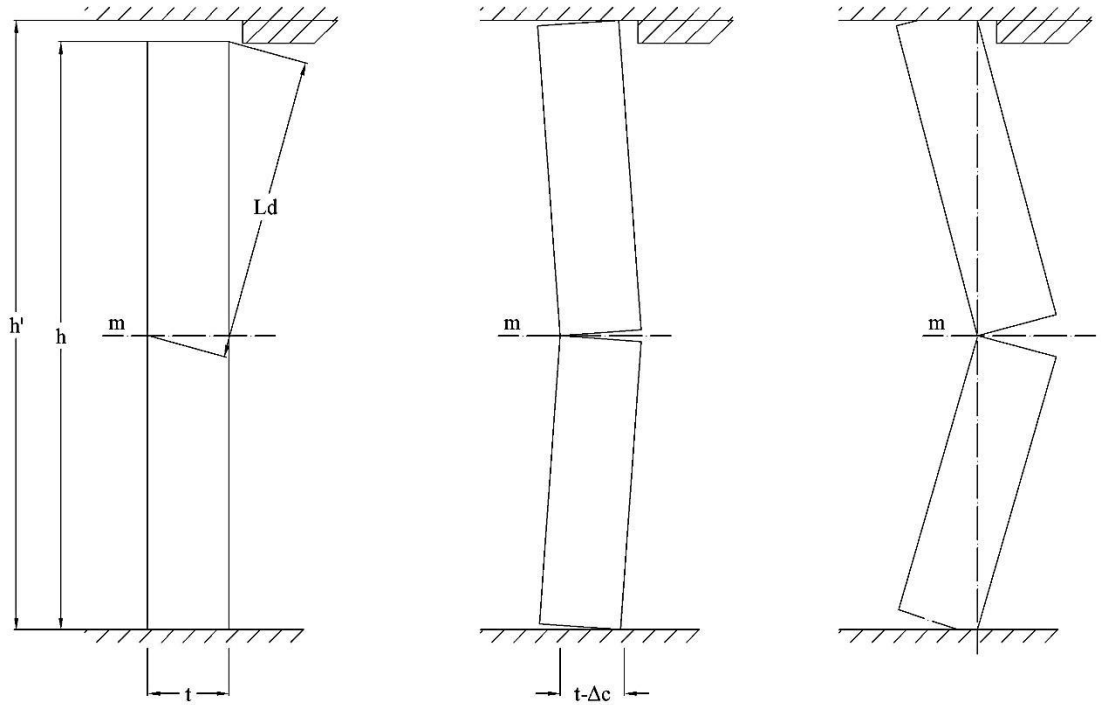

Figure 3.19: UFC (DoD 2008) Gapped Wall Schematic

In the above illustration, the distance the midspan, point m, travels before touching the support is described as Δ_c. While the wall is rotating, only inertial affects are resisting the movement and are considered negligible.

$$\Delta_c = t - \left[L_d - \left(\frac{h}{2} \right)^2 \right]^{1/2} \tag{3.21}$$

$$L_d = \left[\left(\frac{h'}{2} \right)^2 + t^2 \right]^{1/2} \tag{3.22}$$

Shortening of the diagonal at failure along with the elastic modulus will be used to determine the stress in the concrete.

$$\varepsilon_d = \frac{L_d - \frac{h}{2}}{L_d} \tag{3.23}$$

The deflection corresponding to the ultimate resistance is shown in Equation 3.24.

$$\Delta_1 = \frac{(t - \Delta_c)}{E_c \varepsilon_m} + \Delta_c \tag{3.24}$$

The peak resistance is equal to:

$$p_1 = \frac{2}{h^2} f_m^{'} \left[t - \Delta_1\right]^2 \tag{3.25}$$

After the peak resistance, the deflection is incremented until the deflection equals the thickness of the wall.

$$p_2 = \frac{2}{h^2} f_m^{'} \left[t - \Delta\right]^2 \qquad \Delta > \Delta_1 \tag{3.26}$$

When there is no gap present, these equations produce the same curve as the Wiehle method. Many URM walls have a small gap, making the use of the UFC formulas more viable and representative of how the wall will react. Gaps are present to allow for shrinkage and creep. They may also be the result of construction error. The effects of a gap are shown in Figure 3.20.

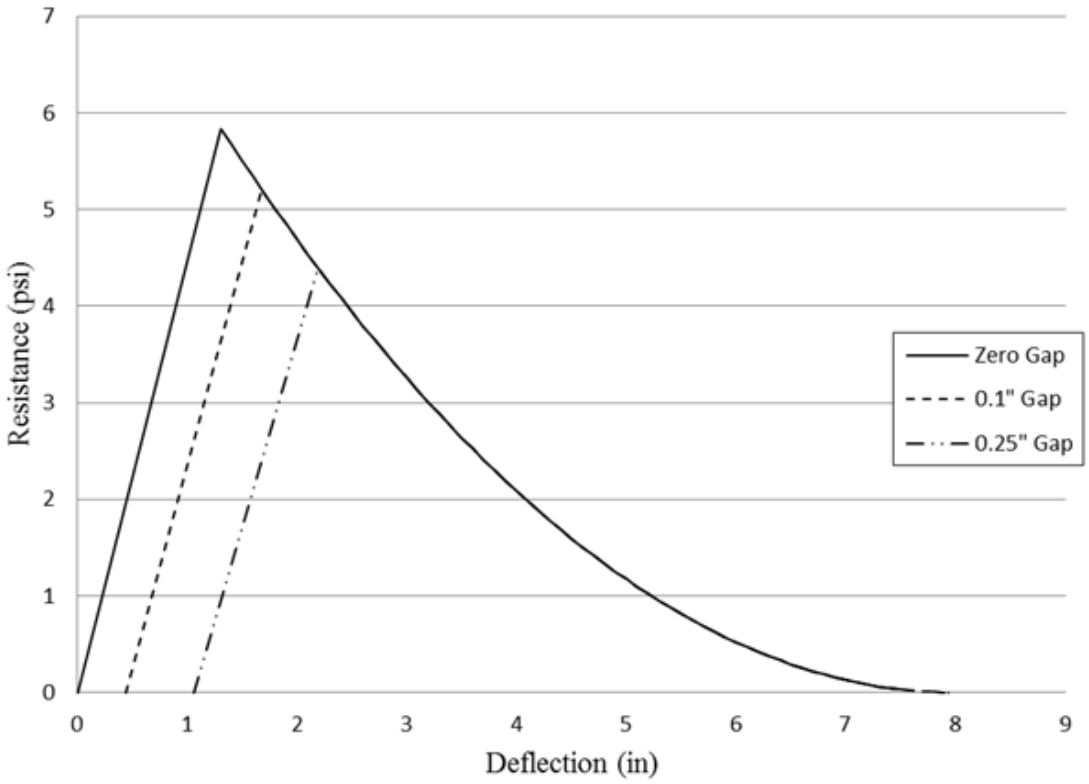

Figure 3.20: UFC Gapped Wall Comparison

The stiffness of the wall is not affected by the addition of the gap. The displacement at the peak resistance is shifted to the right. This is because of the initial deflection required before arching can start. The peak resistance is adversely affected with the addition of a gap. For this reason it is important to incorporate a gap if applicable. The UFC method also does not incorporate an axial load that will produce a conservative curve.

3.3.2 Moradi Arching Resistance Curve

The resistance function created by Moradi et al. (2010) uses mechanics to derive a process to generate a resistance curve. One main difference between the Moradi method

and the Wiehle method is that Moradi included an additional axial load for load bearing walls. The FBD used by Moradi et al. (2010) is shown in Figure 3.21.

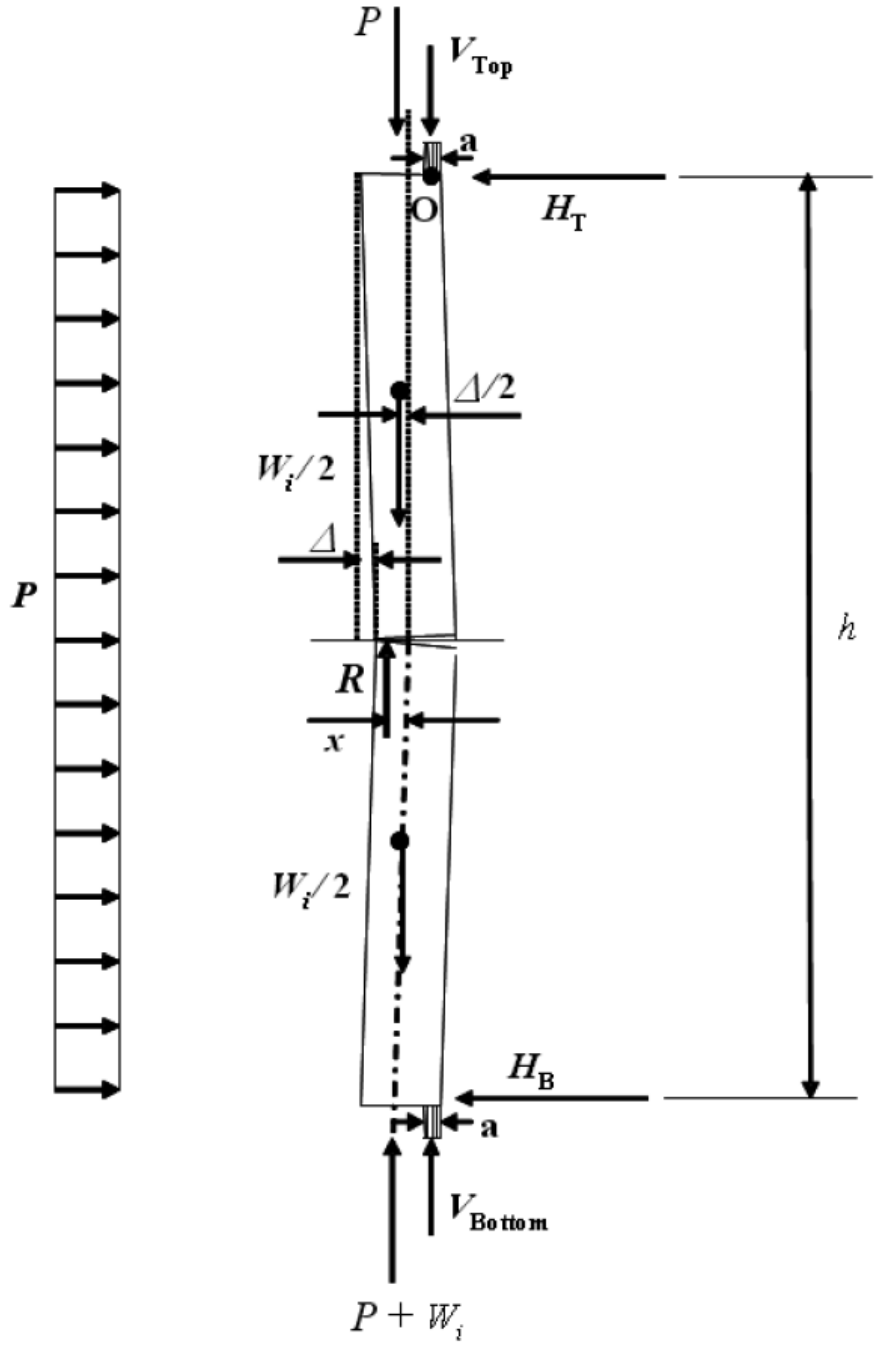

Figure 3.21: FBD of Moradi Arching Wall (Moradi et al. 2010)

An equation was developed for the pressure as a function of displacement, the arching force, and the crack length.

$$p = \frac{8}{h^2}\left(P + V_T + \frac{W_i}{2}\right)\left(\frac{t}{6} - \frac{y}{3} + \frac{t+a}{2} - \Delta\right) - \frac{8P}{h^2}\left(\frac{t-a}{2}\right) - \frac{4W_i}{h^2}\left(\frac{t-a}{2} - \frac{\Delta}{2}\right) \qquad 3.27$$

Where V_T represents the arching force. When the wall is not cracked, the arching force is assumed to be zero along with the crack length. If these values are substituted into Equation 3.27 and solving for displacement results in:

$$\Delta_1 = \frac{\left(P + \frac{W_i}{2}\right)\left(\frac{t}{6}\right) - \frac{ph^2}{8}}{P + \frac{W_i}{4}} \qquad 3.28$$

Before cracking, the wall resists the lateral load due to pure flexural resistance assuming no mortar tensile bond. Using the assumption that the wall ends are fixed, the deflection due to flexure comes from Euler–Bernoulli beam theory.

$$\Delta_1 = \frac{ph^4}{384EI_g} \qquad 3.29$$

Setting Equations 3.28 and 3.29 equal, the pressure that will result in maximum flexural resistance can be determined.

$$p = \frac{\left(P + \frac{W_i}{2}\right)\left(\frac{t}{6}\right)}{\left(\frac{h^4}{384E_cI_g}\right)\left(P + \frac{W_i}{4}\right) + \frac{h^2}{8}} \qquad 3.30$$

Once the resistance is known the displacement can be calculated. The arching force on top of the wall is derived using theory developed by McDowell et al. (1956). The strain

created in the wall due to the shortening of the corner and the support is shown in Equation 3.31.

$$\varepsilon = \frac{2\delta}{\frac{h}{2}} \tag{3.31}$$

Where δ is the shortening of the wall. The definition for the shortening is shown in Figure 3.22 and using the geometry of deformation the definition was developed by Moradi and Davidson (2008).

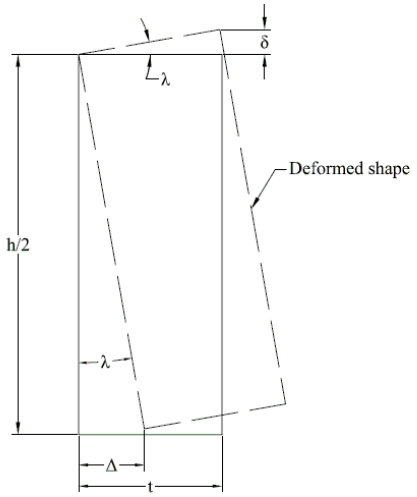

Figure 3.22: Shortening of URM Wall

$$\tan(\lambda) = \frac{\Delta}{\frac{h}{2}} = \frac{\delta}{t} \therefore \delta = \frac{2\Delta t}{h} \tag{3.32}$$

Assuming the masonry is elastic until crushing, Hooke's Law is applicable, σ=Eε.

$$\sigma_{arching} = \frac{4E_c\delta}{h} = \frac{4E_c\frac{2\Delta t}{h}}{h} = \frac{8E_c\Delta t}{h^2} \tag{3.33}$$

$$V_T = \frac{8E_c \Delta t}{h^2} \tag{3.34}$$

To determine the deflection after cracking, Equations 3.6 and 3.7 should be used while incrementing the crack length, *y*. The resultant force is the summation of the axial load, the self-weight, and the arching force.

$$R = P + V_T + \frac{W_i}{2} \tag{3.35}$$

Since the stress relies on the arching force, which is a function of displacement, small incremental steps allow for the use of the stress from the previous iteration to calculate the curvature ratio. Once the deflection is known, the pressure can be determined using Equation 3.27. This process is continued until the resistance of the wall goes to zero which constitutes failure.

The process to develop a resistance curve using the Moradi method is detailed in the flow chart in Figure 3.23 below.

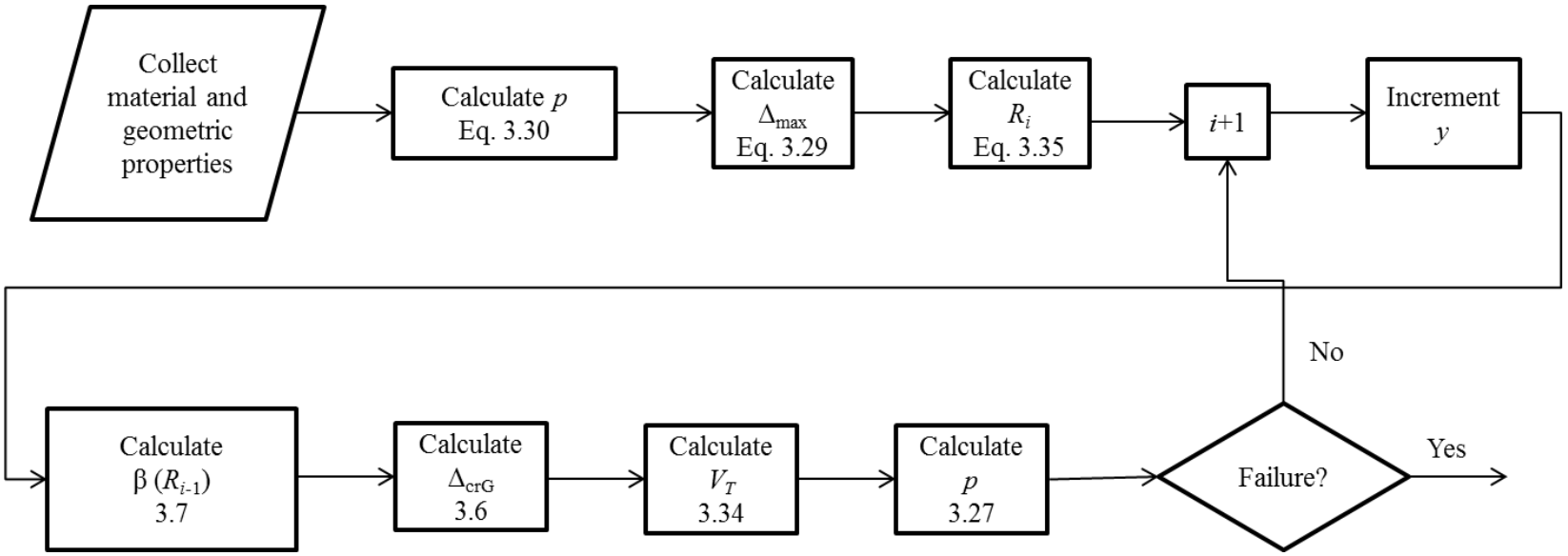

Figure 3.23: Flow Chart of Moradi Arching Resistance Curve Development

3.3.3 SBEDS Arching Resistance Curve

The SBEDS method is similar in the Wiehle method in that it assumes the flexural resistance is significantly less than the arching action. For this reason the flexural resistance is neglected. The methodology used to generate the resistance curve comes from Parks and Gamble (2000) "Reinforced Concrete Slabs". The equations developed neglect the presence of steel, allows for ungrouted voids, and a support movement for gapped walls.

The SBEDS arching resistance curve is constructed using only three points. The first is the displacement of the wall needed to close the gap between the wall and the supports. At this point there is no resistance from the wall and only deflection.

$$\Delta_c = t - \sqrt{\left(\frac{h}{2}\right)^2 + h^2 - \left(\frac{h+\delta_g}{2}\right)^2} \tag{3.36}$$

This is the starting point of the resistance curve. The second point needed is the maximum resistance of the wall and its corresponding deflection.

$$p_{\max} = \frac{8}{h^2}\left[2C_1\left(\frac{t}{2} - \frac{t_{ms}}{2}\right) + 2C_2\left(\frac{t}{2} - t_{ms} - \frac{0.85a - t_{ms}}{2}\right) - \left(C_1 - C_2\right)\Delta_1\right] \tag{3.37}$$

$$a = \frac{t}{2} - \frac{\Delta_1}{2} - \beta h^2\left(\varepsilon' + \frac{\delta_g}{h}\right) \tag{3.38}$$

$$\varepsilon' = \left(\frac{1}{tE_c} + \frac{2}{hS}\right) \times \frac{\left[0.85 f'_{dc}\,\beta_1\left(\frac{t}{2} - \frac{\Delta_1}{4}\right)\right]}{1 + 0.2125\frac{f'_{dc}\,\beta_1\beta h^2}{\Delta_1}\left(\frac{1}{tE_c} + \frac{2}{hS}\right)} \tag{3.38(a)}$$

$$C_1 = 0.85\, f_m^{'}\, t_{ms} \tag{3.39}$$

$$C_2 = 0.85\, f_m^{'}\, k\,(0.85c - t_{ms}) \tag{3.40}$$

$$\Delta_1 = \min\left(\frac{h}{30}, \frac{t}{2}\right) + \Delta_c \tag{3.41}$$

Where: Δ_1 – Midspan deflection at maximum resistance

ε' - Compression strain due to arching forces and support movement strain

δ_g - Gap between edge of wall and rigid supports

t_{ms} - Masonry shell thickness

k - Solid ratio of masonry through webs (k = 0 assumed for horizontal span arching if not fully grouted)

C_1 - Compression force per unit width in shell

C_2 - Compression force per unit width in web

β - Distance from support to yield location divided by span length = 0.5

S – Lateral stiffness of the supports =0.2E_c

$f_{dc}^{'}$ – Dynamic ultimate compressive strength of concrete

β_1 – Ratio of concrete compression block depth to the distance from the compression face to the neutral axis =0.85 for $f'_c \leq 4000$ psi and reduced by 0.05 for every 1000 psi increase in strength but not less than 0.65

E_c – Modulus of elasticity of the concrete

The deflection at ultimate resistance is assumed to be approximate to half the wall thickness based on experimental data presented in Parks and Gamble (2000). Based on the results of the experiments it was observed that the deflection is affected by the stiffness of the supports. For stiffer supports "it would seem that a reasonably conservative estimate of the ultimate load would be obtained at a central deflection of 0.5 the slab thickness" (Parks and Gamble 2000). Once the maximum point has been defined

the last point needed is the point of failure. When the wall exhibits snap through the wall will not be able to resist any loading. The deflection at the point of snap through is defined as:

$$\Delta_{st} = \min\left(0.08h, 0.8t\right) + \Delta_c \le t \qquad 3.42$$

These three points are the only points used to define a resistance curve in SBEDS. Since there are only three points, a triangular resistance curve will always result.

3.3.4 Comparison of Arching Resistance Functions

Three characteristics will be examined to see how these resistance functions will be affected. The first is the thickness of the wall. Three different sized bricks will be selected, 6-in, 8-in and 12-in. The second characteristic of the wall to be examined is the type of brick. The bricks selected are an 8-in CMU, European brick, and a solid adobe brick. The last characteristic is the gap between the walls. A zero gap, 0.1 in. gap, and a 0.25 in. gap will be used. Only two of the resistance functions are designed to incorporate a gap so only these two will be used for this portion. The axial load can influence the resistance; however, since only the Moradi method is capable of incorporating axial loads this characteristic will be neglected.

The first characteristic that was examined was the thickness of the wall. The three wall thicknesses selected were 6-in, 8-in and 12-in CMU. When the thickness of the wall increases the moment of inertia as well as the self-weight of the wall increase. These two values were updated as well. All values correspond to SBEDS Methodology (2008) recommended properties for medium weight CMU. An increase in the wall thickness

should increase the ultimate pressure of the system. The input parameters are shown in Table 3.5 and Figure 3.24 shows the effect of wall thickness on the Wiehle method.

Table 3.5: Input Parameters for Wall Thickness Comparison of Arching Methods

Wall Thickness (in)	6	8	12
Wall Height (in)	144		
Axial Load (lb/in)	0		
Modulus of Elasticity of Mortar (psi)	1350000		
Gross Moment of Inertia (in^4/in)	12.8	28.4	82.4
Weight of Wall (lb/in)	22.9	27.2	33.3
Solid Fractional Ratio (%)	55	49	40
Compression Block (in)	1.25		
f'm (psi)	1350		

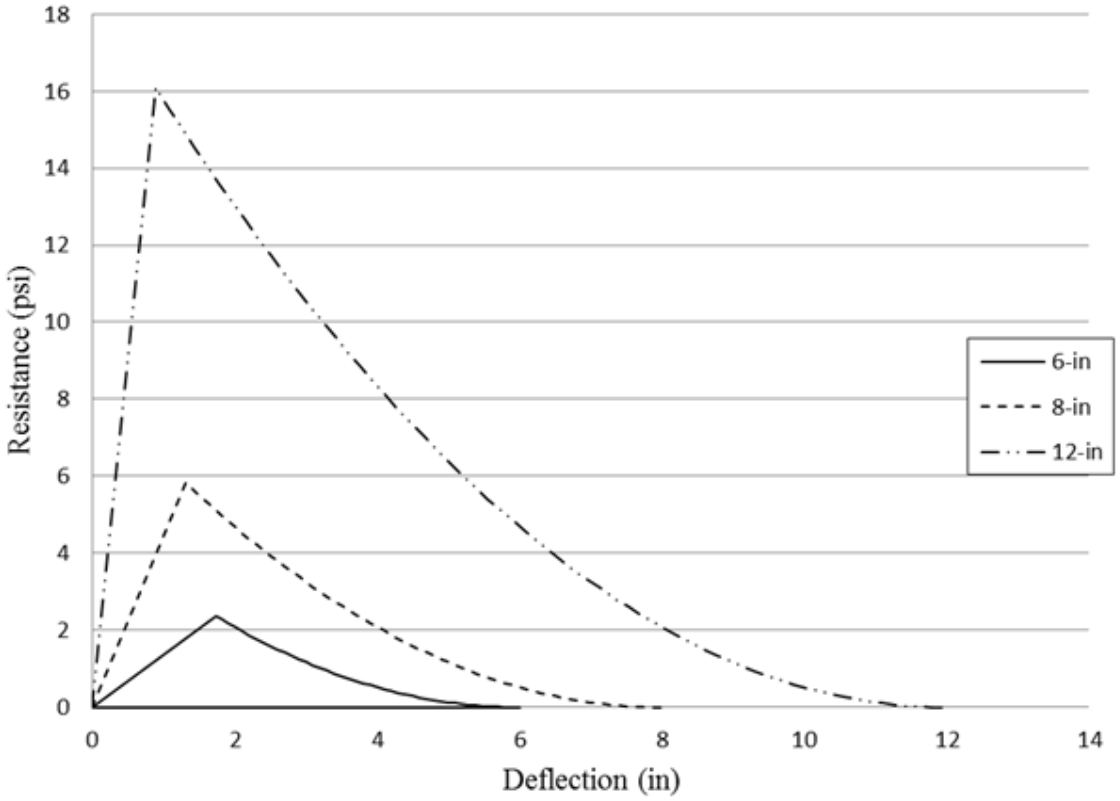

Figure 3.24: Wiehle Arching Variable Wall Thickness

As expected, the larger the wall the greater the peak resistance. The 12-in wall predicts a resistance almost eight times greater than what would be expected for a 6-in thick wall. Because the wall weight increases with increase in thickness, this helps resist the pressures as well as increasing the moment arm of the arching forces. The thicker walls produce a smaller deflection at the ultimate pressure. The effect of wall thickness on the SBEDS method is shown in Figure 3.25.

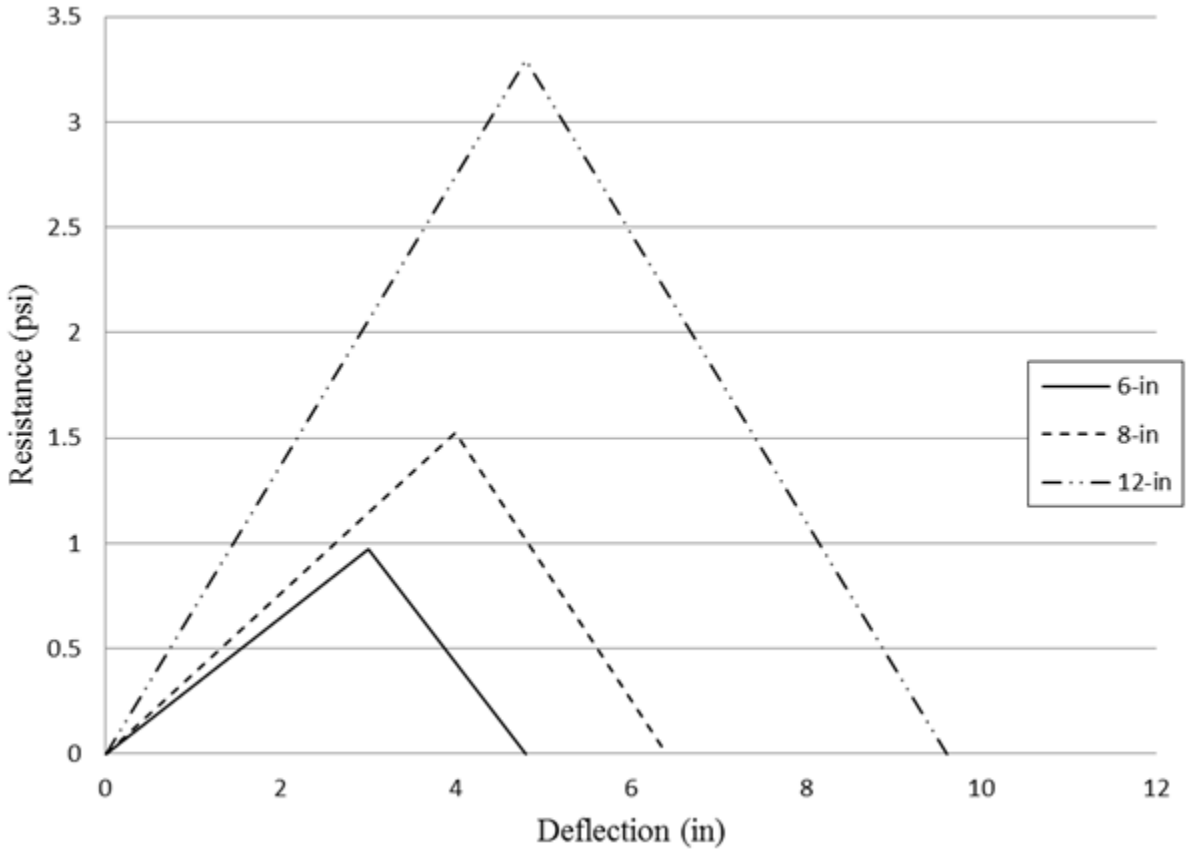

Figure 3.25: SBEDS Arching Variable Wall Thickness

Similar to the Wiehle curves, the peak pressure increases with an increase in the wall thickness. These ultimate pressures are significantly lower than those from the Wiehle model. The deflections are also much greater for the SBEDS method. The snap

through deflection predicts a collapse of the wall at much lower deflections than the Wiehle method. The weight of the wall is not considered for the SBEDS method and could account for the lower pressures. How the Moradi method is effected by the block thickness is shown in Figure 3.26.

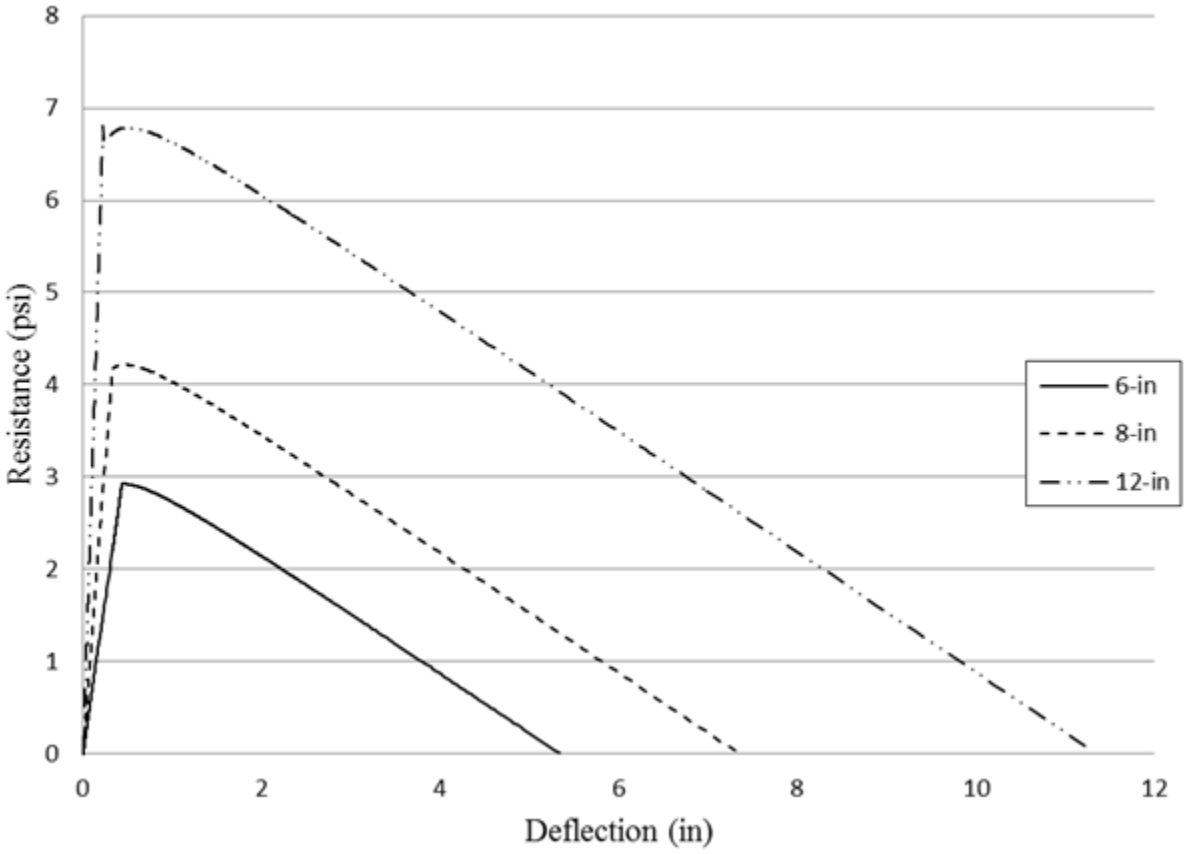

Figure 3.26: Moradi Arching Variable Wall Thickness

The Moradi method produces resistance curves that fall between the other two methods. The stiffness of the walls is not greatly affected by the wall thickness compared to the other two methods. The other two methods show a significant increase in stiffness with a larger wall thickness. This is partly due to the increased moment of inertia of the thicker walls.

The second factor that was looked at is the type of brick. Three common bricks were selected: CMU, European brick, and solid adobe bricks. The CMU block is a common building material in the U.S. and the European brick is used widely overseas. In the Middle East, adobe bricks are still widely used due to the ease of construction and availability. The input parameters for variable brick type are shown in Table 3.6.

Table 3.6: Input Parameters for Brick Comparison for Arching Methods

	CMU	European	Adobe
Wall Thickness (in)	8		
Wall Height (in)	144		
Axial Load (lb/in)	0		
Modulus of Elasticity of Mortar (psi)	1350000	1800000	465100
Gross Moment of Inertia (in^4/in)	28.4	12.8	82.4
Weight of Wall (lb/in)	27.2	27.8	55.6
Solid Fractional Ratio (%)	49	50	100
Compression Block (in)	1.25		
f'm (psi)	1350	1800	465.1

The compression block of the adobe was not changed to reflect that suggested by Drysdale et al. (1994), $a=0.1t$. This was done in order to compare how the different bricks compare as a material. The effect of brick type on the Wiehle method is shown in Figure 3.27.

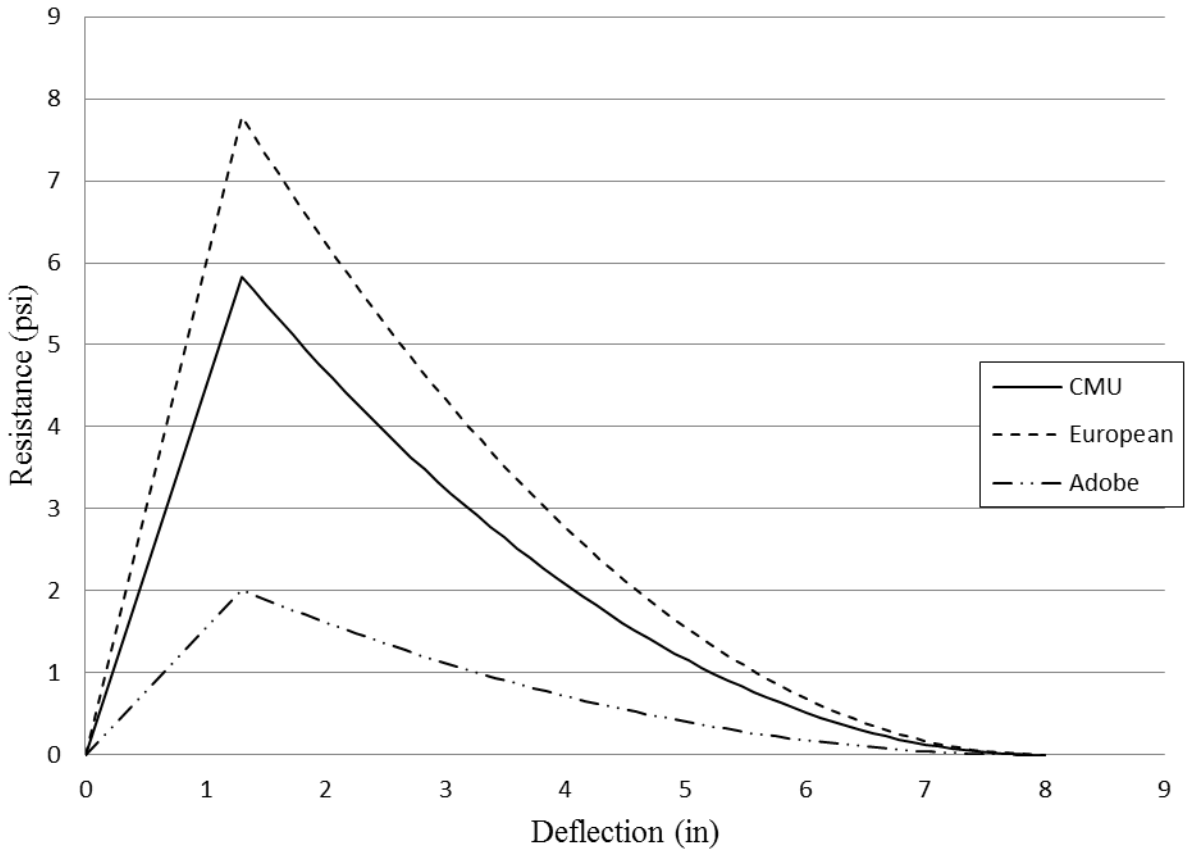

Figure 3.27: Wiehle Arching Variable Brick Type

The European brick produces the largest ultimate pressure according to the Wiehle method. The European brick has a large amount of material in the core of the brick compared to the CMU brick as well as a larger compressive stress. The compressive stress of the adobe greatly affects the peak pressure of the adobe wall. The deflections at the ultimate resistance are directly related to the peak resistance. The European brick produced both the largest ultimate pressure and the largest deflection at peak resistance. The ultimate pressure produced by the European brick is approximately 8 psi. How the brick type effects the SBEDS method is shown in figure 3.28.

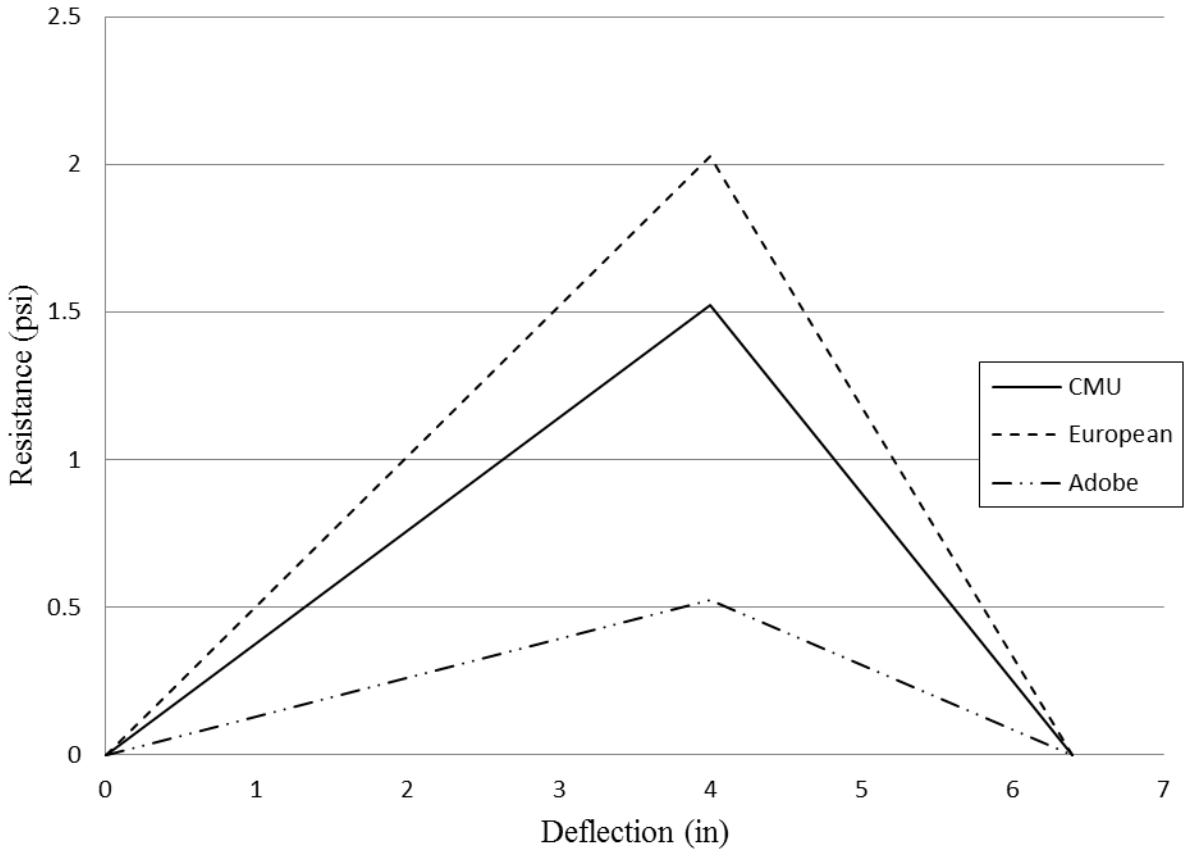

Figure 3.28: SBEDS Arching Variable Brick Type

The SBEDS curves follow the same trend as the Wiehle method, with the European brick producing the largest peak resistance. The deflection corresponding to the ultimate strength is independent of the brick properties. The geometry of the wall dictates this deflection point. The deflection corresponding to the peak resistance is half the width of the wall. These resistances are substantially lower than those produced by the Wiehle method. The maximum resistance produced by the European brick is 2.03 psi. The effect of brick type on the Moradi method is shown in Figure 3.29.

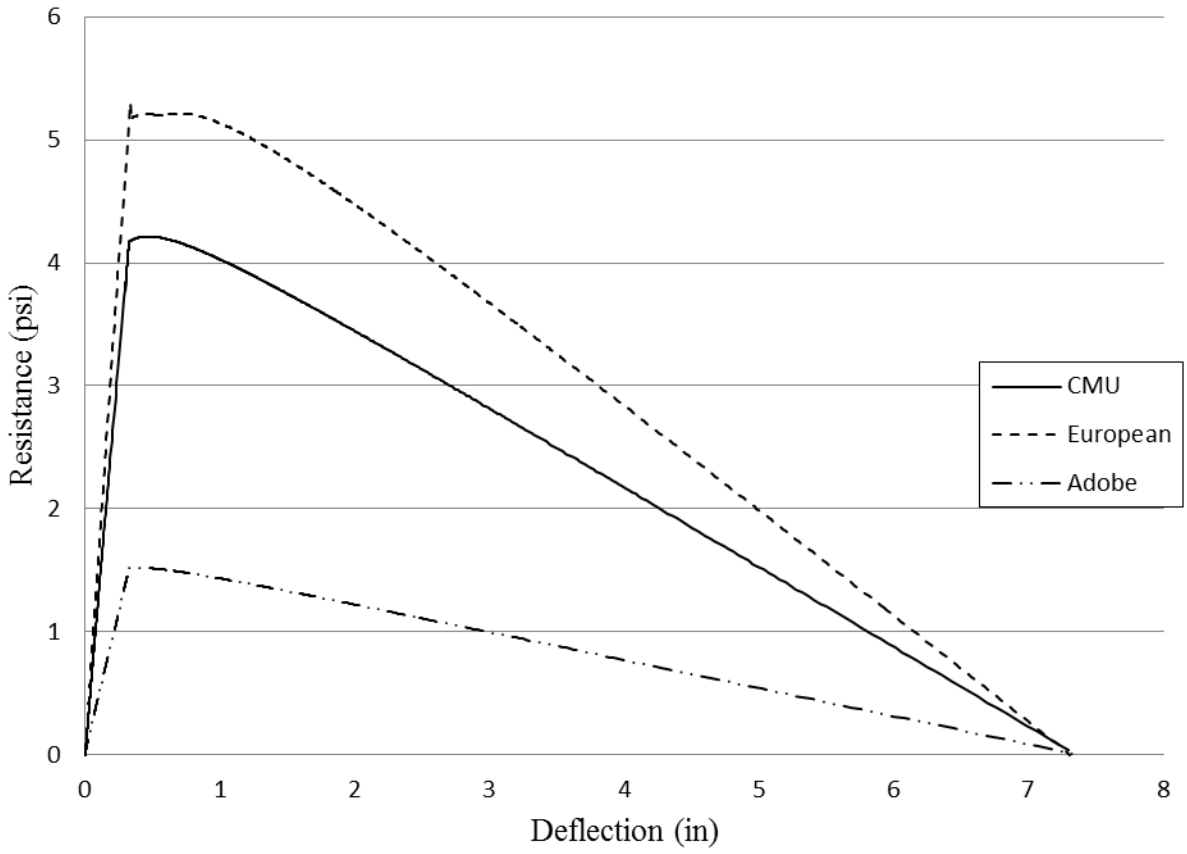

Figure 3.29: Moradi Arching Variable Brick Type

The resistance curves produced by Moradi closely resembles the Wiehle curves. The peak resistances are below the Wiehle resistance but not as significantly as the SBEDS numbers. The resistance of the European brick at the ultimate strength is 5.30 psi and has a deflection of 0.70 in. at the ultimate strength. All of the walls collapse at the same deflection of approximately 7.30 inch.

The final feature to be examined is the gap spacing. The gap will lower the resistance of the wall by approximately 50% (Drysdale et al. 1994) and increase the deflections at the ultimate strength and collapse. Only UFC and SBEDS consider a gap in the development of the resistance curves so the Moradi method will not be considered in

this section. The three gap sizes to consider are zero, 0.1-in and 0.25-in. gaps. The wall will be a standard 8-in. CMU wall with a height of 144 in. between supports. The gap's effect on the UFC method is shown in Figure 3.30.

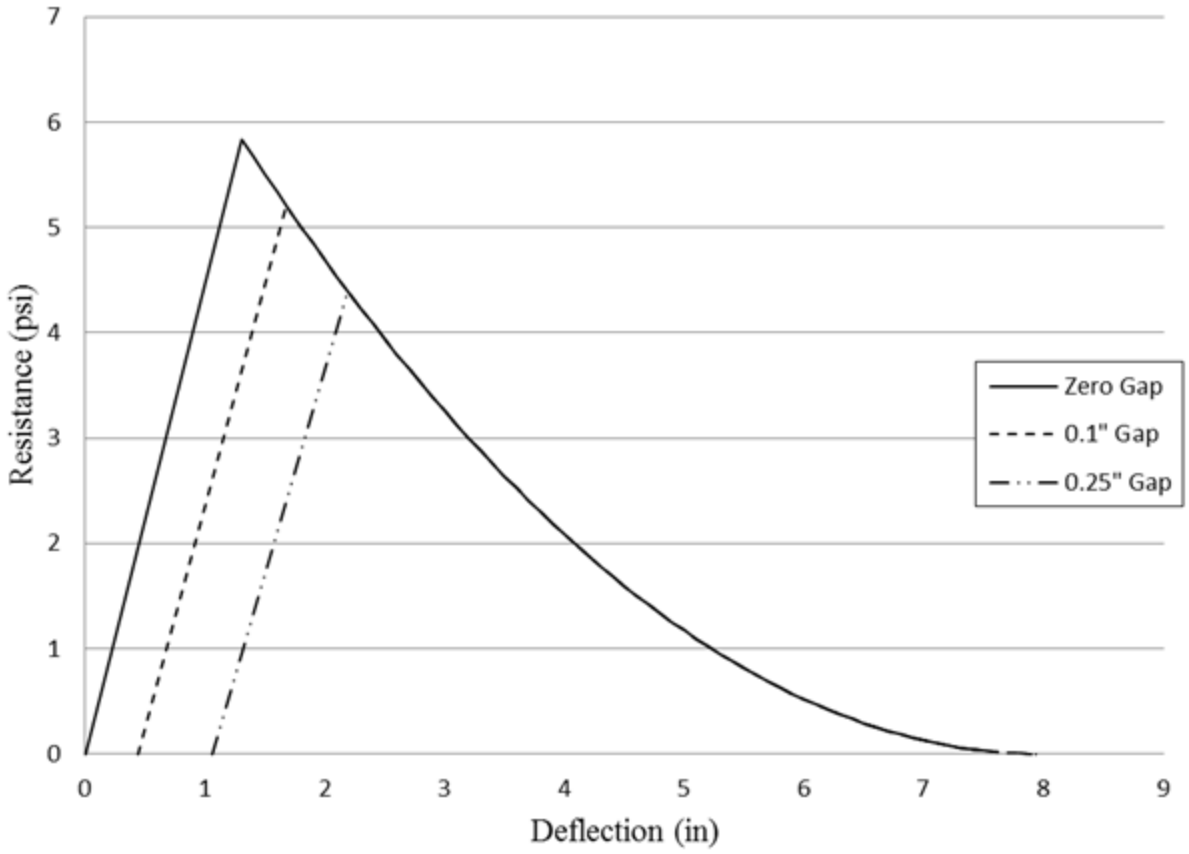

Figure 3.30: UFC Arching Variable Gap Width

The deflection at the start of the resistance curve is heavily influenced by the gap width. The wall must rotate in order to close the gap between the supports and the wall. The deflection at the onset of the resistance curves for the 0.1-in gap and the 0.25 inch gap are 0.43 in. and 1.05 in. respectively. The stiffness of the wall is not affected by the presence of a gap. The peak pressures however are adversely affected as well as the deflection corresponding to the peak pressure. The deflection of the wall at collapse

remains the same for all cases since the method assumes when the wall deflection at collapse equals the wall thickness. The effect of the gap length on the SBEDS method is shown in Figure 3.31.

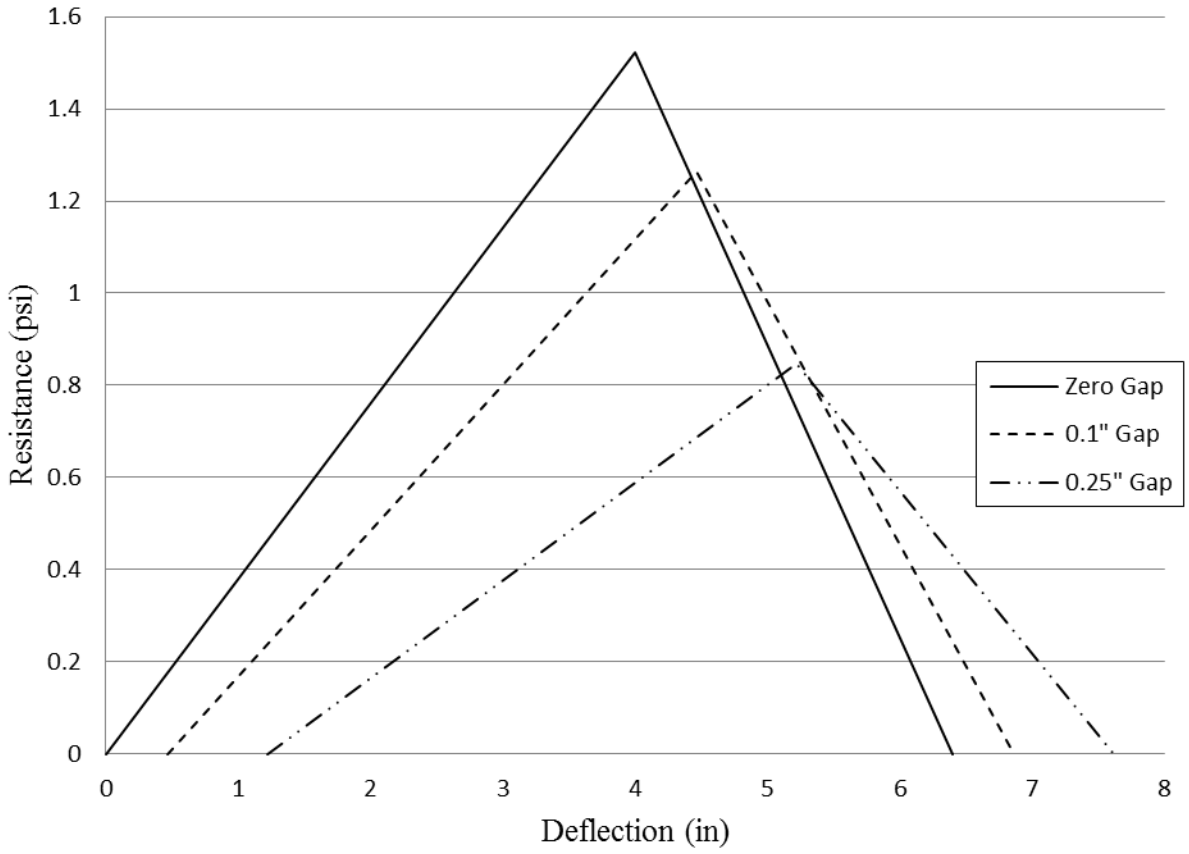

Figure 3.31: SBEDS Arching Variable Gap Width

The deflection at the beginning of the resistance curve is similar to the deflections of the UFC method. The collapse deflection is shifted over by the same amount as the initial deflection. The stiffness of the wall is adversely affected by the presence of a gap unlike the UFC model. The larger gaps have a greater effect on the peak resistance compared to the UFC method.

How the models are affected by an individual characteristic is important. Another critical comparison is how the models compare to one another. Figure 3.32 compares the peak resistance of each of the models. In almost every instance the Wiehle method produced the largest resistance. These resistances were significantly larger in some cases such as the 12-in CMU wall. The Moradi method fell between the other two models in most cases. The SBEDS method always produced the smallest resistance. This is due to the over simplification of the SBEDS method. The low peak resistance can be seen as conservative for design. The European bricks produced a larger ultimate pressure for all methods. As the thickness of the wall increased, the peak resistances increased as well for all methods. The gap width does affect the peak resistance of the wall adversely as expected.

The energy dissipation is an approximate method to determine the effectiveness of a wall's resistance to blast loading. A comparison of the energy dissipation for the different methods is shown in Figure 3.33. For this reason it is used to compare various resistance functions for the same wall. Each class of wall has the same properties the only difference is the method used to calculate the pressure and deflection. The ideal system is one that dissipates more energy. However, the method used to calculate it should not overestimate the resistance of the wall.

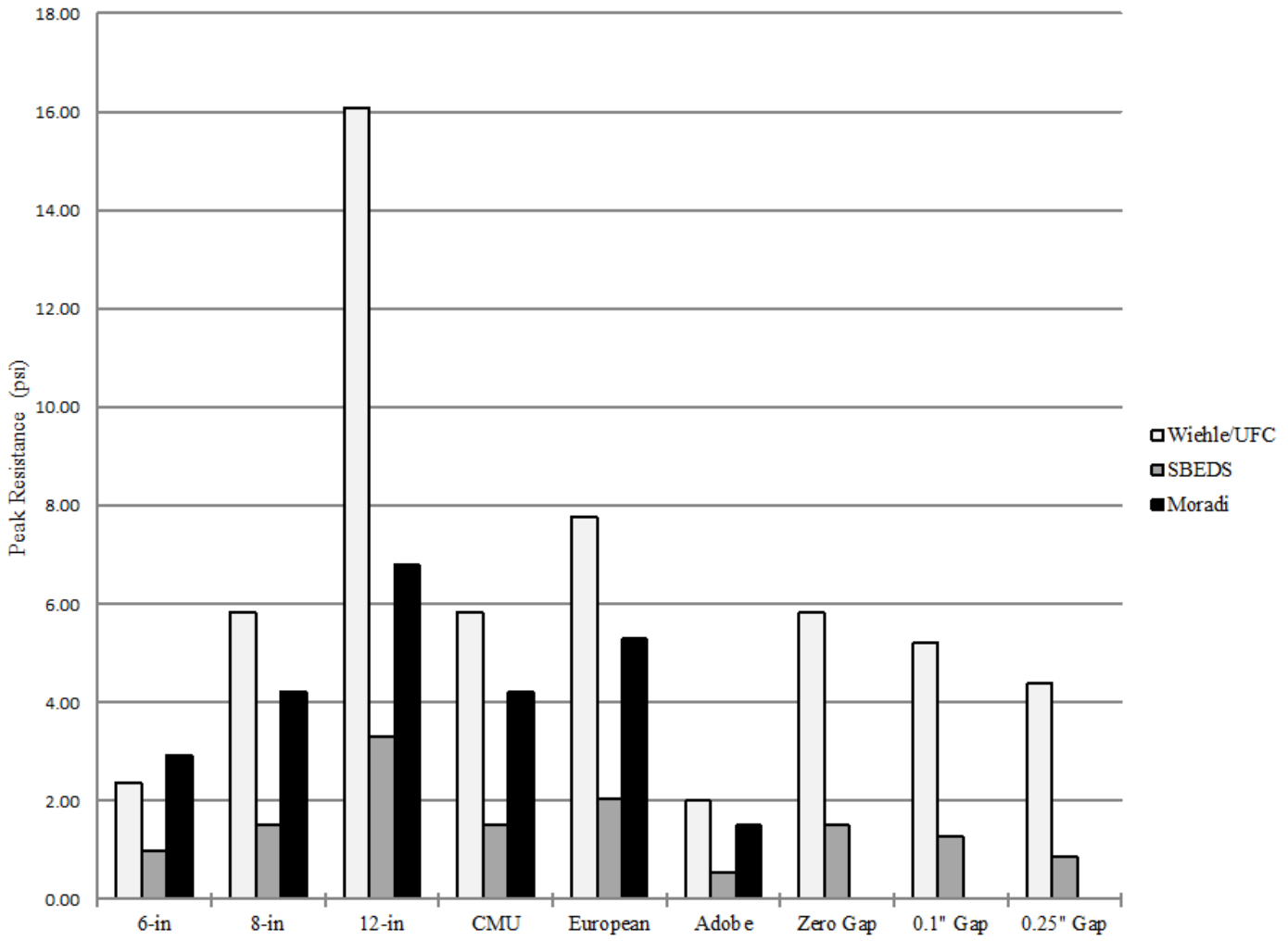

Figure 3.32: Arching Ultimate Resistance Comparison

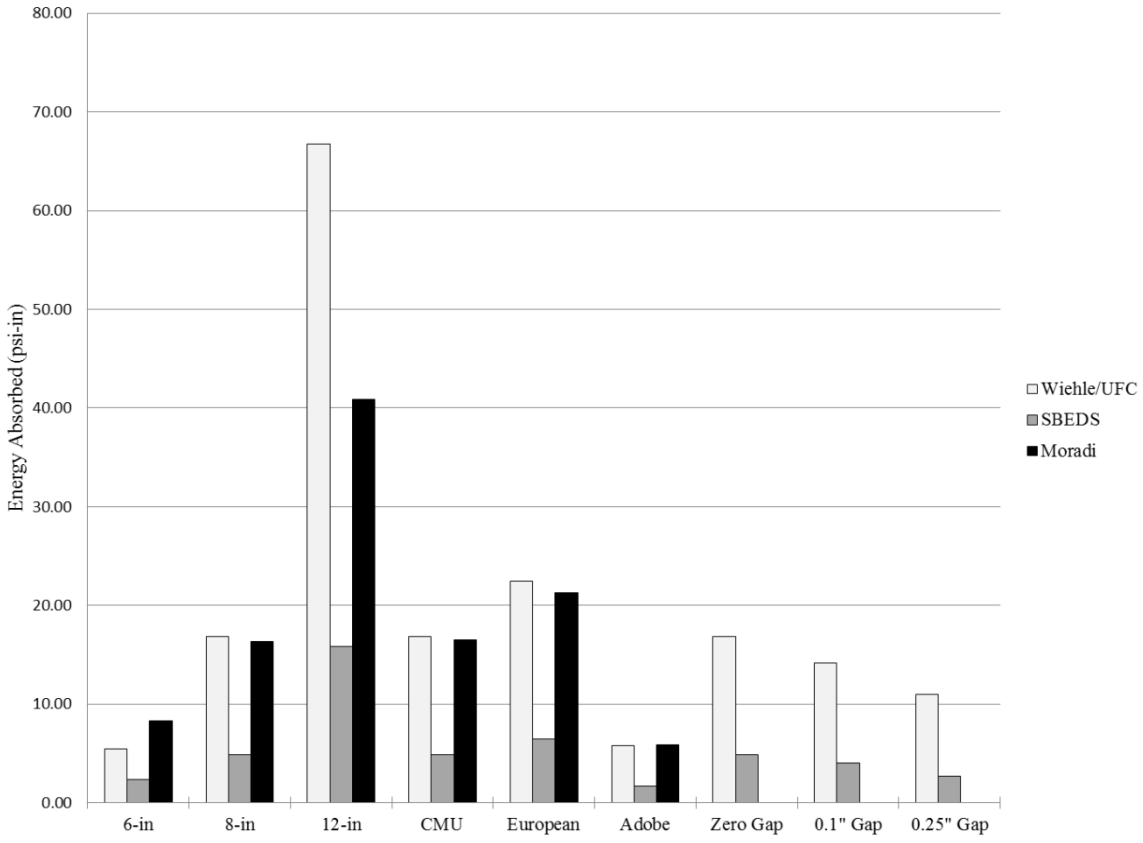

Figure 3.33: Energy Dissipation for Arching Methods

3.4 SDOF Implications

The static resistance function is an integral part of the SDOF model. The concern is not how much energy a wall can dissipate but how much it will deflect under a certain load. The amount a wall deflects must be controlled for blast applications. The response limits proposed by Oswald and Zehrt (2010) are shown in Table 3.7.

Table 3.7: Response Criteria for Masonry Blast Design (Oswald and Zehrt 2010)

Wall Type	Support Rotation (Degrees)		Deflection to Thickness Ratio	
	Category 1	Category 2	Category 1	Category 2
Steel Reinforced Masonry	2.0	8.0	N/A	N/A
Unreinforced Masonry*	1.5	4.0	0.5	0.8
*Only applicable for brittle flexural response followed by compression membrane or axial load arching				

Based on this response criteria a load was selected that would push the limits of a simply supported wall. The loading used is shown in Figure 3.33.

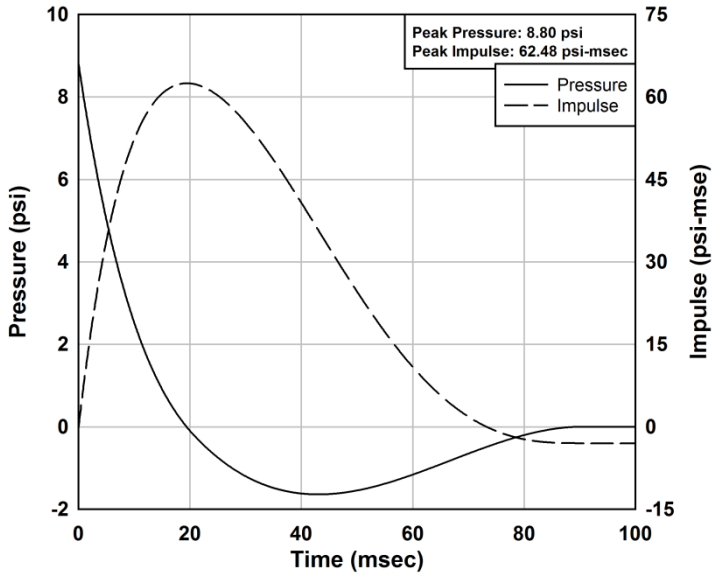

Figure 3.34: Loading used in SDOF

An SDOF model was used to calculate the midspan deflection. Due to the fracturing of CMU during a dynamic load, the properties of the CMU change from the first cycle to the second. The resistance functions do not account for property changes. For this reason the SDOF model is only accurate in determining the first peak. A detailed look at the SDOF process is outlined in Chapter 7. With all of the wall properties

remaining the same as the 8-in CMU wall detailed in Table 3.5 the resistance for each method was plugged into the SDOF model. The results of the dynamic analysis for non-arching walls is shown in Figure 3.35.

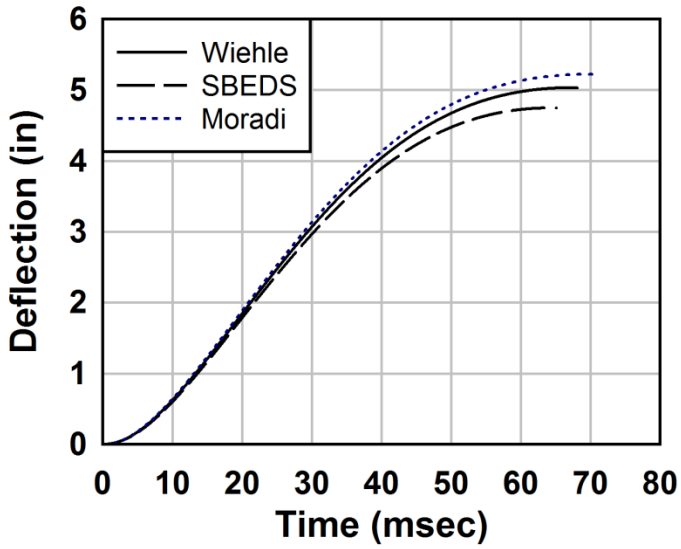

Figure 3.35: Non-Arching Dynamic Response

The Moradi method produces the largest deflection of 5.23 in corresponding to a rotation of 4.2° at the support. The second largest rotation was the Wiehle method with a rotation of 4.0° and lastly was the SBEDS method with a rotation of 3.8°. All three deflections were under the deflection to thickness ratio of 0.8. The percent difference is only 10 percent from the maximum rotation to the minimum. A 10% difference is a reasonable difference given the wide range of assumptions that went into the development of each method.

For arching wall the same loading and wall was used to generate the resistance of the three arching methods. It is expected that the rotation of the arching walls will be less than the non-arching walls since the loading will remain the same. The results of the dynamic analysis for arching walls are shown in Figure 3.36.

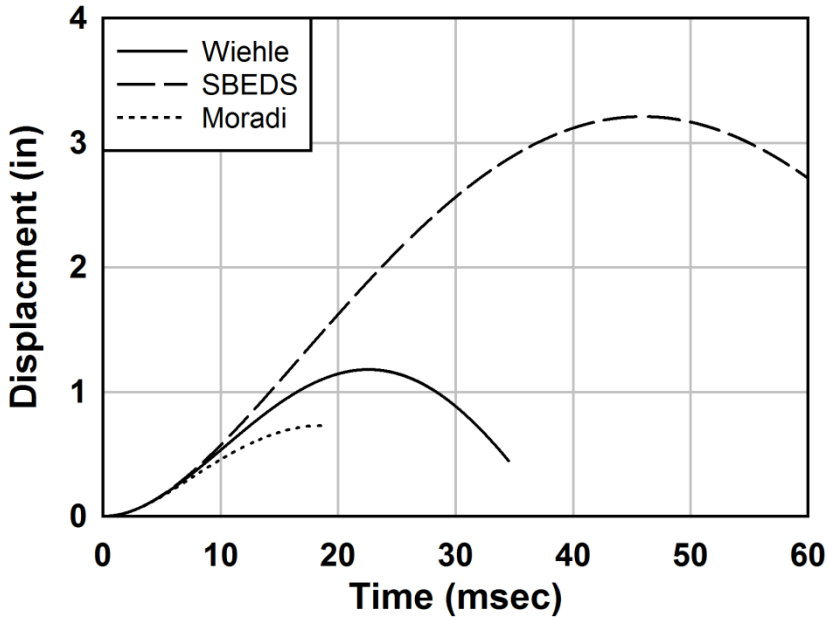

Figure 3.36Arching Dynamic Response

As expected, the deflection of all three arching methods is lower than the deflections observed in the non-arching analysis. There is a large difference in the response of these methods. The method with the lowest deflection is the SBEDS method with a deflection of 3.21 in. and a rotation of 2.6°. The Wiehle method produced the second largest deflection of 1.18 in. and a rotation of 0.94°. The Moradi method produces a deflection of 0.73 in. and a rotation of 0.58°. The difference between the SBEDS method and the Moradi method is 126% and the difference between the Wiehle method and the SBEDS method is 92%. The difference between the Moradi method and the Wiehle method is 47%. These differences are very different and greatly influence the response category the wall will fall into. The Moradi and Wiehle methods fall into Category 1 where the SBEDS method falls into Category 2.

3.5 Dynamic Testing

3.5.1 Testing Overview

A test series was performed by AFRL to investigate the effects that boundary conditions have on plane masonry subjected to blast loading. In this series four walls were constructed all with the same height and wall thickness. Of the four walls constructed, two had non-arching supports and the other two had arching supports. For each support condition, all walls were constructed with 32 lb lightweight blocks. Walls 1 and 3 were constructed as arching walls. Walls 2 and 4 were constructed to simulate non-arching walls. For these non-arching walls, different methods were used to connect the wall to the support that would allow for a horizontal reaction to develop but would not have a moment when the wall rotated. Three support configurations were used. The first used a dowel that would prevent the wall form translating inward but allow rotation at the supports. The second placed the CMU blocks against the support and grouted the gap to prevent any rotation of the wall. The last configuration placed an angle behind the wall. The angle catches the wall and acts similarly to the first configuration. Hoemann et al. (2010) detailed the suggested support conditions shown in Figure 3.37.

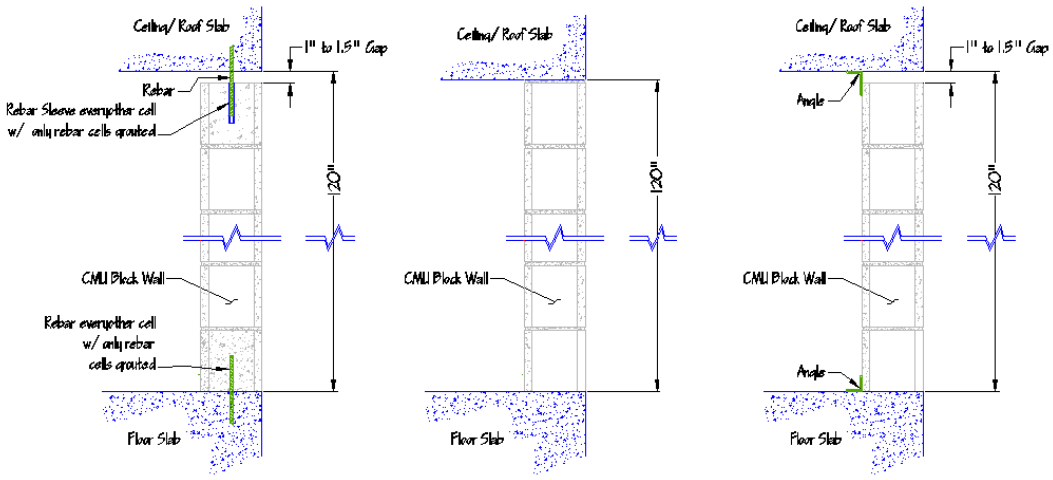

a) Walls 1 and 2 b) Wall 3 c) Wall 4

Figure 3.37: Schematic of Boundary Conditions

The height of all the walls is 120 in. with a wall thickness of 10 in. All the walls were and tested at the same time. The compressive strength of the CMU blocks was reported as 2890 psi and a mortar tensile bond of 100 psi. The support configuration for each wall is shown in Figure 3.37. Pressure gages recorded the pressure for each wall. All four walls had approximately the same pressure.

The loading was the same for each wall. The weight and stand off (distance between explosive charge and wall) was selected to ensure that collapse would not occur. Figure 3.38 presents the normalized measured pressure on Wall 2. The pressure applied to each wall was used in the SDOF model however they are all very similar.

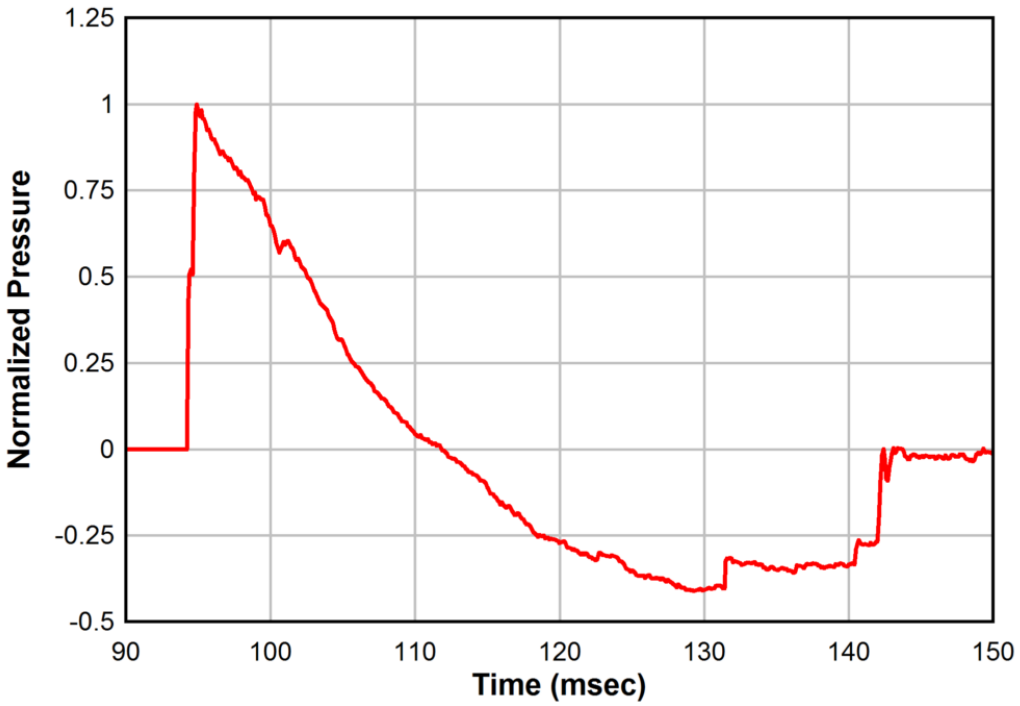

Figure 3.38: Pressure on Wall 2

3.5.2 Dynamic Test Results

Wall 1 exhibited an unexpected response. During the post test inspection it was noticed that the corners of the support framing around the wall were cracked, which likely decreased the stiffness of the wall and allowed for larger deflections. Cracking of the frame is shown in Figure 3.39.

Figure 3.39: Support Cracking of Wall 1

The wall response compaired to the analytical methods is presented in Figure 3.40. Because the support cracked, the largest deflections happened after the first cycle. During the loading significant damage occured in the wall rendering the static resistance function inaccurate after the first peak. This is true for all the resistance curves since cracking of the wall is assumed for all the walls.

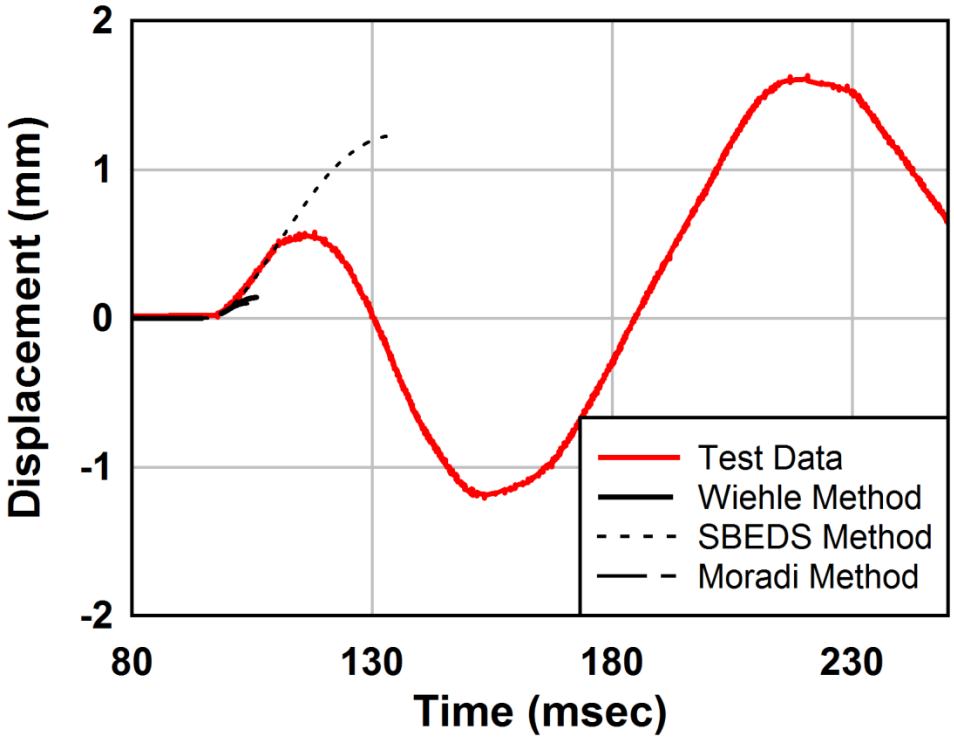

Figure 3.40: Wall 1 Dynamic Response

The SBEDS method produces a much higher deflection while the other two methods generate lower deflections. The maximum deflection of the first phase was 0.54 in. and 1.63 in. for the second phase. The second phase was three times greater than the first phase. The deflection of the negative phase was -1.21 in., 2.24 times larger than the first phase deflection. The maximum deflections for this wall and the other three are reported in Table 3.8.

Wall 2 was constructed with steel dowels grouted into the top and bottom of the wall. It is assumed that the grout in the top and bottom row of the CMU will not add significant resitance. The deflections from the test and the SDOF analysis are shown in Figure 3.41.

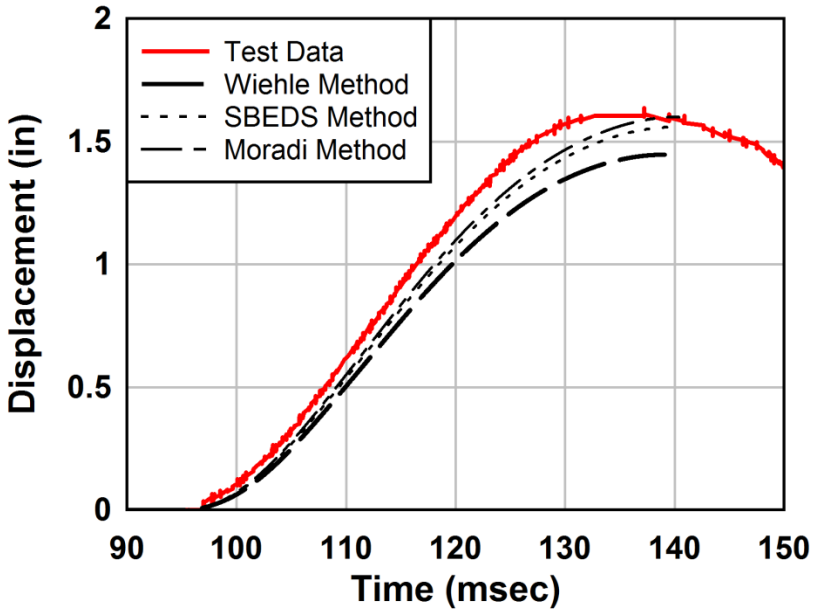

Figure 3.41: Wall 2 Dynamic Response

The deflections generated from the SDOF analysis have a smaller spread and more closely resemble the test results for Wall 2. The methods do not generate significantly different static resistance curves allowing for all three curves to closely resemble one another. The equipment used to measure the deflection stopped at 11.2 msec and continued again at 96.6 msec. Because of this when plotted the response appears to be shifted when it is not. A similar problem occurred with Wall 4.The response of Wall 3 is shown is Figure 3.42. Wall 3 was another arching wall with only the weight of the block and compressive strength changing from Wall 1.

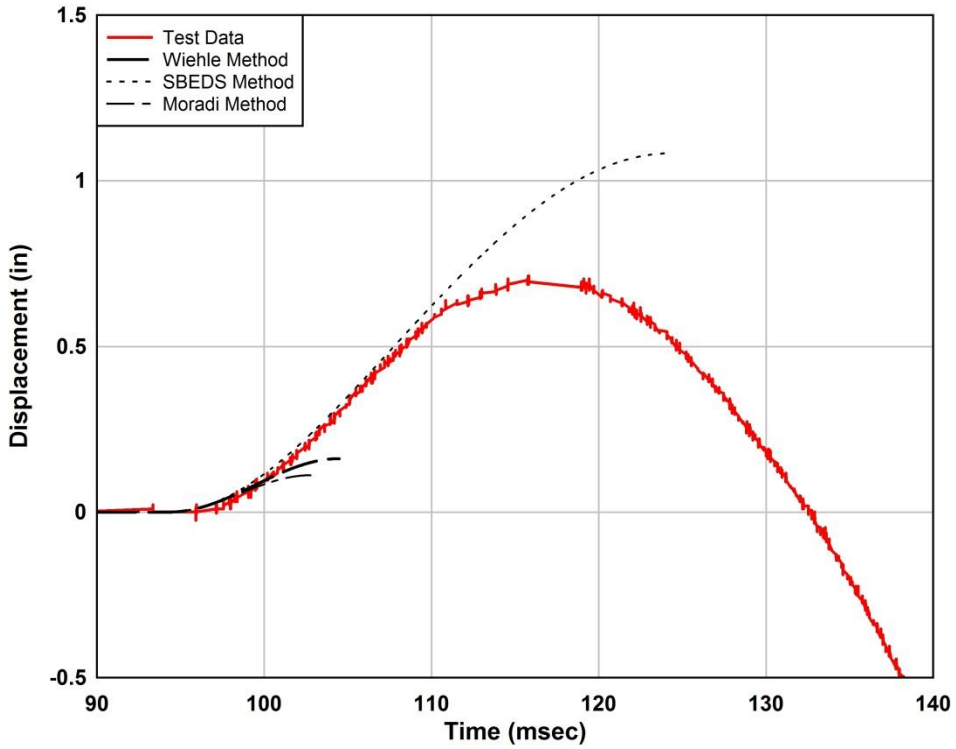

Figure 3.42: Wall 3 Dynamic Response

Wall 3 falls between the SBEDS method and the other two in the same way Wall 1 does. The peak deflection occurs within the first cycle unlike Wall 1 since the support frame did not crack. This could be influenced by the wall being in the center of the support frame where Wall 1 is located at the edge.

Wall 4 was the last wall in this test series and was constructed to represent a non-arching wall. Figure 3.43 shows the boundary conditions of Wall 4.The dynamic response is shown in Figure 3.44.

Figure 3.43 Boundry Condition of Test Wall 4

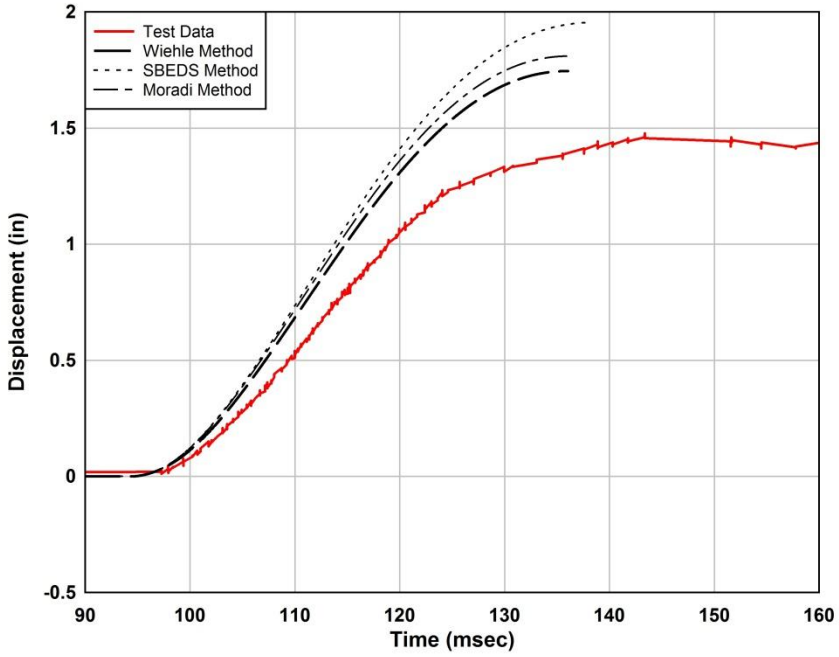

Figure 3.44: Wall 4 Dynamic Response

Wall 4 had a similar response at Wall 2. One important factor is the walls ability to move out of the frame since it is only restrained from moving inward. During the post-

test inspection Figure 3.45 was taken to show how Wall 4 pulled out from the support frame.

Figure 3.45: Wall 4 Pullout of the Frame

This skews the later cycles but does not affect the peak deflection. After the test the wall was pulled 2 in. out of the support frame. All three methods produced deflections greater than the test results.

Table 3.8: Wall Response Comparisons

Wall/ Method	Wiehle	SBEDS	Moradi	Test
	in.	in.	in.	in.
1	0.140	1.23	0.096	0.578*
2	1.446	1.558	1.599	1.636
3	0.161	1.083	0.111	0.782
4	1.746	1.954	1.803	1.478
* Maximum deflection for first cycle only				

Walls 1 and 3, arching walls, have a significant spread with the test data falling in the middle. The first wall has a strange anomaly where the peak deflection occurs on the second cycle. Table 3.8 only lists the deflection of the first cycle; the true maximum deflection is 1.62 in. The SBEDS method was developed with assumptions that overestimating the deflection of the wall. The other two methods produce similar results however these results under predict the maximum deflection making the design unsafe. The non-arching walls, Wall 2 and 4, all had very similar results. This is because the methods used to generate the resistance curves use very similar assumptions and only have slight differences.

3.6 Conclusion

Based on the results presented, conclusions can be made as to which method should be used for design. The non-arching resistance functions produced reasonably close results to the test data whereas the arching methods that over predicted or under predicted the deflection. For design purposes, the method that over predicts deflection will generate a safer design.

The Wiehle method accurately predicted the response of the wall during the dynamic test. For this reason the Wiehle method was chosen as the method to generate the non-arching resistance function in Chapter 7.

None of the arching methods did an accurate job of predicting the response of the wall for the dynamic test. For this reason the method used should generate the safest design without over designing the retrofit. The SBEDS method is the only method that over predicted the deflection. Over predicting the deflection will cause the retrofit to be overdesigned in order to be able to meet the response criteria.

Chapter 4: Comparison of Unbonded Membrane System Analytical Models

4.1 Overview

As previously stated in Chapter 2, three different approaches to the resistance function for the unbonded system have been used and presented in the literature. However, no current used method incorporates the connection ductility in the resistance definition. The development of an analytical method that includes the connections will be discussed in Chapter 5.

The major challenges of developing a resistance function for the membrane are the large displacements and the nonlinear material behavior. The pressure will always act perpendicular to the surface of the membrane. At large displacements, the shape of the surface needs to be known in order to know the force within the membrane that has developed to resist the loading. Since most of the material will exhibit softening the material definition is no longer a linear definition complicating the problem.

It will be shown that these three methods do not coincide with one another but it will be shown that the parabolic method should be used since it coincides with the FE model the most. Because of the large displacements and nonlinear behavior of the material a program should be used to develop a resistance curve since they all require incrementing the deflection or pressure in small steps.

4.2 Cable Analogy Method

The first method developed has the easiest computations. The function was developed for a cable with no flexural resistance subjected to simultaneous lateral and axial loads. This method was presented by Young et al. (2012). The method only uses the cross-sectional area (*A*), length of the membrane (*L*), and the modulus of elasticity (*E*) as a function of stress. The axial tension is assumed to be the only force contributing to the stress. The stress in the membrane is calculated using Equation 4.1, the deflection in terms of pressure can be derived, Equation 4.2. To be able to calculate the stress, the axial force will be needed, Equation 4.3.

$$\sigma = \frac{P_r}{A} \tag{4.1}$$

$$\Delta = L\left(\frac{3pL}{64E_tA}\right)^{1/3} \tag{4.2}$$

$$P_r = \frac{pl^2}{8\Delta} \tag{4.3}$$

Where σ is the stress in the extreme fiber, P_r is the axial load in the retrofit, Δ is the deflection at mid-span, E_t is the tangent modulus of elasticity from the previous step, and p is the uniform lateral load applied. If a unit width is considered, the area of the retrofit reduces to the thickness of the material, $A=t_s$.

This method was originally developed for a linear elastic material. Because of the nonlinear aspect of the material definition an incremental approach was taken. The pressure is incremented and the deflection of that change in pressure is then calculated. To incorporate this additional deflection Equation 4.4 is used.

$$\Delta_i = \sqrt[3]{\Delta^3_{i-1} + \Delta^3_{p,inc}} \qquad 4.4$$

Where Δ_i is the total deflection for that step, Δ_{i-1} is the total deflection from the previous step, and $\Delta_{p,inc}$ is the deflection due to the change in pressure.

The process of developing the resistance curve is detailed in the flow chart in Figure 4.1 and a sample of the calculation is shown in Figure 4.2. The process is continued until the membrane fails. The membrane can fail in one of two ways. The first is if the stress developed within the membrane exceeds the tensile limits of the material. The second failure method is when the membrane exceeds a predetermined displacement. A recommended value for the maximum deflection is between 15 and 20 in. At this displacement the FE model shows that the membrane starts to transition from a parabolic shape to a circular shape. The second reason this deflection is chosen is because the response limits set by UFC 3-340-02 are exceeded at these deflections.

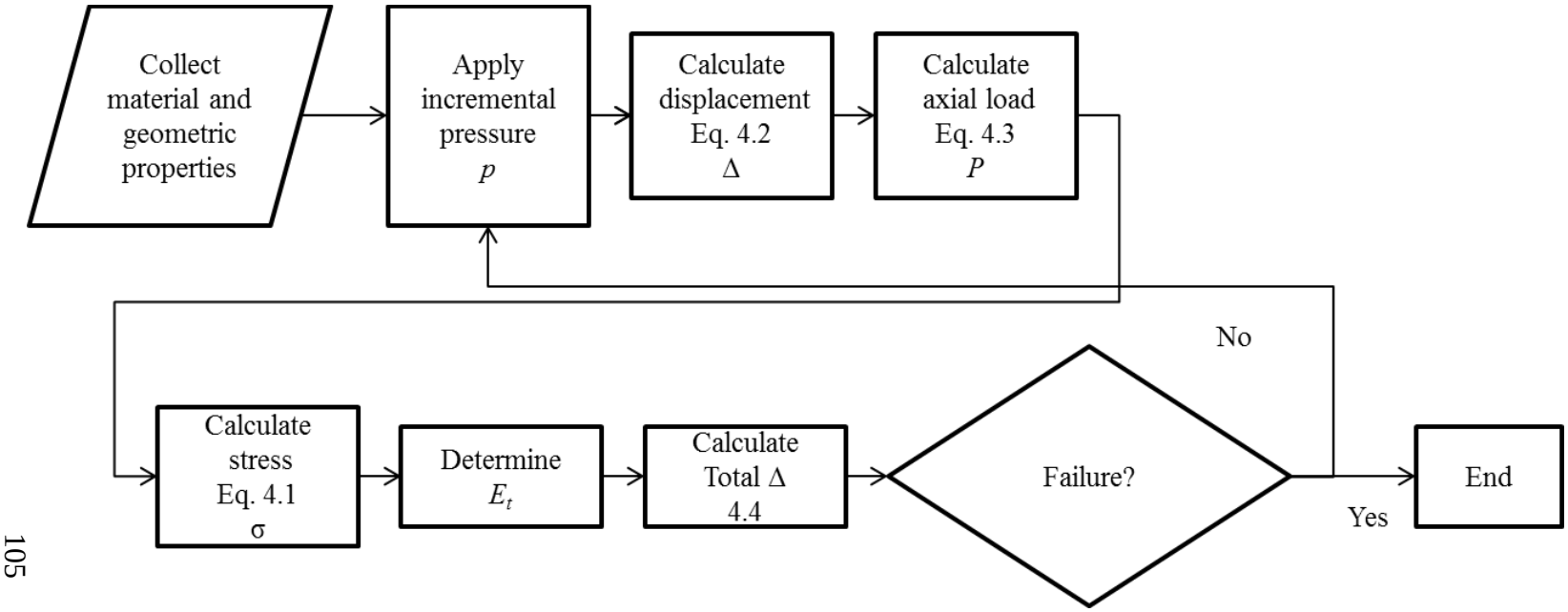

Figure 4.1: Cable Resistance Function Development

L				120	in	
Area				0.079	in^2/in	
Thickness				0.079	in	

Lateral Load	Et (psi)	Δp (psi)	δ from Δp (in)	Total Deflection (in)	Axial Load (lb)	Stress (psi)
0	0	0	0.000	0.000	0.0	0
0.01	1269080	0.01	0.991	0.991	18.2	231
0.02	1269080	0.01	0.991	1.248	28.8	366
0.03	1269080	0.01	0.991	1.429	37.8	480
0.04	1269080	0.01	0.991	1.573	45.8	581
0.05	1269080	0.01	0.991	1.694	53.1	675
0.06	1269080	0.01	0.991	1.800	60.0	762

Figure 4.2: Sample Calculation for Cable Method

4.3 Seide Resistance Function

Paul Seide (1977) generated a formula for large deflections of rectangular membrane. The membranes are assumed to have edges that are fixed against rotation but with no in-plane shear stress and fixed from translation. All edges have these support conditions, which is not how the membrane is attached in reality. The formula developed works reasonably well for walls with larger width to length ratios (Seide 1977). For this reason, Sudame (2004) chose to use this formula to compare to finite element models of a retrofit system. The formula created by Seide (1977) is the simplest method for generating a resistance curve. The two formulas used to generate the resistance curve are Equation 4.5 and Equation 4.6. Equation 4.5 is a constant used to simplify the calculations.

$$j = \sqrt[3]{3*(1-\upsilon^2)} \tag{4.5}$$

The formula for center deflection of the plate in terms of pressure is:

$$\Delta = \frac{j}{4}\, t_s \sqrt[3]{\frac{p\, b^4}{E_t\, t_s^4}} \tag{4.6}$$

In these equations, v is Poisson's ratio, Δ is the center deflection, t_s is the thickness of the membrane, p is the lateral pressure, E_t is the tangent modulus of elasticity and b is the unsupported length of the membrane (Sudame 2004). The strain should be calculated to determine if the membrane has exceeded its ultimate strength and to determine the tangent modulus of elasticity. A formula proposed by Sudame (2004) for the strain at mid-span is presented as Equation 4.7.

$$\varepsilon = \frac{t_s}{2j}\left(\frac{pb}{Et_s}\right)^{\frac{2}{3}} \qquad 4.7$$

This strain definition does not reasonably represent the strain compared to the other methods. For this reason the strain is calculated the same way as the parabolic method presented in section 4.3. The research done by Sudame (2004) concluded that the formula closely resembled the resistance of the finite element model. The analytical function overestimated the pressure by about 5% to 10% around 15 in of deflection (Sudame 2004). The process for developing a resistance curve is simple with the process shown in Figure 4.3. The failure limits are the same as those specified in Section 4.2.

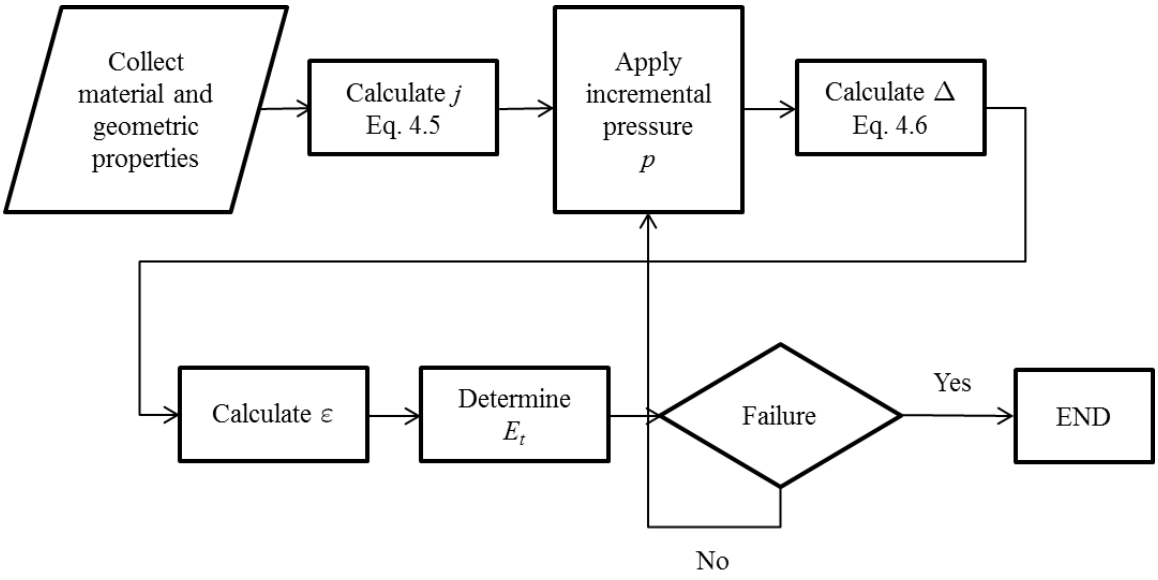

Figure 4.3: Flowchart for Seide Resistance Curve

4.4 Parabolic Deflection Method

The method developed by Lane (2003) assumes that the membrane with a unit width deflects in a parabolic shape. This method starts by using geometric properties to

assess how the membrane reacts and then correlates the change in length to strain and stresses to determine the pressures in the membrane. This method is one of the most widely used methods by researchers to compare experimental works to an analytical model. This model is used by Lane (2003), Fitzmaurice et al. (2006), Salim et al. (2007), Johnson et al. (2009) and Hoemann et al. (2010). The development of this method uses the midspan of the membrane as the origin, refer to Figure 4.4. Assuming a parabolic shape, the general form of the equation is:

$$y(x) = Ax^2 + Bx + C \tag{4.8}$$

Using the boundary conations below, *A*, *B*, and *C* can be determined.

$$\begin{aligned} y'(x) &= 0 \text{ at } x = 0 \\ y(x) &= \Delta \text{ at } x = 0 \\ y(x) &= 0 \text{ at } x = L/2 \end{aligned} \tag{4.9}$$

The slope of the membrane is need and found by taking the first derivative of the general form giving:

$$y'(x) = 2Ax + B \tag{4.10}$$

Using Equations 4.8 and 4.10 and substituting the boundary conditions into them, the coefficients can be determined.

$$\begin{aligned} A &= -\frac{4\Delta}{L^2} \\ B &= 0 \\ C &= \Delta \end{aligned} \tag{4.11}$$

Substituting the coefficients back into Equations 4.8 and 4.9 results in:

$$y(x) = \Delta\left(1 - 4\left(\frac{x}{L}\right)^2\right) \tag{4.12}$$

$$y'(x) = -\frac{8\Delta}{L^2}x \tag{4.13}$$

The next step in deriving the resistance function is to solve for the arc length as a function of mid-span deflection. The equation for arc length is:

$$L' = 2\int_0^{L/2}\sqrt{1+(g'(x))^2} \tag{4.14}$$

Substituting 4.11 in for *g'(x)*, the arc length of the membrane can be solved.

$$L' = \frac{4\Delta}{L}\left[\sqrt{\frac{L^2}{4}+\frac{L^4}{64\Delta^2}}+\left(\frac{L^3}{32\Delta^2}\right)\ln\left(\frac{L}{2}+\sqrt{\frac{L^2}{4}+\frac{L^4}{64\Delta^2}}\right)-\left(\frac{L^3}{32\Delta^2}\right)\ln\left(\frac{L^2}{8\Delta}\right)\right] \tag{4.15}$$

The arc length is used to determine the strain in the membrane at each iteration using Equation 4.16.

$$\varepsilon = \frac{L'-L}{L} \tag{4.16}$$

Using a true stress-strain curve the stress can be determined. Using the FBD in Figure 4.4, the next step is to sum the forces in the y-direction in order to relate pressure to a known variable.

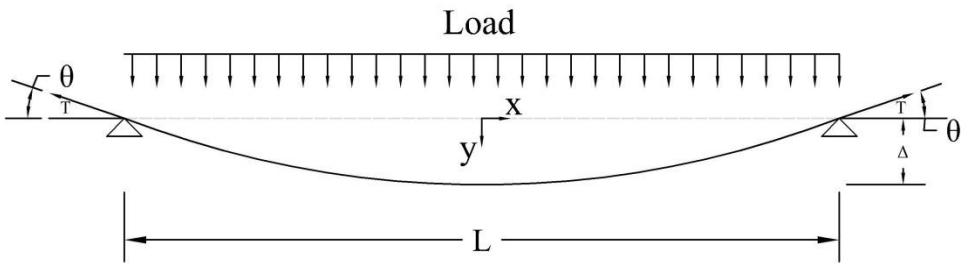

Figure 4.4: Free-Body Diagram of Deformed Membrane

$$\sum F_y = 0 = pL - 2T\sin(\theta) \tag{4.17}$$

Substituting equation 4.11 in to 4.17 and solving for θ results in:

$$2T\sin\left(-\frac{8\Delta}{L^2}x\right) = pL \tag{4.18}$$

It can be shown that $T=\sigma A$ where A is the area of the membrane. If only a unit width is considered the area of the membrane can be reduced to $A=t_s$ where t_s is the thickness of the membrane. Since the angle of interest is at the ends, $L/2$ can be substituted in for x. Implementing these substitutions and solving for pressure gives:

$$p = \frac{2\sigma t_s}{L}\sin\left(\frac{4\Delta}{L}\right) \tag{4.19}$$

This process is complex and requires a true stress true strain curve. The process for creating a resistance curve is detailed in the flow chart in Figure 4.5.

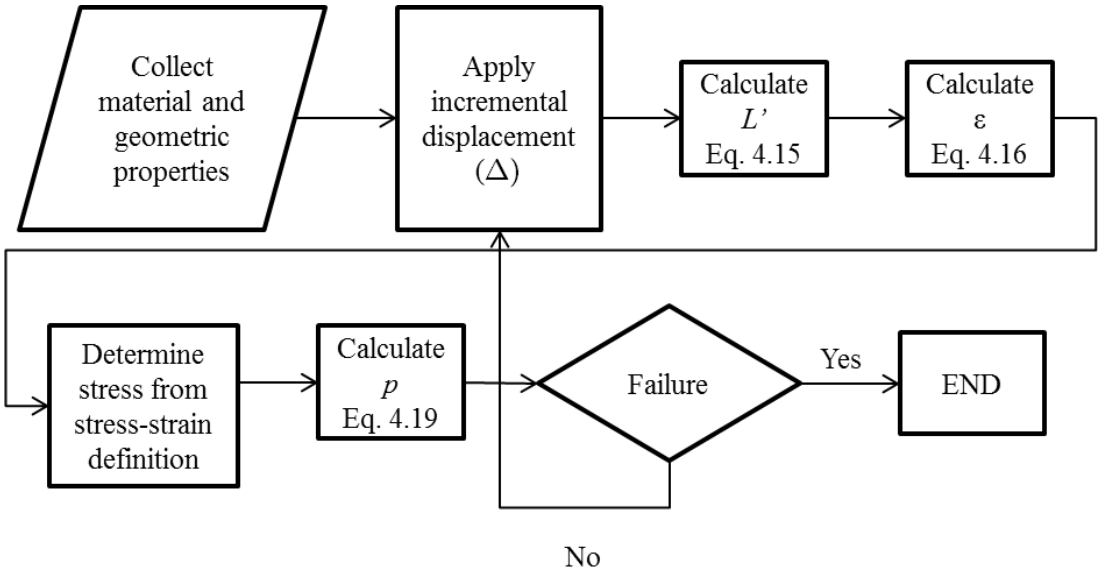

Figure 4.5: Flow Chart of Lane's Resistance Curve

4.5 Stress Strain Conversion

Johnson et al. (2009) discuss the importance of using the true stress conversion from the coupon test. The engineering stress/strain relationship does not consider the change in cross-sectional area as the specimen elongates. The true stress of a material will be larger because of the decrease in area. This larger stress will generate a greater pressure for the same deflection according to Johnson et al. (2009). However, the strain conversion was not considered. Engineering strain is calculated from the arc length and used to find the true stress in the material. The proper way to use the stress strain curve is to use the engineering stresses if the area is assumed constant or to update the area of the membrane and convert the strain values as well.

The engineering strain is only valid for small displacements. As the strain increases the cross-sectional area decreases. Some of the materials considered can have rupture strains of several hundred percent. There is one method to achieve true strain and is derived in Equation 4.20.

$$\varepsilon_t \equiv \int_{L_0}^{L_f} \frac{dL}{L} = \ln(L)\Big|_{L_0}^{Lf} = \ln(L_f) - \ln(L_0) = \ln\left(\frac{L_f}{L_0}\right) \quad 4.20$$

Two methods have been developed to convert engineering stress into true stress. The difference between these methods depends on the use Poisson's ratio. The first method does not use Poisson's ratio. Constant volume is assumed and there are no localized deformations for the first method. This method is derived in Equations 4.21 through Equation 4.24.

$$AL = A_0 L_0 \quad 4.21$$

$$\frac{A_0}{A} = \frac{L}{L_0} \text{ where } \frac{L}{L_0} = \frac{L_0 + \Delta L}{L_0} = 1 + \frac{\Delta L}{L_0} = 1 + \varepsilon_e \quad 4.22$$

$$\therefore A = \frac{A_0}{1 + \varepsilon_e} \quad 4.23$$

$$\sigma_t = \frac{P}{A} = \frac{P}{A_0}(1 + \varepsilon) \quad 4.24$$

Where L_0 and A_0 are the initial length and cross-sectional area, P is the axial load, σ_t is the true stress, ε_e is the engineering strain. The second method looks at the change in cross-sectional area and incorporates Poisson's ratio. The second method for converting stress is derived below.

$$\sigma_e = \frac{P}{ab} \quad 4.25$$

$$\sigma_t = \frac{P}{a'b'} \tag{4.26}$$

$$\text{if } \nu_x = \nu_y = \nu_z \tag{4.27}$$

$$-\nu = \frac{\varepsilon_{t,y,z}}{\varepsilon_{t,x}} \tag{4.28}$$

$$a' = a - \nu\varepsilon_{t,x}a = a(1-\nu\varepsilon_{t,x}) \tag{4.29}$$

$$b' = b - \nu\varepsilon_{t,x}b = b(1-\nu\varepsilon_{t,x}) \tag{4.30}$$

$$A' = a'b' = ab(1-\nu\varepsilon_{t,x})^2 \tag{4.31}$$

$$P = \sigma_e A_0 \tag{4.32}$$

$$\sigma_t = \frac{\sigma_e A_0}{A'} = \frac{\sigma_e ab}{ab(1-\nu\varepsilon_{t,x})^2} = \frac{\sigma_e}{(1-\nu\varepsilon_{t,x})^2} \tag{4.33}$$

The effects of Poisson's ratio can change the outcome substantially. Figure 4.6 shows how these two methods vary. The first method is referred to as the logarithmic stress/strain method and the second is the Poisson's ratio method.

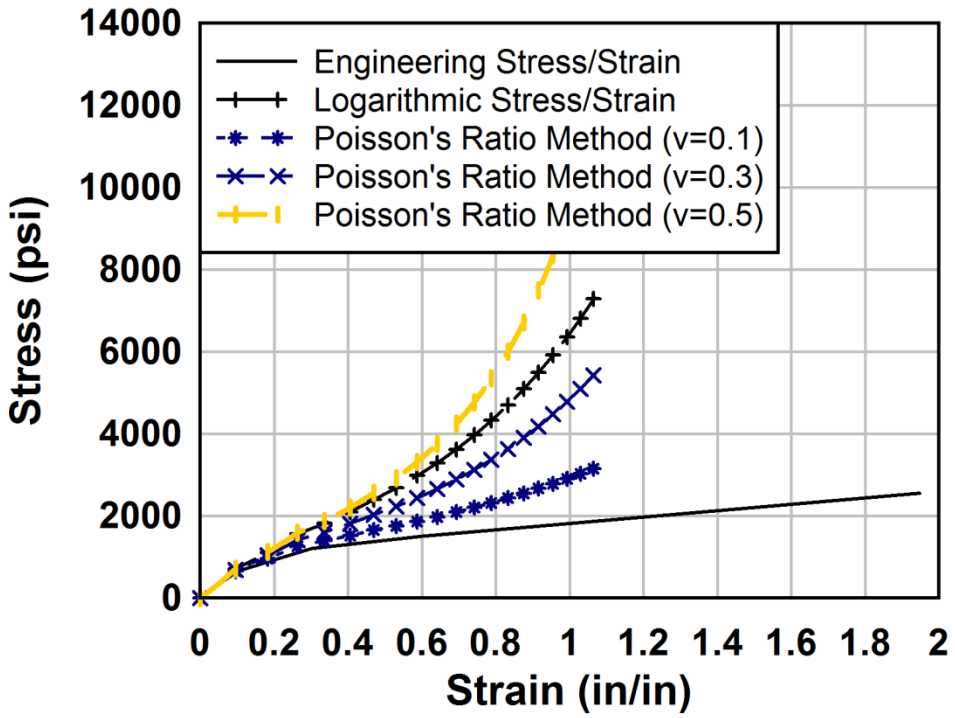

Figure 4.6: Stress Conversion Comparison

While the selection of the proper conversion method is important for high strains there is a limit to the amount of deflection that the wall can exhibit. At a rotation of 16°, double the allowable rotation, for a 10 foot wall the deflection is 17.2 in. and corresponds to a strain of 0.051 in/in. This strain is low enough that the various methods do not have a significant impact.

4.6 Comparison of Resistance Functions

These three methods produce very similar resistance curves. Figure 4.7 is the true-stress true-strain definition used to compare these methods. Figure 4.8 shows how these methods compare to one another. Using a retrofit system that has the properties:

L=120 in

Thickness=0.079 inches

Modulus of Elasticity = 610,000 psi

Yield stress = 2500 psi

Poisons Ratio (ν) = 0.2

And the stress-strain curve in Figure 4.7

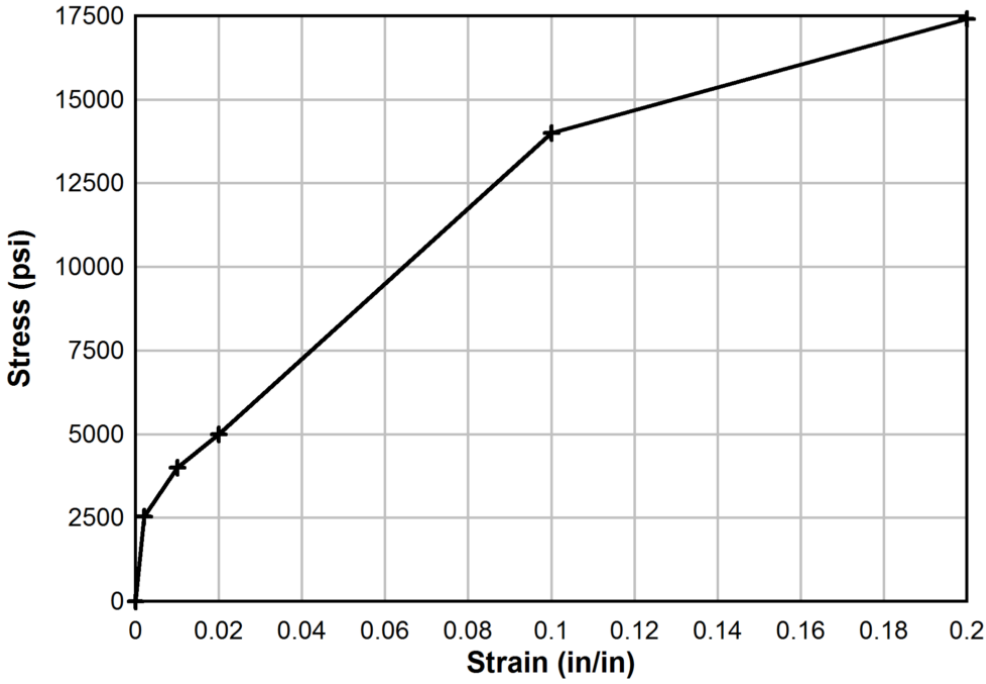

Figure 4.7: True Stress-Strain Curve for Polypropylene

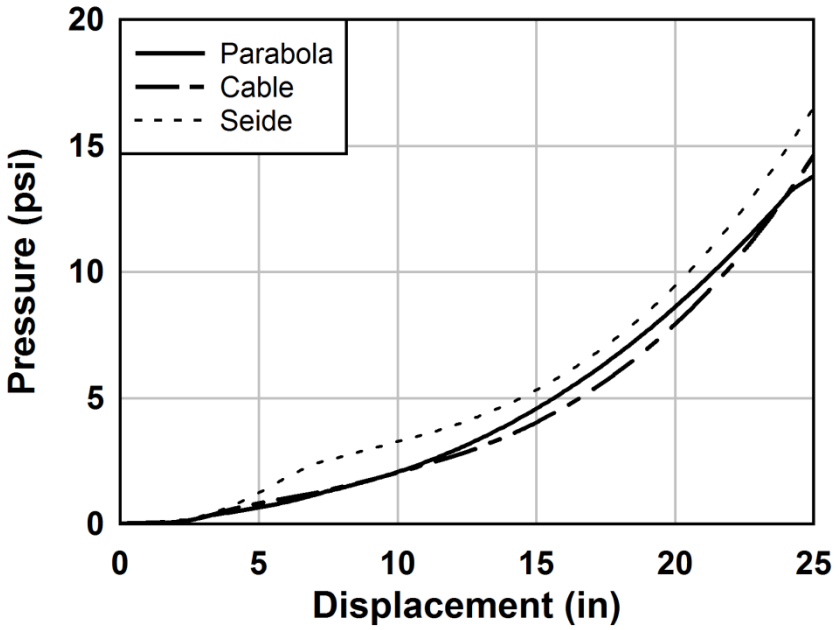

Figure 4.8: Comparison of Membrane Resistance Curves

These methods all produce similar resistance curves despite the different assumptions.

The material used changes how the resistance curves function. How these methods are effected by the use of a different material is shown in Figure 4.9. Using A36 steel greatly increases the elastic phase of the area under the curve.

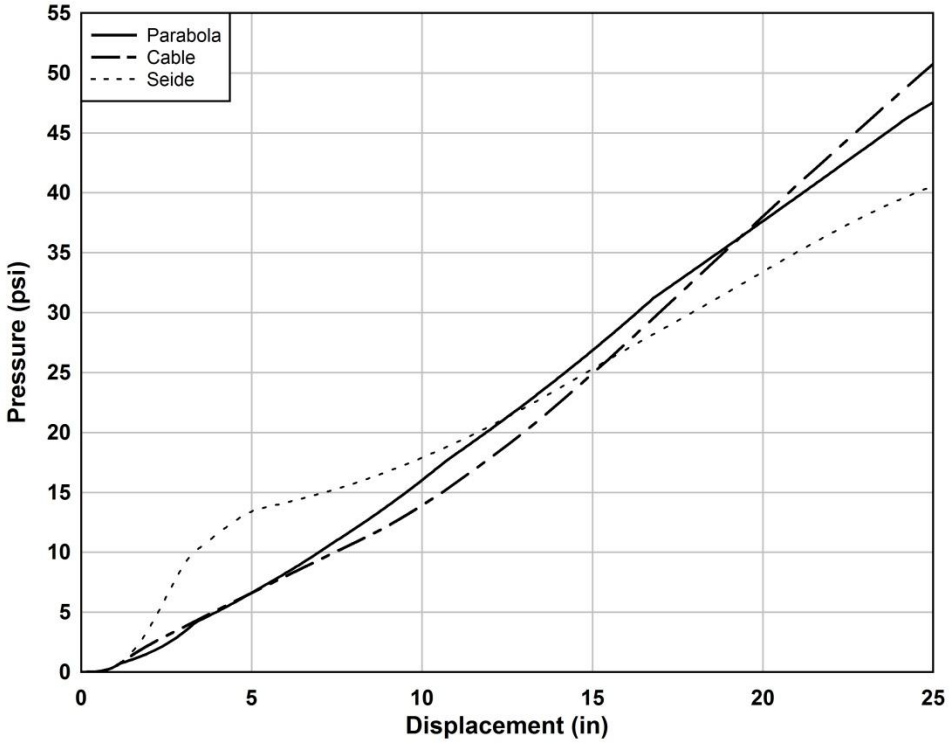

Figure 4.9: Steel Membrane Resistance Curve Comparison

The steel has a higher modulus of elasticity and will allow for much larger pressures to be developed for the same thickness. At 15 in. of deflection all the methods produce a pressure of about 25 psi compared to 5 psi for the polypropylene.

A second important comparison between the models is the height of the wall. The example wall was a 10 ft membrane. A smaller wall will allow for a larger development of pressures and can affect the way the resistance functions develop. A 6-ft wall was chosen to compare how these curves react. This dimension was not selected as a real world example but merely to demonstrate the difference. The effect of wall height on the resistance methods is shown in Figure 4.10.

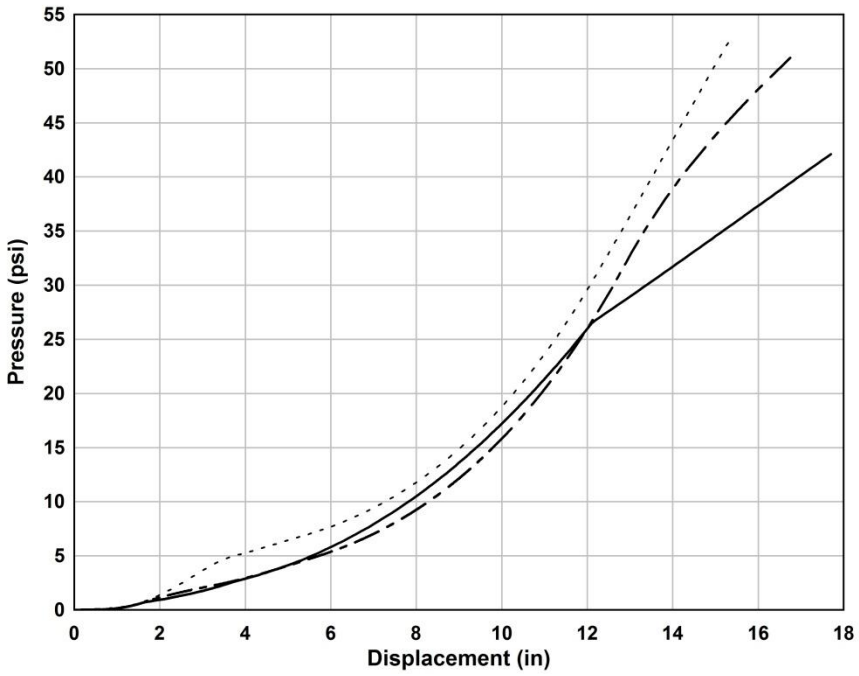

Figure 4.10: Membrane Resistance Curve for 6-ft Wall

The shorter membrane increases the pressures allowed on the wall. The general shape and slopes do not appear to have changed.

The ability to change variables and have a complete resistance curve is imperative. Each system is unique and should be designed as such. For design purposes using the model that produces the strongest wall may reduce the cost of the retrofit but may overestimate the strength of the material while underestimating the deflection. Figure 4.11 illustrates how changing a variable affects the resistance curve for all three methods.

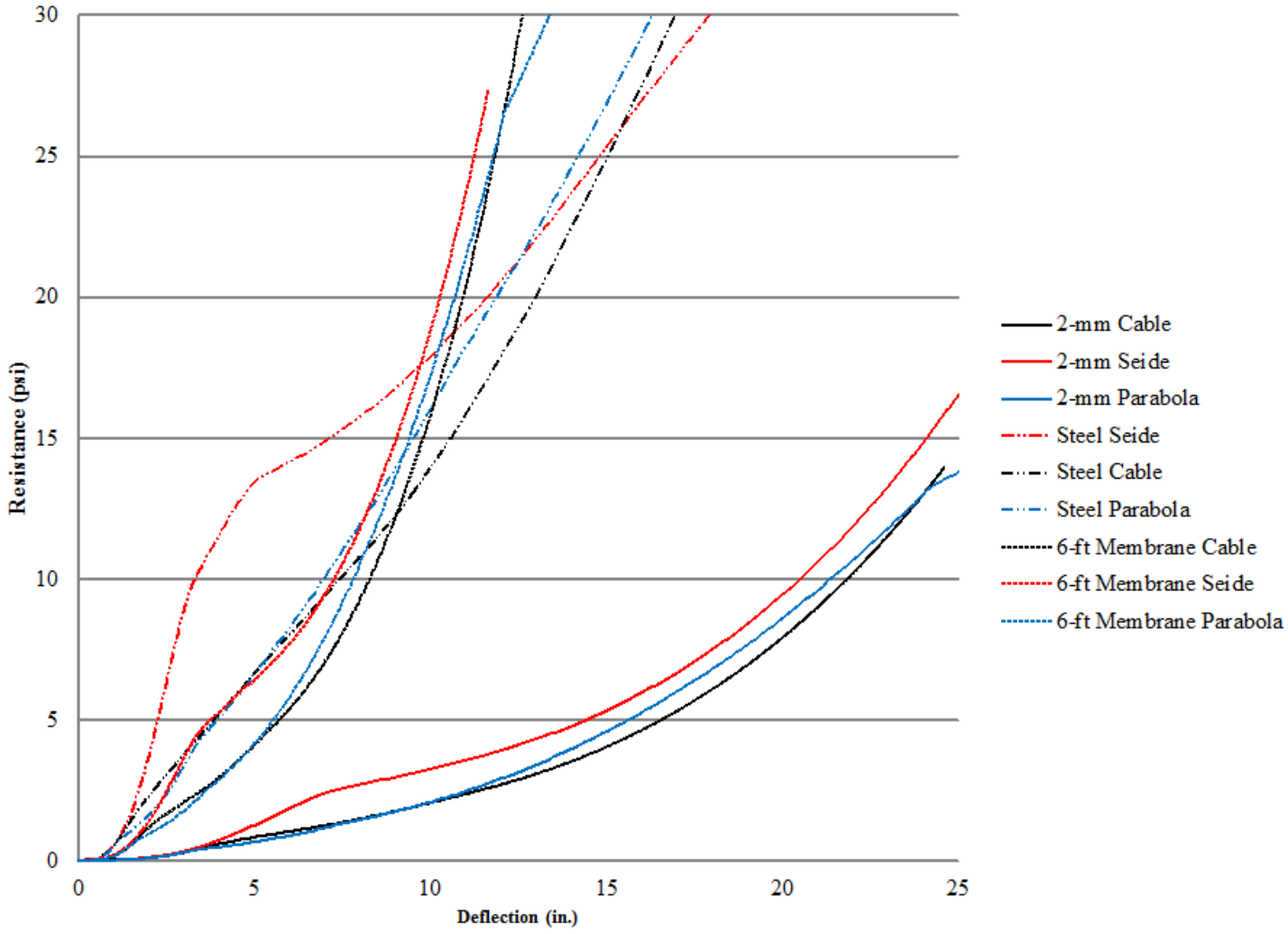

Figure 4.11: Complete Comparison of Resistance Functions with Changing Variables

It is shown that using a shorter membrane with a higher modulus of elasticity and yield point will decrease the deflection of the membrane. These methods tend to follow one another closely. Any could be used for design purposes if only the membrane is considered. However, for the purpose of incorporating the connections a more rigorous method is needed.

The method proposed by Lane (2003) has been studied extensively. Kennedy (2005), Salim et al. (2006 and 2007) Fitzmaurice et al. (2006) and Johnson et al. (2009) have all performed test to evaluate this analytical model. Many of the tests concluded that the analytical model represents the membrane sufficiently. There are some deviations due to the connection ductility and testing errors. At large deflections the 16 point loading frame slips and skews the results (Fitzmaurice 2006).

4.7 Finite Element Validation of Membrane Methods

Abaqus/Standard was used to conduct all finite element modeling. Finite element modeling was done in three stages. The first stage was to compare all the methods described in Chapter 4 assuming a linear stress strain relationship. The second stage compared all the membrane resistance functions for nonlinear stress strain relationships. The final stage was to validate the algorithm detailed in Chapter 5.

4.7.1 Linear Material Definition Validation

For the linear material definition, the membrane was defined using shell elements. A 120 in x 120 in membrane was created. The top and bottom edges were confined using pinned boundary conditions. All nodes were constrained to prevent transverse movement.

This boundary condition was used to simulate an infinite wall. 1 in. x 1 in. elements were created generating 900 elements and 961 nodes, shown in Figure 4.12. Geometric nonlinear effects were taken into account in the FE model.

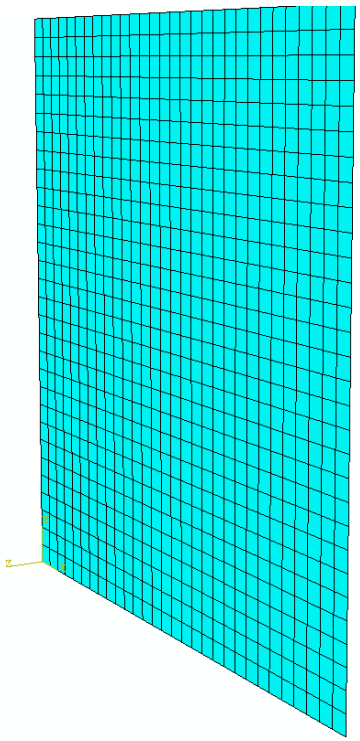

Figure 4.12: Membrane Mesh

The membrane thickness was defined as 0.039 in. and the modulus of elasticity used was 1270000 psi. A lateral pressure was applied and the pressure vs. displacement of the midspan node was plotted against the different resistance definitions, Figure 4.13.

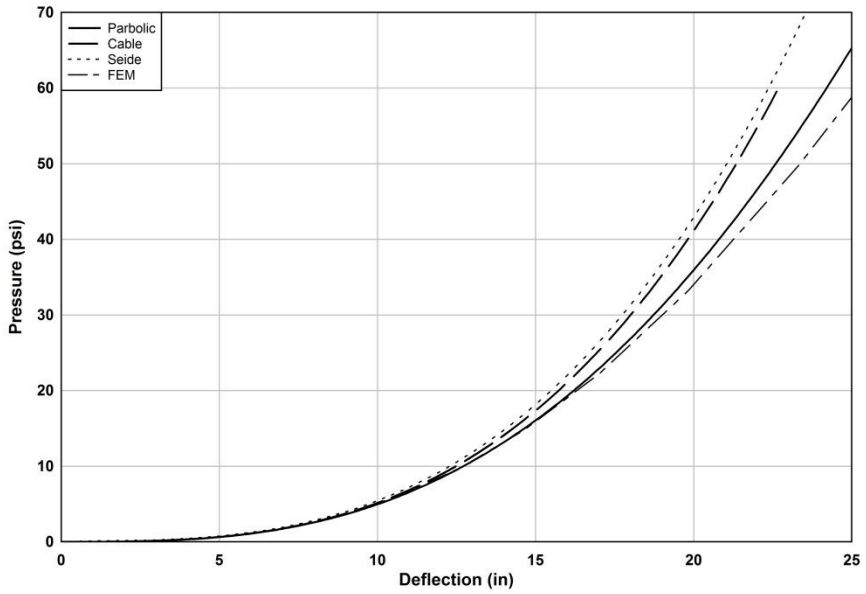

Figure 4.13: Linear Material Resistance Curves

The FE model corresponds well with all the methods. The parabolic method however was closer to the FE results. At larger deflections, the parabolic method deviates slightly due primarily to the change in shape of the membrane. At large deflections and pressures the membrane assumes a cylindrical shape rather than a parabolic shape that is assumed, Figure 4.14.

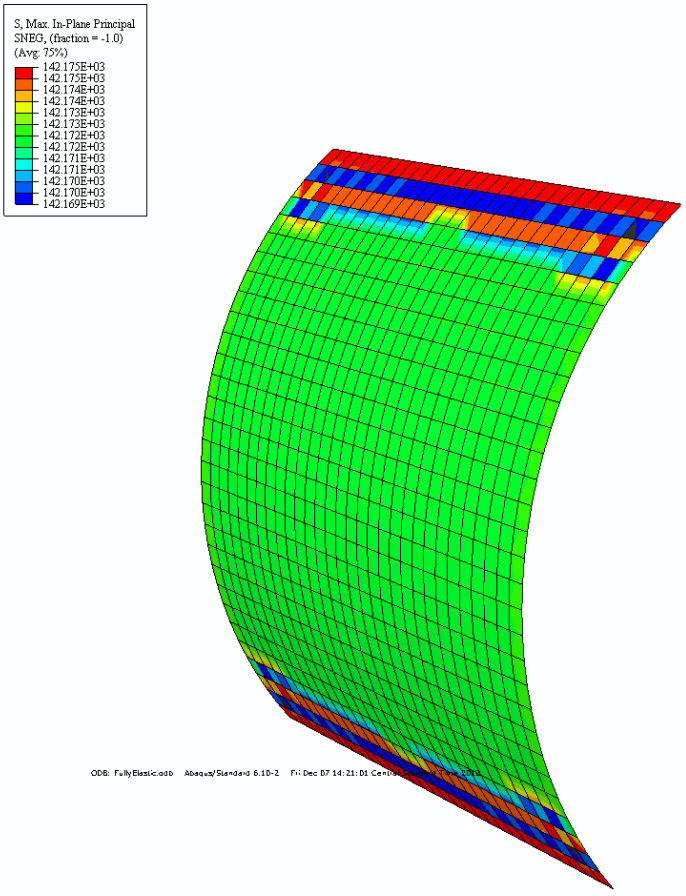

Figure 4.14: In-Plane Stresses of Membrane at 60 psi

The strain is assumed to be constant throughout the height of the membrane in all the algorithms. The FE results show this may not be true; however the percent difference is only 0.004%.

4.7.2 Nonlinear Material Definition Validation

For the nonlinear material modeling, the elastic model was used where only the material properties were changed to allow for a plastic definition to be defined. The stress strain points used for both the FE model and the algorithms is presented in Figure 4.15.

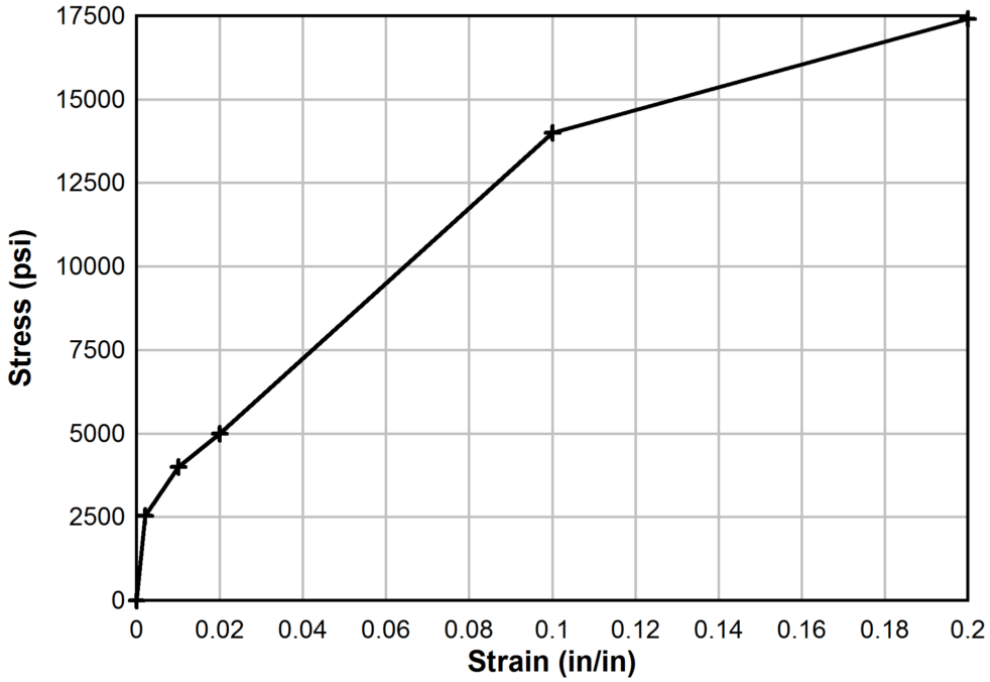

Figure 4.15: Stress Strain for Nonlinear Material Comparison

A more robust definition of the material could be used in the algorithms however the FE model has difficulty with a large amount of data points in the stress strain definition. For comparison purposes however a simple definition will suffice. The results were plotted against the same methods, Figure 4.16, and the same stress-strain points were used in the numerical method.

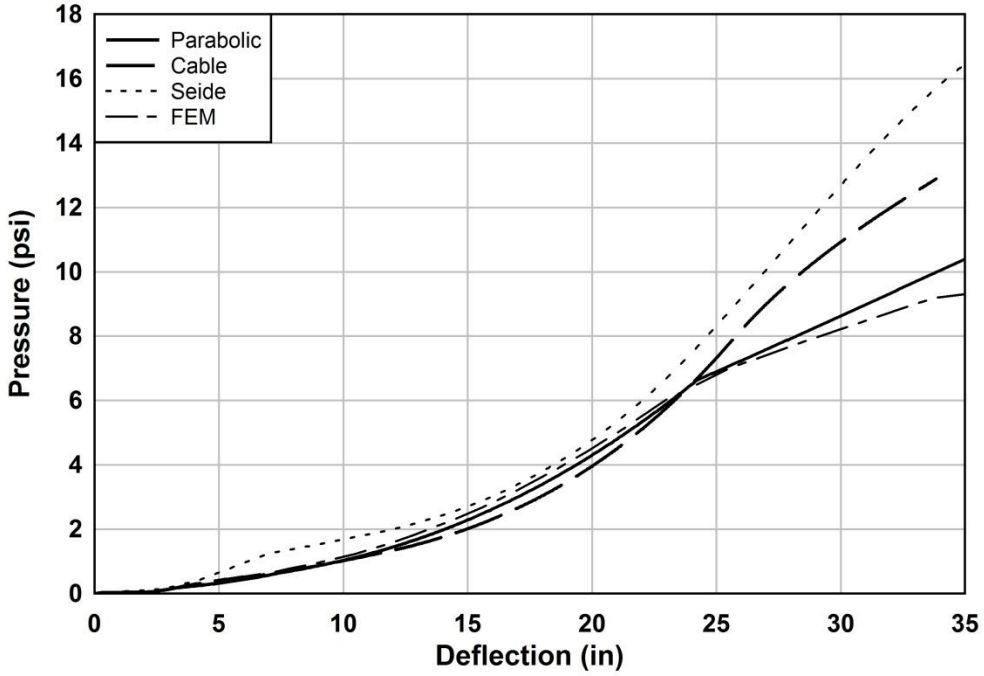

Figure 4.16: Nonlinear Material Comparison

Similar to the linear analysis, the parabolic method better correlates to the FE model. The cable method as well as the Seide method have some difficulties when the stress strain diagram is not perfectly linear. These methods were adapted from their specified use to be able to use a tangent modulus instead of a constant modulus of elasticity. It is assumed that the stress in the membrane is constant throughout the length. Figure 4.17 shows the FEM results of the principal stress throughout the membrane.

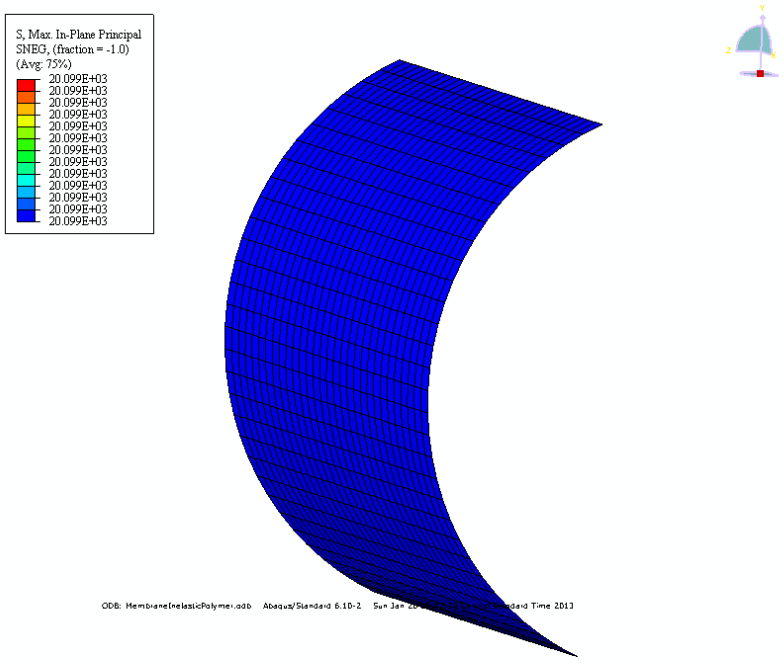

Figure 4.17: Principal In-Plane Stresses for Nonlinear Model

The stresses in the membrane are completely uniform for the nonlinear material definition. The deflected shape at 20 psi shows the non-parabolic shape that result in very large pressures.

Chapter 5: Resistance Function Incorporating Connections

5.1 Overview

Many laboratory tests have been performed to understand how the connection will affect the ductility of the retrofit system (Fitzmaurice et al. 2006, Salim et al. 2007, Johnson et al. 2009, and Hoemann et al. 2010). Johnson et al. (2009) conducted a loading tree test on several samples of a polypropylene composite with several connection configurations. It was observed that the test produced a much more ductile system than the analytical models when the connections are not considered.

Considering an unbonded system with a simple plate that does not allow for local stresses concentrations at the corner of the plates, an analytical model was developed to incorporate the membrane and the connections as one system. The analytical model will be compared to a finite element analysis.

5.2 Unbonded Retrofit Connection Resistance Function Development

To develop a resistance curve for an unbonded retrofit system, the first step was to determine what method should be used for the resistance of the membrane. The parabolic method was chosen because of its accuracy. It is assumed that the membrane will react the same with and without the connections and that the plates will add flexibility to the system as it is bent upwards.

Two significant assumptions were needed to define how the plates will react to the loading. The first is that the plate will be made of a material that behaves elastic-

perfectly plastic and forms a plastic hinge. The second assumption is that the plate can be modeled as a cantilever beam with the fixed support being at the location of the center of the bolt. This assumption is illustrated in Figure 5.1 along with the anticipated curvature of the plate.

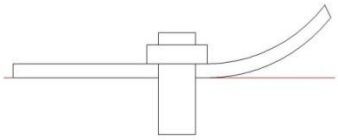

Theoretical Behavior

Static Loading

(Johnson 2009)

Blast Testing by AFRL

Figure 5.1: Plate Response

Depending on the state of the plate, elastic or plastic, one of two methods is used. If the plate is elastic a small displacement is added to the membrane and the rotation of the plate is calculated and the additional displacement from the plate is added to the total displacement. If the plate has reached its plastic moment capacity, a small rotation of the plate is added. With this new rotation, the tension in the membrane is solved, which will generate the plastic moment in the plate. How the plate moves with respect to the elastic and plastic phase is illustrated in Figure 5.2.

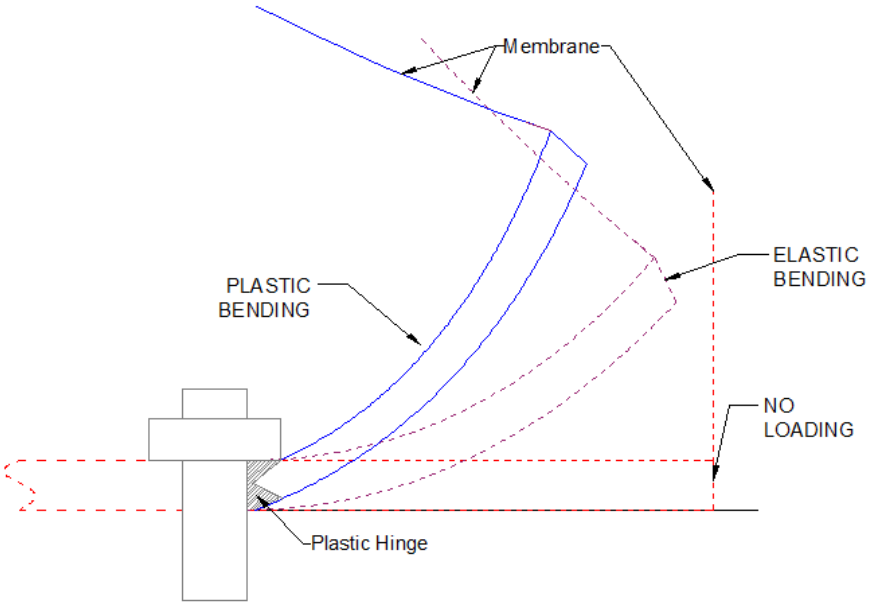

Figure 5.2: Rotation of the Plate for Elastic and Plastic Phases

To start the development of the resistance curve of the retrofit system is similar to the membrane resistance curve. A small displacement, γ, of the membrane is placed on the system and the arc length, L', of the membrane is calculated using the distance between the tips of the plates as L_i. If there is no slack in the system, the initial length and the distance between the supports are the same. At the first iteration $\gamma=\Delta$.

$$L_i' = \frac{4\Delta}{L}\left[\sqrt{\frac{L_i^2}{4}+\frac{L_i^4}{64\Delta^2}}+\left(\frac{L_i^3}{32\Delta^2}\right)\ln\left(\frac{L_i}{2}+\sqrt{\frac{L_i^2}{4}+\frac{L_i^4}{64\Delta^2}}\right)-\left(\frac{L_i^3}{32\Delta^2}\right)\ln\left(\frac{L_i^2}{8\Delta}\right)\right] \qquad 5.1$$

Using the arc length and the original length of the membrane the true strain in the membrane can be calculated.

$$\varepsilon = \ln\left(1-\frac{L_i'-L}{L}\right) \qquad 5.2$$

With this new strain the thickness of the membrane can be updated to account for Poisson's effect.

$$t_i = -\nu\varepsilon t + t \tag{5.3}$$

Using a true stress-strain curve the stress in the membrane can be determined. This process can be adapted if engineering stress strain definition is used. The reason this is allowable is for a 12 ft membrane with 12 in. of deflection the engineering strain is only 2.6%. Once the stress is known the pressure required to cause that stress can be calculated.

$$p = \frac{2\sigma t_i}{L}\sin\left(\frac{4\Delta}{L_i}\right) \tag{5.3}$$

In order to determine the force on the plate, the axial force within the membrane is required.

$$T = \frac{pL}{2\sin\left(\frac{4\Delta}{L_i}\right)} \tag{5.4}$$

The forces applied to the plate are shown in Figure 5.3.

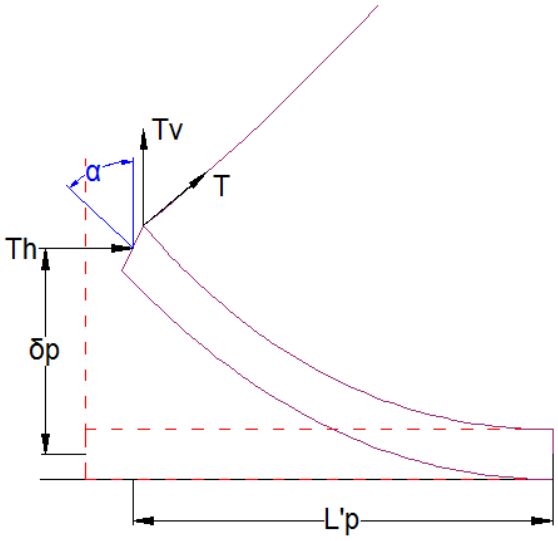

Figure 5.3: Angle Detail of Plate and Membrane

The angle of the retrofit is:

$$\theta = \frac{4\Delta}{L_i} \tag{5.5}$$

The vertical and horizontal components of the tensile force in the membrane at the plate are:

$$T_v = T\cos(\theta) \tag{5.6}$$

$$T_h = T\sin(\theta) \tag{5.7}$$

Using beam mechanics the rotation at the tip of the plate and the vertical displacement can be calculated.

$$\alpha = \frac{T_v L_p^2}{2EI} \tag{5.8}$$

$$\delta_p = \frac{T_v L_p^3}{3 E I} \tag{5.9}$$

The geometric effects from the bending of the plate are taken into account and used to find the moment at the bolt. For the elastic phase the shortening of the plate is assumed negligible.

$$M_{bolt} = T_v L_p + T_h \delta_p \tag{5.10}$$

The moment at the bolt location is checked against the plastic bending moment to determine if the plate is still elastic.

$$M_p = Z f_y \tag{5.11}$$

If the plate is still elastic the rotation of the plate tip increases the angle of rotation of the membrane and increases the deflection. This additional displacement is calculated by taking the change in the plate rotation and calculating how that effects the displacement.

$$\Delta_{plate} = \frac{\partial \alpha L}{4} \tag{5.12}$$

Where $\partial\alpha$ is the change in rotation of the plate. The total displacement of the membrane is the summation of the displacement of the membrane plus the deflection added by the plate.

$$\Delta_{total} = \Delta + \Delta_{plate} \tag{5.13}$$

The total displacement of the membrane is used in the following step with an additional displacement increment.

If the moment of the plate at the bolt reaches the plastic moment capacity a separate process must be used. Instead of incrementing the displacement of the membrane, the plate is rotated about the base.

$$\alpha_i = \alpha_{i-1} + \alpha_{increment} \tag{5.14}$$

For the first step of the plastic phase α_{i-1} is equal to zero. With this new rotation the displacement at the tip of the plate can be calculated. The shortening of the plate is significant from this point forward and used in the calculations.

$$L_p^{'} = L_p(1-\sin(\alpha)) \tag{5.15}$$

$$\delta_p = \delta_{p,elastic} + \sin(\alpha) \tag{5.16}$$

With the upwards deflection of the plate, additional membrane material will be added to the initial length of the membrane. A routine to determine what displacement corresponds to this additional material is needed. This routine finds what deflection will correspond to the zero strain state in the material. Figure 5.4 is the routine created to determine how the slack will affect the deflection.

$$\text{Slack}(L, L_{support}) := \left| \begin{array}{l} \varepsilon \leftarrow 0 \\ \Delta_1 \leftarrow 0 \\ n \leftarrow 2 \\ \text{while } \varepsilon < 0.0000000001 \\ \quad \left| \begin{array}{l} \Delta_n \leftarrow \Delta_{n-1} + 0.001 \\ \text{Arc} \leftarrow 4\dfrac{\Delta_n}{L_{support}} \cdot \left[\sqrt{\dfrac{L_{support}^{\,2}}{4} + \dfrac{L_{support}^{\,4}}{64(\Delta_n)^2}} + \left[\dfrac{(L_{support})^3}{32(\Delta_n)^2} \right] \cdot \ln\left[\dfrac{L_{support}}{2} + \sqrt{\dfrac{L_{support}^{\,2}}{4} + \dfrac{L_{support}^{\,4}}{64(\Delta_n)^2}} \right] - \left[\dfrac{L_{support}^{\,3}}{32(\Delta_n)^2} \right] \ln\left(\dfrac{L_{support}^{\,2}}{8\Delta_n} \right) \right] \\ \varepsilon \leftarrow \left(\dfrac{\text{Arc} - L}{L} \right) \\ n \leftarrow n + 1 \end{array} \right. \\ (\Delta_{n-1}) \end{array} \right.$$

Figure 5.4: Routine to Determine Deflection with Slack in Membrane

With the above routine the deflection of the slack alone can be found. The rotation at ends of the membrane is needed to determine what the tension in the membrane will maintain a plastic hinge in the plate.

$$\theta = \theta_{i-1} + \frac{4\Delta_{slack}}{L} \tag{5.17}$$

With this as an initial trial value for the rotation, the tension in the membrane can be calculated.

$$T = \frac{M_p}{L'_p \cos(\theta) + \delta_p \sin(\theta)} \tag{5.18}$$

Using numeric iteration the deflection that corresponds to this tension can be found. Once the deflection that causes the tension in the membrane is known the deflection associated with the slack is added to this deflection. The actual rotation of the membrane at the support is calculated using Equation 5.5 and the pressure is calculated using Equation 5.3. The complete routine can be found in Appendix A.

The addition of the plate into the routine will increase the deflection of the membrane for a given pressure. A sample resistance curve is shown in Figure 5.6 with retrofit properties listed below and the true-stress true-strain definition shown in Figure 5.5.

Length of Membrane	120 in.
Thickness of Membrane	0.079 in.
Thickness of Plate	0.125 in. and 0.25 in.
Length of Plate (tip to bolt centerline)	3 in.
Yield Stress of Plate	36 ksi

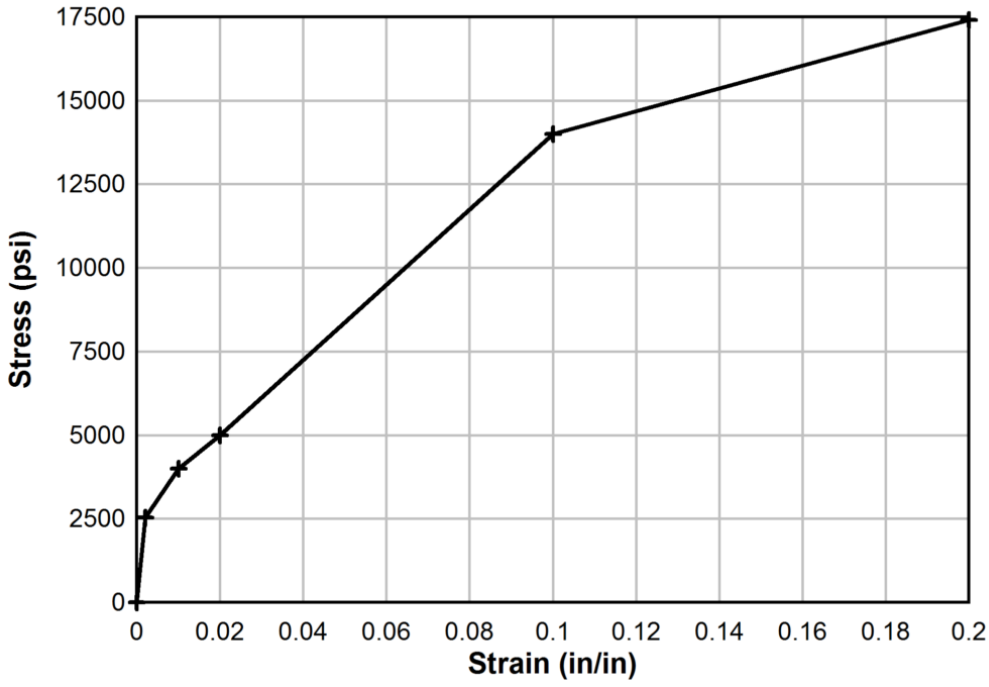

`

Figure 5.5: True Stress True Strain of Membrane

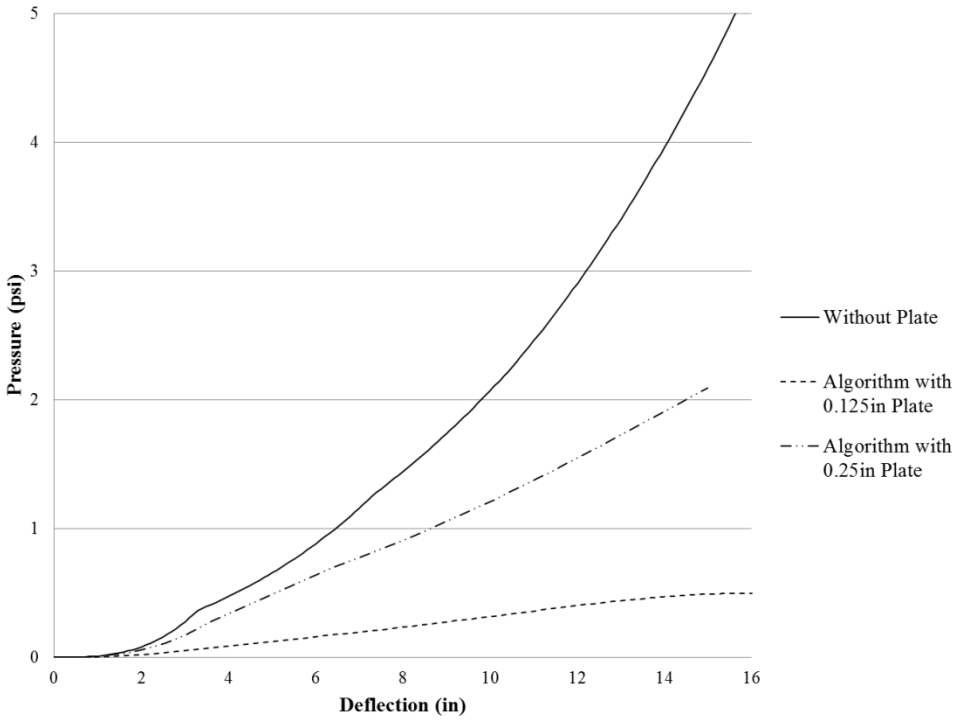

Figure 5.6: Effect of Plate on membrane Resistance

The thickness of the plate contributes greatly to the resistance of the membrane. When a plastic hinge forms in the plate, the resistance of the system is controlled by the yield stress in the plate since the plate is assumed to exhibit elastic-plastic behavior. The ideal system will have a plate that will not yield and allow the membrane to soften.

5.3 Finite Element Validation of the Plate Algorithm

The FE model for membrane with plate connections required a more complex model. Due to its size, only a quarter of the retrofit was modeled and symmetric boundary conditions were used. The bolt spacing and size was not explicitly modeled. The algorithm assumes the bolt spacing is small enough that local effects on the plate are not present.

The reaction block was modeled with 8 node 3-D stress reduced integration solid elements and very stiff material properties. The size of the solid elements are 1 x 1 x ¼ and the elements are fully elastic with a modulus of 29 x 10^9 psi. The membrane was modeled using 4 node full integration shell elements. Unlike with the membrane only models, the membrane not only spanned vertically but also was bent over to be sandwiched between the steel plate and the reaction block. The vertical portion of the membrane used 1x1 elements and the horizontal portion used 1x1/4 elements. The steel plate was modeled using shell elements as well with a mesh size of 1x1/4. The steel plate had to have a small mesh in order to fully encapsulate the stress profile from the line of bolts the tip of the plate. The mesh and geometry of the model is shown in Figure 5.7.

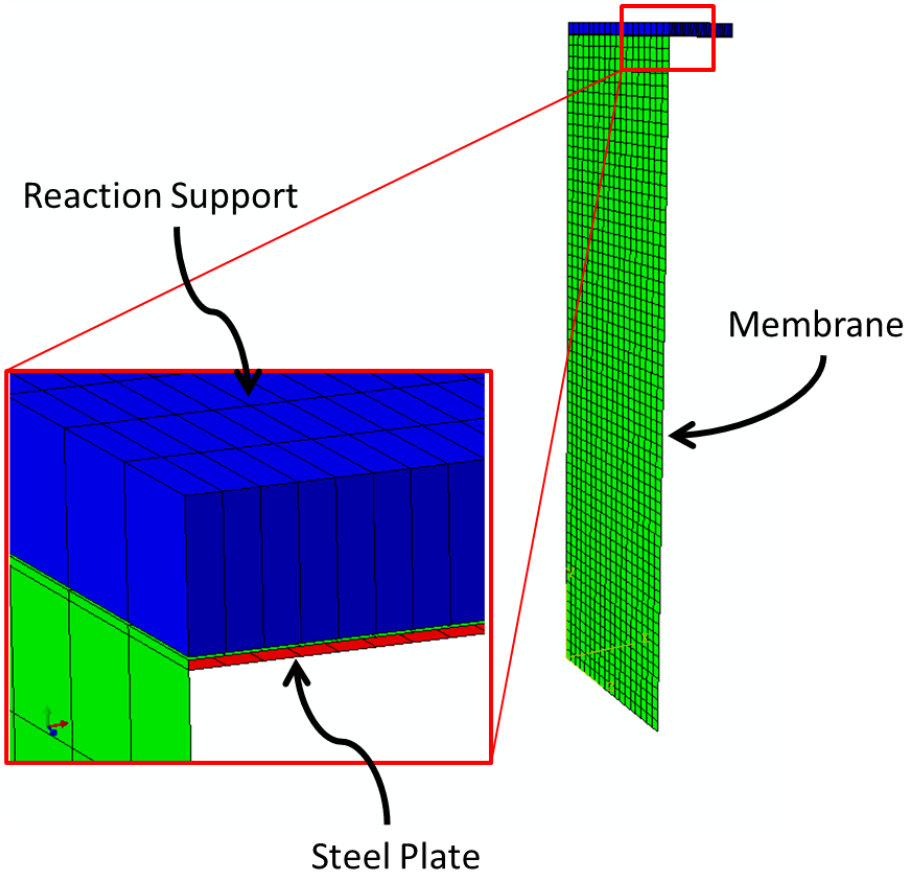

Figure 5.7: Mesh and Geometry of FE Model for Full Retrofit System

The vertical span of the membrane was 60 in. and with a symmetric boundary condition this corresponds to a 120 in. clear span. The depth of the plate and support block were 6 in. and the nodes at the halfway point, 3 in., were tied together to simulate bolt connections. The entire model width is 18 in. with symmetric boundary conditions. In all there are 3040 node and 2376 elements 1944 of which are shell elements.

The purpose of the FE analysis was to determine the validity of the algorithm presented earlier in this chapter. Many different material and cross-section variations were studied. Only a few will be discussed in this chapter the rest can be found in Appendix B.

Two main factors control the strength of a retrofit for a given wall, the membrane material and the membrane/plate thickness ratio. Two types of material were considered for the membrane material, A36 steel and a woven polymer. Three plate thicknesses were considered: 1/8 and 1/4 in. plates. All plates are A36 steel. The membrane thicknesses are 1 and 3 mm for the polymer and 20 ga for the steel. Table 5.1 lists all the different configurations. The results of the analysis for configuration 1 is shown in Figure 5.8.

Table 5.1: Retrofit Configuration

Configuration	Plate Thickness (in)	Membrane Material	Membrane Thickness (in)
1	1/8	Polymer	0.039
2	1/8	Polymer	0.118
3	1/8	Steel	0.0359
4	1/4	Polymer	0.039
5	1/4	Polymer	0.118
6	1/4	Steel	0.0359

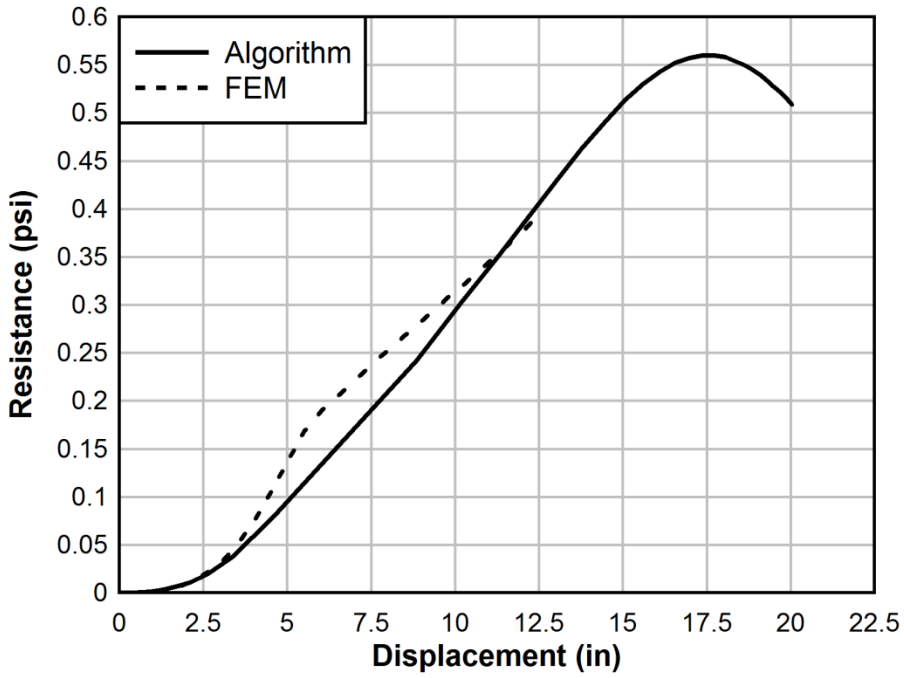

Figure 5.8: Retrofit Configuration 1 for FEM

Configuration 1 produces relatively accurate results with a maximum error of 30% at 6 in. of deflection. The point with the most discrepancy is the point where the plate transitions from elastic to plastic. The cause of the difference is the algorithms ability to make the transition from elastic plate to plastic plate gradually and with small steps. As a result, there is a large jump in deflection when the plate transitions to its plastic state. The last cause for the discrepancy is the membrane will push along the plate's length reducing the moment arm. The results for Configuration 2 are shown in Figure 5.9.

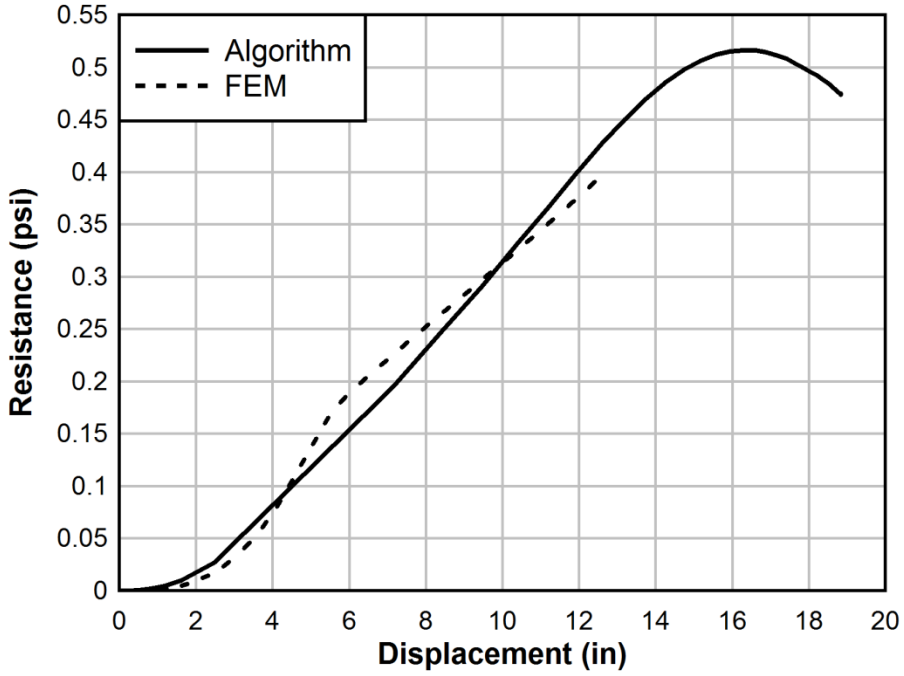

Figure 5.9: Retrofit Configuration 2 for FEM

The same problem with the transition to the plastic plate state persists in configuration 2. However, a more important observation is the increase in membrane thickness does not increase the resistance of the retrofit. As the thickness of the plate decreases, the system starts to be controlled by the strength of the plate. For an economical system, there must be a balance between the thickness of the plate and membrane. The results for Configuration 3 are shown in Figure 5.10.

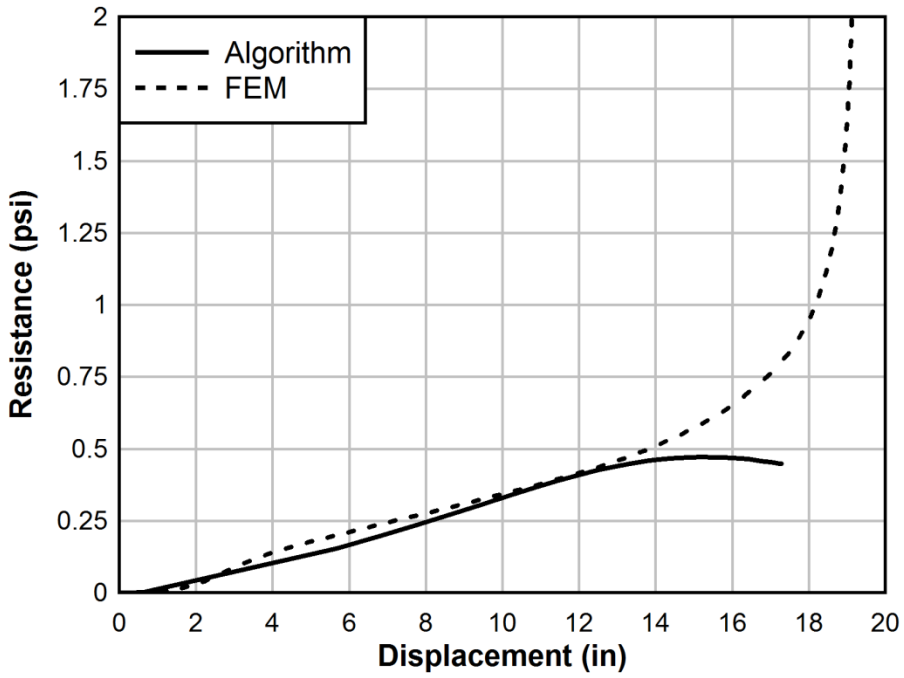

Figure 5.10: Retrofit Configuration 3 for FEM

Configuration 3 uses a steel membrane. One important consideration to notice about the difference between these results is what happens after 13 in. of deflection. The algorithm assumes that the membrane will always bear on the plate and bend it. The FE model shows that after a certain amount of rotation of the plate, the membrane will start to transmit the load directly to the bolts. When the membrane begins to bear directly on the bolts, large stresses are developed and cause the membrane to tear along the line of bolts. In laboratory test, when the membrane starts to bear on the bolts significant bearing stresses rapidly develop and the membrane fails along the bolt line (Johnson 2009). Figure 5.11 illustrates the tension failure observed in testing performed by Johnson (2009). Figure 5.12 is the results of the analyses for configuration 4.

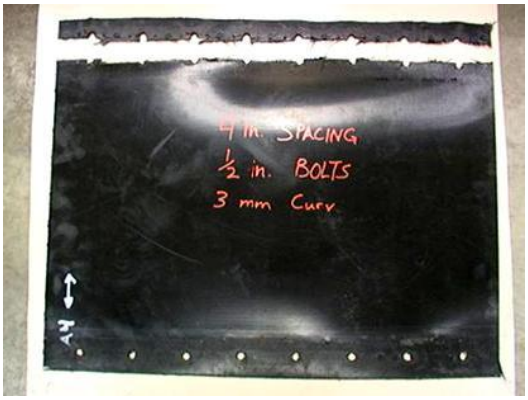

Figure 5.11Bearing Failure of Membrane

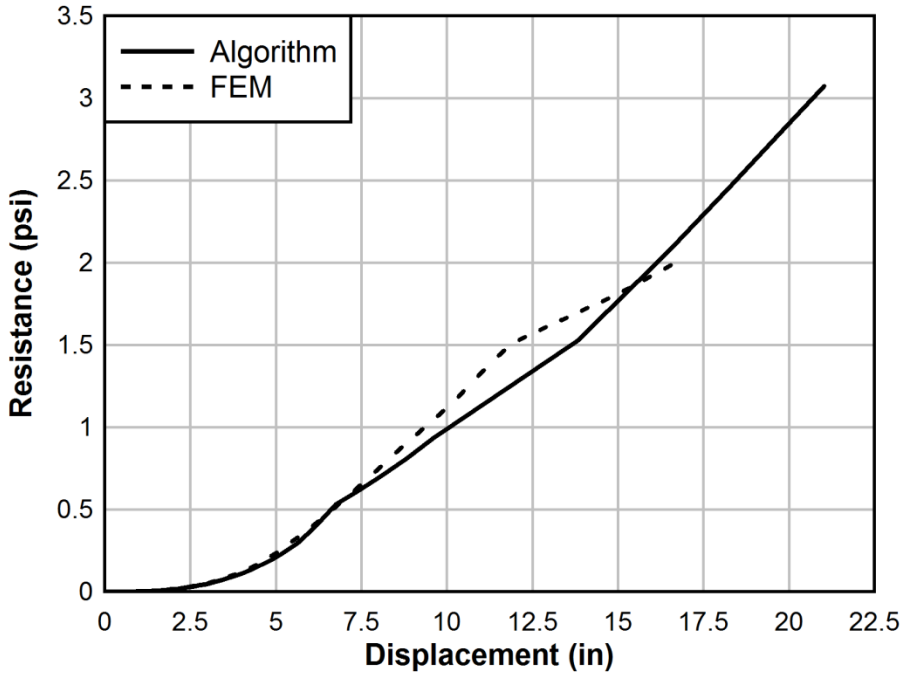

Figure 5.12: Retrofit Configuration 4 for FEM

Configuration 4 is similar to 1 except the plate thickness increases. This increase in plate thickness allowed for the membrane to develop larger tensile forces and greater pressures. From this observation it can be noted that the ability of the plate will control the overall resistance of the system as long as the membrane is strong enough. The results of the analysis for Configuration 5 is shown in Figure 5.13.

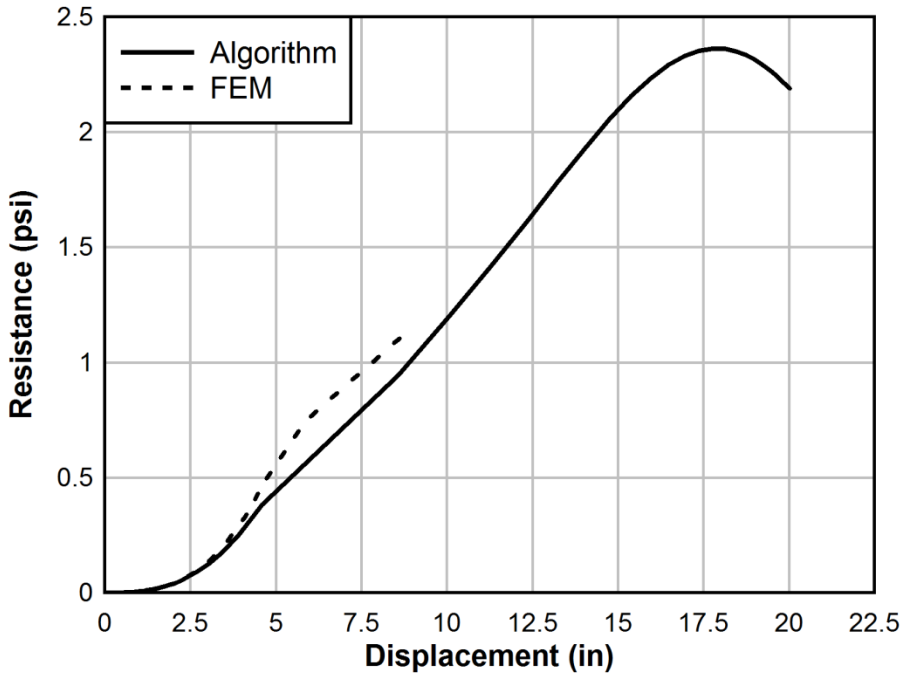

Figure 5.13: Retrofit Configuration 5 for FEM

The FE model for configuration 5 would not run after 1.12 psi of pressure was applied. This is the range in which the plate has reached the plastic moment capacity. The plate has completely yielded at this pressure. The FE model becomes unstable and will no longer run beyond this point unless post-yield hardening slope is defined for the plate. Figure 5.14 show the results of the analyses for Configuration 6.

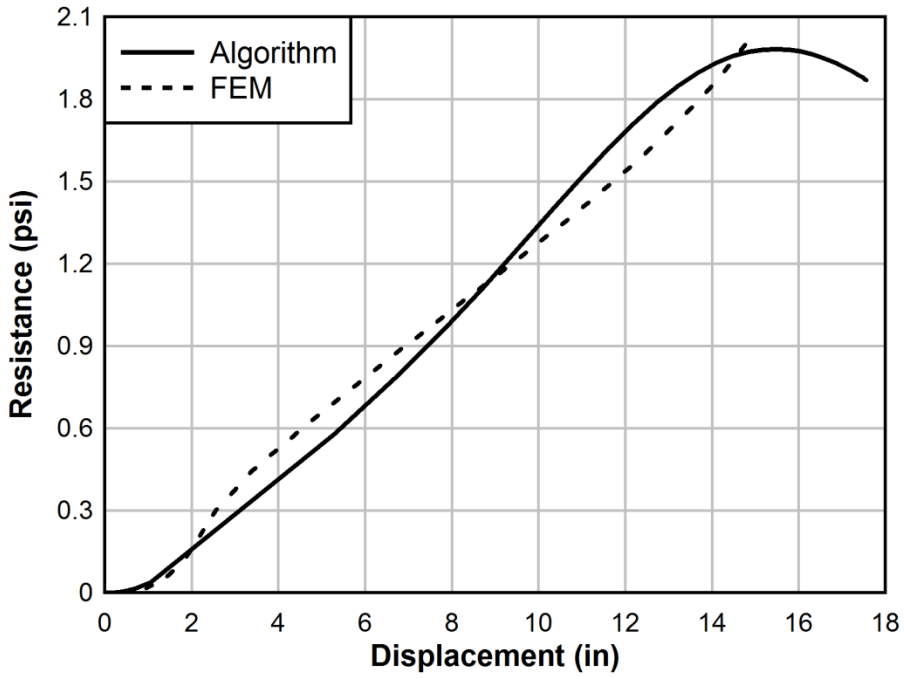

Figure 5.14: Retrofit Configuration 6 for FEM

With a larger plate the membrane does not begin to bear on the bolts as they did in Configuration 3. Even though the steel membrane has a higher modulus of elasticity and significantly higher yield point it did not produce substantially larger pressures. This again is contributed to the plate controlling the system. The tension in the membrane that causes a plastic hinge to form is approximately the same for both materials. Therefore, even though the steel is stronger it will not produce a higher resistance curve.

Overall the results produced by the algorithms at most underestimate the resistance by 30% which is reasonable considering the assumptions made. One consideration that was not made in the algorithm is the idea that the membrane is bearing along the length of the plate. The algorithm assumes the force of the membrane is transmitted to the plate only at the tip. The load is actually distributed along the plate which reduces the moment arm that will generate a moment at the hinge. This will

account for the FE model being larger since the plate will remain elastic longer. For design purposes, the deflection is what will control the design in the SDOF model. For a given deflection the resistance is typically smaller resulting in a conservative design.

Chapter 6: Dynamic Modeling and Comparison

6.1 Overview

SDOF is the most commonly used method for design of wall components. The static resistance is a critical aspect of the SDOF methodology. The SDOF methodology is largely compiled by Biggs (1964), and is general for any linear or nonlinear resistance definition. This methodology does not depend on knowing the elastic and plastic modes.

This chapter will detail the SDOF methodology and the response criteria set by PDC (2008). SDOF will be used to compare the algorithm presented in Chapter 5 against two tests. The first test uses a polypropylene membrane and the second uses a PVC membrane.

6.2 Single-Degree-of-Freedom Development

The system is idealized as a mass suspended from a spring, Figure 6.1 (b). In this system the mass is assumed to remain constant throughout the loading while the resistance and force are time dependent.

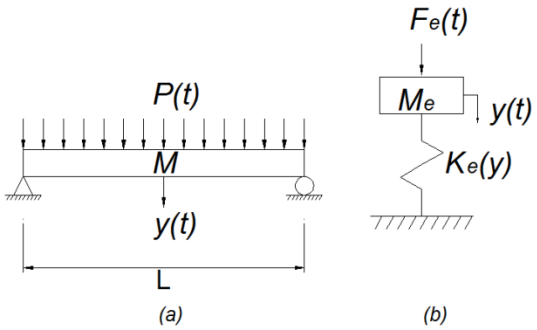

Figure 6.1: SDOF Theory (a) Real System (b) Simplified Model

The equation of equilibrium for dynamic systems is:

$$F(t) - Cy' - k(y)y = My'' \qquad 6.1$$

Where *k(y)* is the resistance as a function of the displacement, *M* is the mass of the structure, *C* is the damping coefficient, *y'* is the velocity, and *y''* is the acceleration. For dynamic analysis of masonry walls the damping force is not typically considered. Three main reasons are stated by UFC:

1) The first cycle and peak response are the only responses of interest which damping has little effect on.
2) Plastic deformations dissipate significantly more energy the normal structural damping.
3) Ignoring damping will generate larger deflections.

A fourth reason is given by Kiger and Salim (1998) is that damping of masonry walls subjected to explosive loading cannot be experimentally evaluated to determine the validity of a damping coefficient. For these reason, damping will not be considered in the following SDOF formulation.

As a simplified approach, equivalent mass and load factors will be used. These factors are generated based on the deformed shape of the structure during the elastic and plastic phases. With these equivalent factors Equation 7.1 reduces to:

$$M_e\, y''(t) + k_e\, y(t) = F_e(t) \qquad 6.2$$

The deflected shapes of the wall are given by Biggs (1963) and the deflected shape of the membrane is assumed to be parabolic as discussed in Chapter 4, these deformed shapes are shown in Figure 6.2.

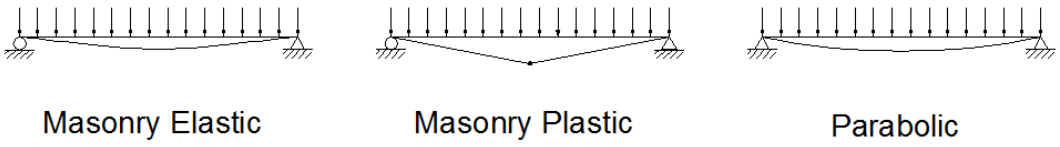

Figure 6.2: Deflected Shapes

The deflected shape for the masonry wall is described by fourth order polynomial for the elastic phase and a triangle for the plastic phase described in Biggs (1963). The parabolic shape for the membrane is defined in Chapter 4. In order to achieve an equivalent factor the deflected shape must be divided by the maximum deflection. This results in the deflection being 1 at midspan for all mode shapes. The elastic phase of the masonry as defined by Biggs (1963) is:

$$\phi(x) = \frac{16}{5L^4}\left(L^3 x - 2Lx^3 + x^4\right) \qquad 6.3$$

The equivalent mass is found by evaluating:

$$M_e = \int^{L} m\phi^2(x)\, dx \qquad 6.4$$

The equivalent mass factor, K_M, is the ratio of equivalent mass to actual load mass.

$$K_M = \frac{M_e}{M_t} \text{ or } K_M = \frac{\int^L m\phi^2(x)dx}{mL} \tag{6.5}$$

Where the actual mass is $M_t=mL$, where m is the mass per unit length. The equivalent load, F_e, is found by evaluating:

$$F_e = \int^L p(x)\phi(x)\,dx \tag{6.6}$$

The equivalent load factor is the ratio of equivalent load to actual applied load, F_t.

$$K_L = \frac{F_e}{F_t} \text{ or } K_L = \frac{\int^L p(x)\phi(x)dx}{pL} \tag{6.7}$$

In order for there to be deformation compatibility, "stiffness is numerically equal to the total load of the same distribution which would cause a unit deflection at the point where the deflection is equal to that of the equivalent system" (Biggs 1963). From this statement it can be said that:

$$K_R = \frac{k_e}{k} = K_L \tag{6.8}$$

Using these equivalent factors Equation 6.1 can be rewritten as:

$$K_m M_t\, y''(t) + K_L K\, y(t) = K_L F(t) \tag{6.9}$$

The resistance of the wall is equal to the stiffness of the wall times the displacement, $R(z) = K\,z$. Dividing both sides by the equivalent load factor and defining $\frac{K_L}{K_M}$ as the load-mass factor, K_{LM}, the final equation of motion can be written as:

$$K_{LM}\,M_t\,y''(t) + R(y(t)) = F(t) \qquad 6.10$$

For a given deflected shape and boundary conditions the load-mass is constant. A wall can have different deflected shapes depending on what stage the wall is in: elastic, plastic, or transition. Biggs (1963) lists these factors for various deflected shapes and loadings. The ones that are most relevant to this type of system and loading are the simply-supported beam and the fixed-fixed beam both with distributed loads. The parabolic load-mass factor was derived using the methods and equations listed above. Table 6.1 list all the factors for both the elastic and plastic phase.

Table 6.1: Equivalent Transformation Factors for One-Way Beams and Slabs

	Equivalent Load Factor K_L		Equivalent Mass Factor K_M		Equivalent Load-Mass Factor K_{LM}	
	Elastic	Plastic	Elastic	Plastic	Elastic	Plastic
Simple Supports	0.64	0.50	0.50	0.33	0.78	0.66
Fixed-Fixed	0.64	0.50	0.41	0.33	0.77	0.66
Parabolic Shape	0.66		0.53		0.80	

For masonry walls retrofit with an unbonded membrane, the initial resistance is dictated by the masonry wall. Once the wall cracks, there is a moment when the membrane may not have the ability to assume the parabolic shape. The resistance of the membrane is much greater than the plastic masonry wall at large deflections. The

membrane will then force the masonry wall to assume the parabolic shape. This transition is very small in terms of both displacement and time. For these reasons the plastic load-mass factor of the masonry will be neglected and only the parabolic load-mass factor will be used after the masonry wall goes plastic.

Many different approximate methods have been developed to solve the problem. Biggs details how to use the constant velocity procedure, linear acceleration method, the Newmark "beta" method, and several finite difference methods. The Newmark "beta" method is one of the most versatile methods. When beta =0 and γ = ½ the Newmark "beta" method is equivalent to the central difference method. The central difference method is a direct approach for solving for the displacement. At any given time the acceleration of the system is:

$$z'' = \frac{y_{i+1} - 2y_i + y_{i-1}}{(\Delta t)^2} \qquad 6.11$$

This formula is presented by Chopra (2007) is an explicit solution and does not require iteration. This formula allows for the deflection at time Δt_{i+1} to be calculated. Substituting Equation 6.11 into Equation 6.10 and solving for y_{i+1} results in Formula 6.12.

$$y_{i+1} = z''\Delta t^2 - y_{i-1} + 2y_i$$

$$\text{Where: } z'' = \frac{F(t) - R(y(t_i))}{K_{LM} M_t} \qquad 6.12$$

This formula only works if the time step, Δt, is constant and small enough. If the time step is too large the results will be meaningless (Chopra 2007). Chopra's time step requirement is:

$$\frac{\Delta t}{T_n} < \frac{1}{\pi} \tag{6.13}$$

Where T_n, the natural period of the wall system presented by Biggs as:

$$T_n = 2\pi\left(\frac{K_{LM}M_t}{K}\right)^{\frac{1}{2}} \tag{6.14}$$

K is defined by SBEDS Methodology (PDC 2008) as the initial elastic stiffness of the system. For simply supported walls this is $\frac{384EI}{5L^3}$ and $\frac{384EI}{L^3}$ for fixed walls. If the time step over the natural period is less than 0.1 the response is adequate. For this reason Chopra (2007) suggest using a time step of 0.01 to 0.02.

Knox et al. (2000) describes the method used to combine the different resistance functions. At a given displacement, the resistance is the sum of all the parts of the wall and the retrofit at that displacement.

6.3 Blast Loading

For design purposes, the airblast loading to the exterior of a building due to an external explosion is typically idealized as a uniform pressure over the surface. The loading is represented as the pressure at a point vs. time and consists of two phases: positive phase and negative phase, shown in Figure 6.3. The positive phase is triangularly shaped and will start at the peak pressure and decay. The negative phase results as negative pressure forms. The negative phase is less important for design of buildings since the peak negative pressure is much less than that of the positive phase. Secondly, ignoring the negative phase generates higher deflections.

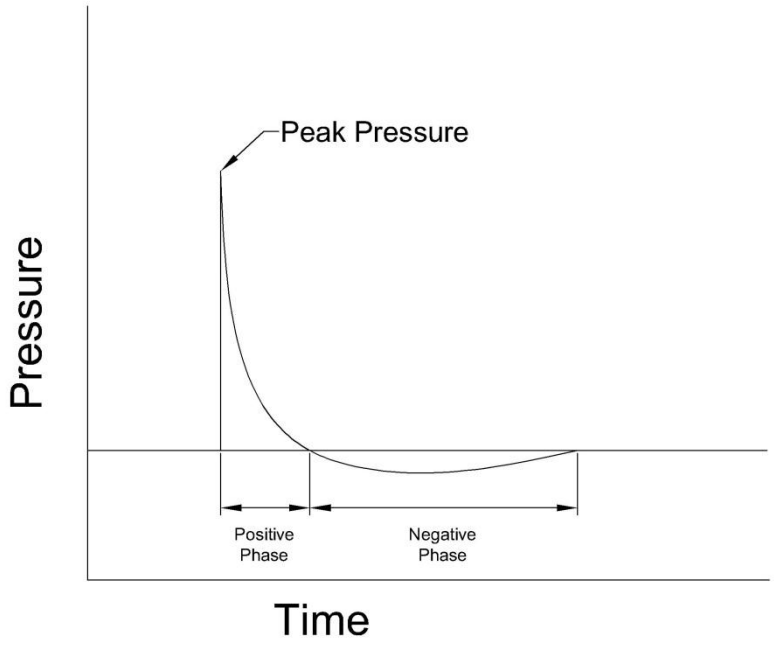

Figure 6.3: Loading Diagram for Free Air Blast

Loading effects from explosives are typically reported as the weight of TNT at a standoff distance. Using these two values the pressure-time data was extracted from SBEDS for use in the design example presented in Chapter 8.

6.5 Dynamic Testing

The Wiehle method is used to generate the resistance of the non-arching walls. The SBEDS method is used to generate a resistance definition for arching walls. The membrane and plate resistance function used is the one described in Chapter 5.

6.5.1 Test 1 Using Polypropylene

Experimental validation was performed using the test data presented in Johnson (2009). The test was performed by AFRL and involves a full scale explosive field test. The height of the wall was 110.2 in. and simulated poor construction of the mortar joints. The CMU block used is shown in Figure 6.5 along with dimensions.

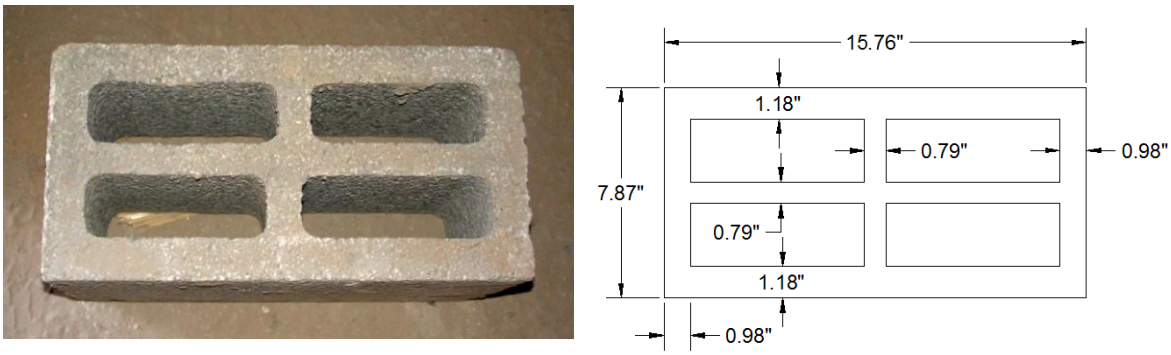

Figure 6.4: (a) CMU Test Block (Johnson 2009) (b) CMU Dimensions

The tensile bond between the mortar and blocks was estimated to be 50 psi. The wall was retrofit with a 0.039 in. thick membrane of polypropylene, whose stress strain curve is shown in Figure 4.6. A steel plate with thickness 0.25 in. and a width of 6 in. was used to connect the membrane to the supports. The plate edge was placed 1.5 in. from the wall. Bolts were placed along the centerline of the plate spaced at 8 in. on center. Washers were used to help connect the bolts to the plate. The washers had a 1.5 in diameter and a thickness of 0.25 in. Figure 6.6 shows both the interior and exterior face of the wall.

Figure 6.5: (a) Interior of Test Wall (b) Exterior of Test Wall (Johnson 2009)

A detailed pressure history was taken for this experiment. The wall was open in the back allowing pressures to develop. This was considered and pressure gages were placed both inside the structure and outside. The net pressure on the wall was calculated and shown in Figure 6.7 below.

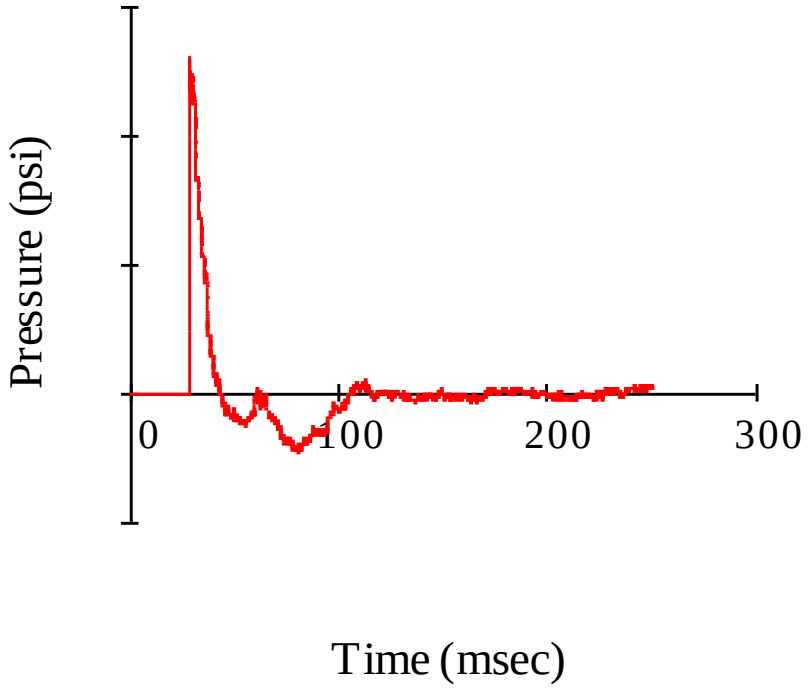

Figure 6.6: Wall Pressure from Test

The algorithm does not incorporate holes in the plate and the additional thickness the washers add. Lastly the algorithm assumes that the plate and membrane are flush against the wall. After the test only the bottom course of CMU remained. Figure 6.8 is the exterior of the wall after the test. The results of the test and the analysis are shown in Figure 6.9.

Figure 6.7: Post Test Wall (Johnson 2009)

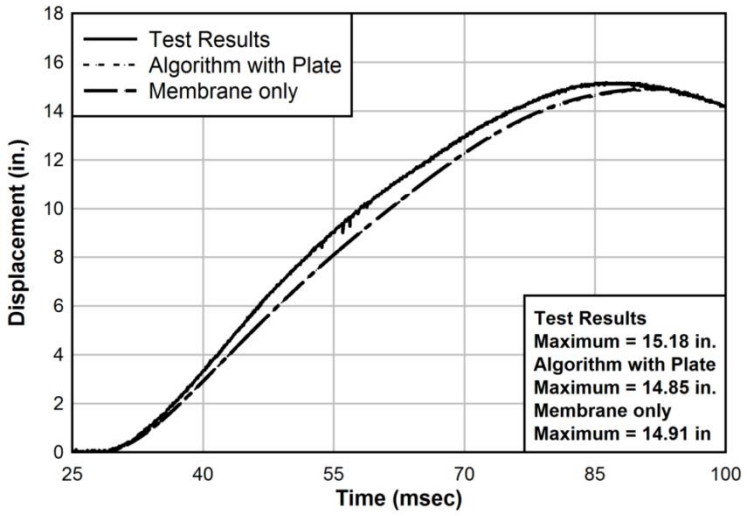

Figure 6.8: Dynamic Response Comparison

The dynamic analysis resulted in a very close approximation to the actual test. The algorithm under-predicted the deflection by 2.3% compared to the measured results. This is reasonable considering the factors that did not go into the analysis, such as holes in the plate, washer stiffness, gaps between the retrofit and the wall, and effects of high strain rate.

6.5.2 Test 2 using PVC Membrane

Test two was conducted by AFRL at Tyndall Air Force Base, Florida, using a PVC liner. The wall was constructed to be 120 in. tall using 8 in. CMU blocks with 49% of the cross-sectional area being solid and a moment of inertia of 28.4 in^4 (PDC 2008). A 1.25 in. gap was present at the top of the wall and steel dowels were grouted into the top cells; refer to Figure 3.35 (a) for support schematic. A 40 mil PVC liner was used as the membrane material; the stress-strain relationship is shown in Figure 6.10. A 0.25 in. aluminum plate, E=10,000 ksi and f_y=37 ksi was used for the connections. A 5 in. plate was fixed to the floor using concrete nails 1 in. from both edges, as shown in Figure 3.11. Figure 3.12 shows the exterior and interior view before testing.

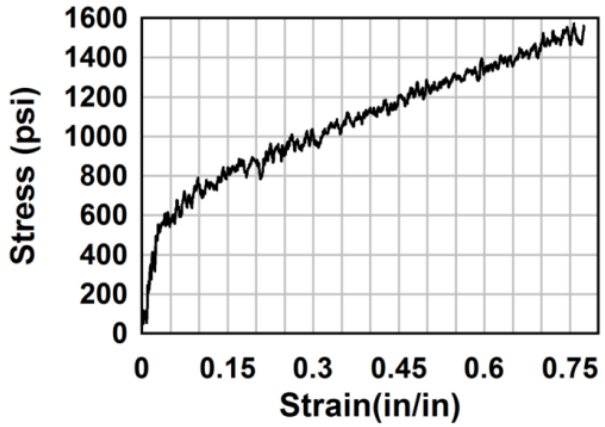

Figure 6.9: True Stress-Strain Plot for PVC Liner

Figure 6.10: Plate Connection for Test 2

(a) Interior (b) Exterior

Figure 6.11: Pretest Constructed Wall (a) Interior (b) Exterior

The loading was selected to generate significant damage to the CMU wall without causing a blowout of the entire wall/retrofit system. Figure 6.13 is a normalized pressure-time plot of the measured pressure.

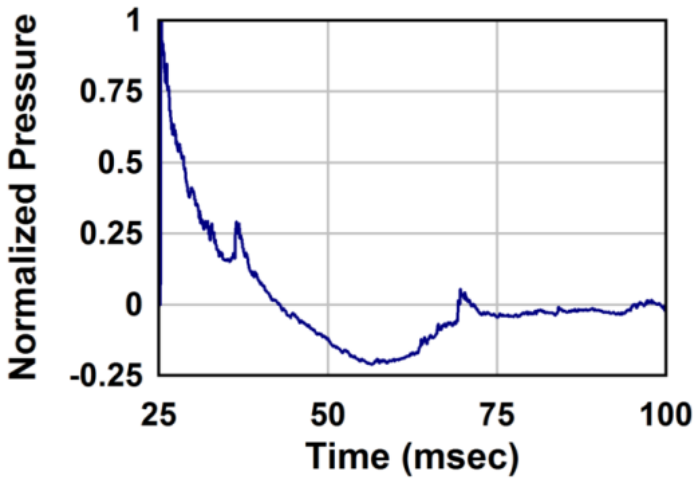

Figure 6.12: Normalized Loading for Test 2

The wall was damaged and exhibited significant deflections during the test. The algorithm over predicted the peak deflection by 8.5%. The peak deflection recorded was 8.03 in. while the algorithm predicted a deflection of 10.3 in. The assumptions that went into the development of the algorithm play a major role in this increased deflection. Figure 6.14 compares the measured deflection and the predicted deflection.

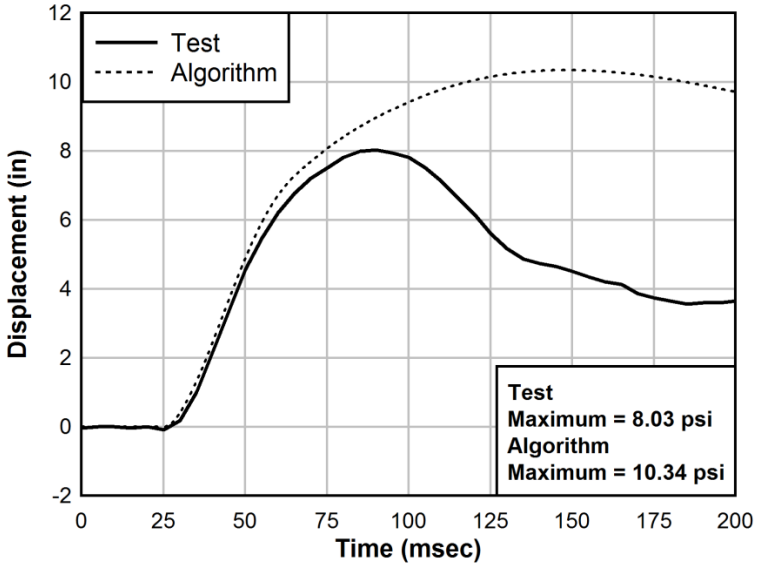

Figure 6.13: Test 2 Deflection Comparison

For this test assumptions that played a role that were not relevant for Test 1 is that the connection plate is assumed to be elastic perfectly plastic. Unlike steel, aluminum does not have a well-defined yield point. A second factor is the exact dimensions and moment of inertia of the CMU blocks were estimated using the SBEDS Methodology (PDC 2008). With deflection being a controlling criteria, the algorithm over predicted peak deflection by 28% making the algorithm conservative. Figure 6.15 is an exterior view of the wall after the test.

Figure 6.14: Post Test Exterior View

The top course of blocks was damaged during the testing. The wall was left with a permanent deflection of 3.6 in. The membrane remained intact and was capable of preventing fragments from entering the building. Figure 6.16 shows a fragment pressing on the membrane after the test did not penetrate the envelope of the building.

Figure 6.15: Post Test Fragment Pressing Against Membrane

Chapter 7: Design Examples

7.1 Overview

The general procedure for the design of a retrofit will be as follows:

For a given loading:

1) Determine the resistance of the masonry alone
2) Determine what level of protection is available
3) Design an initial retrofit system and the complete resistance definition of the wall and retrofit system
4) Determine what level of protection will be provided by the retrofit
5) Modify retrofit system if adequate protection is not provided and iterate

The loading of the structures will be presented as pressure-time data rather than weight and standoff.

7.2 Problem Statement

The owner of an existing two story building, shown in Figure 7.1, wishes to determine the appropriate retrofit to prevent catastrophic failure. There is a high threat to this particular building. The building consists of concrete columns and beams and infill masonry walls; Figure 7.1 and 7.2 detail the geometry of the building. The loading on the building is shown in Figure 7.3 and the material properties for the membrane are shown in Figure 7.4 and Table 7.1 list the wall properties. There are two different walls to

consider for this building. The first wall is ground floor wall. This wall has boundary conditions that allow for it to be considered an arching wall. The second wall is on the second floor and the roof load is transmitted to this wall. The second story wall is assumed to be simply supported at both ends.

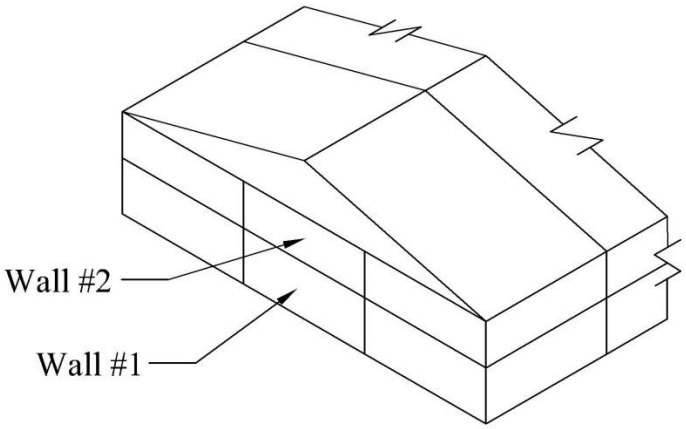

Figure 7.1: Isometric View of Building Identifying Walls

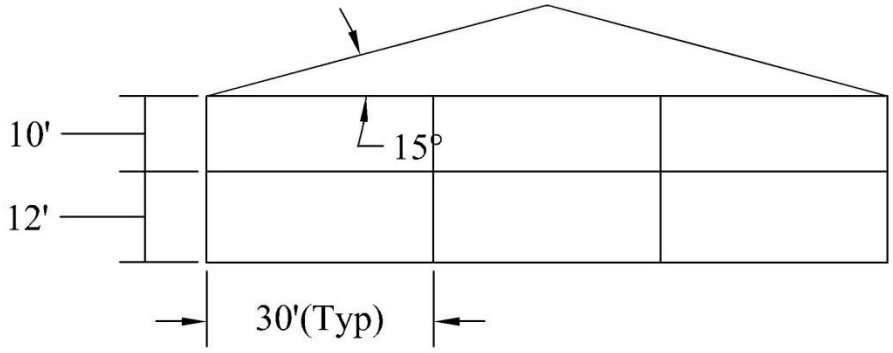

Figure 7.2: Elevation View of Building

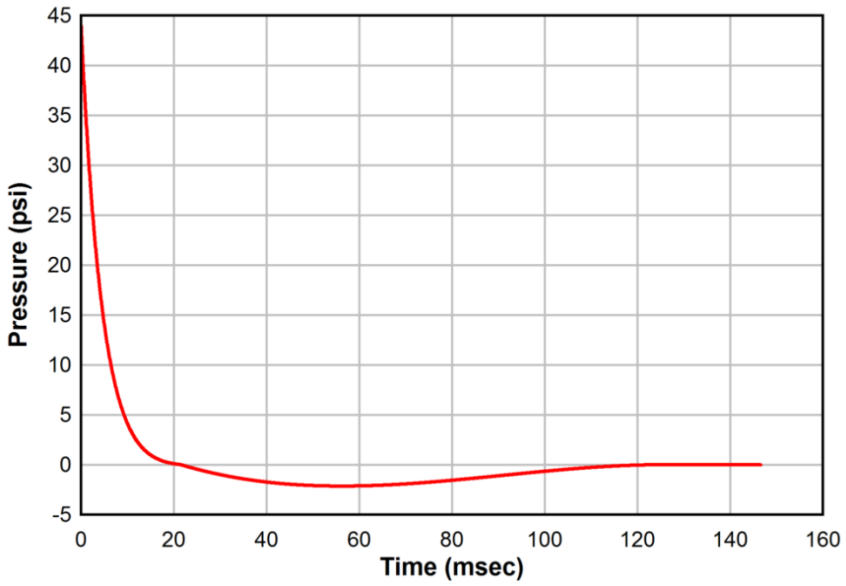

Figure 7.3: Design Loading

The loading on the walls should vary slightly since the second story wall will have a larger standoff distance. However, the difference between these two loadings is small enough to neglect.

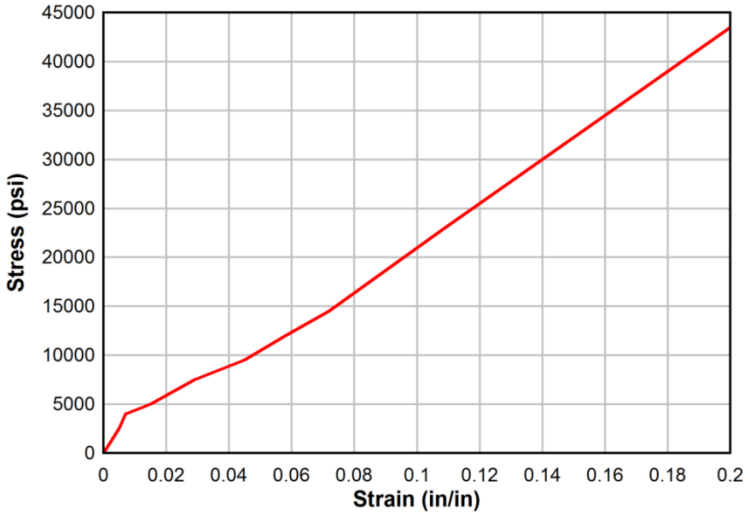

Figure 7.4: Membrane True Stress/Strain

Table 7.1: Wall Properties

Wall	Thickness (in)	Support	Axial Load (lb/in)	Height (in)
#1	8	Arching	NA	144
#2	8	Pin-Pin	100	120

The design process will look at each wall individually starting with Wall #1. The complete design process and calculations are provided in Appendix D

7.3 Wall #1

The first step in the design process is to determine how the wall will react alone to determine if any retrofit is necessary. Assuming arching boundary conditions, the resistance of the wall was determined using the UFC method assuming no gap was present. Figure 7.5 shows the deflection of the wall to its peak deflection.

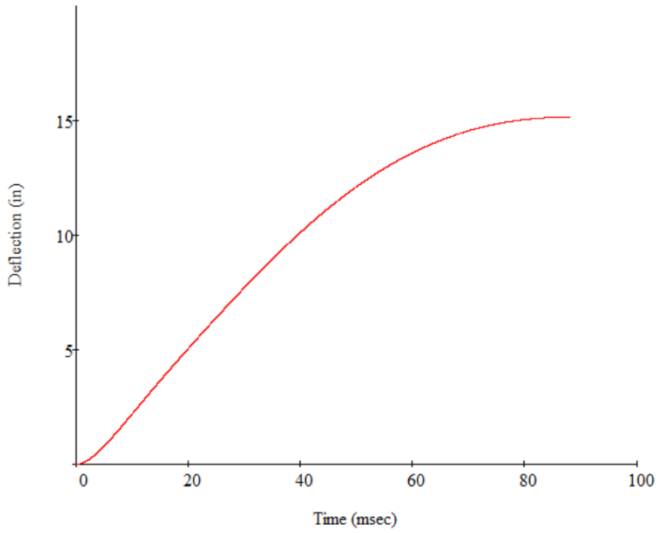

Figure 7.5: Dynamic Results for Masonry Alone

The maximum deflection of the wall alone is 32.1 in. this deflection should be compared to the deflection limits from Table 6.4. To prevent blowout, the rotation must

be less than 8°. With 25.5 in. of deflection the rotation at the support is 24.0° which is larger than what is acceptable. For an initial retrofit design the plate will be 6 in. wide with bolts along the center line at 8 in. spacing on center. The thickness of the plate will be 0.25 in. and the membrane thickness will be 0.79 in.

The maximum deflection with this configuration is 21.7 in. and a rotation of 16.7°. This again is larger than the allowable response limit of 8°. Figure 7.6 is the total resistance of the wall and retrofit system.

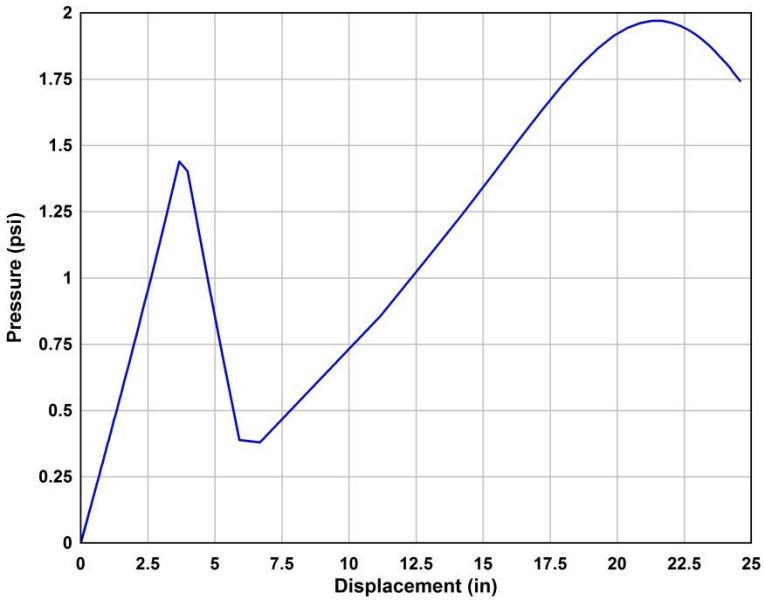

Figure 7.6: Total Resistance of System for Retrofit Trial 1

By inspecting the resistance curve it can be noticed that the steel plate is yielding before the membrane can develop significant resistance. To prevent this, a thicker plate should be used.

For the second trial, a 0.75 in. plate and 0.51-in thick polymer will be used. The results of this trial are that the deflection is 11.9 in. and a rotation of 9.4°. This system is

still not adequate and an increase in membrane thickness should be tried. However, this system is not very cost effective for both material and labor. Because of these reasons the membrane material is changed to A36 steel membrane.

For the third trial, the steel plate will be 0.057 in. and the plate thickness is 7/8 in. The maximum deflection of the system is 10.1 in with a support rotation of 7.97°. based on the response limits outlined in Table 2.4, this system brings the wall out of the blowout range. The steel plate is more difficult to transport than a polymer and both will have to be bent at the support to attach to the supports.

With this configuration, the maximum deflection will be used to determine the forces on the bolts. The axial and shear force on the bolts is 1170 lb and 341 lb, respectively. Using a A325 5/8 in. diameter bolt spaced at 8 in. on center the normal stress in the bolts is 56,700 psi and the shear stress is 16,000 psi. For Grade A325 bolts the normal tensile strength is 90 ksi and the shear strength is 54 ksi. For this configuration the bolt design is adequate.

7.4 Wall #2

The design process for Wall #2 will be the same as Wall #1. The membrane used will also be the steel membrane. The response of the wall is a complete blowout. Mathematically the maximum deflection is 48.6 in. but this simply corresponds to complete catastrophic collapse of the wall.

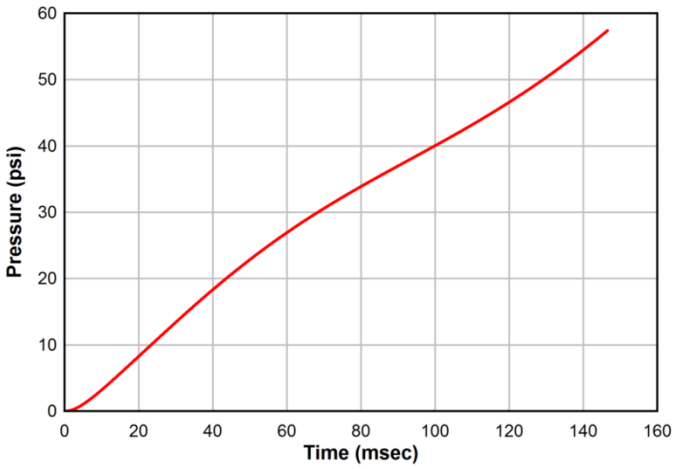

Figure 7.7: Response of Wall #2 without Retrofit

The first trial retrofit will consists of a 0.102 in. steel membrane with ½ in. connection plate. This configuration brings the deflection to 12.3 in. with a rotation of 11.6°. This rotation is still too large.

The second trial will use a 0.229 in. steel membrane and a 13/16 in. connection plate. The response of the system is now 6.80 in. with a rotation of 7.94°. This rotation is within the limit to prevent blow out if the wall is flexural only. There is an axial force applied to the masonry; however, PDC-TR 06-08 states if load is below 20% of the ultimate compressive capacity of the masonry then a flexural response should be used. Figure 7.8 shows how the retrofit affected the response.

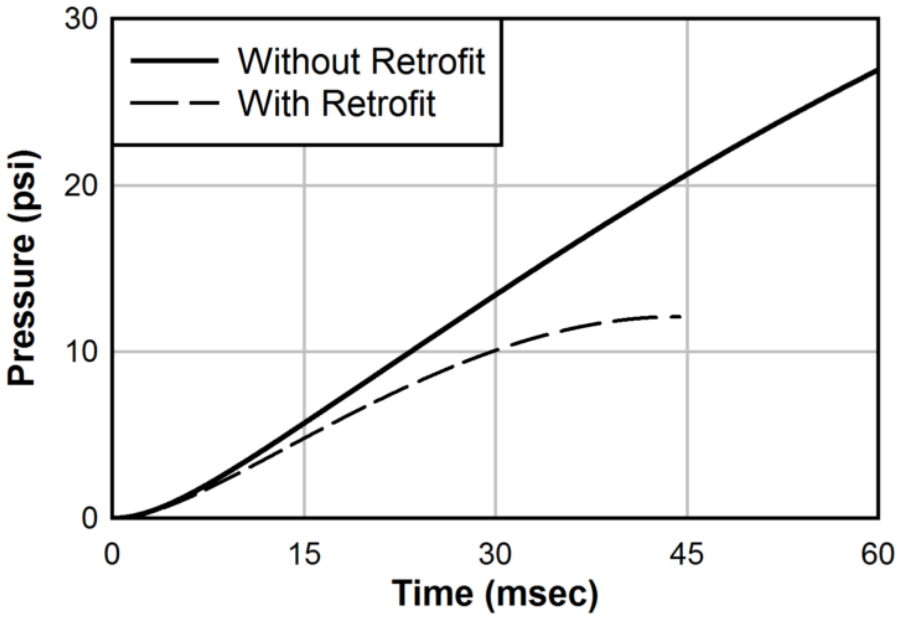

Figure 7.8: Response Comparison of Wall #2

With this configuration, the maximum deflection will be used to determine the forces on the bolts. The axial and shear force on the bolts is 2,336 lb and 670 lb, respectively. Using a A325 5/8 in. diameter bolt spaced at 8 in. on center the normal stress in the bolts is 60,900 psi and the shear stress is 17,500 psi. For Grade A325 bolts the normal tensile strength is 90 ksi and the shear strength is 54 ksi. For this configuration the bolt design is adequate.

Chapter 8: Conclusion

8.1 Masonry Walls

For unreinforced ungrouted masonry, there are many different ways to formulate a resistance curve. The first major distinction that can drastically change the resistance depends on the support conditions. If the supports do not resist rotation the wall can only resist the load using its flexural strength. If rotation is resisted then the wall will have a significant compressive force to restore the wall to its original location.

For non-arching walls, there are three methods to generate a resistance curve. The Wiehle method is the most common and generates a reasonable response. This method accounts for most of the geometric and material properties of the wall. The second method was generated by PDC and detailed in SBEDS Methodology. This method is reasonable and while it generates a graph only using four points, these points correspond closely with the Wiehle method. The last method was developed by Moradi and predicts the lowest resistance. This method has a lower resistance because it does not account for the tensile strength of the mortar bond.

For design purposes the best method is one that is reliable without being overly complicated to formulate. The Wiehle method was selected as the method that should be used. While this method requires more computation than the SBEDS method it can be assumed that a program can be used for this incremental method. While the Moradi

method has the lowest resistance, which may be desirable for design purposes, the computation is rigorous and will result in an over designed retrofit system.

Arching walls generate a significantly larger peak pressure and therefore a larger resistance. However, the use of the arching method can only be used if the supports are significantly stiffer than the wall. The support must have significant strength to resist the rotation of the wall. For arching walls four methods have been developed, the three sources above plus UFC. The Wiehle method is again a simple incremental method. This method is widely used and referenced. The method presented by UFC appears to be more complicated. However, the UFC method accounts for a gap between the wall and the supports. If no gap is present the UFC method reduces to the Wiehle method. The Moradi method is again more complicated to use however this method better aligns with the Wiehle method. The SBEDS method is drastically different than the other two methods. SBEDS should use the method presented in UFC; however, it uses a different method. This new method grossly over estimates the area under the curve compared to the other two methods. Secondly, the deflection at the peak pressure is much greater.

The resistance method that was chosen as the most appropriate for arching walls was the UFC method. This method generates results that are logical without being overly complicated. This method accounts for the gap of the wall which in reality often exists.

8.2 Membrane Resistance Functions

The resistance of the retrofit is what typically provides the strength of the wall system at larger pressures and deflections. Because it is an unbonded membrane, there is a large amount of deflection that is required to generate significant stresses in the

membrane that will resist the lateral loading. For the membrane alone three models have been suggested.

The first method was presented by Seide and was developed for plates subjected to large displacements. This method can generate relatively accurate results even though the boundary conditions that were used to generate this method are not accurate for this system. The second method is to treat the membrane as a cable and use formulas presented in Young (2012). This method more closely follows the anticipated resistance. Both of the previous methods were developed for a linear material definition. These methods were modified to use a tangent modulus so they could account for the softening of the material. The last method was developed using an assumed deflected shape. This last method is the one that has been validated the most with laboratory testing. The deflected shape of the membrane does change with very large displacements; however, because of the response limits, large deflections of the wall are not allowed so this does not have to be changed to a more complex system.

For the development of the algorithm to include the plate, the last method, the parabolic shape function method, was chosen. This method was the one most used and has been validated with testing. This method also allows for forces and stresses in the membrane to be calculated which are needed to incorporate the plate's response.

Finite element modeling was conducted to validate these resistance methods. All of the methods were relatively close to one another especially during the linear phase. The parabolic method most closely followed the FEM and only had significant deviation at large deflections for the reasons stated above.

One notable observation is that the parabolic method proposes using a true stress vs. engineering strain plot to determine what stresses are in the membrane. This was done to account for the larger stresses that will develop in the membrane. However, the stresses are only larger because the thickness of the membrane is decreasing and this is not accounted for in the parabolic method. The proper way to use the stress strain curve is to use the engineering stresses if the area is assumed constant or to update the area of the membrane and convert the strain values as well.

8.3 Full Resistance Curve Including Plate Connections Algorithm

The algorithm developed that would incorporate the plate generates a lower resistance curve than the FE model. The plate is assumed to deflect as a cantilever beam with the fixed base being at the center line of the bolts. While the membrane reacted against the length of the plate it was assumed that the membrane will transmit the load only at the tip of the plate.

This last assumption has a large impact on lowering the resistance. The load will have a larger moment arm causing plastification of the plate to happen at lower pressures. This assumption was made to eliminate the geometric changes of the plate and the frictional resistance that can result from the membrane sliding across the surface of the plate.

This algorithm was validated using finite element modeling. It was shown that the algorithm produces lower resistance. Many deferent geometries and materials were used in the FEMs to ensure that the algorithm was not specific to a single case. It was shown that the plate can drastically decrease the resistance of the retrofit. If the plate is too thin

it will yield early and diminish a large amount of the strength that may be assumed if the membrane is sufficiently attached to the supports. Larger plates however do not increase the resistance beyond what the membrane alone can do. The most a plate can do is allow the membrane to generate sufficient stresses to resist the lateral load. Another notable point that was observed is that for a given system the use of a stiffer membrane material will not generate larger resistance. The plate will control what the maximum pressure will be as long as the membrane does not fail before the plate. The advantage of stiffer materials is that a thinner membrane can be used which will help with both material cost and labor cost.

8.4 Single-Degree of Freedom Analysis

Biggs (1964) is the standard that has been used to determine the maximum deflection of the system. The deflected shapes of the masonry wall are well defined and using the simplified equivalent load mass factors for the masonry alone can be selected from Biggs. However, the membrane has a different deflected shape than the plastic phase of the masonry. The load-mass factor for a parabolic membrane was created to accurately model the system.

References

American Institute of Steel Construction (AISC). Steel Construction Manual. 14th ed. 2010. Print.

ASCE/SEI. Blast Protection of Buildings. Reston, VA: American Society of Civil Engineers/Structural Engineering Institute, 2011. Print.

Biggs, John M. Introduction to Structural Dynamics. New York: McGraw-Hill, 1964. Print.

Buchan, P., and J. Chen. "Blast Resistance of FRP Composites and Polymer Strengthened Concrete and Masonry Structures – A State-of-the-art Review." Composites Part B: Engineering 38.5-6 (2007): 509-22. Print.

Chopra, Anil K. Dynamics of Structures: Theory and Applications to Earthquake Engineering. Upper Saddle River, NJ: Pearson/Prentice Hall, 2007. Print.

Department of the Air Force. "Engineering Technical Letter (ETL) 00-9: Airblast Protection Retrofit for Unreinforced Concrete Masonry Walls." 2000.

Drysdale, Robert, Ahmad Hamid, and Lawrie Barker. Masonry Structures: Behavior and Design. Englewood Cliffs: Prentice-Hall , 1994.

Federal Bureau of Investigation (FBI). "FBI 100 - 1993 Trade Center Bombing." *FBI*. N.p., 19 Feb. 2008. Web. 18 June 2012. <http://www.fbi.gov/news/stories/2008/february/tradebom_022608>.

Fitzmaurice, Salis, Hani Salim, Robert Dinan, and Elizabeth Trawinski. "Blast Retrofit Design of CMU Walls Using Polymer Sheets." May 2006.

R. Park, and Gamble, W. L. *Reinforced Concrete Slabs.* New York, NY: Wiley, 2000.

Hoemann, John, James Davidson, Robert Dinan, and Bryan Bewick. "Boundary Condition Behavior and Connection Design for Retrofitted Unreinforced Masonry Walls Subjected to Blast Loads." *Strucures Congress.* 2010. 2021-2032.

Johnson, Rhett, Hani Salim, John Hoemann, Keith Nelson, Bryan Bewick, and Michael Hammons. "Validation and Design of Sheet Retrofits." December 2009.

Jones, Patricia A. S. *WAC: An Analysis Program for Dynamic Loadings on Masonry and Reinforced Concrete Walls*. Thesis. Mississippi State University, 1989.

Kiger, Sam, and Hani Salim. "Use and Misuse of Structural Damping in Blast Response Calculations." *ACI SPECIAL PUBLICATIONS* 175.7 (1998): 121-30. Print.

Knox, Kenneth, Michael Hammons, Timothy Lewis, and Jonathan Porter. "Polymer Materials for Structural Retrofit." 2000: 1-17.

Lane, Jordan W. *Modeling and Design of Explosion-Resistant Steel Stud Wall Systems*. Thesis. University of Missouri--Columbia, 2003.

McDowell, E. L., K. E. McKee, A.M. ASCE, and E. Sevin. "Arching Action Theory of Masonry Walls." *Journal of the Structural Division* 82.2 (1956): 1-8.

Moradi, Lee G., and James S. Davidson. *Resistance of Membrane Retrofit Concrete Masonry Walls to Lateral Pressure*. 2008.

Moradi, Lee G., Robert J. Dinan, Bryan T. Bewick, and James S. Davidson. *Resistance of Concrete Masonry Walls with Membrane Catcher Systems Subjected to Blast Load*. 2010.

Nassr, Amr, Ghani Rasaqpur, Michael Tait, Manual Campidelli, and Simon Foo. "Single and Multi Degree of Freedom Analysis of Steel Beams under Blast Loading." Nuclear Engineering and Design 242.January (2012). Print.

National Research Council (NRC). (1995). Protecting Buildings for Bomb Damage: Transfer of Blast-Effects Mitigation Technologies from Military to Civilian Applications. Washington D.C.: National Academy Press.

Newman, Craig. "Timeline: From Boston Marathon to Chicago Haymarket Riots - Bombings in U.S. History - Sun-Times News." *Timeline: From Boston Marathon to Chicago Haymarket Riots - Bombings in U.S. History - Sun-Times News*. Chicago Sun-Times, 15 Apr. 2013. Web. 16 May 2013. <http://blogs.suntimes.com/news/2013/04/timeline_us_bombings_boston_marathon_chicago_haymarket.html>.

Paulay, T., and M. J. N. Priestley. *Seismic Design of Reinforced Concrete and Masonry Buildings*. New York: Wiley, 1992.

Protective Design Center. "Engineering Technical Letter (ETL) 110-3-494: Airblast Protection Retrofit for Unreinforced Concrete Masonry Walls." 1999

Protective Design Center. *Methodology Manual for the Single-Degree-of-Freedom Blast Effects Design Spreadsheets (SBEDS)*. Tech. no. TR-06-01. 2008.

Protective Design Center. *Single-Degree-of-Freedom Structural Response Limits for Antiterrorism Design*. Tech. no. TR 06-08. 2008. Print.

Protective Design Center. *User's Guide for the Single-Degree-of-Freedom Blast Effects Design Spreadsheets (SBEDS)*. Tech. no. TR-06-02. 2008.

Sadame, Sushant. *Development of Computational Models and Input Sensitive Study of Polymer Reinforced Concrete Masonry Walls Subjected to Blast*. Thesis. University of Alabama at Birmingham, 2004.

Salim, Hani, Robert J. Dinan, and John Kennedy. *Blast-Retrofit of CMU Walls Using Steel Sheets*. 2006.

Salim, Hani, Robert Dinan, and John Hoemann. *Blast-Retrofit of Gravity Infill Walls Using Ductile Thin Sheets*. 2007.

Seide, Paul. "Large Deflections of Rectangular Membranes Under Uniform Pressure." *International Journal of Nonlinear Mechanics.* 12 (1977): 397-406.

Slawson, Thomas R. *Wall Response to Airblast Loads: The Wall Analysis Code (WAC)*. 1995.

"Terrorist Through America's History." (2004) American History. <http://americanhistory.about.com/library/fastfacts/blffterrorism.htm>

The Mason Contractors Association of America. "Masonry Facts." *Masonry Facts*. The Mason Contractors Association of America. Web. 16 May 2013. <http://www.masoncontractors.org/aboutmasonry/masonryfacts/>.

Thornburg, Danica L. *Evaluation of Elastomeric Polymers Used for External Reinforcement of Masonry Walls Subjected to Blast*. Thesis. University of Alabama at Birmingham, 2004.

Unified Facilities Criteria (UFC). UFC 3-340-02 Structures to Resist the Effects of Accidental Explosions. 2008. 1635-649. Print.

Wiehle, Carl K., James Bokholt, and Stanford Research Institute Menlo Park California. Existing Structures Evaluation Part I: Walls. Tech. 1969. Print.

Young, Warren C., Richard G. Budynas, Ali M. Sadegh, and Raymond J. Roark. *Roark's Formulas for Stress and Strain*. New York: McGraw-Hill, 2011. Print.

Appendix A

Routine for Resistance Definition of Retrofit with Plate Connections

Appendix A

$$\text{StaticResistance}(L, t, L_p, E, t_p, \nu, f_y, \text{Membrane}, \beta) :=$$

$\Delta_1 \leftarrow 0.001$

$p_1 \leftarrow 0$

$I \leftarrow \frac{t_p^3}{12}$

$Z \leftarrow \frac{t_p^2}{4}$

$M_p \leftarrow Z \cdot f_y$

$M_{plate} \leftarrow 0$

$\theta_1 \leftarrow 0$

$\delta_1 \leftarrow 0$

$\text{Phase} \leftarrow \text{"Elastic"}$

for $i \in 2..2000$

  if $\text{Phase} = \text{"Elastic"}$

    $\Delta_i \leftarrow \Delta_{i-1} + 0.01 \cdot \Delta_{i-1}$

    $\text{ArcLength}_i \leftarrow 4\frac{\Delta_i}{L}\cdot\left[\sqrt{\frac{L^2}{4}+\frac{L^4}{64\cdot(\Delta_i)^2}}+\left[\frac{L^3}{32(\Delta_i)^2}\right]\cdot\ln\left[\frac{L}{2}+\sqrt{\frac{L^2}{4}+\frac{L^4}{64\cdot(\Delta_i)^2}}\right]-\left[\frac{L^3}{32(\Delta_i)^2}\right]\ln\left(\frac{L^2}{8\Delta_i}\right)\right]$

    $\varepsilon_i \leftarrow \ln\left(1+\frac{\text{ArcLength}_i - L}{L}\right)$

    $\sigma_i \leftarrow \text{linterp}\left(\text{Membrane}^{\langle 1\rangle}, \text{Membrane}^{\langle 2\rangle}, \varepsilon_i\right)$

    $t_{membrane_i} \leftarrow -\nu \cdot t \cdot \varepsilon_i + t$

    $p_i \leftarrow \frac{2\cdot\sigma_i\cdot t_{membrane_i}}{L}\cdot\sin\left(\frac{4\Delta_i}{L}\right)$

    $T_i \leftarrow \sigma_i \cdot t_{membrane_i}$

Appendix A

$$\theta_i \leftarrow \frac{4 \cdot \Delta_i}{L}$$

$$M_{plate_i} \leftarrow T_i \cdot \cos(\theta_i) \cdot L_p + T_i \cdot \sin(\theta_i)\, \delta_{i-1}$$

$$\sigma_{Plate_i} \leftarrow \frac{M_{plate_i} \cdot \frac{t_p}{2}}{I}$$

$$\delta_i \leftarrow \frac{T_i \cdot \cos(\theta_i) \cdot L_p^{\,3}}{3E \cdot I}$$

$$\lambda_i \leftarrow \frac{T_i \cdot L_p^{\,2}}{2E \cdot I}$$

$$\Delta\lambda \leftarrow \lambda_i - \lambda_{i-1}$$

$$\Delta_{plate} \leftarrow \frac{\lambda_i \cdot L}{4}$$

$$\Delta_i \leftarrow \Delta_i + \Delta_{plate}$$

$$\alpha_i \leftarrow 0$$

$$\delta_{elastic} \leftarrow \delta_i$$

$$n_i \leftarrow \text{"Elastic"}$$

$$Tol_i \leftarrow \text{"Elastic"}$$

$$T_{elastic} \leftarrow T_i$$

$$Lprime_{p_i} \leftarrow 3$$

$$Phase \leftarrow \text{"Plastic"} \quad \text{if} \quad M_{plate_i} \geq M_p$$

break if $\Delta_i > 30$

if $Phase = \text{"Plastic"}$

$\alpha_i \leftarrow \alpha_{\ldots} + \beta$

Appendix A

if Phase = "Plastic"

$\alpha_i \leftarrow \alpha_{i-1} + \beta$

$Lprime_{p_i} \leftarrow L_p \cdot (1 - \sin(\alpha_i))$

$\delta_i \leftarrow \delta_{elastic} + \sin(\alpha_i) L_p$

$\Delta_{slack} \leftarrow Slack(L, L - 2 \cdot \delta_i)$

$\theta_i \leftarrow (\theta_{i-1}) + \frac{4 \cdot \Delta_{slack}}{L}$

$T_r \leftarrow \frac{M_p}{Lprime_{p_i} \cdot \cos(\theta_i) + \delta_i \cdot \sin(\theta_i)}$

for $j \in 1..1$

$n_i \leftarrow 3$

$def_1 \leftarrow 0$

$def_2 \leftarrow \Delta_{i-1}$

$Tol_i \leftarrow 1$

while $|Tol_i| > 0.001$

if $Tol_i < 0$

$\Delta_2 \leftarrow def_{n_i-1} + \left| \frac{def_{n_i-2} - def_{n_i-1}}{2} \right|$

$ArcLength_i \leftarrow 4 \frac{\Delta_2}{L} \cdot \left[\sqrt{\frac{L^2}{4} + \frac{L^4}{64 \cdot (\Delta_2)^2}} + \left[\frac{L^3}{32 (\Delta_2)^2} \right] \cdot \ln \left[\frac{L}{2} + \sqrt{\frac{L^2}{4} + \frac{L^4}{64 \cdot (\Delta_2)^2}} \right] - \left[\frac{L^3}{32 (\Delta_2)^2} \right] \ln \left(\frac{L^2}{8 \Delta_2} \right) \right]$

$\varepsilon_i \leftarrow \ln \left(1 + \frac{ArcLength_i - L}{L} \right)$

$\sigma_i \leftarrow linterp(Membrane^{\langle 1 \rangle}, Membrane^{\langle 2 \rangle}, \varepsilon_i)$

$t_{membrane_i} \leftarrow -\nu \cdot t \cdot \varepsilon_i + t$

$Tol_i \leftarrow t_{membrane_i} \cdot \sigma_i - T_r$

$\Delta_i \leftarrow \Delta_2$

$def_{(n_i)} \leftarrow \Delta_2$

$n_i \leftarrow n_i + 1$

break if $n_i > 200$

if $Tol_i > 0$

$\Delta_2 \leftarrow def_{n_i-1} - \left| \frac{def_{n_i-2} - def_{n_i-1}}{2} \right|$

$ArcLength_i \leftarrow 4 \frac{\Delta_2}{L} \cdot \left[\sqrt{\frac{L^2}{4} + \frac{L^4}{64 \cdot (\Delta_2)^2}} + \left[\frac{L^3}{32 (\Delta_2)^2} \right] \cdot \ln \left[\frac{L}{2} + \sqrt{\frac{L^2}{4} + \frac{L^4}{64 \cdot (\Delta_2)^2}} \right] - \left[\frac{L^3}{32 (\Delta_2)^2} \right] \ln \left(\frac{L^2}{8 \Delta_2} \right) \right]$

$\varepsilon_i \leftarrow \ln \left(1 + \frac{ArcLength_i - L}{L} \right)$

$\sigma_i \leftarrow linterp \left(Membrane^{\langle 1 \rangle}, Membrane^{\langle 2 \rangle}, \varepsilon_i \right)$

$t_{membrane_i} \leftarrow -\nu \cdot t \cdot \varepsilon_i + t$

$Tol_i \leftarrow t_{membrane_i} \cdot \sigma_i - T_r$

$\Delta_i \leftarrow \Delta_2$

$def_{(n_i)} \leftarrow \Delta_2$

$n_i \leftarrow n_i + 1$

break if $n_i > 200$

$T_i \leftarrow t_{membrane_i} \cdot \sigma_i$

$\Delta_i \leftarrow \Delta_i + \Delta_{slack}$

$\theta_i \leftarrow \frac{4 \cdot \Delta_i}{L}$

$p_i \leftarrow \frac{2 \cdot (T_i)}{L} \cdot \sin(\theta_i)$

$M_{plate_i} \leftarrow T_i \cdot \sin(\theta_i) \cdot \delta_i + T_i \cdot \cos(\theta_i)\, Lprime_{p_i}$

break if $\Delta_i > 30$

if $\Delta_i < \Delta_{i-1}$

$\Delta_i \leftarrow \Delta_{i-1} + 0.00001$

break

$\Delta_1 \leftarrow 0$

$Result \leftarrow augment(\Delta, p, T, \theta)$

Result

Appendix B

Finite Element Results Compared to Algorithm

Table B-1: Additional Test Configurations

#	Height (in)	Material	Plate Thickness (in)	Membrane Thickness (in)	Length of Plate (in)
1	120	Polymer	0.5	0.039	3
2	120	Polymer	0.75	0.039	3
3	120	Steel	0.5	0.039	3
4	120	Steel	0.75	0.039	3
5	120	Polymer	0.25	0.079	3
6	120	Polymer	0.5	0.079	3
7	120	Steel	0.25	0.079	3
8	120	Steel	0.5	0.079	3
9	72	Polymer	0.25	0.039	3
10	120	Polymer	0.25	0.039	5

Appendix B

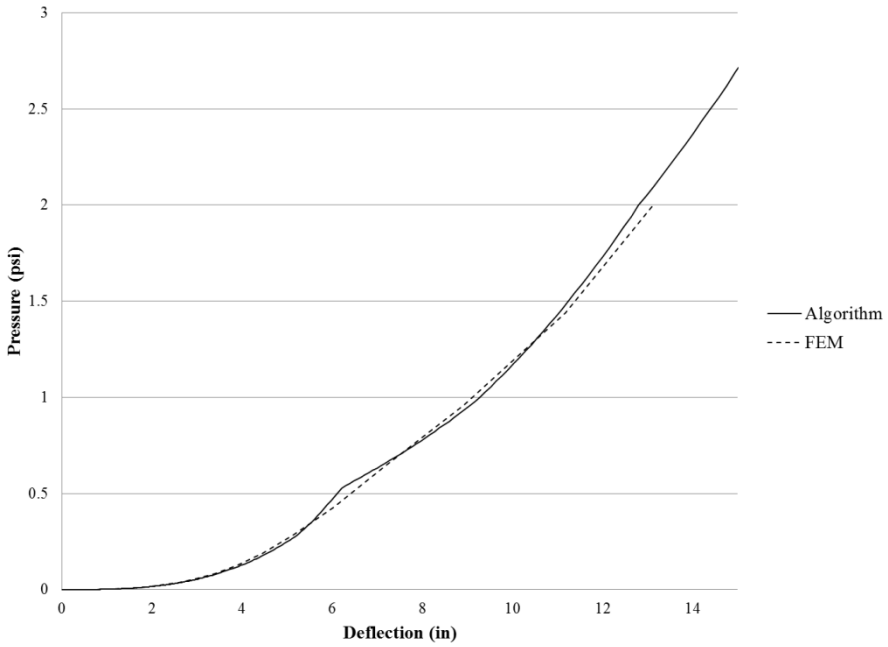

Figure B-1: Configuration 1

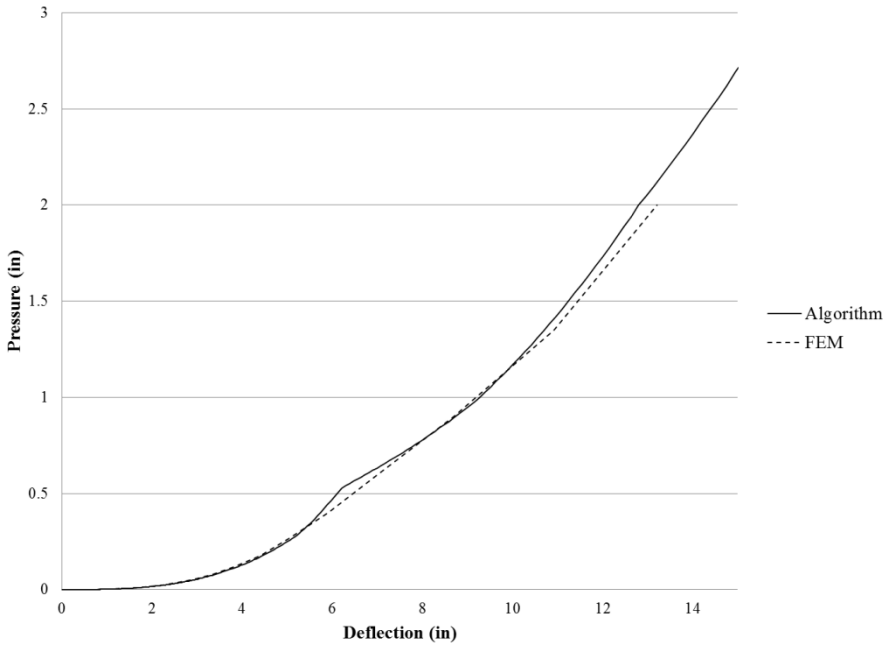

Figure B-2: Configuration 2

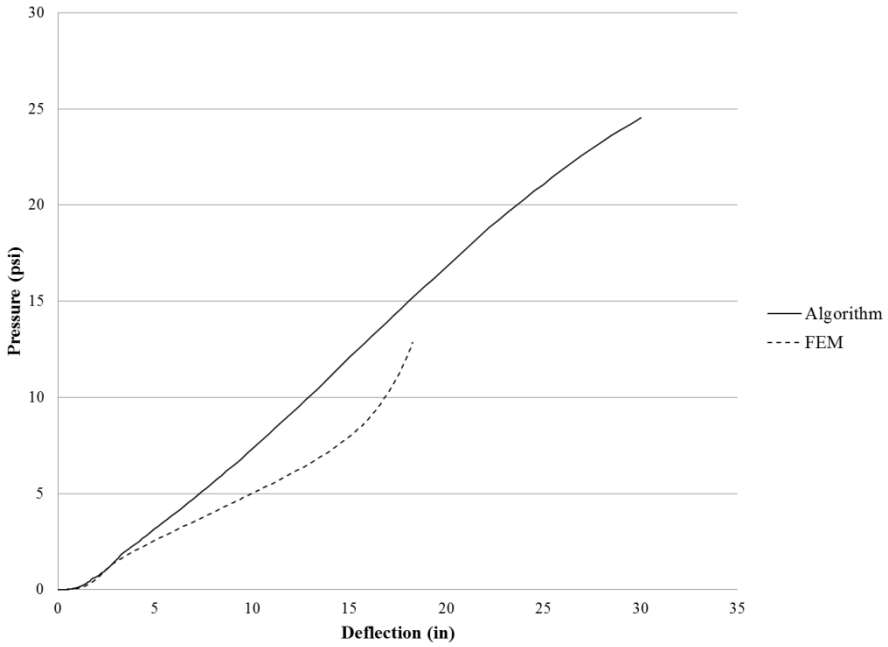

Figure B-3: Configuration 3

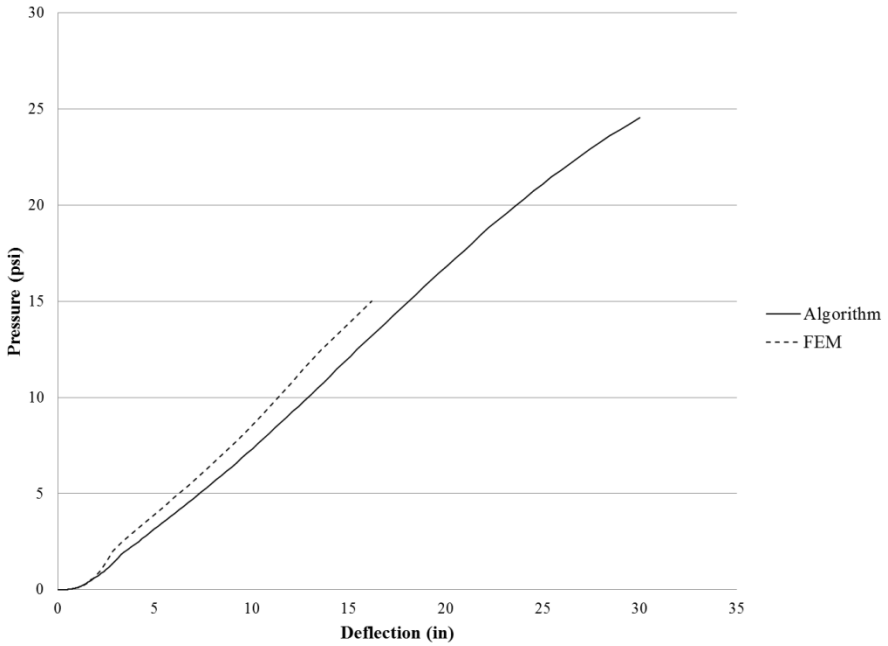

Figure B-4: Configuration 4

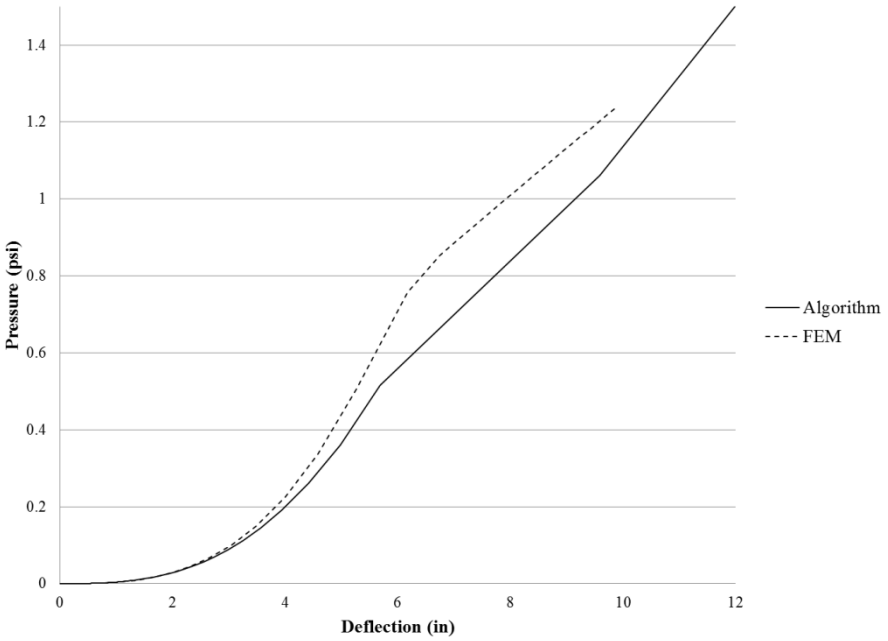

Figure B-5: Configuration 5

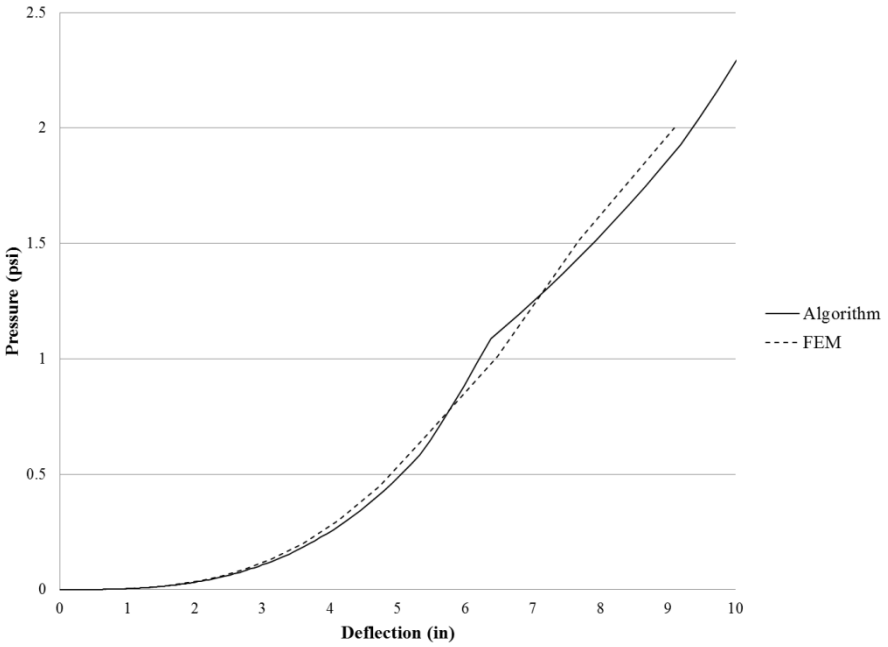

Figure B-6: Configuration 6

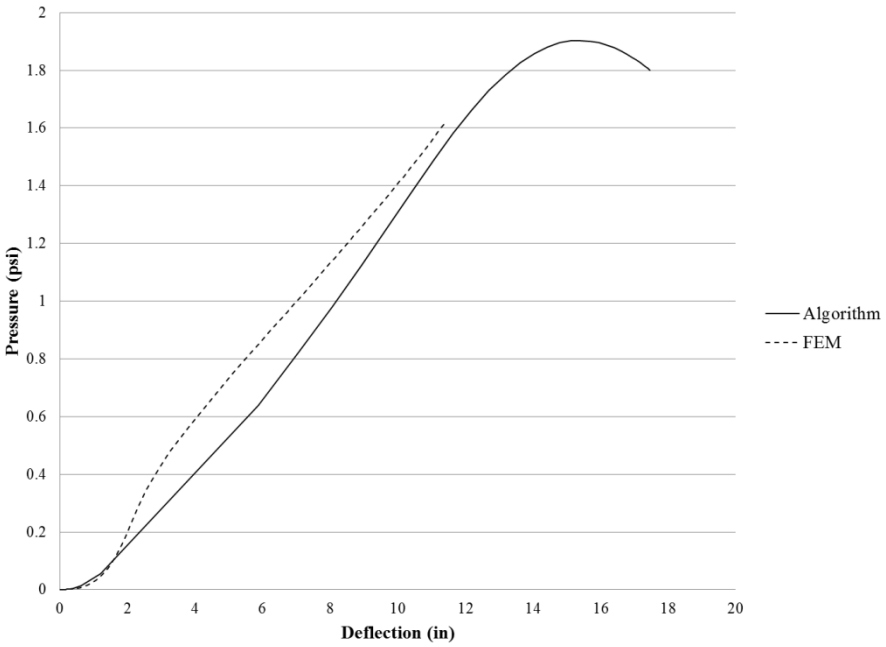

Figure B-7: Configuration 7

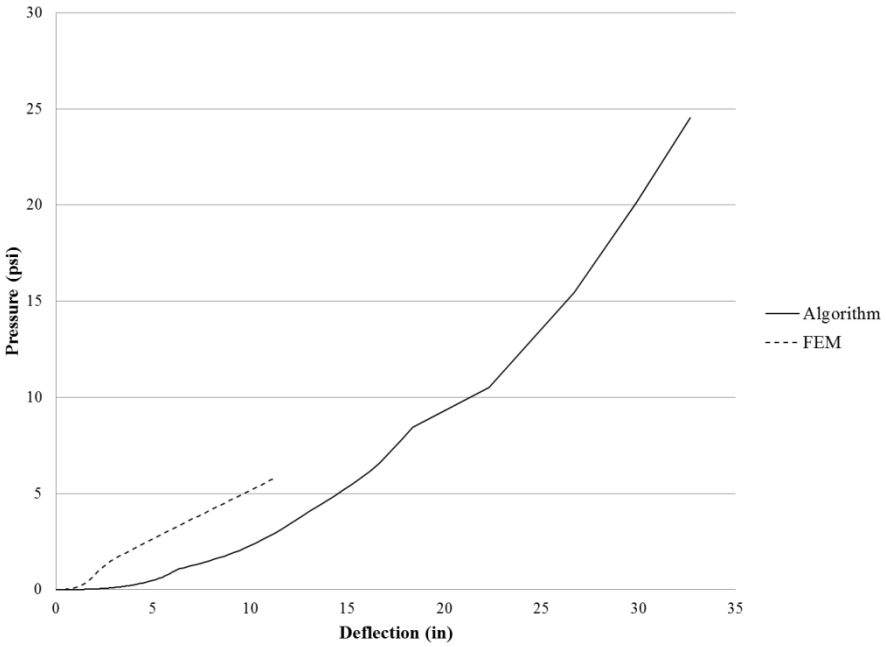

Figure B-8: Configuration 8

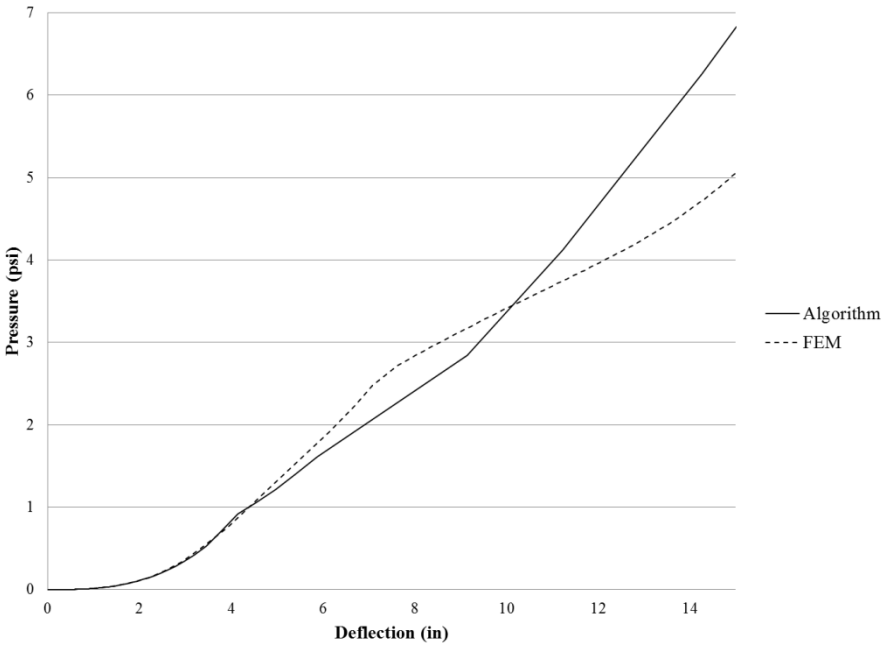

Figure B-9: Configuration 9

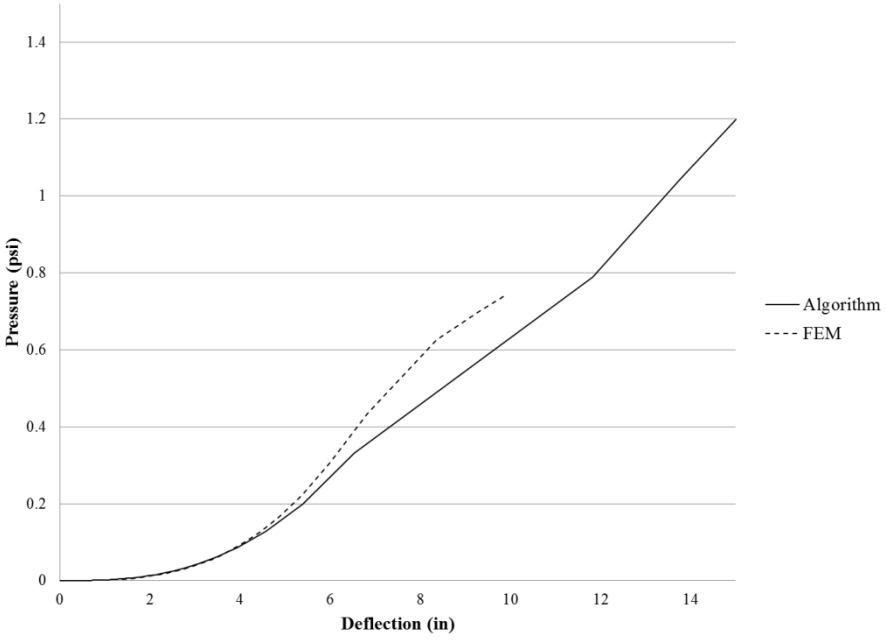

Figure B-10: Configuration 10

Appendix C
Other Routines

Appendix C

$$\text{CombineResistance}(\text{Wall}, \text{Membrane}) := \left| \begin{array}{l} N \leftarrow \text{rows}(\text{Membrane}) \\ \text{for } i \in 1..N \\ \quad \left| \begin{array}{l} R_{wall} \leftarrow \text{linterp}\left(\text{Wall}^{\langle 1 \rangle}, \text{Wall}^{\langle 2 \rangle}, \text{Membrane}_{i,1}\right) \\ \Delta_i \leftarrow \text{Membrane}_{i,1} \\ p_i \leftarrow R_{wall} + \text{Membrane}_{i,2} \end{array} \right. \\ \text{augment}(\Delta, p) \end{array} \right.$$

$$\text{WiehleNonArching}(E, t, L, P, F, I, w) := \left| \begin{array}{l} \Delta_1 \leftarrow 0 \\ p_1 \leftarrow 0 \\ p_2 \leftarrow \frac{4 \cdot t}{3 \cdot L^2} \cdot (F \cdot t + P) \\ \Delta_2 \leftarrow \frac{5 \cdot p_2 \cdot L^4}{384 \cdot E \cdot I} \\ i \leftarrow 2 \\ \text{while } \Delta_i < t \\ \quad \left| \begin{array}{l} i \leftarrow i + 1 \\ \Delta_i \leftarrow \Delta_{i-1} + 0.01 \\ p_i \leftarrow \frac{4}{L^2} \cdot \left(t - \Delta_i\right) \cdot \left(P + \frac{w}{2}\right) \end{array} \right. \\ \Delta_i \leftarrow t \\ p_i \leftarrow 0 \\ \text{Results} \leftarrow \text{augment}(\Delta, p) \\ \text{Results} \end{array} \right.$$

SBEDS method adapted for one way spanning CMU wall with arching along vertical face. Therefor c, C2 and ε are not used. Assumes face shell, ts, is 1.25 in.

$$\text{SBEDSArching}(t, L, f_m, F_r, E, \text{Gap}) :=$$

$\Delta_g \leftarrow t - \sqrt{\left(\frac{L}{2}\right)^2 + t^2 - \left(\frac{L + \text{Gap}}{2}\right)^2}$

$\Delta_1 \leftarrow 0$

$p_1 \leftarrow 0$

$\Delta_m \leftarrow \min\left(\frac{L}{30}, \frac{t}{2}\right) + \Delta_g$

$s \leftarrow 0.2E$

$B_1 \leftarrow 0.85$

$C_1 \leftarrow 0.85 f_m \cdot 1.25$

if $\text{Gap} > 0$

- $\Delta_2 \leftarrow \text{Gap}$
- $p_2 \leftarrow 0$
- $\Delta_3 \leftarrow \Delta_m$
- $p_3 \leftarrow \frac{8}{L^2} \cdot \left[2 \cdot C_1 \cdot \left(\frac{t}{2} - \frac{1.25}{2}\right) - C_1 \cdot \Delta_m\right]$
- $\Delta_4 \leftarrow \min\left(\min(0.08L, 0.8) + \Delta_g, t\right)$
- $p_4 \leftarrow 0$
- $p_5 \leftarrow 0$
- $\Delta_5 \leftarrow 100$

if $\text{Gap} = 0$

- $\Delta_2 \leftarrow \Delta_m$
- $p_2 \leftarrow \frac{8}{L^2} \cdot \left[2 \cdot C_1 \cdot \left(\frac{t}{2} - \frac{1.25}{2}\right) - C_1 \cdot \Delta_m\right]$
- $\Delta_3 \leftarrow \min\left(\min(0.08L, 0.8) + \Delta_g, t\right)$
- $p_3 \leftarrow 0$
- $p_4 \leftarrow 0$
- $\Delta_4 \leftarrow 100$

$\text{augment}(\Delta, p)$

$$\text{Transition}(\text{WallResults}) := \left| \begin{array}{l} N \leftarrow \text{rows}(\text{WallResults}) \\ \text{Max} \leftarrow \max\left(\text{WallResults}^{\langle 2 \rangle}\right) \\ \text{for } i \in 1..N \\ \quad \Delta \leftarrow \text{WallResults}_{i,1} \text{ if } \text{WallResults}_{i,2} = \text{Max} \\ \Delta \end{array} \right.$$

$$\text{SDOFpinpin}(m, L, \text{Load}, \text{Resistance}, \Delta t, K_{LM}, \text{Trans}) :=$$

$n \leftarrow \text{rows}(\text{Load})$

$N \leftarrow \dfrac{\text{Load}_{n,1}}{\Delta t}$

$M_t \leftarrow m \cdot L$

$\Delta_1 \leftarrow 0$

$\Delta_2 \leftarrow 0$

$t_1 \leftarrow 0$

$\text{Phase} \leftarrow \text{"Elastic"}$

for $i \in 2..N$ if $\text{Phase} = \text{"Elastic"}$

- $t_i \leftarrow \Delta t + t_{i-1}$
- $w \leftarrow \text{linterp}\left(\text{Load}^{\langle 1 \rangle}, \text{Load}^{\langle 2 \rangle}, t_i\right)$
- $R \leftarrow \text{linterp}\left(\text{Resistance}^{\langle 1 \rangle}, \text{Resistance}^{\langle 2 \rangle}, \Delta_i\right)$
- $z'' \leftarrow \dfrac{w \cdot L}{K_{LM_1} \cdot M_t} - \dfrac{R \cdot L}{K_{LM_1} \cdot M_t}$
- $\Delta_{i+1} \leftarrow z'' \cdot \Delta t^2 - \Delta_{i-1} + 2 \cdot \Delta_i$
- $j \leftarrow i$
- $\text{Phase} \leftarrow \text{"Plastic"}$ if $\Delta_{i+1} > \text{Trans}$
- $\text{trace}(\text{Phase}, i)$
- break if $\Delta_{i+1} < \Delta_{i-1}$

for $i \in j..N$ if $\text{Phase} = \text{"Plastic"}$

- $t_i \leftarrow \Delta t + t_{i-1}$
- $w \leftarrow \text{linterp}\left(\text{Load}^{\langle 1 \rangle}, \text{Load}^{\langle 2 \rangle}, t_i\right)$
- $R \leftarrow \text{linterp}\left(\text{Resistance}^{\langle 1 \rangle}, \text{Resistance}^{\langle 2 \rangle}, \Delta_i\right)$
- $z'' \leftarrow \dfrac{w \cdot L}{K_{LM_2} \cdot M_t} - \dfrac{R \cdot L}{K_{LM_2} \cdot M_t}$
- $\Delta_{i+1} \leftarrow z'' \cdot \Delta t^2 - \Delta_{i-1} + 2 \cdot \Delta_i$
- break if $\Delta_{i+1} < \Delta_{i-1}$

$t_{i+1} \leftarrow t_i + \Delta t$

$\text{Result} \leftarrow \text{augment}(t, \Delta)$

Result

Appendix D
Design Example Computations

WALL #1

Wall Properties:

Non-Arching $t_{wall} := 7.625$ $P := 0$ $F_r := 65$ $Ec := f_m \cdot 1000$ $L := 144$

$Gap := 0$ $w_{wall} := 29.30$ $f_m := 1350$

$$m := \frac{w_{wall}}{144 \cdot \left(3.861 \times 10^{-4}\right)} = 526.994$$

Resistance Function

$Wall := SBEDSArching\left(t_{wall}, L, f_m, F_r, Ec, Gap\right)$

SDOF

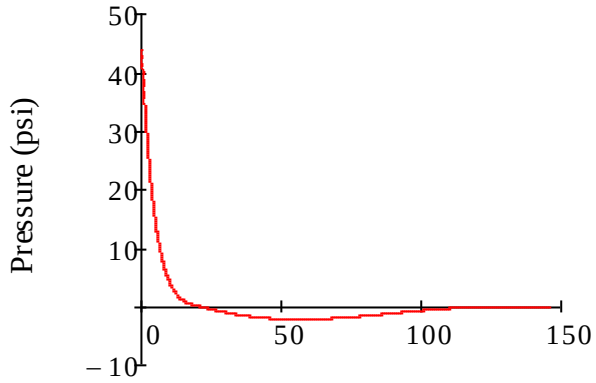

$\Delta t := 0.01$ $Trans := Transition(Wall) = 3.813$ $K_{LMWall} := \begin{pmatrix} 0.77 \\ 0.66 \end{pmatrix}$

$SDOF_{wall} := SDOFpinpin\left(m, L, Load, Wall, \Delta t, K_{LMWall}, Trans\right)$

Response Limits

$$B2 := \tan(1.5\text{deg}) \cdot \frac{L}{2} = 1.885$$

$$B3 := \tan(4\text{deg}) \cdot \frac{L}{2} = 5.035$$

$$B4 := \tan(8\text{deg}) \cdot \frac{L}{2} = 10.119$$

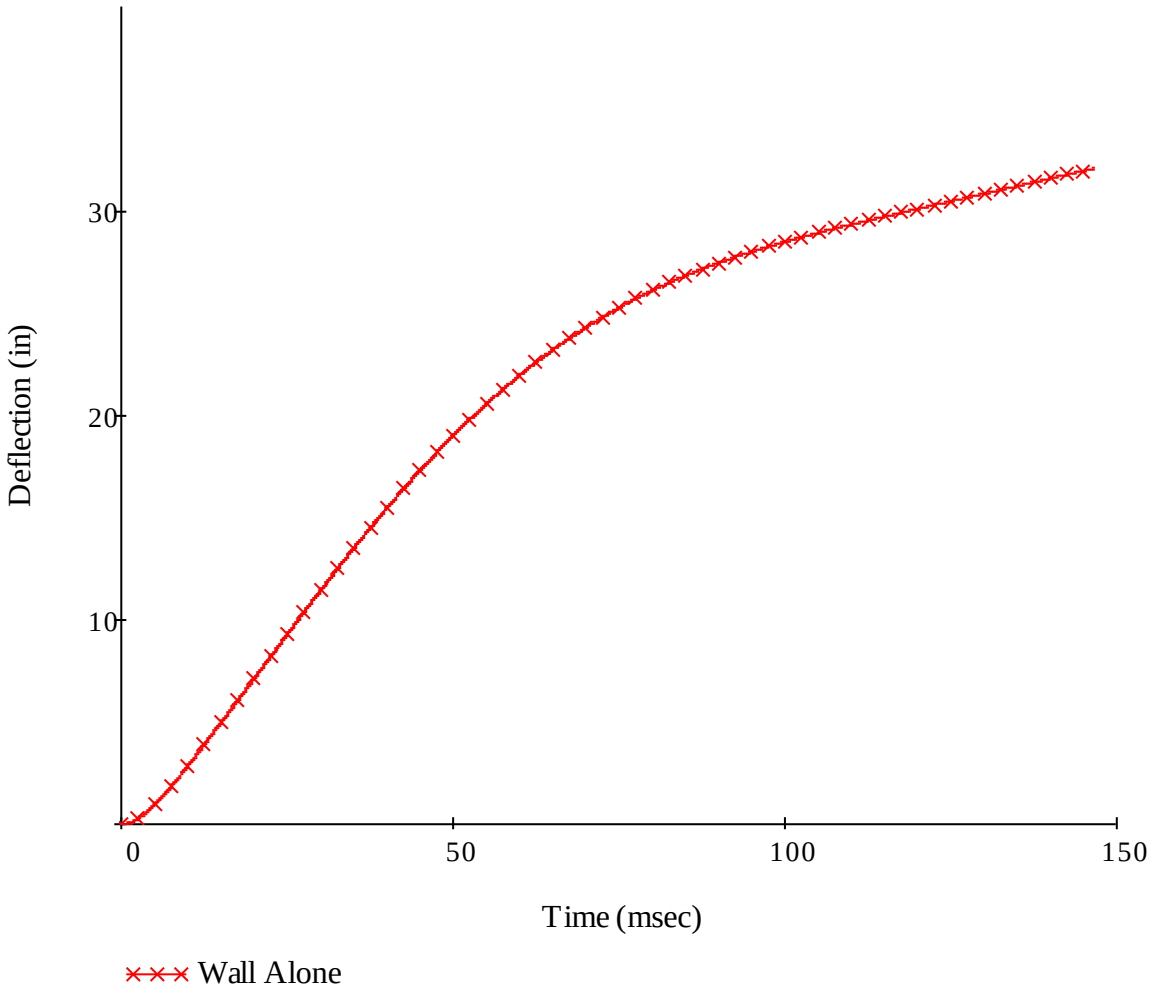

$$Max\Delta_{wall} := \max\left(SDOF_{wall}^{\langle 2 \rangle}\right) = 32.121 \qquad angle := \operatorname{atan}\left(\frac{Max\Delta_{wall}}{\frac{L}{2}}\right) = 24.043 \cdot \text{deg}$$

Trial 1

Membrane Properties:

$L := 144$

$t := 0.0359 \cdot 2$

$f_y := 36000$

$L_p := 3$

$E := 29000000$

$\beta := 5 \cdot 10^{-2}$

$t_p := .25$

$\nu := 0.2$

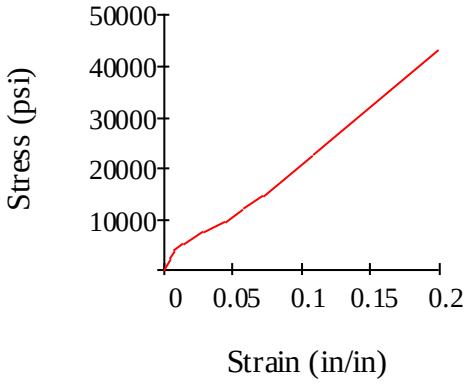

Resistance Definition:

$Membrane := StaticResistance(L, t, L_p, E, t_p, \nu, f_y, Polymer, \beta)$

$TotalResistance := (CombineResistance(Wall, Membrane))$

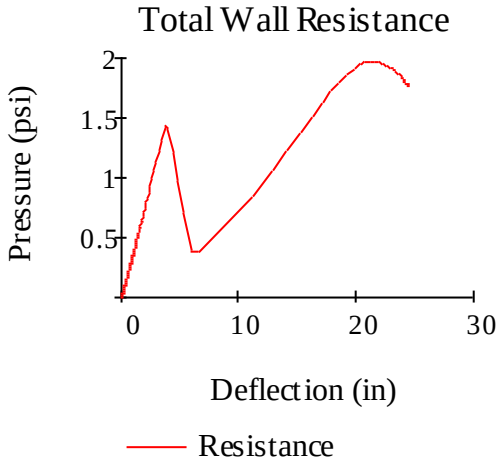

SDOF:

$$K_{LM} := \begin{pmatrix} 0.77 \\ 0.8 \end{pmatrix}$$

$SDOF := SDOFpinpin(m, L, Load, TotalResistance, \Delta t, K_{LM}, Trans)$

$MaxDeflection := \max(SDOF^{\langle 2 \rangle}) = 21.659$ $\quad angle := \operatorname{atan}\left(\frac{MaxDeflection}{\frac{L}{2}}\right) = 16.742 \cdot deg$

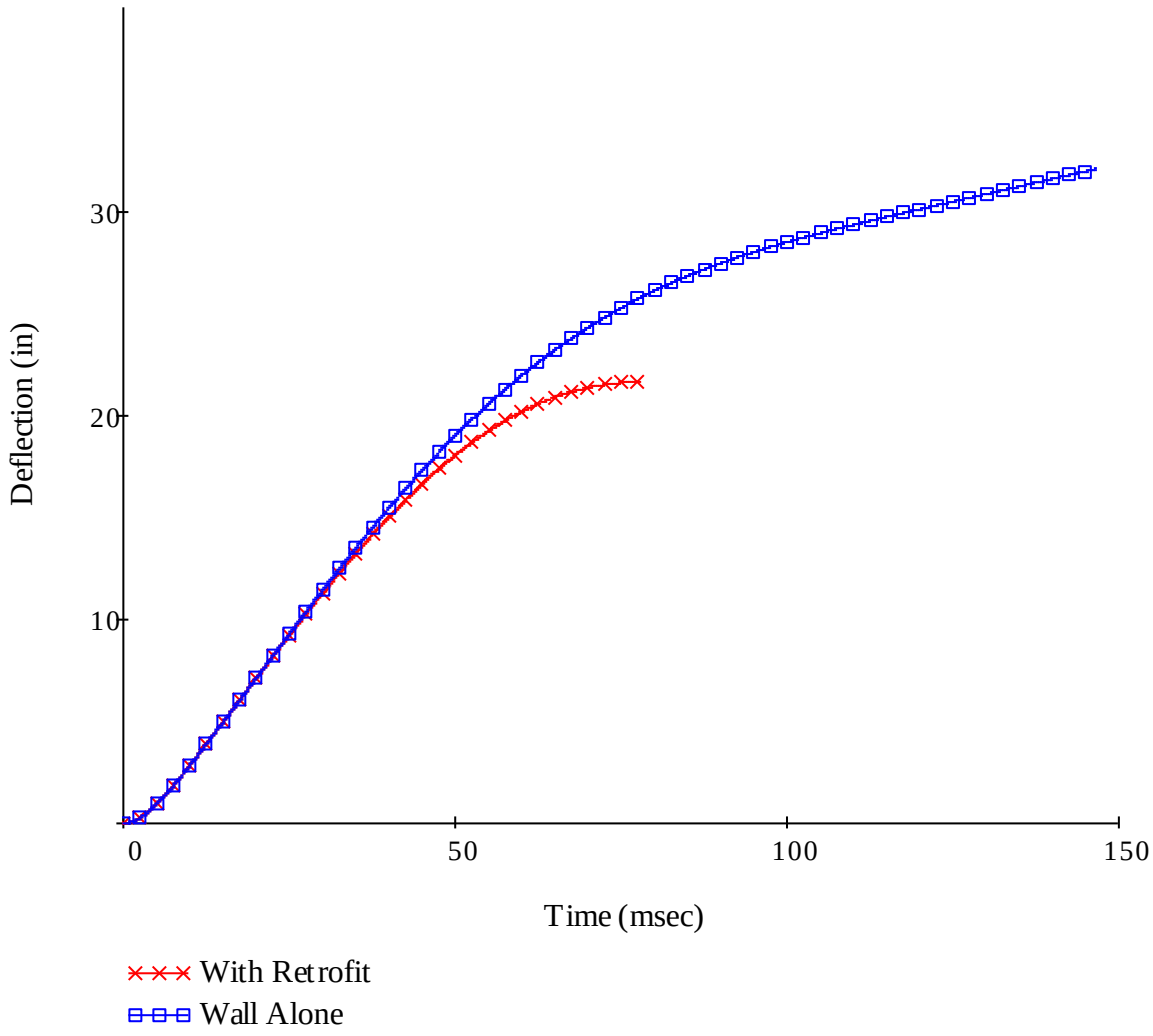
Deflection (in)
30
20
10
0
50
100
150
Time (msec)
With Retrofit
Wall Alone

Trial 2

Membrane Properties:

$L := 144$

$t := 0.0359 \cdot 13$

$f_y := 36000$

$L_p := 3.00$

$E := 29000000$

$\beta := 5 \cdot 10^{-2}$

$t_p := 0.75$

$\nu := 0.2$

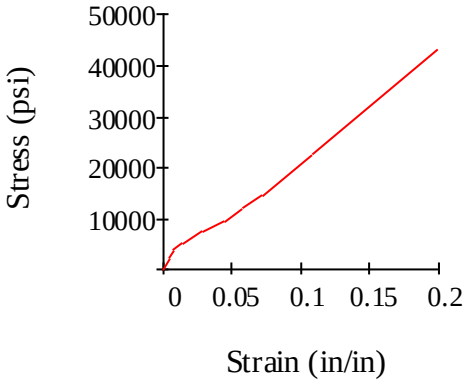

Resistance Definition:

$Membrane := StaticResistance(L, t, L_p, E, t_p, \nu, f_y, Polymer, \beta)$

$TotalResistance := (CombineResistance(Wall, Membrane))$

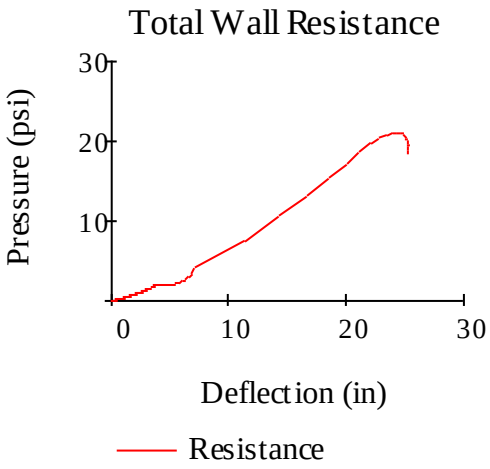

SDOF:

$$K_{LM} := \begin{pmatrix} 0.77 \\ 0.8 \end{pmatrix}$$

$SDOF := SDOFpinpin(m, L, Load, TotalResistance, \Delta t, K_{LM}, Trans)$

$MaxDeflection := \max(SDOF^{\langle 2 \rangle}) = 11.943$ $\quad angle := atan\left(\frac{MaxDeflection}{\frac{L}{2}}\right) = 9.418 \cdot deg$

Appendix D

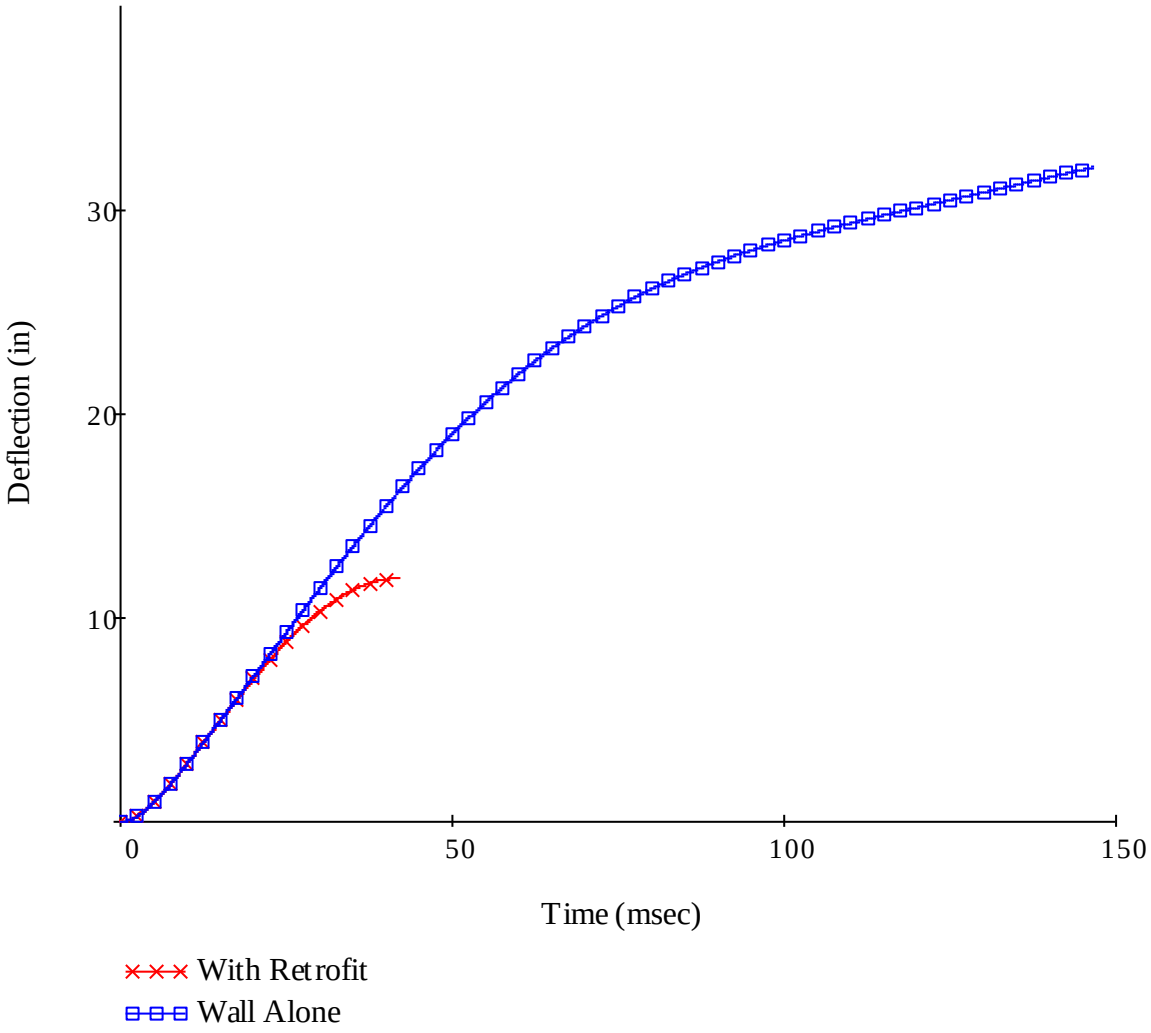
Deflection (in)
30
20
10
0
50
100
150
Time (msec)
With Retrofit
Wall Alone

Trial 3

Membrane Properties:

$L := 144$

$t := 0.0673$

$f_y := 36000$

$L_p := 3.00$

$E := 29000000$

$\beta := 5 \cdot 10^{-2}$

$t_p := \frac{7}{8}$

$\nu := 0.2$

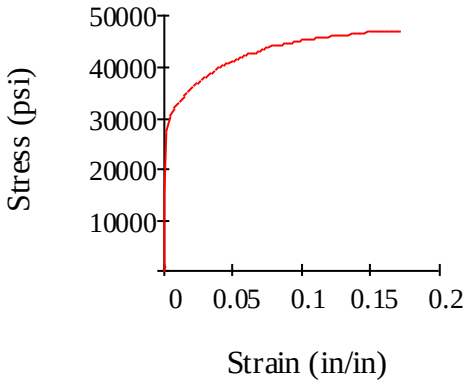

Resistance Definition:

Membrane := StaticResistance(L, t, L_p, E, t_p, ν, f_y, Plate, β)

TotalResistance := (CombineResistance(Wall, Membrane))

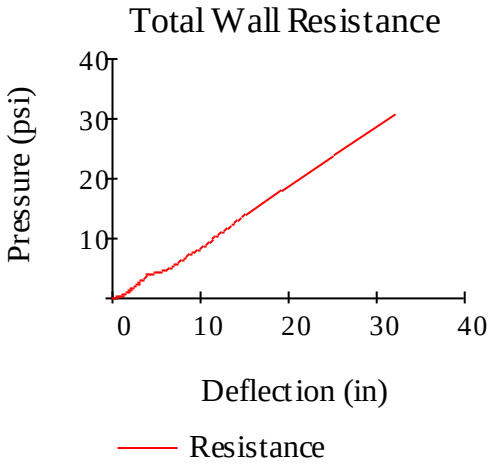

SDOF:

$$K_{LM} := \begin{pmatrix} 0.77 \\ 0.8 \end{pmatrix}$$

SDOF := SDOFpinpin(m, L, Load, TotalResistance, Δt, K_{LM}, Trans)

MaxDeflection := $\max(SDOF^{\langle 2 \rangle}) = 10.082$

$$angle := \operatorname{atan}\left(\frac{MaxDeflection}{\frac{L}{2}}\right) = 7.971 \cdot deg$$

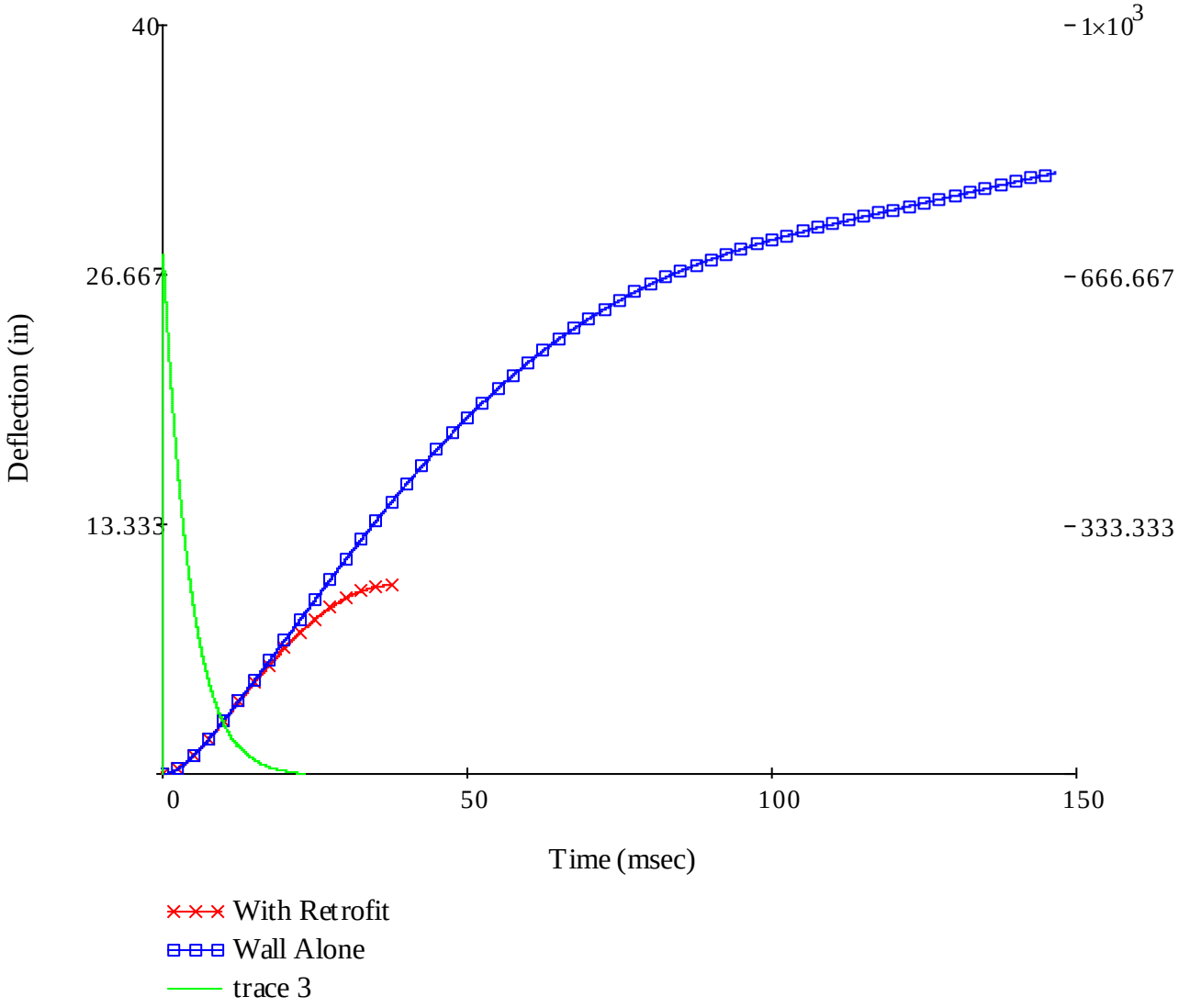

Bolt Loads:

$$T_{Axial} := linterp\left(Membrane^{\langle 1 \rangle}, Axial(Membrane), MaxDeflection\right) = 2175.1$$

$$T_{Shear} := linterp\left(Membrane^{\langle 1 \rangle}, Shear(Membrane), MaxDeflection\right) = 610.8$$

$$Area_{Bolt} := \frac{\left(\frac{5}{8}\right)^2 \cdot \pi}{4} = 0.307$$

$$\sigma_{normal} := \frac{T_{Axial} \cdot 8}{Area_{Bolt}} = 56717.1 \quad psi$$

$$\sigma_{shear} := \frac{T_{Shear} \cdot 8}{Area_{Bolt}} = 15927.7 \quad psi$$

WALL #2

Wall Properties:

$f_m := 1350$ $t_{wall} := 7.625$ $P := 100$ $F_r := 65$ $L := 120$

$Gap := 0$ $w_{wall} := 29.30$ $I := 28.4$ $Ec := f_m \cdot 1000$

$$m := \frac{w_{wall}}{144 \cdot \left(3.861 \times 10^{-4}\right)} = 526.994$$

Resistance Function

$Wall := WiehleNonArching(Ec, t_{wall}, L, P, F_r, I, w_{wall})$

SDOF

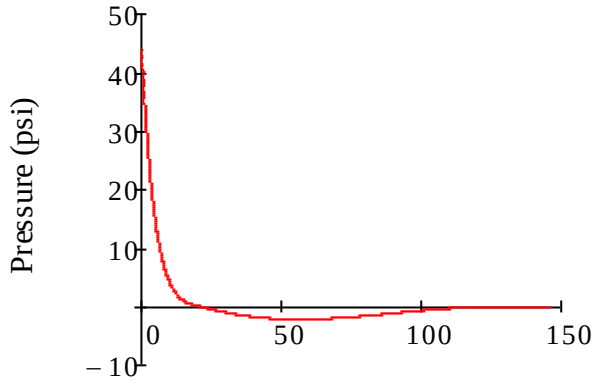

$\Delta t := 0.01$ $Trans := Transition(Wall) = 0.03$ $K_{LMWall} := \begin{pmatrix} 0.77 \\ 0.66 \end{pmatrix}$

$SDOF_{wall} := SDOFpinpin(m, L, Load, Wall, \Delta t, K_{LMWall}, Trans)$

Response Limits

$$B2 := \tan(1.5\text{deg}) \cdot \frac{L}{2} = 1.571$$

$$B3 := \tan(4\text{deg}) \cdot \frac{L}{2} = 4.196$$

$$B4 := \tan(8\text{deg}) \cdot \frac{L}{2} = 8.432$$

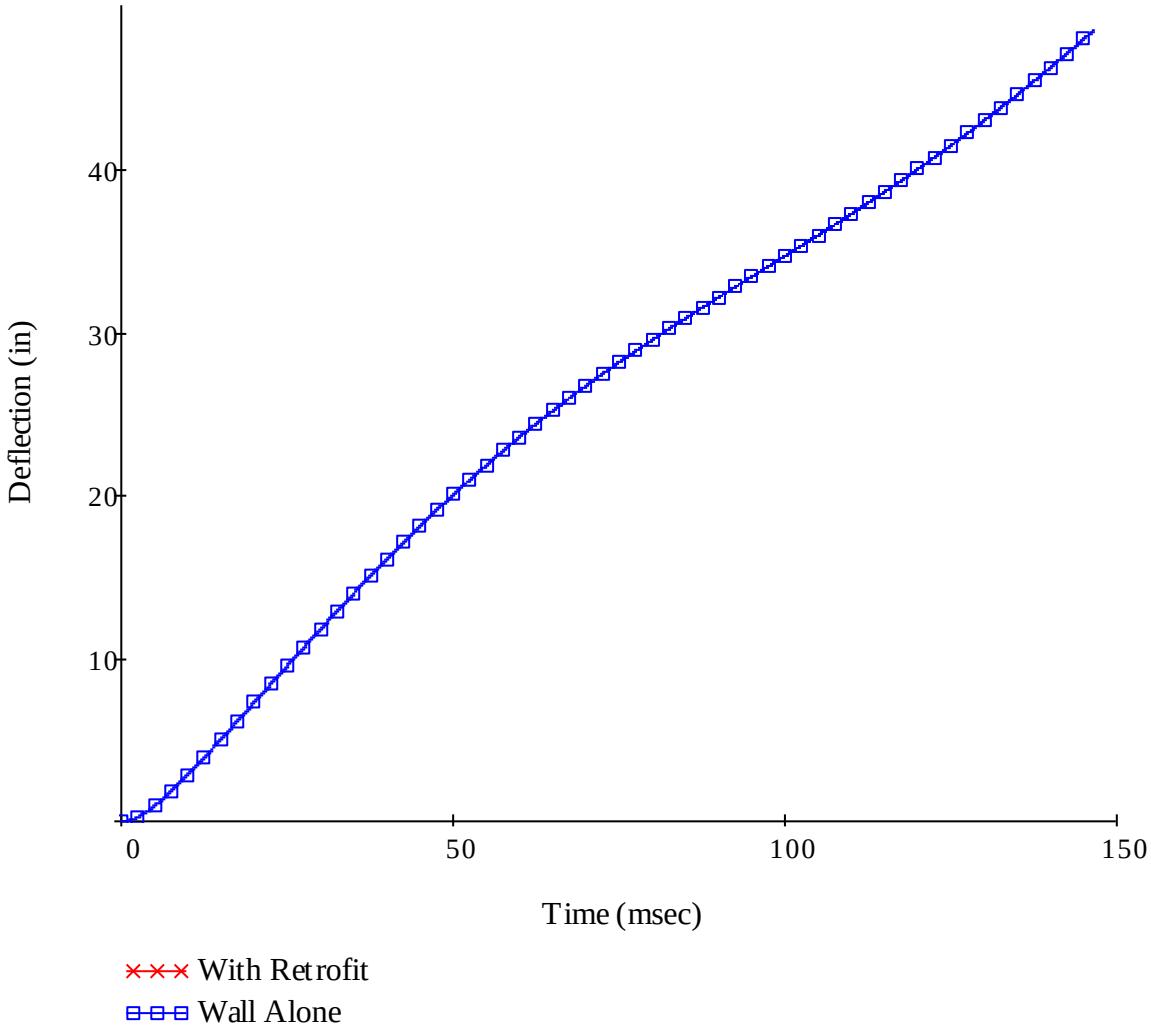

$$\text{Max}\Delta_{\text{wall}} := \max\left(\text{SDOF}_{\text{wall}}^{\langle 2 \rangle}\right) = 48.552 \qquad \text{angle} := \text{atan}\left(\frac{\text{Max}\Delta_{\text{wall}}}{\frac{L}{2}}\right) = 38.98\,\text{deg}$$

Trial 1

Membrane Properties:

$L := 120$

$t := 0.1345$

$f_y := 36000$

$L_p := 3$

$E := 29000000$

$\beta := 5 \cdot 10^{-2}$

$t_p := 0.50$

$\nu := 0.2$

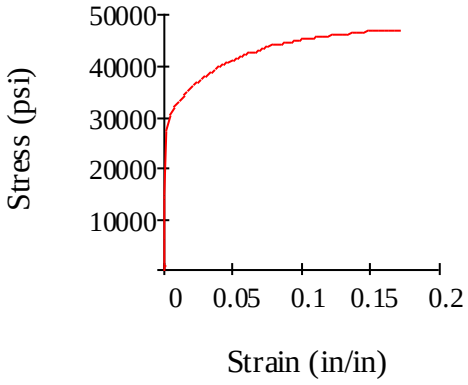

Resistance Definition:

Membrane := StaticResistance$(L, t, L_p, E, t_p, \nu, f_y, Plate, \beta)$

TotalResistance := (CombineResistance(Wall, Membrane))

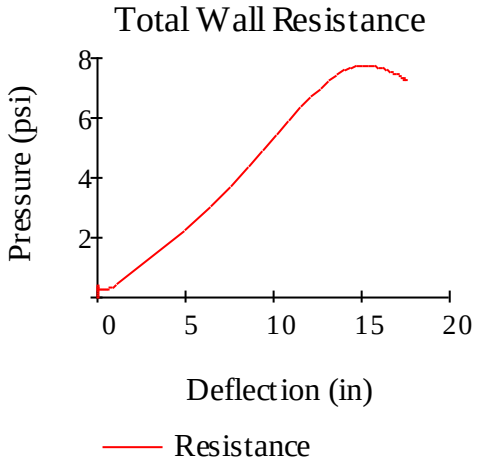

SDOF:

$$K_{LM} := \begin{pmatrix} 0.77 \\ 0.8 \end{pmatrix}$$

SDOF := SDOFpinpin$(m, L, Load, TotalResistance, \Delta t, K_{LM}, Trans)$

MaxDeflection := $\max(SDOF^{\langle 2 \rangle}) = 12.277$ angle := $\operatorname{atan}\left(\frac{MaxDeflection}{\frac{L}{2}}\right) = 11.564\,deg$

Appendix D

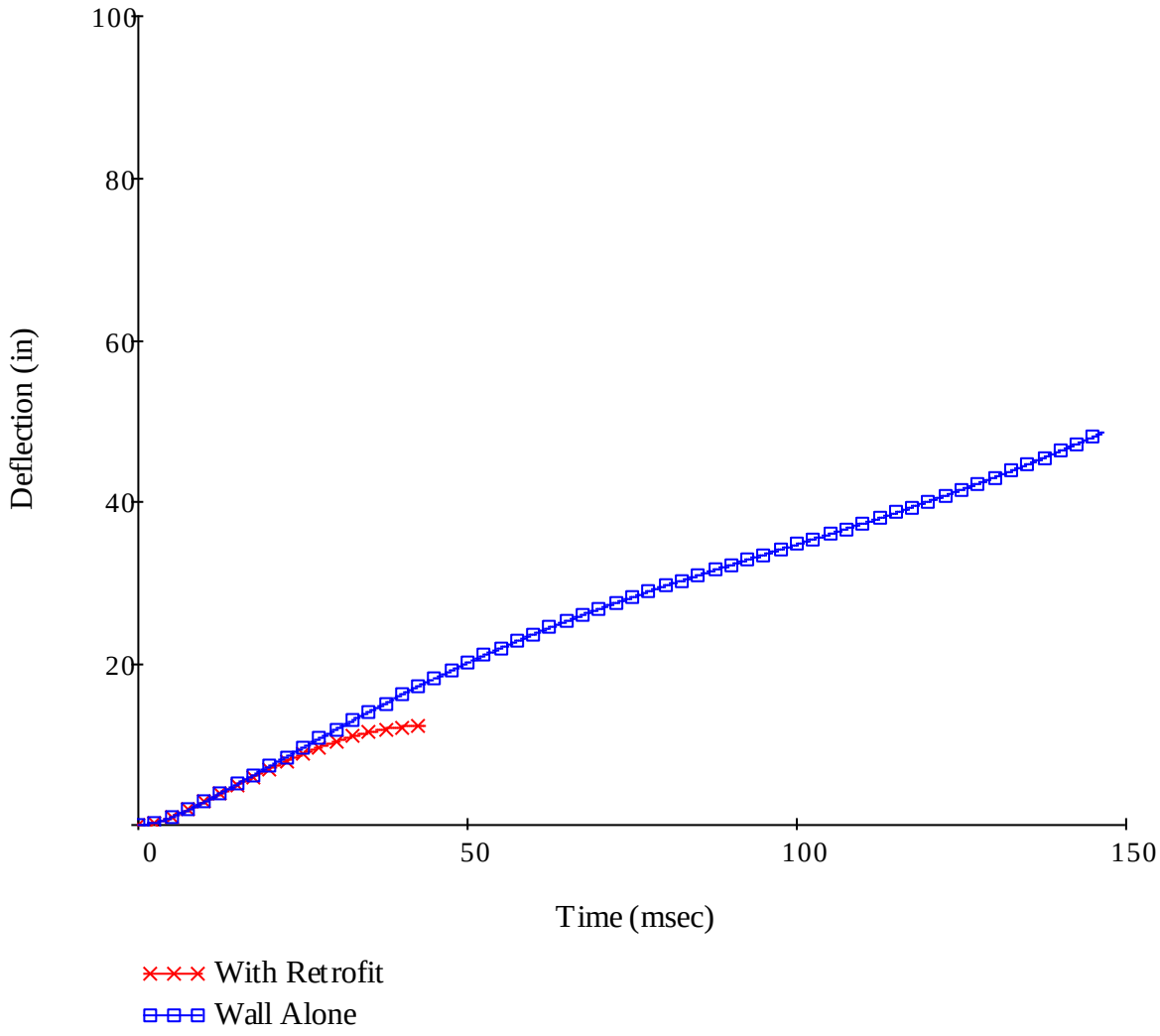
100
80
60
40
20
Deflection (in)
0
50
100
150
Time (msec)
With Retrofit
Wall Alone

Trial 2

Membrane Properties:

$L := 120$

$t := 0.239$

$f_y := 36000$

$L_p := 3$

$E := 29000000$

$\beta := 5 \cdot 10^{-2}$

$t_p := \frac{13}{16}$

$\nu := 0.2$

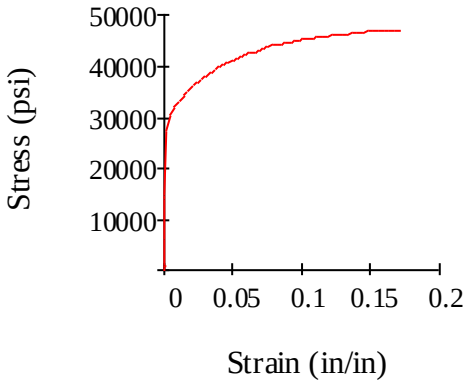

Resistance Definition:

Membrane := StaticResistance(L, t, L_p, E, t_p, ν, f_y, Plate, β)

TotalResistance := (CombineResistance(Wall, Membrane))

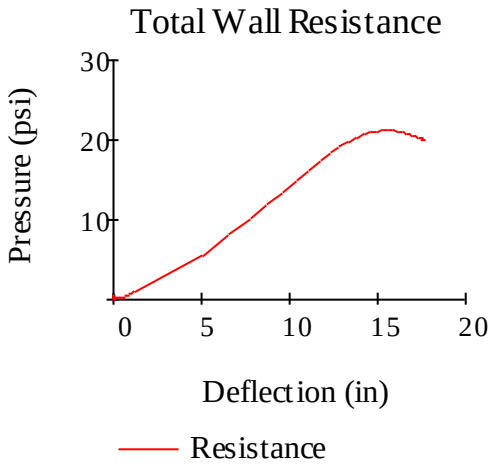

SDOF:

$$K_{LM} := \begin{pmatrix} 0.77 \\ 0.8 \end{pmatrix}$$

SDOF := SDOFpinpin(m, L, Load, TotalResistance, Δt, K_{LM}, Trans)

MaxDeflection := $\max(SDOF^{\langle 2 \rangle}) = 8.371$ angle := $\operatorname{atan}\left(\frac{\text{MaxDeflection}}{\frac{L}{2}}\right) = 7.942\,\text{deg}$

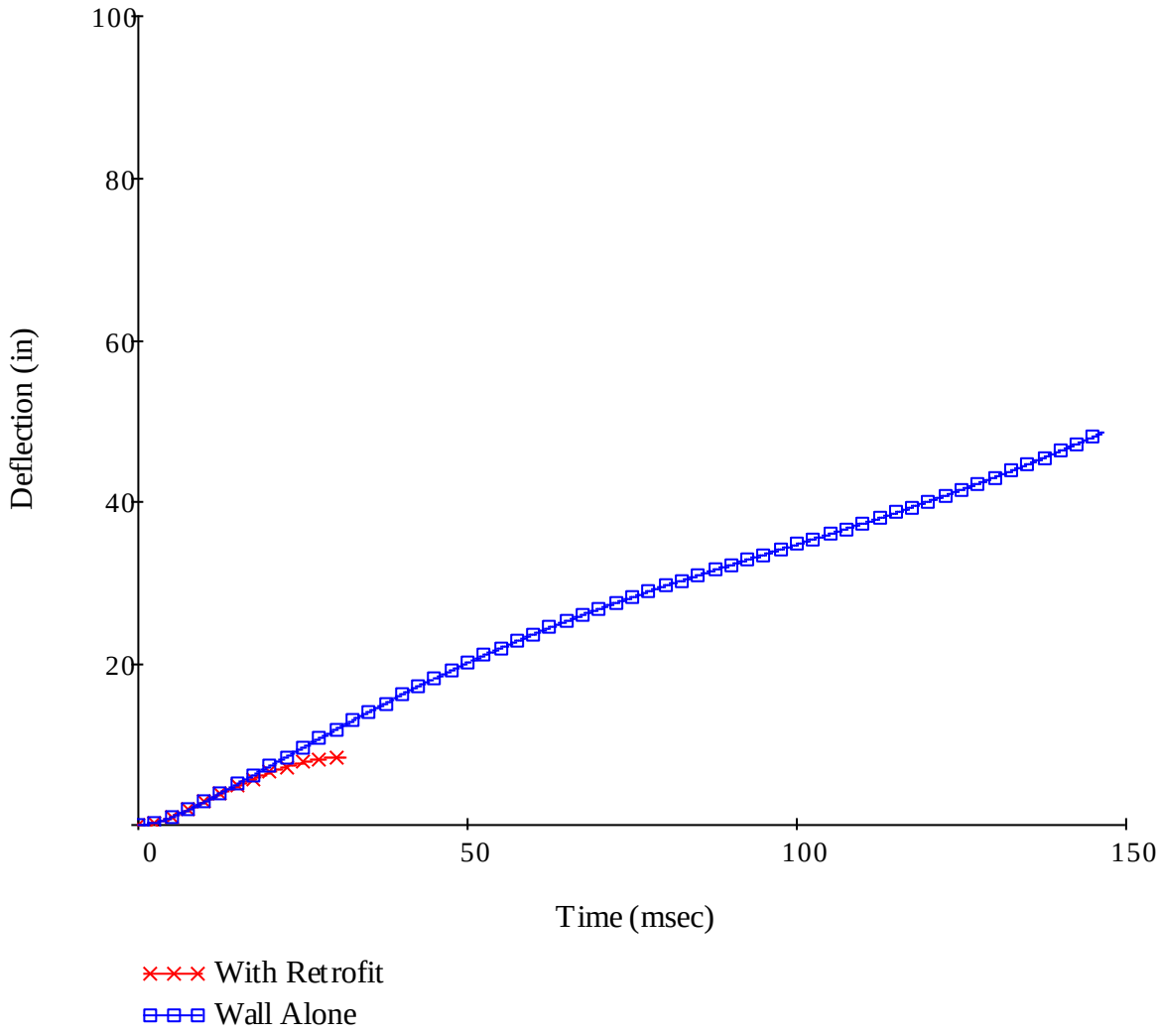

Bolt Loads:

$$T_{Shear} := linterp\left(Membrane^{\langle 1 \rangle}, Shear(Membrane), MaxDeflection\right) = 670.4$$

$$T_{Axial} := linterp\left(Membrane^{\langle 1 \rangle}, Axial(Membrane), MaxDeflection\right) = 2336.6$$

$$Area_{Bolt} := \frac{\left(\frac{5}{8}\right)^2 \cdot \pi}{4} = 0.307$$

$$\sigma_{normal} := \frac{T_{Axial} \cdot 8}{Area_{Bolt}} = 60928.9 \ psi \quad \sigma_{shear} := \frac{T_{Shear} \cdot 8}{Area_{Bolt}} = 17480.1 \ psi$$

Appendix D